

**Novel Thermally Conductive and  
Flame-Retardant Substrates for  
Printed Circuit Boards**  
**- *Structure-Property Relationships* -**

Von der Fakultät für Ingenieurwissenschaften  
der Universität Bayreuth  
zur Erlangung der Würde einer  
Doktor-Ingenieurin (Dr.-Ing.)  
genehmigte Dissertation

von

*M.Sc. Christin Pawelski-Höll*

aus

*Bad Frankenhausen*

Erstgutachter: *Professor Dr.-Ing. Volker Altstädt*

Zweitgutachter: *Professor Dr. Hans-Werner Schmidt*

Tag der mündlichen Prüfung: *01. Dezember 2021*

Lehrstuhl für Polymere Werkstoffe  
Universität Bayreuth  
2021

## Acknowledgments

A long journey comes to an end...!

This research work was completed during my time as a scientific employee at the Chair of Polymer Engineering of Prof. Dr.-Ing. Altstädt at the University of Bayreuth between 2015 and 2018.

During this journey, I met inspiring people for who I am deeply thankful.

Foremost, I am deeply thankful for Prof. Dr.-Ing. Altstädt allowed me to join his group in November 2015. Prof. Dr.-Ing. Altstädt did not only introduce me to the material science of polymers but also their engineering part. He encouraged me in different ways but giving me the freedom to work independently broadened my horizon both scientifically and personally. Thank you for being my mentor and for the support in technical discussions.

This journey started with my master thesis with Dr. Julia Gensel, who, to date, is my superhero. She taught me how to work in a scientific way and motivated me to go beyond my boundaries. Stepping outside the comfort zone is not always easy, but the personal growth which comes with that is priceless. Thank you!

In addition, the saying „*it takes a village to raise a baby*“ can be correlated with earning a Ph.D. degree. I am deeply thankful for all members of the Polymer Engineering Chair. I always look back with a huge smile and teary eyes. Especially, the group „*thermosets*“ guided me through my journey. Gökhan Bakis, thank you for the constant discussions and your input as my group leader and mentor. Also, a big thank you to Martin Demleitner, Markus Häublein, and Fabian Hübner, who never hesitated to support me and discuss scientific topics.

Ute Kuhn, thank you not only for conducting some of the thermal characterizations but also for sharing an office with me. Christian Bauer, thank you for your support during the numerous prepreg-trials. Anneliese Lang, Milena Spörl, Tobias Standau. I don't need to say many words about you; just a simple thank you for always being there for me. Ute, Christian, Anne, Standau and Milli constantly encouraged me. The biggest “Thank you” goes out to you.

Anneliese Lang, Annika Pfaffenberger, and Jaqueline Uhm for conducting SEM, TEM and EDX measurements and helping me with tips to measure some SEM-EDX by myself.

I also like to thank Alexander Brückner and Andreas Mainz for giving me an introduction to the vast world of mechanical testing and also constantly supporting my students' work. I thank Andreas Edenharter and Florian Puchtler from the Chair ACI for supporting me at the Cone Calorimeter and UL-94.

I cannot thank enough my *students* and *Hiwis*, who contributed to this research work with their results in the form of bachelor's and/or masters' thesis. Not only did they learn from me, but most importantly, I learned a lot from them. I tried to teach all my students to work hard to reach a goal, and so did I! A special thanks goes out for their intricate and precious work: Gohar Sani, Enpu Kang, Clara Clute, Liu Honglin, Khushdeep Sharma, Sagar Bhagwat, Alexandra Anastasijevic and Simon Oberländer (in order of their appearance during my research work).

Hauke, we share the same passion, flame retardancy, and thermoset resins. I am very proud to say that I will follow in your footsteps. Thanks for your valuable time and your feedback on my first draft.

This research work was financially funded by the Federal Ministry of Economic Affairs and Energy (public-funded project "*Smart PVI Box*", BMWi 0325916F). I am also profoundly thankful to Nabaltec AG and OLIN Corp. for their material supply throughout my research.

This work is dedicated to my beloved parents and my dear husband. I am deeply thankful for their constant support, motivation, and being a "rock" during these rocky times.

***Ein guter Anfang braucht Begeisterung,  
ein gutes Ende Disziplin.***

*Chemist Prof. Dr. Hans-Jürgen Quadbeck-Seeger*

## Kurzfassung

Neue technologische Trends gehen mit steigenden Anforderungen an Materialeigenschaften einher. Prepreg-basierte Materialien, wie sie in Leiterplatten (LP) verwendet werden, sind keine Ausnahme, da die kurz- und langfristigen Einsatztemperaturen dramatisch zugenommen haben. Ein Versagen des Trägermaterials ist oft die Folge. Darüber hinaus haben RoHS-Konformität und gesetzliche Vorschriften den Einsatz von bleihaltigen Lötprozessen eingeschränkt. Bleifreies Löten erfordert Temperaturen, die um etwa 40 °C höher liegen als bisherige Blei-basierte Verfahren, wodurch das Wärmemanagement zu einer der Schlüsseleigenschaften moderner PCB-Basismaterialien wird. Derzeitig verfügbare PCB-Materialien auf Polymerbasis, wie beispielsweise glasfaserverstärkte (GF) Duroplaste, haben diese Anforderung aufgrund ihrer geringen inhärenten Wärmeleitfähigkeit nicht.

Die Kombination von Baugruppen aus Metallen und polymeren Materialien in Leiterplatten, zeigen bei Temperaturwechselbeanspruchungen ein unterschiedliches Ausdehnungsverhalten (CTE). Neben dem Auftreten von Hot-Spots ist auch Materialversagen (= Delamination) die Folge.

Die aktuelle Herausforderung liegt darin, das breite Spektrum der Anforderungen, die erfüllt werden müssen, zu kombinieren. Die Erhöhung der Wärmeleitfähigkeit und anderer thermischer Eigenschaften geht in der Regel einher mit der Verschlechterung anderer notwendiger Eigenschaften von PCB, wie der Wasserabsorption, dielektrische und mechanischen Eigenschaften.

Wie macht man das Unmögliche möglich?

Bei der Suche nach dem „Heiligen Gral“ in den Bereichen der PCB-Substrate wird nach einem Material (-Kombination) gesucht, dessen Verarbeitung kostengünstig ist, aber auch einen kurzen Produktionszyklus erfordert (Serienproduktion), und im industriellen Maßstab abbildbar ist. Darüber hinaus muss das Basismaterial den geltenden Vorschriften entsprechen und die Anforderungen erfüllen, die sich aus anspruchsvolleren und neuen Anwendungen in schwierigen Umgebungen ergeben.

Ziel dieser Doktorarbeit ist es, ein Verfahren zu konzipieren, das umweltfreundlich, kostengünstig und im industriellen Maßstab anwendbar ist. Das hoch-T<sub>g</sub>-Basismaterial ist auf eine gleichzeitige Erhöhung der Wärmeleitfähigkeit und des Flammschutzes ausgerichtet, ohne dass andere wichtige Eigenschaften (d. h. Wasserabsorption, dielektrische Eigenschaften)

beeinträchtigt werden. Dazu wurden verschiedene Füllstoffe unterschiedlicher Natur, unterschiedlicher Füllstoffgröße und -konzentrationen verwendet. Außerdem werden Füllstoffkombinationen und deren Verhältnisse untersucht. Die Verteilung und Orientierung der Füllstoffe sind entscheidende Faktoren, die durch das optimierte, lösungsmittelfreie Verarbeitungsverfahren beeinflusst werden kann.

Experimentelle Studien werden in verschiedenen Stadien durchgeführt: gefüllte Harzplatten, Prepregs und ihre GF-verstärkten Lamine. Eine Struktur-Eigenschafts-Beziehung wird durch den Vergleich der Gesamtergebnisse unter besonderer Berücksichtigung der Wirkung von GF hergestellt. Das Hauptziel besteht darin, die Auswirkungen der kombinierten Füllstoffe und die Variation des Faservolumengehaltes (FVG) auf die Filtration von Füllstoffen, die Ausbildung des Füllstoffnetzwerks und den daraus resultierenden Eigenschaften zu verstehen. Die Übertragbarkeit von Kompositen auf deren faserverstärkte Systeme wird mit Fokus auf die thermischen Eigenschaften untersucht. Es ist es von großem wissenschaftlichem Interesse, die Abhängigkeit von unterschiedlichen Faservolumengehalten (FVC) auf die thermischen Eigenschaften zu verstehen und die Basis für Vorhersagen oder modellmäßige Beschreibungen zu schaffen.

## Abstract

New trends in technology come at the cost of increasing demands on material properties. Prepreg-based materials as used in **Printed Circuit Boards (PCBs)** are no exception. The short and long-term temperature range which they need to operate in has increased dramatically, critical material failures are often the consequence. Additionally, RoHS compliances and governmental regulations limit the use of i.e., lead-based soldering processes have their share as well. Lead-free soldering requires temperatures about 40 °C higher than *State-of-the-Art* technologies, making thermal management one of the critical properties of modern PCB base materials. *State-of-the-Art* polymer-based PCB materials such as glass-fiber (GF) reinforced thermosets lack this requirement due to their low intrinsic thermal conductivity. Pairing high thermally conductive metals that also possess a low CTE with polymers in PCBs creates a challenge as both material classes show a different dimensional behavior under thermal cycling, and PCB delamination or hot-spot formation is the result.

The current research is challenged by the broad spectrum of requirements that need to be fulfilled. Increasing thermal conductivity and other thermal properties usually come at the cost of other must-have properties of PCBs, like water absorption, dielectric and mechanical properties.

So how does one make the impossible possible?

Searching for the “holy grail” in the fields of PCB substrates is finding a material (combination) whose processing is *cost-efficient* material-wise with a *short production cycle* at an industrial scale. In addition, the base material must comply with current regulations and has to meet the requirements coming from more demanding and new applications in challenging environments. Therefore, this doctoral thesis, aims to design a process and material that are environmental-friendly and cost-efficient and applicable in industrial scale. The high- $T_g$  base material is tailored towards a simultaneous increase in thermal conductivity and flame retardancy without deteriorating other essential properties (i.e., water absorption, dielectric properties). The workflow involves the screening of different fillers of different nature, different filler sizes, and concentrations in feasibility studies. In addition, filler combinations and their ratios are investigated. The fillers’ dispersion and orientation are vital factors that can be triggered by an optimized processing method.

Experimental studies are conducted in different stages: filled resin plates, prepregs, and their corresponding GF-reinforced laminates. The structure-property-relationship is established by comparing the overall results with special attention to the effect of GF. The main aim is to understand the impact of (synergistic) filler combinations, and the increasing FVC on filtration of fillers, filler network formation and the final laminate properties. The transferability between filled resin plates to their fiber-reinforced systems is studied to focus on thermal and mechanical properties. It is of great scientific interest to understand the inter-dependency of different fiber volume contents (FVC) with the thermal properties to describe models and give forecasts.

# Table of Contents

<b>Acknowledgments</b> .....	<b>II</b>
<b>Kurzfassung</b> .....	<b>IV</b>
<b>Abstract</b> .....	<b>VI</b>
<b>Table of Contents</b> .....	<b>VIII</b>
<b>Abbreviations</b> .....	<b>X</b>
<b>1 Introduction and Motivation</b> .....	<b>1</b>
<b>2 State of the Art</b> .....	<b>4</b>
2.1 Electronic Packaging & Thermal Management .....	4
2.1.1 Printed Circuit Boards – <i>The Evolution of FR-4 towards High-Temperature Applications</i> .....	4
2.1.2 Thermal and Mechanical Properties of FR-4 Substrates .....	11
2.1.3 Benchmarks - <i>Market Overview of High-Temperature Substrates</i> .....	15
2.1.4 Thermal Management - <i>Heat Dissipating Components in FR-4 PCBs</i> .....	16
2.1.5 Thermal Conductive Mechanisms in (filled) Polymers .....	20
2.1.6 Review of the current <i>State-of-the-Research – (filled) Resins</i> .....	24
2.1.7 Overall Conclusion of the State of Research .....	47
2.2 Fire Behaviour & Flame Retardancy of Polymers and their filled Resins .....	49
2.2.1 Thermal Degradation of Polymers & the Modes of Action of Flame Retardants.....	49
2.2.2 Characterization of the Fire Behavior .....	52
2.2.3 State of the Research – <i>Flame Retardancy</i> .....	56
<b>3 Objective and Structure of the Thesis</b> .....	<b>61</b>
<b>4 Materials &amp; Methods</b> .....	<b>67</b>
4.1 Materials .....	67
4.1.1 Resin Matrix .....	67
4.1.2 Fillers .....	68
4.1.3 Glass Fabrics .....	71
4.1.4 Benchmarks .....	72
4.2 Processing .....	74
4.2.1 Processing of filled Resin Plates.....	74
4.2.2 Prepreg Manufacturing .....	74
4.2.3 Production of the Laminates – <i>Hand-Lay-Up and Autoclave</i> .....	76
4.3 Characterization Methods .....	79

4.3.1	Thermo-Analytical and Physical Methods .....	79
4.3.2	Pyrolysis and Fire Behaviour .....	83
4.3.3	Mechanical Properties .....	85
4.3.4	Morphological Characterization .....	85
<b>5</b>	<b>Results and Discussion .....</b>	<b>87</b>
5.1	Material Selection .....	87
5.1.1	Matrix .....	87
5.1.2	Fillers .....	90
5.2	Processing of filled Resin Plates and their Thermal Properties .....	92
5.2.1	Process Optimization – <i>filled Resin Formulations</i> .....	92
5.2.2	Optimization towards the desired Thermal Conductivity .....	92
5.2.3	Optimization towards the desired Flame Retardancy .....	107
5.3	Thermal Conductive and Flame-Retardant Properties of Laminates .....	122
5.3.1	Solvent-free direct <i>in-line</i> Impregnation – <i>Prepreg Properties</i> .....	122
5.3.2	Thermal Conductivity of filled GF Prepreg Laminates .....	131
5.3.3	Pyrolysis- and Fire Behaviour of filled GF Laminates .....	148
5.4	Other PCB-relevant Properties.....	178
5.4.1	Mechanical Properties – <i>Flexural Three-Point Bending</i> .....	178
5.4.2	Coefficient of Thermal Expansion (z-CTE) .....	180
5.4.3	Dielectric Properties .....	182
5.4.4	Water Absorption .....	184
<b>6</b>	<b>Summary and Outlook.....</b>	<b>187</b>
<b>7</b>	<b>References.....</b>	<b>194</b>
	<b>Curriculum Vitae.....</b>	<b>212</b>
	<b>Publications .....</b>	<b>213</b>
	<b>Annex .....</b>	<b>215</b>

## Abbreviations

Al	Aluminum
Ag	Silver
AR	Aspect Ratio
ATH	Aluminum trihydrate
BN	Boron Nitride
CFRP	Carbon-fiber reinforced polymer
Cu	Copper
CPT	Cured Ply Thickness
CTE	Coefficient of thermal expansion
DETDA	Diethyl toluenediamine
DMTA	Dynamic-mechanical thermal analysis
DSC	Differential Scanning Calorimetry
EDX	Energy-dispersive x-ray spectroscopy
E&E	Electrical & Electronics
EPN	Epoxy-Novolac
FIGRA	Fire Growth Rate Index
FVC	Fiber volume content (vol%)
FR	Flammschutzmittel (engl. <i>Flame Retardant</i> )
FR-4	Flame Retardant Grade 4 (4 <sup>th</sup> generation)
GF	Glass-fiber reinforced polymer
GFRP	Glass-fiber reinforced
HRR	Heat release rate
MCPCB	Metal-Core PCB
MEK	Methyl ethyl ketone
MLB	Multilayer Board
PCB	Printed Circuit Boards
Prepreg	Preimpregnated fibers
PHRR	Peak heat release rate
RC	Resin content (in wt.% or vol.%)
RoHS	Restriction of Hazardous Substances

SE	Synergy Index
SEM	Scanning Electron Microscopy
TBBA	Tetrabrombisphenol-A
TC	Thermal Conductivity ( <i>dt. Wärmeleitfähigkeit</i> )
TGA	Thermal Gravimetric Analysis
THB	Transient Hot Bridge
T <sub>d</sub>	Thermal Decomposition Temperature
T <sub>g</sub>	Glass Transition Temperature
t <sub>ig</sub>	Time to Ignition
TSP	Total Smoke Production
PHRR	Peak Heat Release Rate
PTH	Plated Through Hole

## 1 Introduction and Motivation

Power electronics is one of the most crucial technologies for promoting resource-saving and regenerative braking in electromobility. Because of the increased demand for sophisticated infotainment and autonomous driving solutions (Figure 1), it is not surprising that the market growth of PCB modules in the automotive sector is expected to grow by a further 8% by 2023 [1,2].

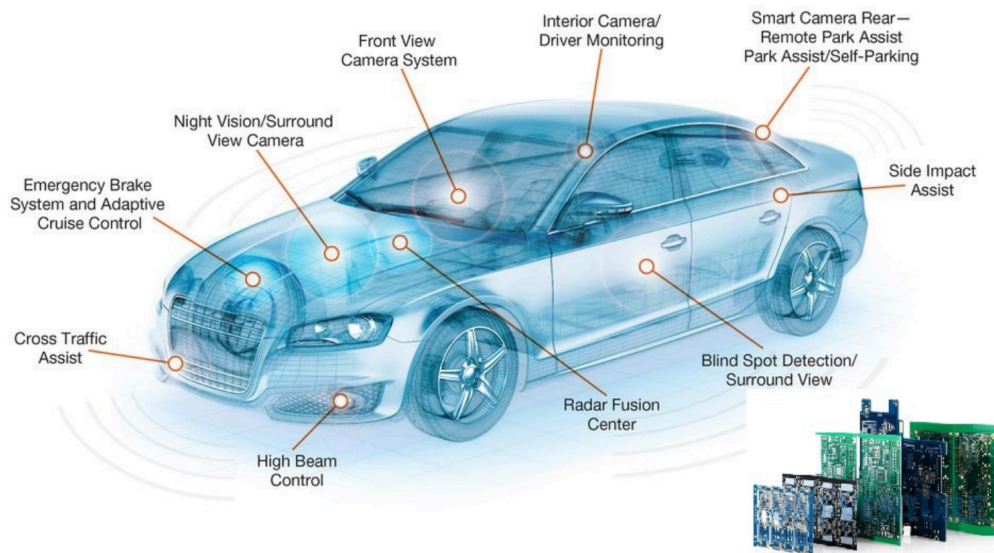


**Figure 1 Future of PCBs in automotive – electrification of sensor techniques, and info-& entertainment [3].**

According to the International Energy Agency (IEA), 50 % of vehicles worldwide should be emission-free by 2030 and CO<sub>2</sub>-neutral by 2050 [4], which goes in hand with finding solutions for *quicker, wireless charging* for electric mobiles. These *electronic devices* are primarily manufactured using *printed circuit boards* (PCBs) which are structural, glass fiber reinforced epoxy laminate sandwich boards. Onto PCBs, electronic components such as semiconductor chips and capacitors are connected with the board, providing the electrical interconnections between those components [5].

In addition to this growth, a revolution is taking place in the PCB industry as a result of the Restriction of Hazardous Substances (EU Directive 2002-96-EC-27, *RoHS*) and the Waste

Electrical & Electronic Equipment (EU, 2002, 96, EC, *WEEE*) [5] directive. Both directives limit the use of certain toxic substances in the electronic industry. Toxic heavy metals such as *lead* (Pb) must be eliminated from the manufacturing of printed circuit boards. This impacts the *soldering process*, as the melting point of lead soldering alloys is around 180 °C. Lead-free tin-silver or tin-copper-based alloys, on the other hand, only melt at about 220 °C but are 20 % higher in production costs. With lead-free soldering processes, the material must withstand briefly elevated temperatures without softening or degradation.

Current technological drivers in the electronic industry beyond *miniaturization & cost reduction* are *high-performance* and *long-term product reliability*. The major drawback with these trends is the significant *heat production* by power components, which must, in some cases, operate under harsh environments with frequent deep thermal cycling. Local heat spots occur close to the embedded chip (Figure 2a)). If heat is not removed correctly, the electronic system will result in lower *efficiency*, less *reliability*, shorter *service life*, and even become a potential hazard (Figure 2b)).

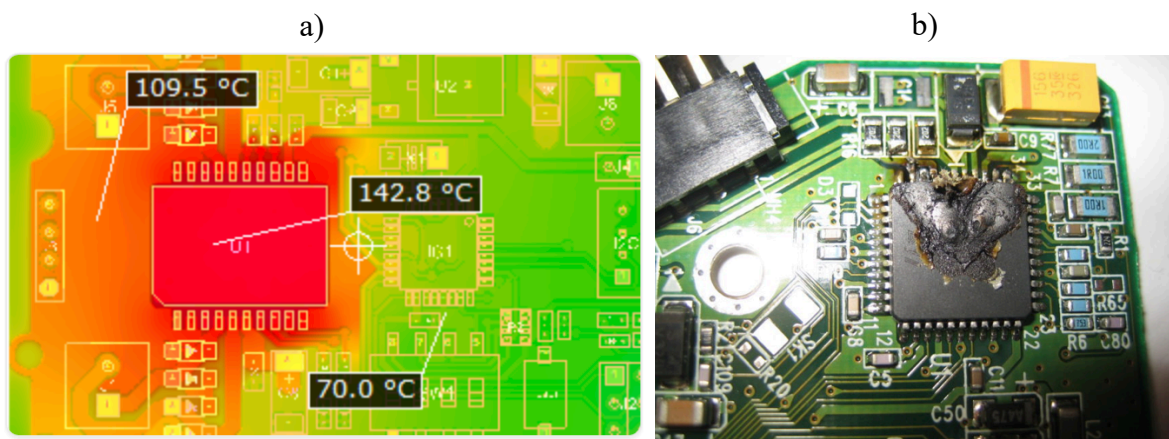


**Figure 2** Current FR-4 PCBs: a) Heat spot detection close to the embedded chip [6]. The generated heat cannot be adequately managed in current FR-4 materials leading to severe degradation (b) [7]).

The long-term stability of the electronic devices decreased by 10% with an increase of temperature by 2° C and decreased lifetime by factor 2 [8,9]. Current *State of the Art printed circuit boards* (PCB) and *FR-4* laminates for lead (Pb) solder assembly will not withstand the higher temperatures of Pb-free processing and are therefore not considered compatible with lead-free assembly. Early material failure due to insufficient heat dissipation often manifests as

delamination in the interlayer between the polymeric matrix (insulator) and the metallic-based assembly parts (highly thermally conductive). The use of ceramic-based substrates may avoid these problems, but their high cost makes them niche market products, such as high-frequency applications. Current assembly concepts for cooling printed circuit boards are at odds with the current trend towards miniaturization. The generated heat must be managed by the assembled parts and the environment of the PCB [10]. Assembled components such as heat sinks and or thermal vias increase the assembly time, which increases the overall cycle time, and requires a lot of designed space [11].

Therefore, a novel approach is, therefore, the modification of the base material to sufficiently distribute and manage heat. Organic matrices have a thermal conductivity of 0.2 – 0.3 W/mK, which is poor compared to target values of  $> 0.7$  W/mK. An increase in thermal conductivity is only possible with the integration of fillers. In literature, it is well known that incorporating ceramic fillers (i.e., AlN, BN, or Silica) with high intrinsic thermal conductivity (TC) will increase the overall epoxy resins' thermal transport behavior [12,13].

*State-of-the-Art* PCB materials based on polymers have not been able to meet these requirements as their thermal conductivity is  $< 0.4$  W/mK. Development work must be carried out here, with the goal to produce a base material that offers simultaneously a higher  $T_g$ , higher  $T_d$ , lower expansion of materials (CTE), and higher thermal conductivity [14]. Glassfiber-fabric (GF) in PCBs provide structural/dimensional stability and bending strength. A possible filtration and aggregation of the particles might occur with the prepreg processing route, due to their small gaps (*intratow-region*). However, very few studies have investigated the impact on processing, filtration effects, and overall laminate properties [15,16]. A further trend is to move away from industrial standard *solvent-based* impregnation towards a *completely solvent-free route*. The use of hazardous materials for the production of PCBs, such as formaldehyde or dimethylformamide, which are known to be reproductive toxins and carcinogenic with exposure of 6 times above the of 5 ppm [5].

The primary motivation is to develop a novel multifunctional, high-temperature base material that applies to PCBs, with increased thermal conductivity and improved flame retardancy.

This doctoral thesis is based on research work as part of the public-funded project „*Smart PVI box*“ (BMW i 0325916F), supported by project partners Siemens AG, Robert Bosch GmbH, Isola GmbH, Schweizer Electronic AG, Lackwerke Peters, Fraunhofer IZM, ECPE European Center of Power Electronics) and Huntsman Advanced Materials.

## 2 State of the Art

### 2.1 Electronic Packaging & Thermal Management

#### 2.1.1 Printed Circuit Boards – *The Evolution of FR-4 towards High-Temperature Applications*

A printed circuit board (PCB) is a board or a substrate on which an electrical circuit is printed or electronic assemblies of capacitors, resistors, inductors, and switches are mounted [10,17]. The interconnection of integrated circuit chips, their signal and power transmission, and environmental protection can be summarized as *Electronic Packaging*. Dr. Paul Eisler developed the first printed circuit boards in 1943 during World War II [18]. Initially, the material used in PCB laminates could be almost anything, from thin pieces of wood to Bakelite and Masonite. With the widespread commercialization of transistors from the 1950s through to the 1960s, demand for printed circuit boards expanded significantly. The laminate substrate materials also shifted from paper-fiber to glass-fiber-thermosetting resins [19]. Automated mass production of PCBs started in the late 1960s [17]. Glass fiber-reinforced epoxy laminates have been the base substrate material in printed circuit boards for decades now. The challenging demands of PCBs in aerospace, military, and computing applications have led to multi-layer- and rigid-flexible-structures.

The PCB has two essential components: the *base material* (an insulating material that acts as a mechanical supporting structure) and the *conductor material* (high-purity copper, which interconnects the electrical junctions) [17]. The primary *conductive material* used in PCBs is Cu foil or CU sheets with a thickness between 12 and 70  $\mu\text{m}$  and weights between 107 and 610  $\text{g}/\text{m}^2$  [17]. Base materials can be divided into *organic* and *inorganic* substrate materials. Organic base materials are phenolic or epoxy impregnated paper or woven / nonwoven glass. Inorganic substrates are composed of ceramics and metals (e.g., Al, Cu). The electrical components are generally soldered to the electrically insulating substrate. In addition, layers (depending on the PCB type) of the thin copper sheets are attached to the top layers of the PCB to conduct heat and electricity (Figure 3). Usually, the primary function of the substrate or the base material is to provide insulation to the electric components, and act as a support on which

different electrical components can be etched or printed. The highly thermally and electrically conductive layers consist of aluminum (Al) or copper (Cu) foils [10].

The base material (the “*dielectric core*”) of the PCB consists of a polymer, in general, a thermoset, the reinforcement, woven fiber glass fabrics, the conductive foil, and (inorganic) fillers [18,20]. These consist of woven fiberglass fabric to give structural stability, impregnated with Epoxy resin, and exhibits excellent mechanical, electrical and thermal properties (Figure 3).

Applications include computers, telecommunication devices, satellites, automobiles, aerospace, and industrial controls [18,21]. The demand for higher switching frequencies, the PCB components (e.g., inductors, capacitors, energy storage devices) need to be designed to be drastically smaller but must also withstand harsh higher temperatures. Currently, PCBs applicable in automotive, such as wireless charging devices, are realized using *ceramic substrate materials*. These ceramic PCBs are high-temperature stable but require lengthy processing times and are therefore very high in costs. Currently available *polymer-based* circuit board substrates, the “FR-4” substrates have glass transition temperatures between 130 and 200 °C [22,23]. Polymers such as cyanate esters or polyimides with glass transition temperatures of > 200 °C are not in a competitive situation due to their high material costs (factor 2-7) [24].

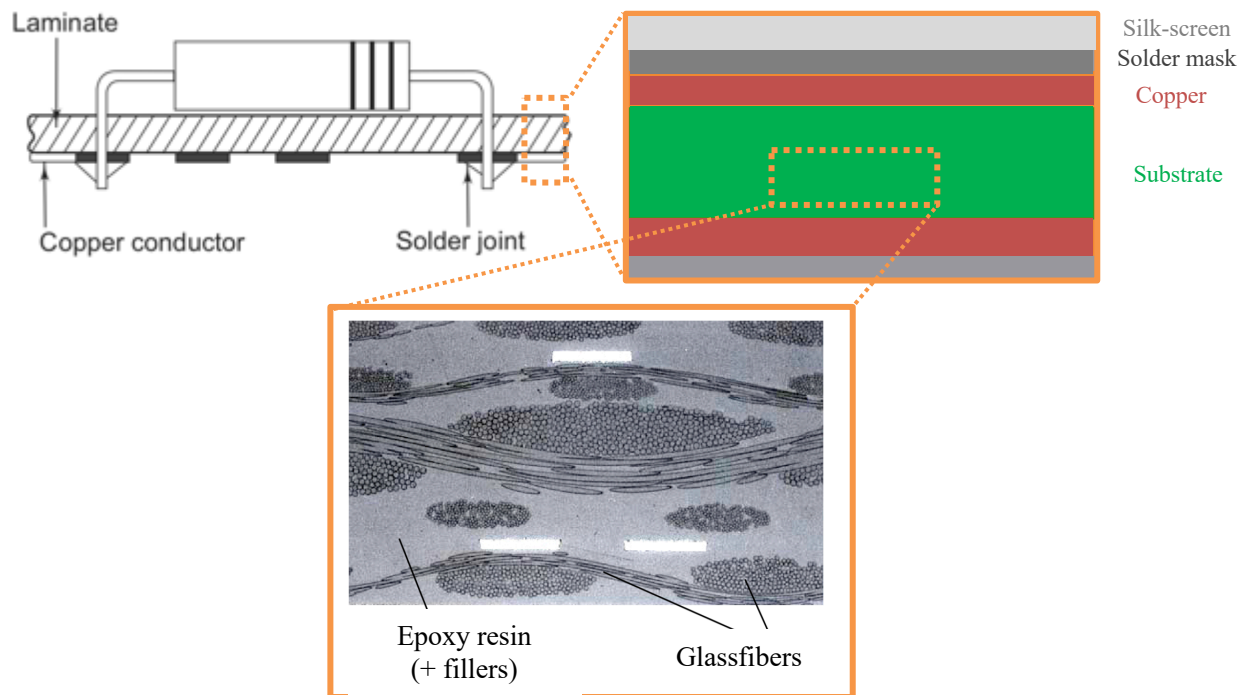


**Figure 3 Schematic set-up of a double-layer PCB (left), its layered structure (right) and cross-section through the prepreg substrate laminate (bottom) [17,24].**

In recent years, some variations of FR-4 substrates with higher  $T_g$  of up to 200 °C were introduced into the market (Table 1). *These FR-4 have a very low thermal conductivity (between 0.2 to 0.4 W/mK), which is unsuitable for HT-PCB applications.*

**Table 1 Summary of common FR-4 substrates with their corresponding properties [18].**

Specification Sheet	Resin System	T <sub>g</sub> / °C	Properties/Comments
IPC-4101/82	Epoxy/Multi-functional Epoxy; Flame resistant	110 °C	UL-94 V1, Kaolin, or inorganic filler
IPC-4101/83	Epoxy/Multi-functional Epoxy	< 200 °C	UL-94 V1, Kaolin, or inorganic filler
IPC-4101/92	Epoxy/Multi-functional Epoxy; Phosphorous flame retardant	< 150 °C	UL-94 V1
IPC-4101/93	Epoxy/Multi-functional Epoxy; Aluminum Hydroxide flame retardant	< 150 °C	UL-94 V1
IPC-1401/97	Di-functional/Multi-functional Epoxy	110 °C	UL-94 V0, inorganic fillers
IPC-1401/121	Di-functional/Multi-functional Epoxy; Modified (5 wt.% max)	110 °C	UL-94 V0; z-CTE, and time to delamination requirements
IPC-1401/124	Epoxy/Multi-functional Epoxy; Modified (5 wt.% max)	150 °C	UL-94 V0; z-CTE, and time to delamination requirements
IPC-1401/126	Epoxy/Multi-functional Epoxy; Modified (5 wt.% max)	170 °C	UL-94 V0; inorganic fillers

In general, *polymers* are extensively used in electronic packaging and thermal management systems such as packaging, molding, encapsulation, thermal adhesives, PCB substrates, and thermal interface materials (TIMs) [10]. Compared to thermoplastics, *thermosets* possess improved temperature performance (T<sub>g</sub>) and thermal stability (T<sub>d</sub>) due to their 3-D crosslinking, which occurs during thermally- or chemically induced curing. During curing, the resin undergoes a gradual conversion of its functional groups (gelation) [25]. However, thermosets are used in niche applications like high-frequency and recyclable PCBs [10,26–28].

Common thermosets are *Bismaleimide-triazine (BMI) epoxy*, *cyanate esters*, *polyimides*, *polyurethanes*, and *phenolics*. *Epoxy* resins are the most common thermosets for PCB applications. Epoxy resins can vary with a T<sub>g</sub> between 160 and 185 °C, whereas Epoxy Novolac thermosets can reach glass transition temperatures from 180 and above 200 °C [29]. *Di-*

**functional epoxy resins** have a  $T_g$  below 120 °C. These epoxies can be used in double-sided PCBs or blended with other epoxies to provide superior temperature stability [18]. **Tetra-/ or multi-functional epoxies** have more than two epoxide groups per molecule, which results in higher crosslink efficiency. These epoxies have elevated thermal properties, i.e,  $T_g$ ,  $T_d$ , but are usually more brittle and expensive. The  $T_g$  ranges from 125 to 175 °C [18].

To reach a  $T_g > 175$  °C, one must switch from epoxy to the phenolic resin chemistry, which is a promising candidate. Two types of **phenolics** are commercially available: **novolacs** and **resols**. **Novolac** can be used as is or as an intermediate reacting with an amine-based hardener to create a 3-D structure. **Resole** is a multifunctional reactant and undergoes thermally-induced curing [30]. Novolac needs a curing agent to crosslink, whereas resoles are self-curable [29,33]. In a second reaction with Epichlorohydrin, Epoxy-Novolac (EPN) is formed [31] (Figure 4). The reaction to novolac at higher temperatures under a condensation reaction of methylol phenol with phenol and or / methylol phenol releasing water as a by-product [30,32].

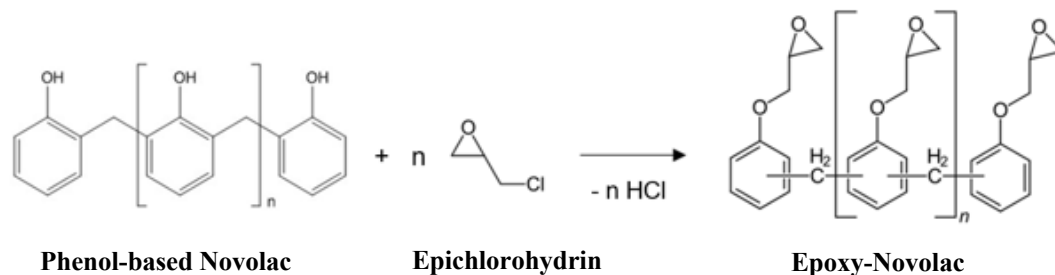


**Figure 4** Reaction scheme of Phenol-Novolac with Epichlorohydrin [33].

A correlation between  $T_g$  increase, CTE, and costs can be observed with the various Epoxies: the higher the  $T_g$ , the higher the relative costs, and the lower the  $\alpha$ -CTE. An even higher  $T_g$  range is only achievable by using cyanate esters or BMI epoxies. However, the raw material price would increase by factor 2-3.

The most commonly used **reinforcement materials** are woven fiberglass fabrics, papers, or aramid fibers. The advantage of woven glass is not only good mechanical and electrical properties but also its price. In the PCB industry, carbon-based fibers are very uncommon.

Glass fiber (GF) reinforcement not only gives structural and dimensional stability but also offers a low thermal expansion, high tensile strength, and low electrical conductivity (=

isolators) [18,24,32]. **E-glass** (major component: *boron silicate*) is the most used fabric for PCBs as it combines good electrical, mechanical, and chemical properties at an acceptable cost. The CTE of E-glass is about 5.5 ppm/°C, its dielectric constant  $D_k$  is 6.6, and its dissipation factor  $D_f$  is 0.0012, both measured at 1 MHz. NE-glass has slightly better dielectric properties but is more expensive [18]. The weaving process can produce different fiber orientations: *unidirectional fiber bundles*, *woven fabric*, or *multi-directional woven* [30]. GF fabrics consist of two rectangular *crossing warps* (in production direction) and *weft threads* and therefore have a bi-directional strengthening effect [32]. In general, woven fabrics have good strength and stiffness in two directions. Their areal weights vary between 20 up to 1.000 g/m<sup>2</sup> [34]. They may also benefit from an applied *surface finish* (epoxy- or amino silanes) [18] to enhance the interaction in the interface between the glass and the polymeric matrix. The surface finish decreases water absorption and increases tensile and shear strength due to enhancing the interfacial adhesion [32].

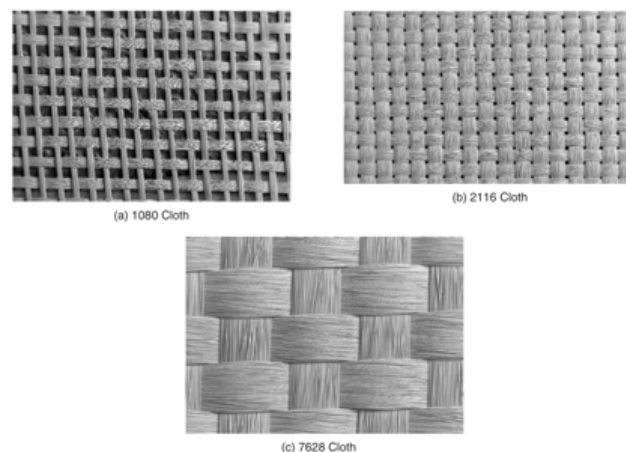


**Figure 5** The most common fiberglass fabrics in plain-weave: a) US Style 1080, b) US Style 2116, and c) US Style 7635 with increasing warp and fill count leading to an increased cloth weight [18]. The SEM micrographs are to be seen as schematics as scale bars are missing.

An international nomenclature has developed for woven GF, starting with *US-style 106* with a thickness of 0.0013” (0.033 mm) up to *US-style 7635* with a thickness of 0.008” (0.2032 mm). While the thickness of the cloths does not vary much, the gaps between warp and fill yarn decrease (Figure 5).

The design of the laminate structure can positively influence the overall cost and the final laminate properties. Within the development, reverse engineering usually starts with the end-use and then drafts and simulates the PCB design concept. The substrate thickness can be triggered by using different US-style fabrics. With an increase in fabric thickness, the FVC increases, and the resin content decreases. This leads to lower costs and a difference in the final properties of this prepreg, such as thermal, mechanical, and electrical properties [24].

The *resin content* is directly dependent on the used GF style (refer to Figure 6). The lower the resin content, the lower the impact on thermal expansion since polymers have a higher CTE value in  $z$ -direction than the glass fibers. To improve dimensional stability, the resin content should therefore be kept low. The GF cloths have an average  $x/y$ -CTE of 22.2, 18.1, and 15.6 ppm/K US Style 106, US Style 1080, and US Style 2116, respectively [18]. Higher FVC also reduces the resin costs, help with dimensional stability, and can create issues with fabrication steps, such as drilling (breakage!).

However, high resin content can positively impact the overall dielectric properties, since GF has a higher  $D_k$  than resins and can help achieve a smooth surface finish of the prepreg [18]. Regarding prepreg manufacturing, the resin content can vary for each type of GF cloth within a range of  $\pm 10\%$ . Higher resin contents aid in filling, i.e. circuit patterns, and directly influences the ply thickness [18].

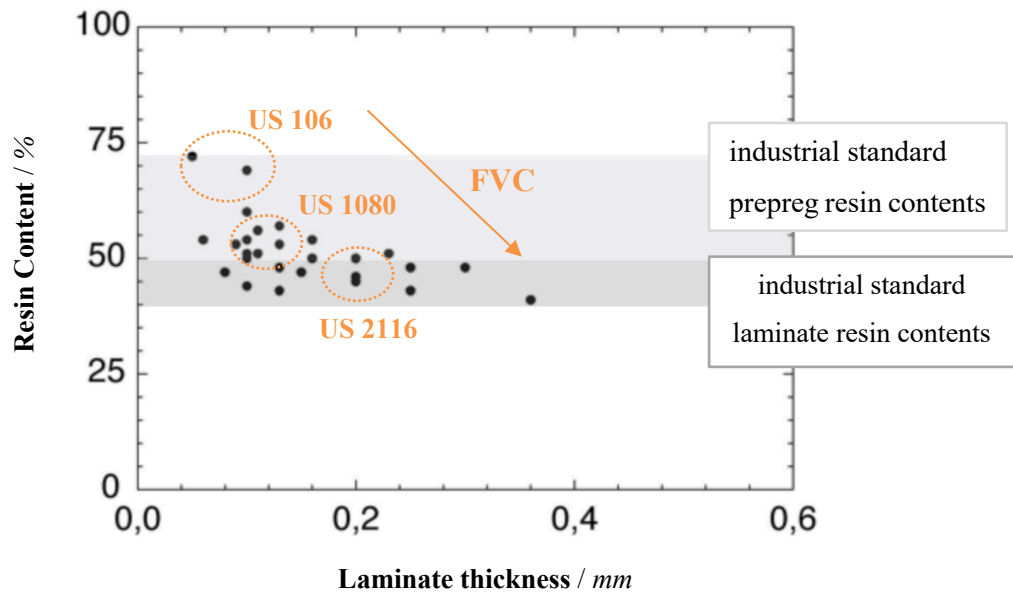


**Figure 6** *State of the Art*-laminate thicknesses, and their corresponding resin contents exemplarily for US 106, US 1080 and US 2116 [18,35].

### 2.1.2 Thermal and Mechanical Properties of FR-4 Substrates

**High-temperature** applications are defined as the inflection point of performance decrease, in definition between 150 °C to 300 °C [36–38]. The first critical parameter in HT-electronic applications is **thermal stability**. A low degradation temperature can lead to adhesion loss and delamination. The point at which degradation begins, usually indicated as  $T_{d,2\%}$  or  $T_{d,5\%}$  for material decomposition of 2 % and 5 %, is a crucial parameter. At this point, volatiles can be released, leading to overall mass reduction. *State of the Art* FR-4 materials, with a  $T_g$  of < 170 °C, commonly have a  $T_{d,5\%}$  of 345 °C. Novel developments shall at least have  $T_g$  values above 200 °C and a  $T_{d,5\%}$  of > 350 °C [18] (Figure 7).

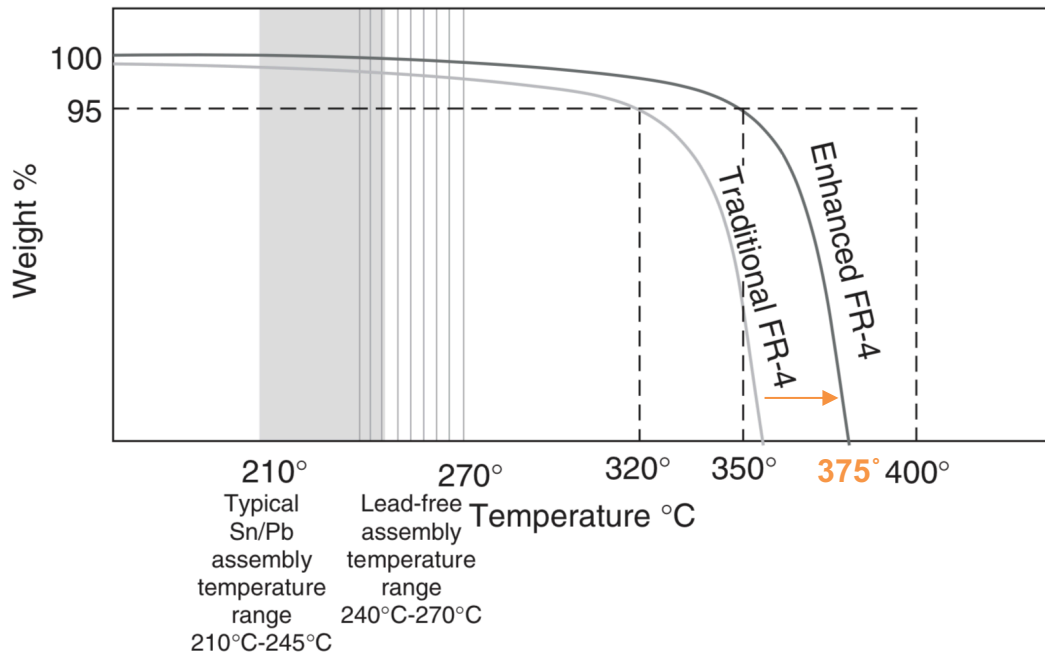


**Figure 7 Schematic decomposition curves (TGA) for traditional FR-4 material and enhanced FR-4 materials. With lead-free soldering processes, the  $T_g$  and the  $T_d$  values materials have to withstand are shifted to higher values [18].**

The **glass transition temperature**,  $T_g$ , of a base material is a critical parameter in PCB design since operation below this temperature (rigid state) or above (softened state) can cause different properties. In the softened state, the material undergoes physical, especially volumetric changes. Thermosets increase the relative mobility of their linkages at  $T_g$ , resulting in lower mechanical strength. The glass transition is influenced by the degree of cure and the reinforcing matrix [18]. A mismatch due to the difference in coefficient of thermal expansion (CTE) values will cause deformation in the  $z$ -direction of copper pads on the surface of printed circuits, i.e., in between the copper film and the base material. Sufficient thermal stresses from this deformation might result in delaminations causing early failure. It is important to note that the  $z$ -CTE is usually determined *below*  $T_g$  (known as  $\alpha_1$ -transition) [18]. Table 2 gives a summary of the  $T_g$  and CTE values of *State-of-the-Art*-base materials.

**Table 2 Thermal properties,  $T_g$ , and CTE of *State-of-the-Art-FR4* materials [18].**

Material	$T_g / ^\circ C$	$z$ -CTE / ppm/K	$x/y$ -CTE / ppm/K
FR-4	140	4.5	13 - 16
Enhanced FR-4	140	4.4	13 - 16
Enhanced FR-4 (filled)	150	3.4	13 - 16
Enhanced FR-4 (filled), high $T_g$	175	2.8	12 - 15
Halogen-free, filled, high $T_g$ FR-4	175	2.8	13 - 16

The  $T_g$  values are a result of different Epoxy base resins, i.e., *di-functional* or *multi-functional* crosslinking.  $T_g$  higher than 180 °C can only be achieved with blend systems or cyanate esters [14].

Regarding the *flammability* of a base material, the trend shifts to the use of “green electronics”. Demand for non-toxic smoke forming, halogen- and lead-free PCB materials [18,39]. The flame retardancy can be increased by using of different flame retardant (FR) fillers: non-halogenic, phosphorus, or aluminum hydroxide (ATH). The reduction of CTE values arises from the incorporation of inorganics fillers, such as  $Al_2O_3$ , which is a commonly used FR in the PCB market.

The demand for printed circuit boards that operate at high frequency requires materials with good permittivity and loss characteristics. Some conventional PCBs cannot be used for such high-speed devices due to their high *dielectric constants* ( $D_k$ ) (= permittivity) and *loss tangents* ( $D_f$ ), which describe the insulating behavior of the base materials. The dielectric constant can easily be influenced by the applied frequency, temperature, and humidity.  $D_k$  gives the capacity of a material to store electric charge. The dissipation factor  $D_f$  is the ratio of the power loss within a material to the product of voltage and current in a capacitor. FR-4 materials have a  $D_k$  at 1 MHz of 4.7 and at 1 GHz of 4.3. The dissipation factor is for 1 MHz 0.023 - 0.025 and at 1 GHz 0.016 - 0.018. The dielectric properties strongly depend on the chosen resin system, the

resin content, and frequency. With epoxy systems, the values for  $D_k$  are in the range of 4-5 (at 1 MHz); for cyanate esters, the range is between 3.5 -4.5 (at 1 MHz) (also see listed values in Table 3).

With decreasing resin content, the  $D_k$  decreases. In contrast, the  $D_f$  increases with increasing resin content. With increasing frequency,  $D_k$  values decrease. Regarding water absorption, both values increase in direct proportion to water content. The curing agent also influences the electrical properties: dicy-based curing agents usually perform better than phenolic-based concerning  $D_f$  [17,18,39].

**Table 3 Overview of *State-of-the-Art* dielectric properties of high- $T_g$  laminate materials [17,18,40].**

PCB Material	$T_g / ^\circ C$	$D_k$ (at 10 GHz)	$D_f$ (at 10 GHz)
FR-4	140	4.3 – 4.5	0.0016
FR-4 (filled)	150	4.4	0.0016
Enhanced FR-4 (tetrafunctional Epoxy)	175	4.4	0.0020
Enhanced FR-4 (filled), high $T_g$	175	4.3	0.0018

The **moisture absorption** resistance of the base material (either from the air or water immersion) is essential for printed circuit board reliability. Water has a relative dielectric constant  $D_k$  of 78. In addition, the most critical effect of absorbed moisture is the declining ability of a material to oppose conductive anodic filament (CAF) formation when a bias is applied to the circuit. Besides, because HT-PCBs may be exposed to high temperatures, evaporation of water will influence structural stability and affect the performance of the PCB. Standard FR-4 products have a moisture absorption between 0.1 - 0.5 % after 24 h exposure; halogen-free materials have higher uptake [18].

### 2.1.3 Benchmarks - *Market Overview of High-Temperature Substrates*

Currently, available prepregs for high-temperature PCBs range between  $T_g$  values of 150 – 200 °C (Figure 8). Higher glass transition temperatures can only be achieved with PI matrices. The thermal degradation at 5 % has an average of 330 - 350 °C. Higher  $T_{d,5\%}$  are only achieved with the addition of fillers (whereas the suppliers do not list these on their SDS or TDS due to confidential IP that is also protected by patents! (refer to [41–45]). Only PI matrices can reach  $T_{d,5\%} > 400$  °C, and with PTFE  $T_{d,5\%} > 500$  °C. Whereas the latter is only used in particular niche applications, such as high frequency. The high-frequency ranges from 300 MHz to 300 GHz, with applications in aerospace (satellite communication) or automotive (radar systems).

The overview below shows that there is still some gap (area in green) where more development work can be done, of  $T_g > 220$  °C and  $T_{d,5\%} > 380$  °C. Depending on the application or the frequency in the end-use, one can either use thermoset-based substrates or switch to PTFE-based substrates. One must consider the overall costs as PTFE follow non-conventional processing. However, PTFE has excellent electrical properties [46]. PTFE based material is used for antennas (24 GHz) or sensors (77 – 79 GHz).

Rogers' "92ML<sup>TM</sup>" prepreg, applicable for power electronics, is advertised as a halogen-free prepreg filled with ceramic fillers. Attaching an aluminum plate to the assembled PCB would result in a  $z$ -thermal conductivity of 1.6 W/mK. The  $T_g$  is about 160 °C, with a  $T_{d,5\%}$  of around 350 °C [47].

Isola's "TerraGreen®" [48] and "PCL 370 HR®" [49], have  $T_g$  values of 180 – 200 °C, with "Terra Green" having a superior  $T_{d,5\%}$  of about 390 °C compared to  $T_{d,5\%}$  of PCL 370HR of 340 °C.

**In summary, all current suppliers of PCB prepregs materials do not offer Epoxy-based systems with a TC of  $> 0.7$  W/mK, nor with a  $T_g > 220$  °C and  $T_{d,5\%}$  of  $> 350$  °C without the need to switch to a different polymer (indicated in Figure 8, "gap"). Almost all current prepregs have a TC of  $< 0.4$  W/mK, unless additional cooling methods such as aluminum heat sink. Standard FR-4 substrates made of E-Glass (at unknown FVC) have a TC of 0.3-0.4 W/mK, PTFE ceramic based substrates a TC of 0.5-0.6 W/mK [50].**

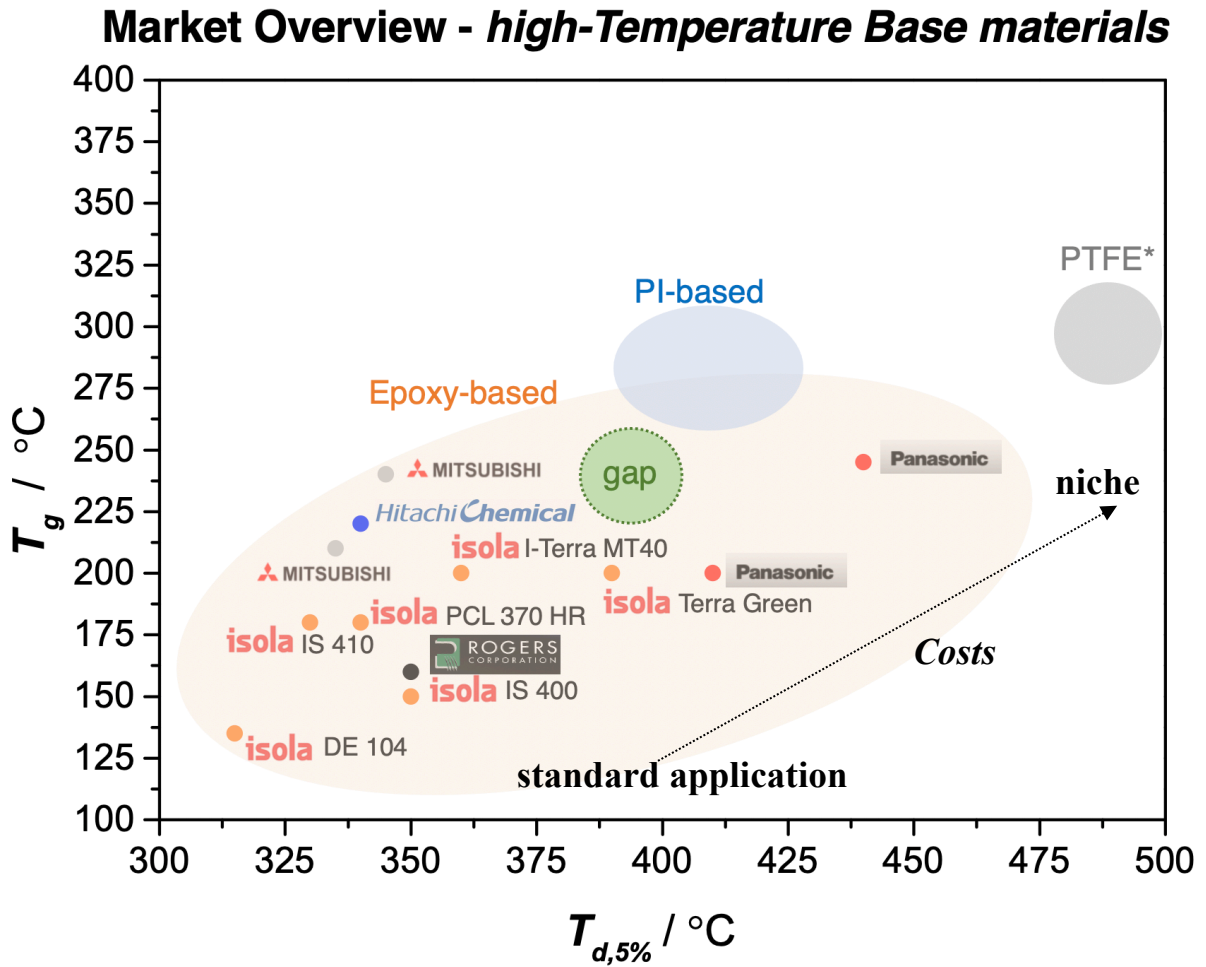


Figure 8 Market overview of current *State-of-the-Art* high-temperature base materials (= prepregs) for PCBs. (\* =  $T_{crystallization}$ ) [47–49,51–58]

#### 2.1.4 Thermal Management - *Heat Dissipating Components in FR-4 PCBs*

Over the years, *thermal management* has become an integral design consideration in today’s electronic industry [59] (Figure 9).

Heat can be dissipated in different ways. The board-level techniques include thermal conductive materials or assembled parts, such as heat sinks. On the chip level, i.e., microchannel cooling or cooling by using conductive copper materials. The overall packaging can be cooled with air fans.

With the size limitation, the current research needs to find ways to incorporate thermal conductive materials on the chip level into the base material. Choosing the right thermally conductive material without sacrificing other essential properties, such as CTE,  $D_k$ , or even the lightweight design [60].

Convection and Radiation apply directly to the PC boards' surface mounted components and surface layers (Figure 10). They are predominantly dependent on the board's environment, which usually cannot be changed. Furthermore, forced convection, such as the help of ventilation, is not possible in some cases because PCBs are in a sealed environment or because this is not attainable for small applications. Thus, for heat management, getting an excellent thermal conduction is more dominant in the design of PCBs. The goal is to produce the most efficient thermal path with good heat conduction to the heat sink or environment [38].

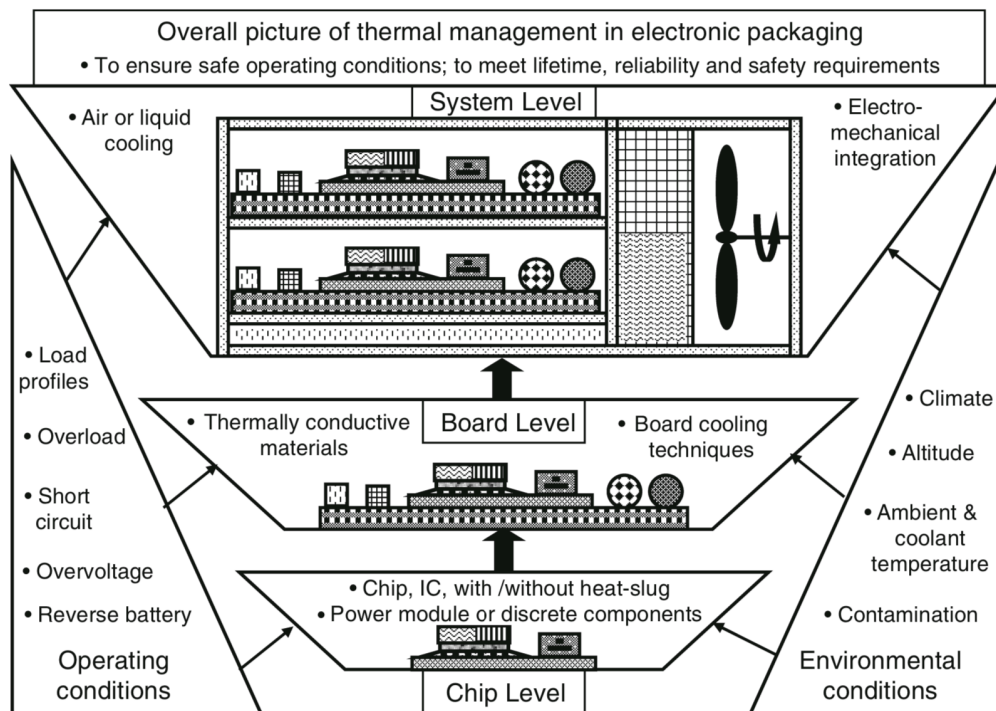
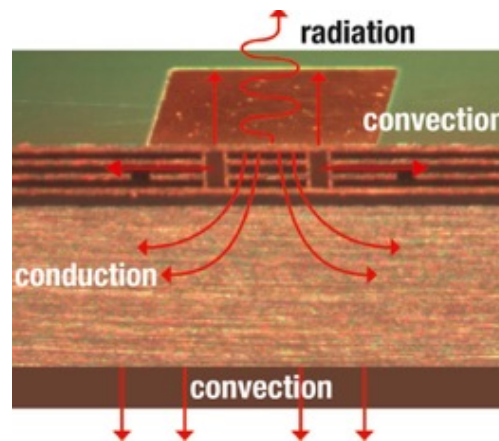
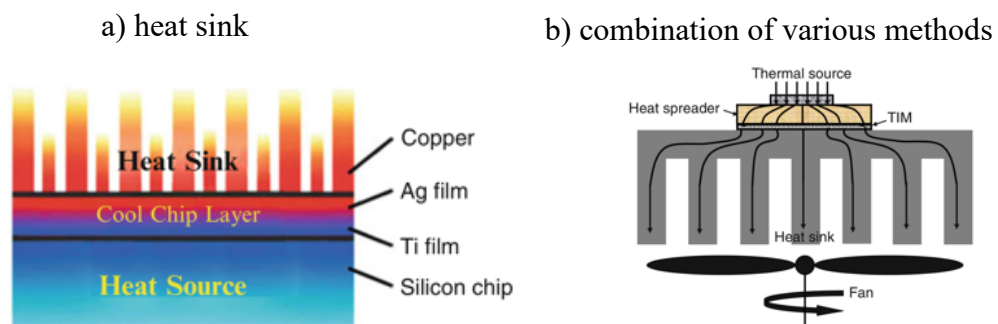


Figure 9 Thermal management in different levels of electronic packaging [11].



**Figure 10** Three heat transfer mechanisms in a 4-layer Printed Circuit Board attached to an aluminum heat sink [61].

Inefficient thermal management in PCBs will result in loss of efficiency, reliability, and lifetime. Reliability reports have exhibited that almost 50 % of electronic system failures are caused by high-temperature applications [62–64]. Several thermal management strategies are currently used to cool the electronic components, which can be divided into two areas: *primary material-specific* thermal conductivity and the actual *secondary cooling units* such as blowers, cooling fins, or heat pipes and other currently used cooling systems include air-cooled *heat sinks (passive cooling)* and *radiators, forced air-flow and pumped liquid loops* [10] (Figure 11).



**Figure 11** Latest heat management Components in Electronics. a) Active air cooling example using a heat sink and b) Combination of heat spreading, heat sink and fan [10].

Heat spreaders are highly conductive plates (e.g., made of Al) serving as heat exchangers between the heat source (chip) and the heat sink. Dielectric heat spreaders are applied between

a high-power semiconductor to a PCB to transfer thermal energy. They are commonly thermally conductive but electrically insulating material (i.e., BN, BeO, AlN, or Al<sub>2</sub>O<sub>3</sub>).

Conventionally, a combination between heat spreading, heat sink, and air cooling (fan) is used when a high-powered system must be cooled.

Another method to distribute heat from the chip is via *thermal vias*. Thermal vias are mechanically drilled, open through holes with a Cu plating thickness of 35  $\mu\text{m}$ . Thermal vias act as connectors to the Cu insert  $x/y$ -plane and remove heat efficiently in the  $z$ -direction (Figure 13).

*Buried vias* are structures that connect two or more layers of a board buried inside the base material board. Meanwhile, a blind via is a plated through-hole (PTH) which connects the surface layer with the internal layers of the board (Figure 13) [17,18,65].

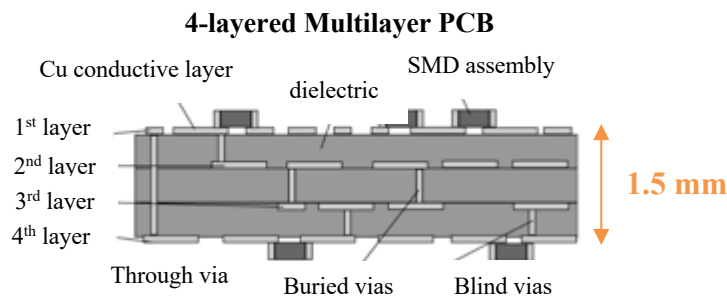


**Figure 12** Set-up of a multilayer PCB [24] in cross-section.

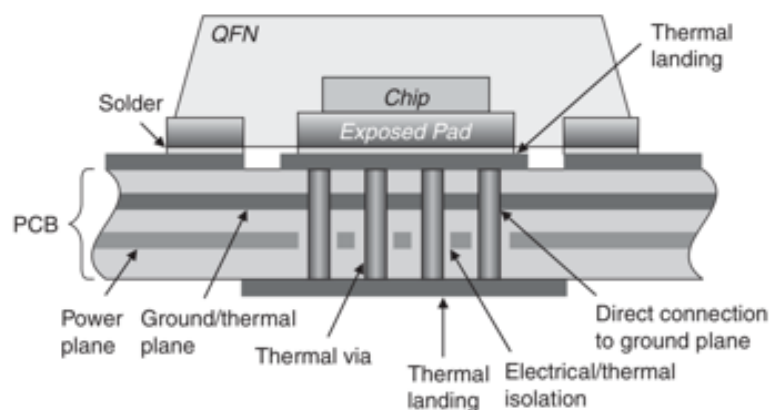


**Figure 13** Application of thermal vias in a four-layer PCB (cross-sectional view) [18].

The PCB design, as described above, determines its performance and its end-use, i.e., high-frequency applications. A standard FR-4 board is not suitable as it cannot withstand the thermally dynamic environment. The overall design and development process balances between choosing the suitable materials, cost, and requirements.

### 2.1.5 Thermal Conductive Mechanisms in (filled) Polymers

Heat is, in general, transferred by a *movement of energy* induced by temperature difference. In contrast, *heat flow* is described as the movement of thermal energy, which is linked to the kinetic energy of atoms or molecules [10]. The higher the materials' temperature, the higher the linear and vibrational motion of molecules. *Heat* is the actual transfer between two adjacent particles and describes how much energy is transferred and how quickly and in which direction. Heat directly correlates to thermal conductivity [66]. *Fourier's law* describes the heat flow path ( $dx$ ) in solid materials as proportional to the ambient temperature gradient ( $dT$ ). The constant of this proportionality is called thermal conductivity  $\lambda$  ( $\frac{W}{mK}$ ) [67].

$$\mathbf{q} = -\lambda \frac{dT}{dx} \quad [10] \quad \text{Equation 1}$$

*Thermal Conductivity*  $\lambda$  is a material constant describing thermal heat conduction, independent of material size, shape, or orientation [10,68].

Burger *et al.* describes in their review paper the correlation between thermal energy, heat, and temperature [66]. *Thermal energy* is the vibration of particles on a microscopic level, whereas *temperature* is a physical property that specifies the amount of the thermally vibrating particles. **Conduction** is when heat flows through a solid, liquid, or gas or between several mediums that are in intimate contact. Conduction through dielectric solids (isolators) is basically due to lattice vibrations (= phonons), as the electrons of the atoms are tightly bound. These are susceptible to scattering effects that occur at interfaces. Free electrons conduct heat much more efficiently and faster than phonons and are less vulnerable to scattering effects. Metals, therefore, have a significantly higher thermal conductivity than ceramics or polymers. The heat conduction through metallic solids and carbon-based additives (carbon nanotubes (CNT), graphite, graphene) are transported by free electrons [10,61,66,69,70].

In *polymers*, the primary mechanism of conduction is based on *phonon transfer*, i.e., atoms vibrating due to induced thermal energy in the molecule direction [67]. Polymers show a low thermal conductivity due to their low atomic density. Amorphous polymers, compared to crystalline, exhibit a higher number of defects, therefore higher scattering effects, leading to even lower TC values (Figure 14). *Polymer matrices* play an important role when determining the overall thermal properties. In general, crystalline polymers (e.g., PE) show higher thermal conductivity than amorphous (e.g., PS or PI). Moreover, defects (e.g. impurities, chain ends, or entanglements) lead to a heat flow loss due to scattering [70] (Figure 14). The presence of heavy atoms or side chains can lead to higher TCs (e.g., HD-PE vs. PA and PS) [70]. Thermosets, such as Epoxy and Phenol resins, results in 0.17 – 0.4 W/mK and 0.24 – 0.29 W/mK, respectively [70].

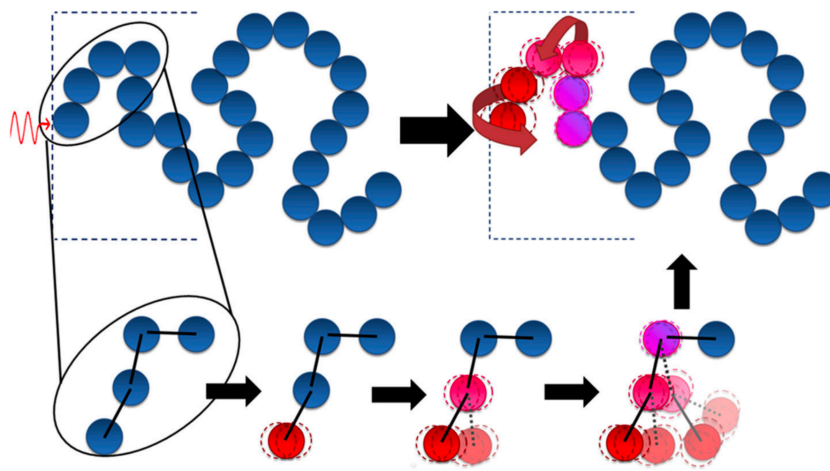


**Figure 14 Thermal transfer in (amorphous) polymers caused by phonon transfer, i.e., vibration of molecules [66].**

The thermal conduction mechanism can be described as an ideal Newtonian pendulum. The heat transfer in amorphous substances is significantly inhibited since the vibration energy cannot spread in a wave-like manner in the disordered structure of the material. The heat diffuses into the material due to the uneven vibrational states of the molecular atoms; there is phonon scattering [66]. The different vibrational states of the molecular atoms mean that the heat is transferred significantly slower, and the material heats - the *material's thermal resistance*. In polymers, the thermal resistance is strongly dependent on the molecular length

and the degree of crosslinking. Still, defects such as pores and foreign substances also increase the thermal resistance due to thermal interface resistance.

The **addition of fillers** will influence mechanical properties or inherent flame retardancy and increase the TC [67]. The acoustic and vibrational mismatch between the polymeric matrix and the fillers can lead to a high scattering degree at their interfaces. These scattering processes decrease the TC along the heat flow path (Figure 15).

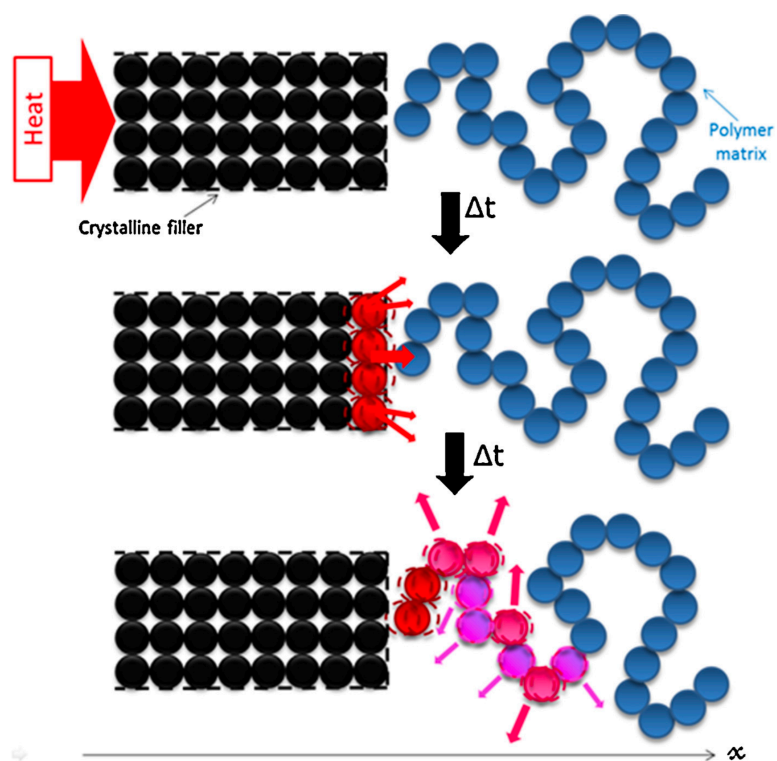


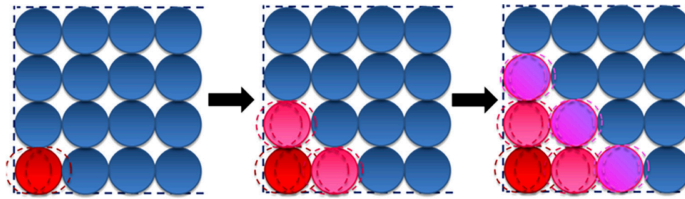
**Figure 15 Heat transfer in a filled polymer – interface between the filler and polymer is causing an acoustic mismatch, leading to scattering effects and inefficient thermal transfer [66].**

The *formation of tight, continuous filler network paths* in all three dimensions is inalienable. Therefore, the *nature of the fillers is dominating the TC*, i.e., the crystal structure and lattice. Figure 16 shows the thermal transfer in the crystalline matter. The vibrations of the crystalline lattice result in a uniform thermal transfer in the material. In a crystalline material, such as *hexagonal boron nitride (h-BN)*, thermal energy firstly reaches surface atoms, gaining vibrational energy. The thermal energy then propagates as a wave (phonon) and diffuses

through the filler. Due to its high degree of crystallinity, phonons can propagate quicker [66]. The spread of the phonon oscillation in crystalline materials depends on their intrinsic hardness, the atomic density of their crystal lattice, and the bonding forces of the atoms. It is only inhibited by defects such as grain boundaries, vacancies, or foreign atoms in the crystal lattice [66].

### Thermal conduction crystalline matter

#### a) Temperature gradient



#### b) TC mechanism

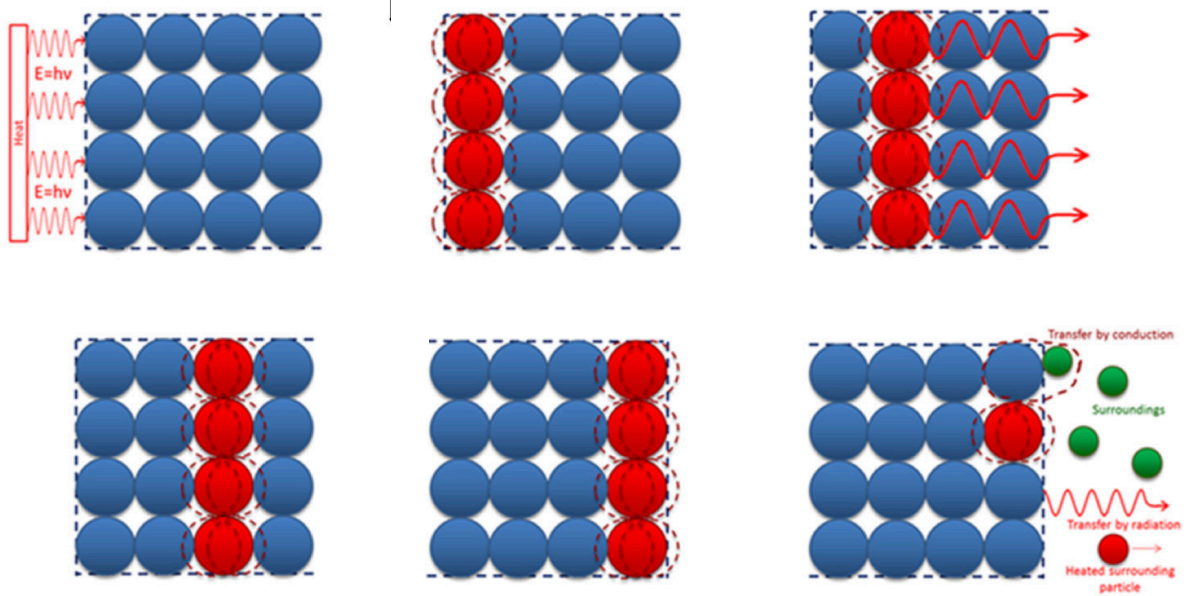


Figure 16 Schematic of the thermal transfer in the crystalline matter: a) induced by a temperature gradient and b) induced by thermal conductivity mechanism [66].

### 2.1.6 Review of the current *State-of-the-Research* – (*filled*) *Resins*

The intrinsic thermal conductivity range of neat (= unfilled) Epoxy resins is in the range of 0.19 - 0.21 W/mK [71]. In literature, it is well known that incorporating ceramic fillers (i.e., AlN, BN, or Silica) with high intrinsic thermal conductivity (TC) increases the overall Epoxy resins' thermal transport behavior [12,13]. Many composite-based studies show that the *filler size* [72–78], *geometry* [9,73,75], *concentration* [72–78], and the *fillers aspect ratio* [79] play a crucial role in the 3D network formation of the fillers to build up a continuous channel for heat passing through. Moreover, the thermal conductivity can be further enhanced by *combining of two fillers of different sizes* [9,78] and of *varying nature* [74,80]. The *filler dispersion, distribution, and alignment can affect* the overall packing density [10]. In addition, the *wettability* of fillers with the matrix is important due to chemical or polar interactions, which can result in a good interphase [10]. The matrix viscosity is dictated by the (maximum) filler volume fraction concerning processing. Also, the higher the volume content, the higher the resulting viscosity [81]. The more significant the difference between filler and polymer, the higher the need for a high viscosity avoiding *floating or sinking effects* [81] causing filler gradients. Therefore, it is primarily of scientific interest what happens during resin curing. Is the network governed by the formulation preparation (*ex-situ*) or during composite processing (*in-situ*) [81]. The interphase can also be improved by the *surface modification* of the filler [10].

High-performance composite materials provide tremendous advantages over conventional materials for electronic packaging thermal control, including extremely high thermal conductivities (more than twice that of copper), low tailorable CTEs, weight savings up to 80 %, extremely high strength and stiffness, low-cost, net-shape fabrication processes; and cost reductions as high as 65 % [10,25]. *Polymer-matrix*-based composites are increasingly used in the E&E sector. The polymeric matrix is reinforced with either filler, fibers, or fabrics. Whereas the reinforcement acts as a performance enhancer, the fillers usually improve thermal, optical, and flame-retardant properties. For the last decade, literature dealing with the increase of TC in polymers especially filled Epoxies, is of great interest. However, the filled resin processing method strongly restricts the filler(s) [81].

The research has different opinions on what causes the increase of the TC. Some conclude that a *continuous filler network* is a reason, analog to electrical conductivity, with an existing

percolation threshold. In contrast, other authors state that the *polymer-filler interaction* is essential. The mismatch between the polymeric matrix and the filler is usually responsible for scattering effects, therefore lowering efficient phonon transport [82].

### **Influence of Polymer Matrix and Filler Nature**

The *key to increasing the TC within the base material of a PCB substrate is the addition of fillers*. Many studies in the last decade show that the addition of BN, AlN, diamond, glass, ceramic fibers, or even carbon-based fillers improve the polymer's properties regarding its thermal behavior. When polymeric matrix, the heat is diffused and progressing at a much slower velocity over time compared to the filler [66] (Figure 15).

To improve the thermal conductivity of thermosets, either metallic, carbon-based, or ceramic fillers are used. Because of their *availability, oxides such as aluminum oxide ( $Al_2O_3$ ) and silicon dioxide ( $SiO_2$ ) are often used for printed circuit board materials*, which should also be electrically insulating. Ceramic fillers are thermally conductive and electrically insulating because, unlike metallic or carbon-based fillers, they have no free electrons. In particular, non-oxide ceramics such as boron nitride (BN), aluminum nitride (AlN), silicon nitride ( $Si_3N_4$ ), and silicon carbide (SiC) have high thermal conductivities because of their strong atomic bonds and high crystallinity. On the one hand, the disadvantages of these fillers are their high dielectric constant of  $\sim 9$  at 1 MHz of  $Al_2O_3$  and the moderate thermal conductivity of  $SiO_2$ , which only makes a minor contribution to the overall thermal conductivity with 1.5 – 3 W/mK [90]. Figure 17 summarizes common filler types and Epoxy resin plotted as TC with CTE.

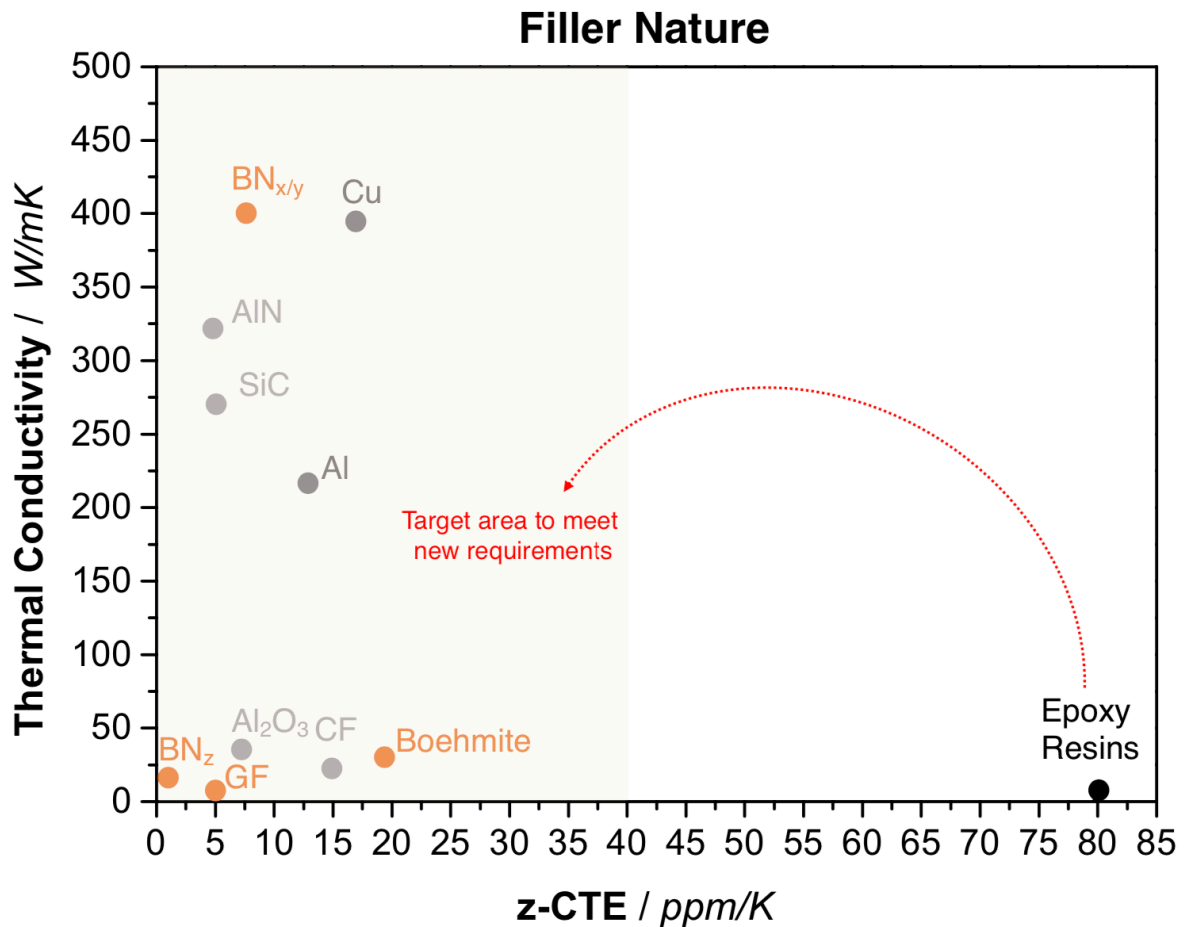


**Figure 17** Physical properties of various matrices and filler materials from literature [59,67,68,70,81,83–89].

Concluding Figure 17 above, polymers, in particular, Epoxy resins have a very low TC of  $< 0.3$  W/mK on average. In addition, metal-based fillers offer the highest TC, followed by carbon-based fillers. **Neither of both candidates is suitable for the application in PCBs, as they are electrically conductive.**

E-glass has a TC of  $0.9$  W/mK on average due to its main component, boron silicate. Inorganic, nitride-based fillers show a conductivity in the intermediate range (depending on their orientation). **Especially *h*-BN seems to be an ideal candidate to increase the overall TC.** In addition, metal oxides have a low dielectric loss at higher frequencies [90].

Currently, Silica is predominantly used due to its low CTE, good insulating properties, low cost.

Aluminum-based fillers are currently trending. Up to date, reported TC values are usually below 5 W/mK. Higher values usually only can be attained with very high loadings and pressing techniques, where the resin is used as a binder rather than a predominant matrix. However, the costs are higher due to the filler amount used, processing techniques are not relevant for industrial applications. Since carbon- and metal-based fillers cannot be used in these applications, non-oxide, inorganic fillers are preferred (*h*-BN or Silica). Al<sub>2</sub>O<sub>3</sub> or SiC are higher in their hardness compared to BN. BN is a filler of softer nature, which can easily be deformed, leading to a higher packing density and also to a higher thermal conductivity [91].

Hill *et al.* studied the effect of different platelet-shaped fillers with different intrinsic thermal conductivities and found a correlation between the TC and the inherent filler *hardness* and *filled resin densities*. With a concentration of 50 vol.% Al<sub>2</sub>O<sub>3</sub> in the Epoxy Novolac matrix, a TC of 3.5 W/mK was achieved. According to the microstructure (Figure 18), at this concentration, the fillers show a *strong alignment* in the 2D- direction of measurement, which causes the increase in TC. TC measurements perpendicular to it resulted in much lower TC.

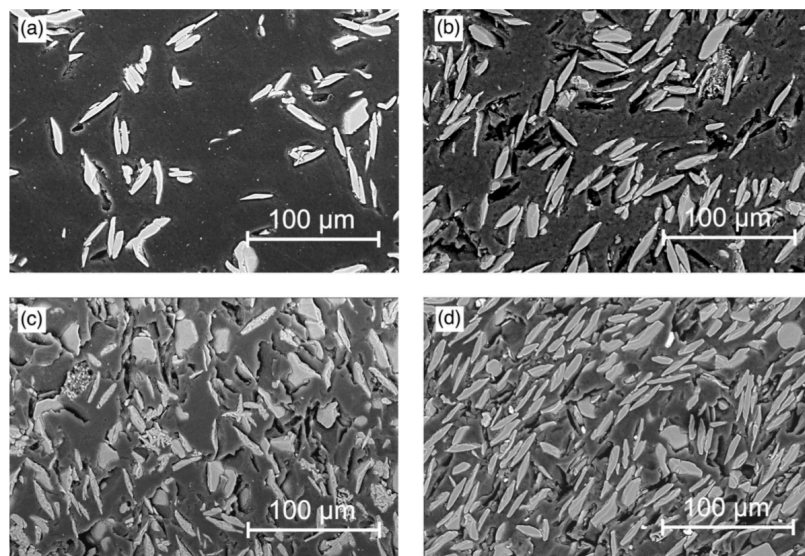


**Figure 18** SEM micrographs of the cross-sections of Al<sub>2</sub>O<sub>3</sub>-filled composites. a) 10 vol.%, b) 22 vol.%, c) 40 vol.% and d) 50 vol.%. With increasing content, the platelet fillers show a preferred alignment in the measurement direction [91].

According to the findings above, it seems that BN is a promising filler candidate to increase TC efficiently. Therefore, the focus of the following chapters will be laid on this filler.

BN currently in trend as it is known for its exceptional thermal resistance, low density, and favorable processing influence (i.e., viscosity additive). The main advantage of BN is its soft nature. Therefore a higher packing density can be reached at lower contents contributing with its larger surface area in a better contact to the matrix [92]. BN was first synthesized from boric acid and potassium cyanide, though in 1842, W.H. Balmain devised a method using  $\text{NH}_3$  or Melamine [88]. The crystalline structure of hexagonal boron nitride (*h*-BN) can be seen in Figure 19 and is similar to the structure of graphite, with alternatively linked boron and nitrogen atoms ((BN)<sub>3</sub>-rings) [87,88,93]. The hetero-B-N bond is partially ionic. Compared to a covalent C-C bond, the  $\sigma$ -bonds localize the electrons closer to the N, whereas in the  $\sigma$ -bond the electrons of the nitrogen are less delocalized than the  $\pi$ -electrons in the C-C link. The electrons can move freely, hence the electrical conductivity of graphite. The differences in properties (optical, electrical, and chemical) compared to graphite are based on this phenomenon [87,88]. *Hexagonal BN (h*-BN) has a smooth surface with no functional groups available for chemical bonding. However, at the edge of each plane, there are hydroxyl (-OH) and amino groups (-NR<sub>3</sub>) available for chemical linkages [82]. Mechanical reinforcement and lubricious properties arise from its intralayer  $\sigma$ -bonds and interlayer weak van der Waals forces [87]. The non-toxic BN offers electrical insulation, a wide band gap, superior thermal (up to 3000 °C), and chemical resistance [87,94]. Ishida [95,96] published a patent, using 80 vol% of *h*-BN flakes with a D<sub>50</sub> of 225  $\mu\text{m}$  in a polybenzoxazine matrix, a TC value of 37 W/mK was achieved. Rheological, mechanical, or fire-retardant aspects were not part of the study.

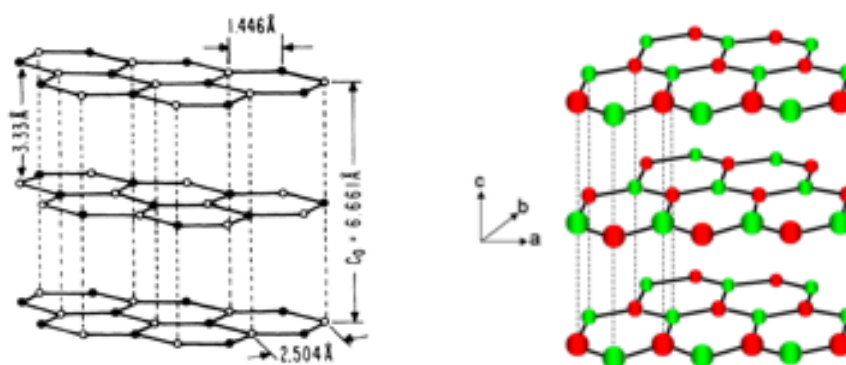


Figure 19 Crystalline structure of hexagonal BN with N and B atoms in A-B crystal plane [59].

The intrinsic filler TC is critical, which is mainly governed by its perfect lattice or crystal structure. However, fillers with different natures also have other scattering effects at the interface of different phases [66,89].

### **Influence of Filler *Geometry, Concentration, and Microstructure***

In addition to the intrinsic properties of the fillers, the *structure and shape* of the filler particles also can influence the thermal conductivity. Many studies on filled resins show that the **filler size and aspect ratio**, their **geometry**, and the total **filler content** play a crucial role in the 3D network formation [9,72–79].

Filled resin systems can have two configurations: *random* and *segregated* [81]. The random state is governed by the percolation effect, whereas the network arrangement governs the segregated state. In the case of *high filler contents* > 20 vol.%, the literature describes a *heat conduction path* as the fillers are lined up in the matrix and close to one another.

Figure 20 shows the change in properties in dependency of the filler content, with a higher loading, the higher the TC but also the costs. The elongation at break and the ease of processing decreases directly proportional to it. Whereas the strength decreases above a critical filler content.

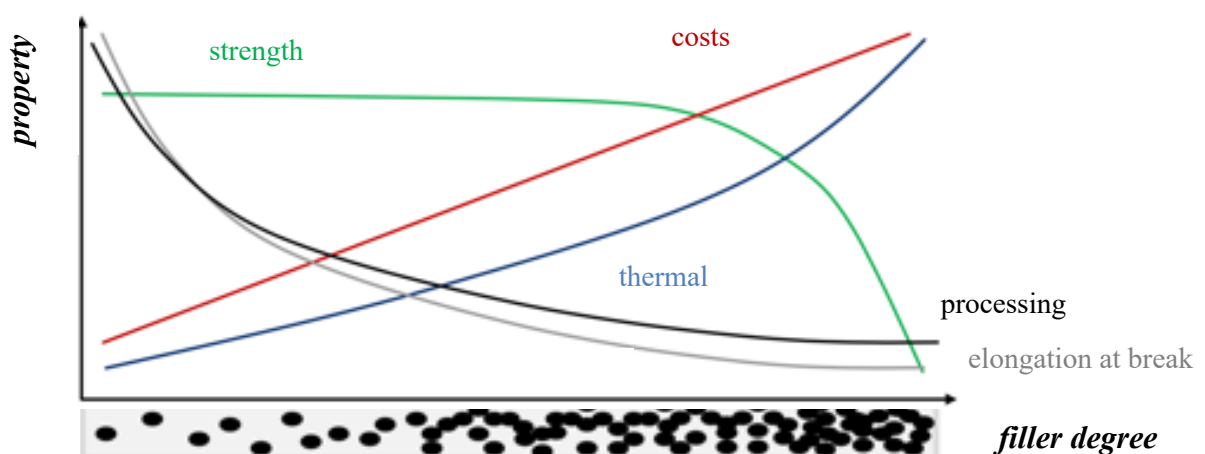


**Figure 20** Change in properties of a filled resin by adding electrically and thermally conductive fillers with a higher modulus of elasticity than the matrix material [68,97,98].

The effect of *particle size* of BN on the thermal conductivity of filled Epoxy also draws much attention [72,73,75–78,99]. The **common understanding is that the larger particle size provides higher thermal conductivity for the same type of filler at the same loading level.** Heat transfer in most polymers is driven by the flow of phonons or lattice vibrational energy. Various phonon scattering processes such as *phonon–phonon scattering*, boundary scattering, and defect or impurity scattering are the source of thermal resistance [77]. Therefore, the larger BN helps to decrease the interfacial area between fillers and polymer matrix, leading to the improvement of thermal conductivity of filled Epoxy resin by reducing the interfacial phonon scattering.

The *particle size* also has a significant impact on the thermal conductivity of fillers. The *particle size* also affects the dispersion properties - smaller particles result in a higher viscosity. Smaller particles (*nano-particles*) have a higher thermal resistance than large ones because they have a higher relative surface area, where interface effects can occur [82,100]. The *Kusy model* describes the critical volume fraction and particle size ratio: segregated for large particle size ratios, random for small particle size ratios [81]. According to literature, there are controversial studies in particular the *nm vs. μm* filler size [70,101]. In most cases, *μm*-size fillers perform better [66], *nm*-size can only reach high TC values when a controlled aggregation of the fillers can be achieved. Therefore, a small number of larger fillers is more favorable than a larger number of smaller fillers [89]. The concentration is especially important in terms of processing. High loadings increase the viscosity and the risk of void formation tremendously. A good filler dispersion is hindered and can create a barrier [66]. In Zhu's *et al.* research [78], a filler loading of 21.7 vol.% lead to a thermal conductivity of 1.2 W/mK and 0.7 W/mK by using micro-sized BN particles (7 μm) and nano-sized BN particles (70 nm), respectively. However, large BN particles have less edge plane areas than small particles, which may result in difficulties in obtaining uniform dispersion and chemical bonding of BN-Epoxy [99]. Kim *et al.* [99] achieved thermal conductivity of 2.92 W/mK with 12 μm BN particles and 2.15 W/mK with 1 μm BN particles at a filler content of 70 wt.%.

The *aspect ratio* (AR) of fillers plays a vital role and results from the ratio of the surface to the volume or the length to the thickness of the particle. With the same composition, fibers and rod-like fillers have a higher aspect ratio leading to a low-inter-filler distance at a lower

concentration [102]. Spherical particles have the lowest thermal conductivity and, at the same time increase, the viscosity to a higher degree due to their high surface area [70]. High AR particles are favorable for network formation, as explained in Figure 21 [103]. Higher aspect ratio fillers perform better as their inter-particle spacing is lower at low concentrations [81]. Burger *et al.* demonstrate that small, spherical-shaped fillers have more boundaries which cause more scattering effect and therefore induce a loss in heat transfer. Long fibrous or platelet fillers, even in lower concentrations, have a higher ability for filler-filler-interaction (Figure 21).

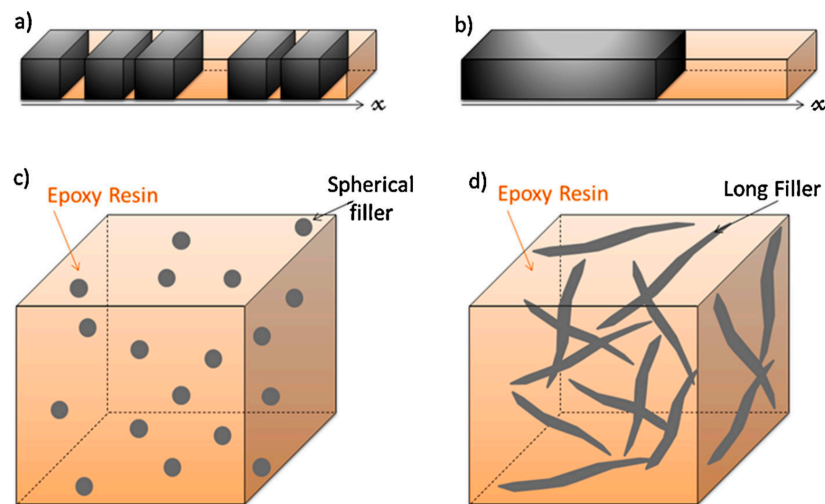


**Figure 21** Schematic of difference in filler geometry and its impact on thermal conductivity. a) spherical filler and b) fibrous filler [66].

Kochetov *et al.* state that BN with a *platelet* geometry has a higher potential to increase the thermal conductivity than a *spherical* shaped BN. In particular, the filler distance of the platelets is much smaller as their aspect ratio is much higher, and therefore, the heat flow is enhanced (Figure 22) [104].

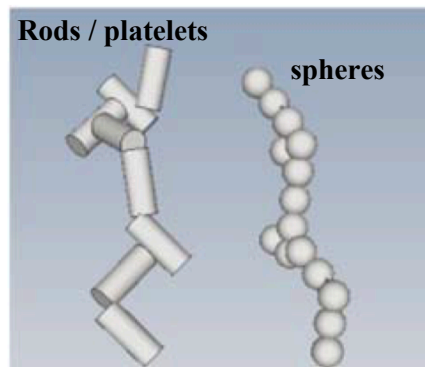


**Figure 22 Influence of filler aspect ratio on the effective formation of thermally conductive paths [105].**

In addition, Kochetov [76] illustrated that an Epoxy resin filled with smaller particle size (0.5  $\mu\text{m}$ ) of BN has a higher thermal conductivity compared to larger (5  $\mu\text{m}$ ) BN particles because the larger one has a spherical shape and the smaller ones are in the shape of platelets. Below 50 vol.%, a particle network is formed; above 50 vol.%, a pathway is formed [81]. In general, adding a filler to the matrix instantly decreases the overall CTE [81].

Kim *et al.* [9], Huang *et al.* [73], Gaska *et al.* [75], and some other groups [76,78] demonstrated that enhancement of thermal conductivity of filled Epoxy resins depends strongly on the *geometry* of BN fillers.

*Platelet*-shaped particles are strongly anisotropic and tend to orientate in a specific direction and considerably decrease the thermal conductivity if measured perpendicularly to that plane. Therefore, parameters such as mixing and curing must be considered to obtain a uniform dispersion and optimal thermal pathway [79].

Hill *et al.* reported that the orientation along the *x*-direction increases for platelet-shaped particles with increasing filler content. These platelet shape particles tend to orientate in parallel due to their crystal structure during processing [106]. *Orientation* of the fillers is influenced by the processing, i.e., extrusion, injection molding, or thermoset-based impregnation techniques [70]. Some research “forces” a particle alignment with the help of an external field or by pressing methods. The TC in this particular direction is increased [70]. *Elliptical* particles show behavior in a fluid flow similar to fibers and platelets, but fibers have one preferred axes, whereas platelets have two preferred axes [98,107]. In constant fluid flow, platelets constantly rotate [98]. The higher the AR of the filler platelets, the more the elliptical particles stay parallel to the actual shear flow. In diluted systems, the distance between the particles is high, with no interaction. In higher concentrated systems, the probability of contact is given. The higher the

AR of fibers, the higher their propability to interact. The transition happens in a lower concentration area. For ellipticals, it is valid in lower concentrations since the transition is depending on their AR. The transition at higher concentrations is influenced by the filler loading.

*Chen et al.* established a model for critical, distinct angles for platelet fillers [108]. They described h-BN and the matrix as a unit cell (two-coordinate system with x/y-coordinates with:  $0^\circ$  as *perpendicular* (factor of 1) to measurements direction and tilted as  $45^\circ$  which results in a factor of 0.5,  $90^\circ$  parallel orientation. The orientation is directly correlated to the filler-filler-interaction; the higher the concentration, the more likely is the interaction, and therefore, the platelets can rotate around their axis.

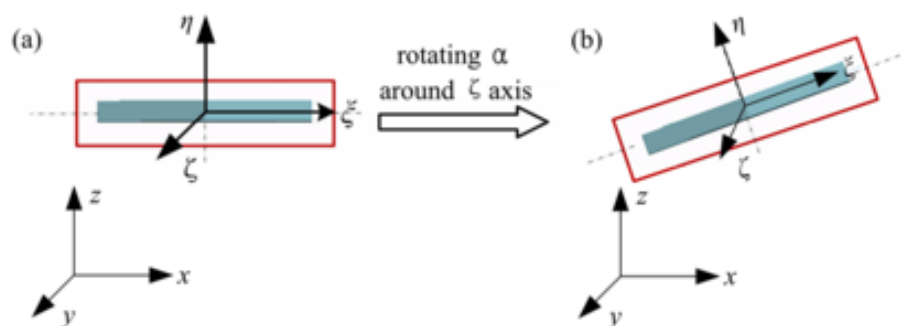


**Figure 23** Schematic to describe the orientation and rotation of h-BN platelets [108].

With *h*-BN having an oval/elliptical, platelet-shape, the thermal heat spreading is, therefore, more prominent in the planar level (300-600 W/mK), whereas in the perpendicular level, the TC is as low as 2-30 W/mK [68]. *In-plane*, the heat is transferred via lattice vibrations of the crystal structure, while scattering effects occur in the *z*-direction. A study by Yu *et al.* shows that with the forced alignment through applied vacuum-filtration of platelet BN, the TC reaches values up to 9 W/mK with a 44 wt.% loading in-plane [109]. However, this procedure involves additional processing steps increasing the cycle time, and only a 2D-heat transfer is resulting, whereas the targeted application of PCBs requires a 3D heat spread.

The research of Donnay *et al.* [72] had shown that overall **filler weight percentage** had the most substantial effect on thermal conductivity compared to other studied factors. The addition of BN filler effectively increased the thermal conductivity of neat resin. An increase of up to 275%

with 20 wt% nano-BN was achieved. Even when the filler morphology appears as BN nanosheets (BNNS), the same trend is presented in [74].

Isarn *et al.* studied the effect of BN related to *size* and *concentration*. They found a linear increase in TC with a maximum reached 0.97 W/mK by using 40 wt.% of 6  $\mu\text{m}$  BN, whereas the addition of 80  $\mu\text{m}$  BN led to 1.75 W/mK [82].

Tsekmes *et al.* showed that at a *filler concentration below 20 vol.%, the thermal conductivity of the matrix is still more dominant*. In addition, the authors demonstrated that a *surface modification* of fillers is only prevalent with decreasing filler size in *nm*-range rather than affecting the thermal conductivity in  *$\mu\text{m}$* -range [105].

Figure 24 summarizes *h*-BN incorporated in various polymer matrices, and the resulting TC values based on multiple effects, i.e., surface functionalization, concentration increase, or even increased particle size.

Concluding the *State of Art* regarding ***filler nature, content, geometry, and morphology***, firstly, the intrinsic TC plays a crucial role (= filler nature). One-dimensional fillers increase TC (fibers, rods, whiskers, platelets) with increasing AR [70]. Platelets with a high AR have a low percolation threshold, and their thickness creates a 2-D TC and leads to anisotropy. According to the figure below (Figure 24), the optimum filler degree is between 15 to 20 vol.%. However, the studies show that only platelet sizes in the smaller filler size (nm or < 5  $\mu\text{m}$ ) or larger size range (> 80  $\mu\text{m}$ ) were studied. Both filler sizes would not be applicable for the processing of prepregs. Larger platelets would migrate into the GF fabric and will break. Filler sizes below 5  $\mu\text{m}$  or in the nm range would cause a tremendous increase in viscosity due to their higher surface area. Surface functionalization only has a minimal effect on the increase of the TC.

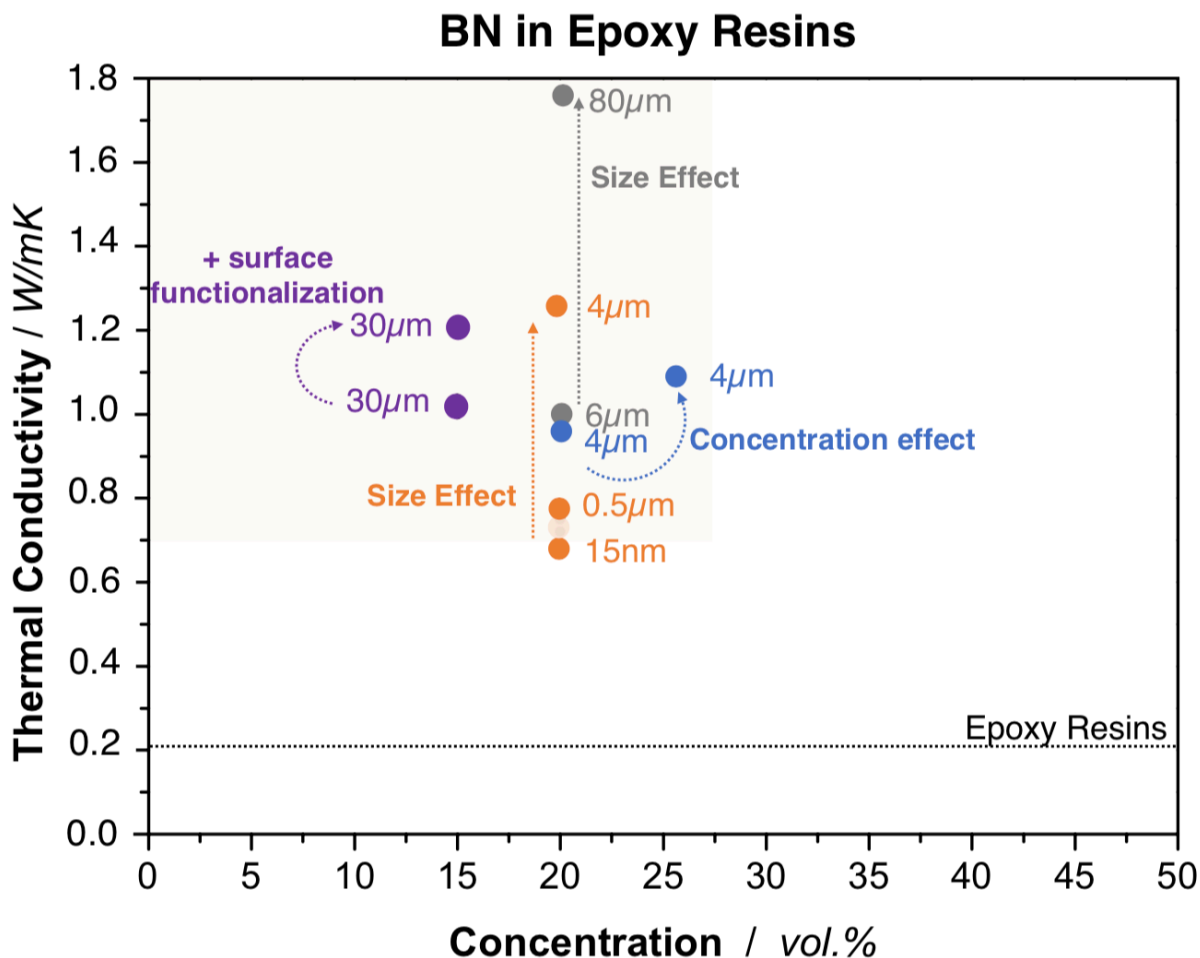


Figure 24 Overview of the effect of concentration and BN filler size in Epoxy (Novolac) resins [77,82,94,95,110–114].

### Relevance of Filler Combinations – *Bimodal and Hybrid Mixtures*

Recent research work focuses on optimizing *the packing density* and *lowering the percolation threshold* by using two or more fillers [66,70,89]. Figure 25 summarizes literature findings on fillers combinations with BN.

Usually, combining two fillers of the same nature leads to *bimodal* filler size (distribution) differing in filler size, i.e., AR [9,78]. *Hybrid* combinations include using two fillers of different chemical nature or size [74,115]. With these binary filler distributions, one or more functionalities are often simultaneously introduced and combined (= *synergism*). Mixing two

different filler sizes leads to a filler network formation and improves the thermal bridging [81]. Creating a high interface density within a nanolaminate material has produced a very effective barrier to heat transfer and a material with a thermal conductivity three times smaller than a conventional insulator. The heat flow is limited at the interface as the differences in lattice vibrations between the materials restrict the transfer of energy across the interface [10]. Packing density decreases proportionally with increasing AR. Packing densities with bimodal distribution have packing coefficients of up to 84 % and trimodal of up to 88 % [88].

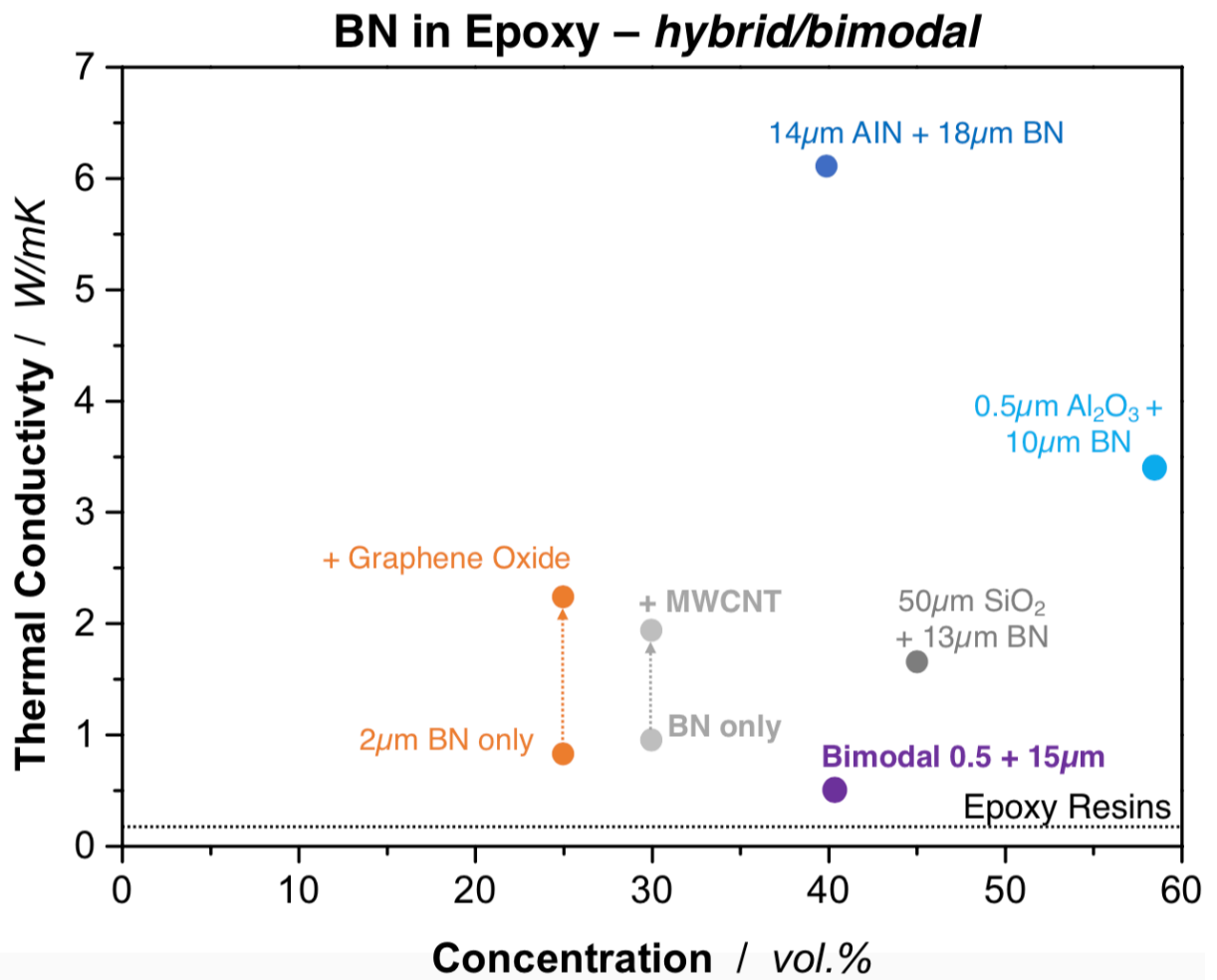


Figure 25 Summary of published work on bimodal and hybrid filler combinations focusing on the use of *h*-BN in Epoxy matrices [115–119].

### ***Bimodal combinations***

According to Zhu *et al.* [78], at the same filler loading of 21.7 vol.%, the thermal conductivity of Epoxy filled with 70 nm BN, 7  $\mu\text{m}$  BN, 70 nm + 7  $\mu\text{m}$  BN are 0.7 W/mK, 1.2 W/mK, 1.39 W/mK, respectively (Figure 26 a)). Epoxy resin filled with bimodal BN combination led highest thermal conductivity. The authors suggest that the nano-BN fillers may fill into the voids in the packed structure generated from micro-sized BN particles. This exhibits the higher packing density, and good conductive pathways inside the matrix when mixed fillers are used. This is also shown in the SEM micrographs in Figure 26 b).

#### **a) TC results as function of filler content**

#### **b) corresponding microstructure**

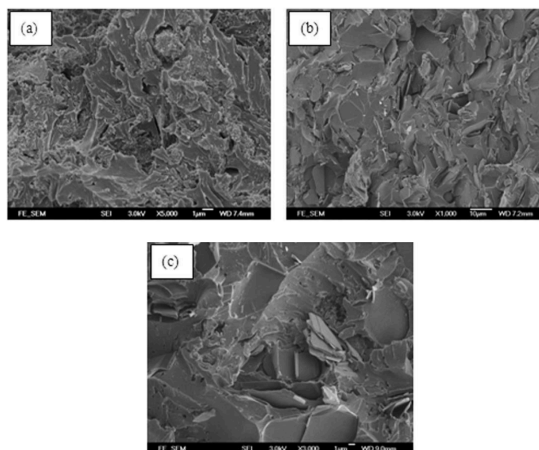
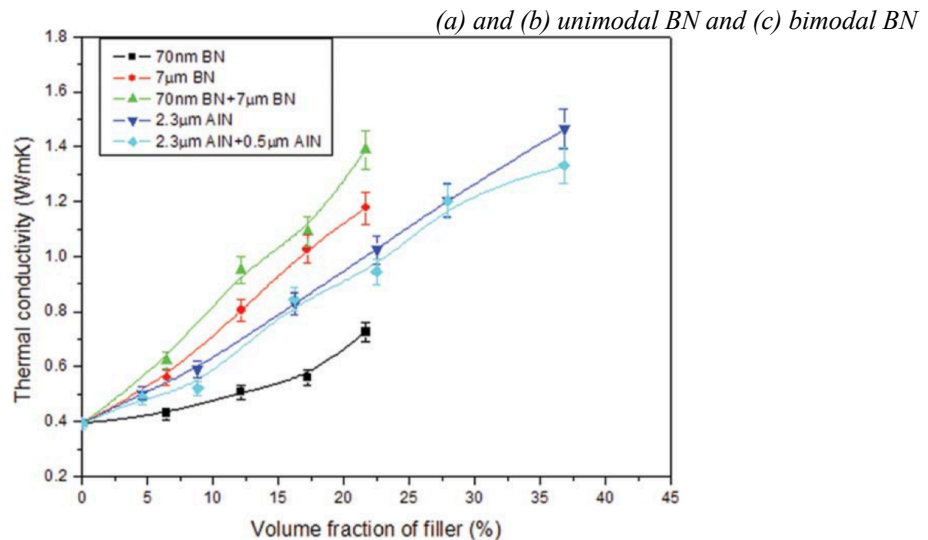


**Figure 26 a) Thermal conductivity of bimodal BN-filled composites in dependency of concentration and b) morphology of hybrid combinations in the corresponding SEM micrographs [78].**

### ***Hybrid Combinations***

The combination of BN with two or more fillers in a polybenzoxazine matrix, mainly ceramic fillers (Silica, Al<sub>2</sub>O<sub>3</sub>, AlN) to reduce the overall costs, is described in Ishida's patent [120]. In addition, Hong *et al.* [115] explored Epoxy resin filled with high thermal conductivity fillers of aluminum nitride (AlN) and boron nitride (BN). The *effect of the particle size* and the *relative composition* on the thermal conductivity of composites were identified. They achieved the highest thermal conductivity of 8 W/mK when the volume ratio of AlN : BN is 1:1, and their particle size is nearly the same. They demonstrated with their experimental methodology that enhancement of thermal conductivity needs two factors. One is the two different particles should be packed well to fill up the interstitial space. The other one is the contact resistance, and the contact area of the fillers should also be optimized. Three different cases were used in the research, which is case 1 ( $D_{\text{AlN}} > D_{\text{BN}}$ ), case 2 ( $D_{\text{AlN}} \approx D_{\text{BN}}$ ), and case 3 ( $D_{\text{AlN}} < D_{\text{BN}}$ ). The result of thermal conductivity is shown in Figure 27.

Platelet fillers generate a higher packing density compared to whiskers or (short) fibers. Higher volume contents can be achieved, resulting in even lower CTEs or TCs [81]. However, with these volume fractions, the ductility and the fatigue behavior are impaired [81].

Fu *et al.* studied the combination of  $\mu\text{m}$ -sized BN (0.5  $\mu\text{m}$ ) with nm-sized Al<sub>2</sub>O<sub>3</sub> (range of 20 nm up to 500 nm) in Epoxy adhesives. They found a synergy at a concentration of 40 wt% in a ratio of 1:3 (smaller Al<sub>2</sub>O<sub>3</sub> with the  $\mu\text{m}$ -sized BN) for all properties studies, i.e., thermal conductivity, electrical insulation, and mechanical strength [121]. Figure 28 shows the corresponding SEM micrographs. The authors explain that the larger BN fillers form a network due to their inter-filler contact, whereas the smaller particles fill the gaps.

Hong *et al.* evaluated BN-containing polymer composites and the effect of adding metal, BN, and AlN particles (1:6:6 ratio) to a DGEBA matrix. They reached a TC value of approximately 10 W/mK [122].

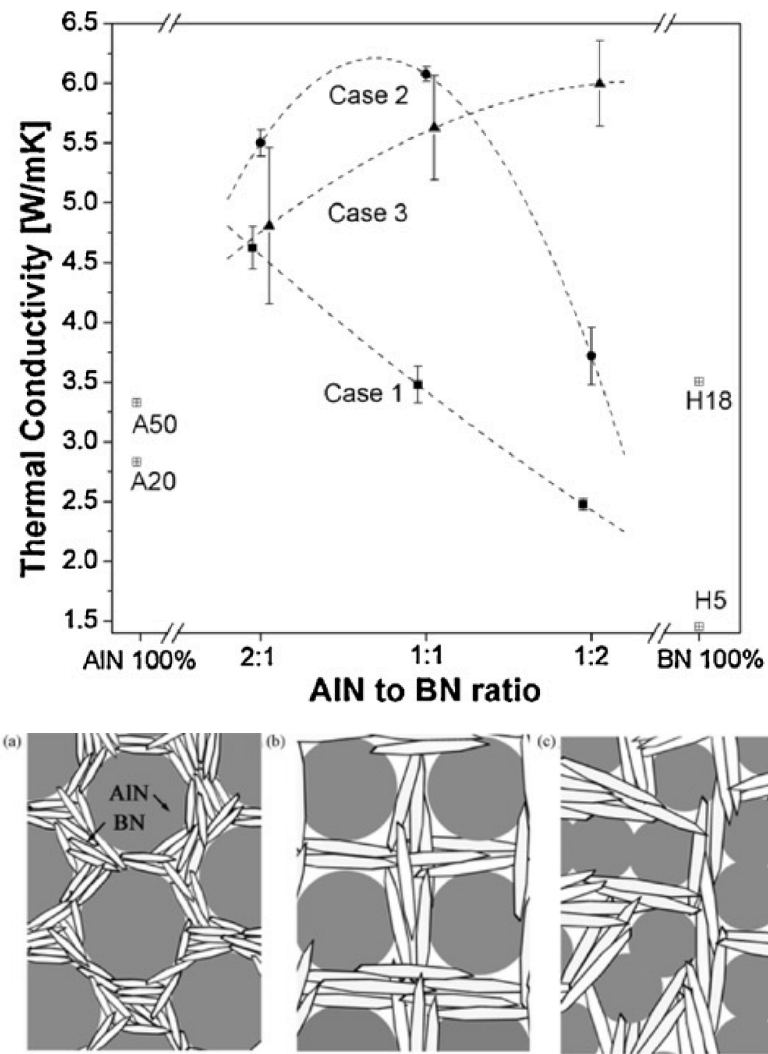
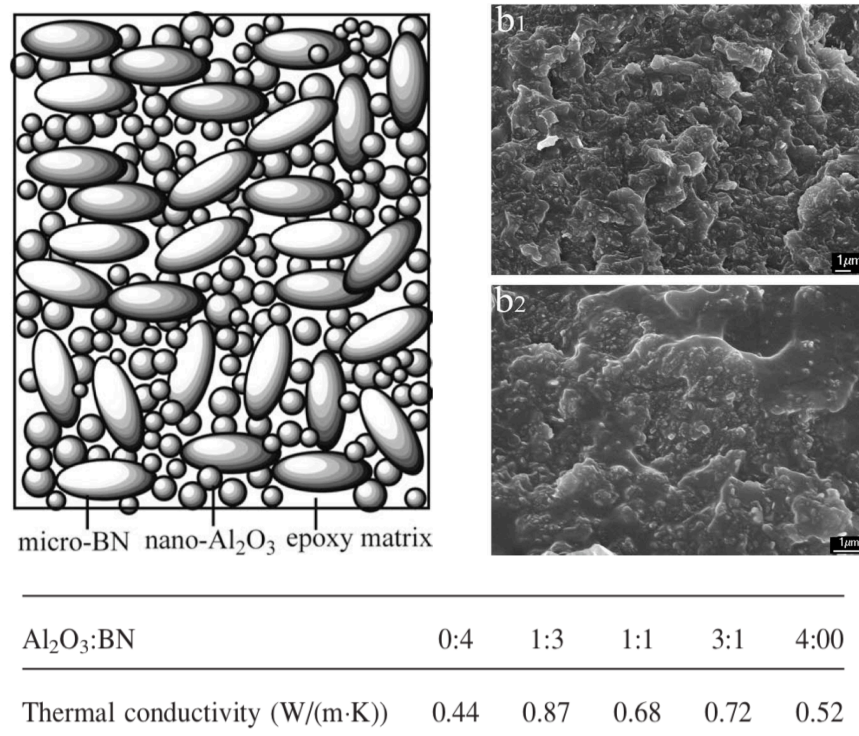


Figure 27 Thermal conductivity and schematic of the morphology schematic of the filler combination between AlN and BN in dependency of their ratios [115].



**Figure 28** Hybrid combination of nano-Al<sub>2</sub>O<sub>3</sub> with micro-*h*-BN in various ratios. Schematic of the filler network, corresponding SEM micrographs, and TC results [121].

To summarize the findings in the literature (Figure 25), the bimodal combination of two BN sizes must not necessarily be the most efficient. Hybrid combinations can be more efficient and can lead to higher TC values. The combination of carbon-based (MWCNT or graphene) with *h*-BN shows lower TC values than combining BN with another inorganic filler. The ratio between two fillers also plays a crucial role. BN in a higher composition with an oxide filler seems to be the most effective but can have a negative impact on the price.

### **Influence of Glassfibers - *Thermal Conductivity in Laminates***

The incorporation of glass-fibers or a glass-fabric (GF) is necessary to give structural stability and bending strength in PCBs needed during operation. The intrinsic TC of the E-glass is 0.9 - 1.35 W/mK, according to the literature [123]. The incorporation of E-glass with Epoxy as FR-4 resulted in a TC value of 0.3 - 0.4 W/mK, according to Vasoya *et al.* [60].

With the fiber incorporation, the particles' filtration and/or aggregation during processing is possible due to the tight mesh and the overlapping strand that form small gaps (intra-tow region) between the 0/90° - GF tows. The incorporation of GF into filled resins can lead to a lower z-plane heat transport due to the barrier effect of the fibers. However, very few studies exist on the relevance of processing, filtration effects, and the overall laminates' properties [15,16,124]. Only very few studies on thermal conductivity in filled resins reinforced with fibers.

Devendra *et al.* studied the effect of incorporating thermally conductive fillers in glass-fiber reinforced (GFRP) laminates produced with the hand-lay-up technique. The authors observed that 10 vol.% of SiC particles the TC of the laminates from 2.89 W/mK up to 3.51 W/mK. They suggested the formation of a conductive pathway, which contributed to enhanced heat transfer [15]. However, the authors did not study the overall resulting microstructure.

Fan *et al.* incorporated 1  $\mu\text{m}$ , BN into a carbon-fiber-reinforced (CFRP) bisphenol-F Epoxy resin. At 20 vol.% of 1  $\mu\text{m}$  BN leads to a thermal conductivity of 7.9 W/mK (no reference value given for 0 % of BN, also unknown fiber areal weight). A proper morphological qualitative study that elaborates the structure-property relationship is missing [16]. SEM micrographs are shown below. The authors also claim that there is only a weak bonding between the smooth BN filler surface and the fibers.

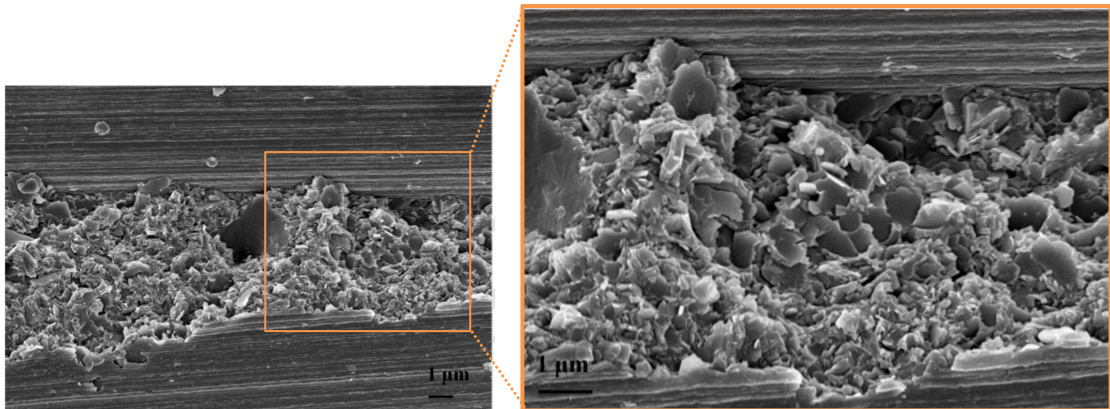


**Figure 29 Morphology of 1  $\mu\text{m}$  BN (20 vol.%) incorporated into a carbon-fiber reinforced laminate [16].**

Suchitra *et al.* [125] studied ATH (2.6  $\mu\text{m}$ , 5wt.%),  $\text{SiO}_2$  (12 nm, 2 wt.%), and  $\text{Al}_2\text{O}_3$  (12 nm, 3wt.%) in Epoxy (DGEBA) glass-fiber reinforced (FVC: 75 wt.%) produced via pultrusion. Overall, all filler types increase the TC and thermal stability. The thermal conductivity of the unfilled laminate was 0.28 W/mK. The hybrid combination with all three fillers reached a TC value of 0.43 W/mK. The authors did not correlate the TC results with the microstructure to explain the thermal pathway.

Ge *et al.* [126] introduced *h*-BN (15 – 30  $\mu\text{m}$ , irregular shape) into a Polyphenylene ether resin used to produce copper-clad laminates via the prepreg direct impregnation route. The BN filler was studied as is and coated with  $\text{SiO}_2$ . The  $\text{SiO}_2$  particles only can adhere to the BN edges. The thermal conductivity increased from ca. 0.3 W/mK to 1.08 W/mK at 48 wt.% filler content (Figure 30). The authors suggest that at > 40 wt.%, a continuous filler network is formed, which helps to increase the TC. However, the  $\text{SiO}_2$ -surface coated BN did not lead to the same TC increase as the uncoated filler, as the  $\text{SiO}_2$  only adhere to the BN filler edges. They propose barrier effects and the formation of pores within the laminate to be the reason for the lower TC results.

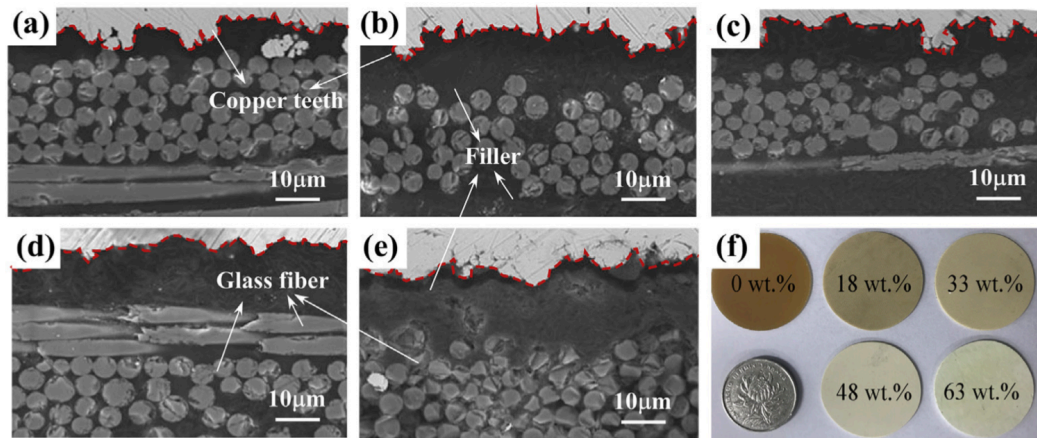


**Figure 30** Thermal conductivity results of BN-filled GF laminates with and without SiO<sub>2</sub> surface coating and their corresponding microstructure with increasing filler content [126].

### Theoretical Modelling of the Thermal Conductivity

The intrinsic thermal conductivities of the components of a composite material limit their theoretically achievable thermal conductivity. There are various analytical models for predicting the thermal conductivity of filled resins. The simplest model is the *rule of mixture* - also called *parallel model* - in which an isotropic, perfectly mixed material without interface effects is assumed. The influence of the filler geometry is also neglected in this model, which leads to an overestimation of the thermal conductivity if discontinuous fillers (particles) are used. However, this model is relevant (Chen *et al.* [70]). The thermal conductivity of a composite material made of resin matrix (M), glass fibers (GF), and thermally conductive filler (F) can therefore be calculated using the following equation (2) if the effective thermal conductivity of the filler in the composite (without fibers)  $\lambda_{F,eff}$  was determined.

$$\lambda = \varphi_M * \lambda_M + \varphi_{GF} * \lambda_{GF} + \varphi_F * \lambda_{F,eff} \quad \text{Equation 2}$$

Due to their high aspect ratio, thermally conductive fibers or platelets achieve higher thermal conductivities in the composite compared to spheres or irregularly shaped particles at the same filler proportion. However, the maximum expected increase in thermal conductivity due to the addition of fillers is limited to a factor of 100 of the matrix thermal conductivity (efficiency

threshold) for a filler content below 60 vol.%. In electrical conductivity, there is no percolation threshold for the heat transfer [127]. According to the Nielsen's prediction, the potential of a highly thermally conductive filler can only be used efficiently at very high filler contents [89]. The Nielsen model relates to the increase in the thermal conductivity of a composite material by adding fillers and is plotted as the ratio of filled matrix  $\lambda$  to unfilled matrix  $\lambda_m$  over the filler content. Figure 31 below shows the Nielsen forecast for different percentages of the thermal conductivities of filler particles  $\lambda_p$  to  $\lambda_m$ .

The comparison of the dark blue and purple curve in Figure 31 shows that from a ratio  $\lambda_p/\lambda_m = 100$ , there is no additional increase in thermal conductivity due to the increase in the filler content up to 60 vol.%. According to the Nielsen model, the limitation of the effective thermal conductivity is referred to below as the *efficiency rule*.

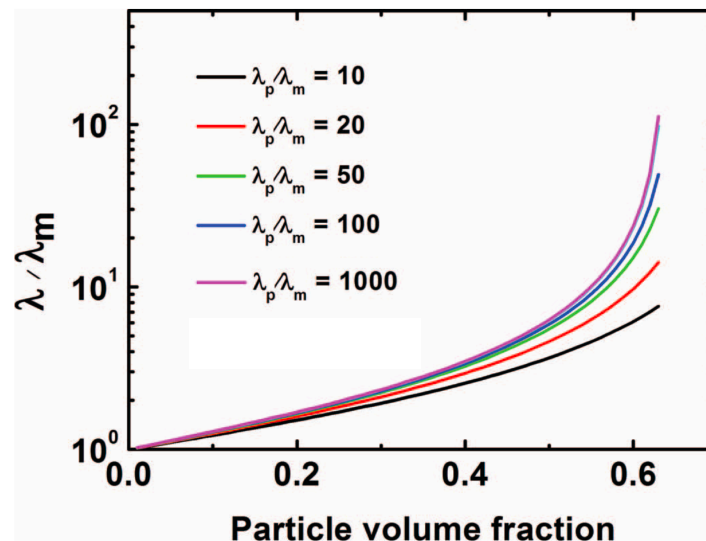


Figure 31 Nielsen's prediction of the TC of composites in dependency on content (adapted from [89]).

*Hatta-Taya* published in 1986 an explicit theoretical model based on a bi-component system, i.e., matrix and filler, where the matrix defines the fundamental property (TC of the matrix). This model calculates the TC based on filler volume and geometry, especially platelet or elliptical shaped fillers with an aspect ratio are included in this model [68,98,128–131].

$$\lambda_c = \lambda_m + \frac{\phi \lambda_m}{S_i \cdot (1-\phi) + \frac{\lambda_m}{(\lambda_f - \lambda_m)}} \quad \text{Equation 3}$$

$S_i$  describes the filler geometry. For anisotropic fillers, the following equations are valid [98]:

*for x/y-plane of the TC*

$$S_{x/y} = \frac{\pi a_z}{4 a_x} \quad \text{Equation 4}$$

*for z-plane of the TC*

$$S_z = \frac{\pi a_z}{2 a_x} \quad \text{Equation 5}$$

with  $a_x$  the diameter of the platelet, and  $a_z$  the thickness.

Soga *et al.* [131] published thermal conductivity studies with elliptical  $\text{Al}_2\text{O}_3$  fillers ( $D_{50}$  of  $6 \mu\text{m}$ ) focusing on their orientation. Platelet fillers are two-dimensional but can have a three-dimensional orientation in the matrix, i.e., *in-plane* and *out-of-plane* or even a shift of  $45^\circ$  [132] (Figure 32).

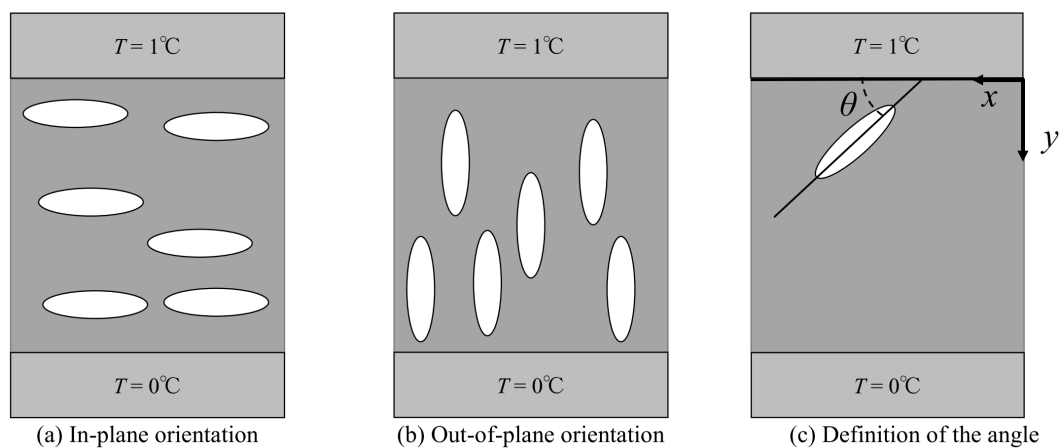


**Figure 32** Theoretical orientation states of platelet/ elliptical fillers in a two-phase system: a) in-plane, b) out of plane, and c)  $45^\circ$  shift [131,132].

Soga states that low *aspect ratio* (AR) fillers give a high TC in *in-plane*, whereas high AR fillers result in high TC in *out-of-plane* direction [131]. With a low AR, the average filler distance is much smaller than with high AR fillers. **A higher number of low AR fillers in a two-phase system increases the heat flux.** They showed that the Hatta-Taya model is in good alignment with their results, especially at lower conductivities ( $< 10$  W/mK). At higher TCs, the models approach a plateau (Figure 33).

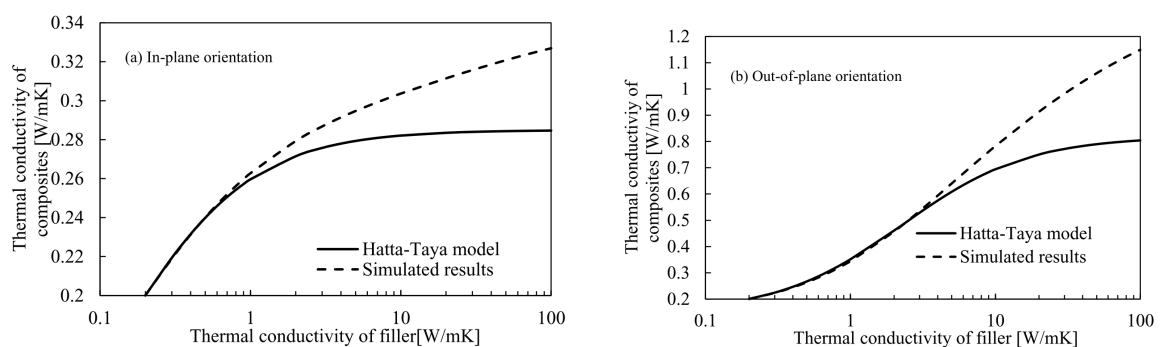


**Figure 33 Thermal conductivity of a filled resin in dependency on intrinsic filler conductivity and its orientation [131].**

In conclusion, the higher the filler concentration, the higher the TC increase. *The increase in TC is non-linear.* The fillers may have to interact to form continuous paths [10]. According to literature, *Hatta-Taya* delivers the most exact modeling for elliptical particles and high filler degrees as orientation and geometry are considered. The major disadvantage is the overestimation of the TC values compared to predicted TC as the model does not consider the interaction between fillers [131].

### 2.1.7 Overall Conclusion of the State of Research

Summary of the findings in the previous chapters [66,70]:

- **Concentration:** TC depends on the chosen two-phase system consisting of the *low conductive matrix* and intrinsic filler and intrinsic conductivity. Filled resins show higher values in TC since the microstructure/percolating path dominates [133], especially at concentrations  $> 15$  vol.%. At lower filler loadings, the matrix is predominating as being a thermal barrier. A specific *concentration threshold* of fillers is needed to increase the TC. High loadings are easier achievable and processible with “softer” fillers [91].
- **Filler Morphology and Size:** geometry and AR, and the interfacial area play an essential role in efficient heat transfer. In literature, *fibers or platelets are known to perform better than spheres*. However, there are very inconsistent findings in the literature about the filler size effect. Therefore, each study is to be treated as a case-by-case study or a proof of concept, as literature findings are strongly depending on processing and measurement techniques.
- **Filler combinations:** to improve the packing density in the matrix and introduce a dual functionality into the resin, e.g., flame-retardancy (hybrid combination) to exhaust synergistic effects.
- **Surface functionalization:** only plays a minor role in the increase in TC. Especially below 20 vol.%, the TC increase only up to 0.1 W/mK, which is not in relation to economic reasons (long production times) [113]. BN only has very few active functional groups on its surface available for functionalization at their edges [134]. Yung *et al.* [77] pointed out that the coating layer on the particles must be thick enough to make the modification work. However, if the coating is too thick, the coating will become a thermal barrier itself, hence decreasing the thermal conductivity. Similar findings are published in [71,112,133–136].
- **Orientation:** anisotropy can be an enhancing effect, depending on the chosen processing method. Particularly, the filler orientation, dispersion, and distribution (3-D approach) need to be process-controlled.

- **Processing techniques:** pressing, sonication, roll-milling, mixing can improve the dispersion but increase cycle time/production cost tremendously.
- **Thermal conductive pathway formation:** What happens during curing? When and how is the filler network formed?
- **Role of GF:** not well described in the literature. In GF reinforced systems, the filler orientation and location are even more critical since filler filtration may occur. To overcome the thermal barrier caused by the GF, thermally conductive fillers need to be introduced into the GF strands. There are very few studies on filled laminates but almost no scientific studies on the increase in FVC.

The most efficient system described from the literature is a system containing a **platelet filler** with a low AR in  **$\mu\text{m}$ -size** (anisotropy is preferred!). Best performances are shown in combination with another filler (**hybrid combination**) to evaluate possible synergistic effects. Literature shows TC, thermal stability, CTE,  $D_k/D_f$ , and mechanical studies, but almost **no published work on Flame Retardancy for BN particles or filler combinations!**

## 2.2 Fire Behaviour & Flame Retardancy of Polymers and their filled Resins

### 2.2.1 Thermal Degradation of Polymers & the Modes of Action of Flame Retardants

The development of fire is generally influenced by the following factors: *energy/heat/fuel*, *oxygen (concentration)*, and the *polymer material* itself.

In general, *polymer degradation* follows a cycle and influenced by energy, oxygen, and the fuel, the polymeric material. The heat, which is generated is transported back to the polymer surface. The polymer softens and decomposes into small fragments. The produced volatiles (radical polymeric fragments) are constantly providing fuel [137] (Figure 35). The volatiles migrate into the *flame zone*, into the gas-phase, and react with oxygen supplied from the ambient air in a free-radical chain reaction. A fire develops through different stages (Figure 34): the *ignition* of the polymer material, where the ambient temperature is relatively low. The *fire grows* if enough oxygen and fuel are available (= fire growth state). Simultaneously, the ambient temperature increases. Locally, on the polymeric surface, a *fully developed* fire can reach temperatures up to 1200 °C. An exothermic chain reaction between fuel, oxygen, and the free radicals occurs (= thermal coupling). The so-called *flash-over* is indicated by the sharp rise of temperature and the generation of heat. *Smoke* is a mixture of complete and incomplete combustion, resulting in H<sub>2</sub>O and CO<sub>2</sub> or CO and soot, respectively. The remaining solid, the residual char, mainly consists of carbon and ash [137–141].

EPA published a study on the major combustion by-products at different temperatures and environments (pyrolysis *versus* oxidation atmosphere) when using no flame retardants. These include phenol, toluene, and benzene [142].

Epoxy resins differentiate in their intrinsic flame retardancy. Aromatic groups offer higher thermal stability compared to aliphatic and are also known as char-promoting agents [18,30].

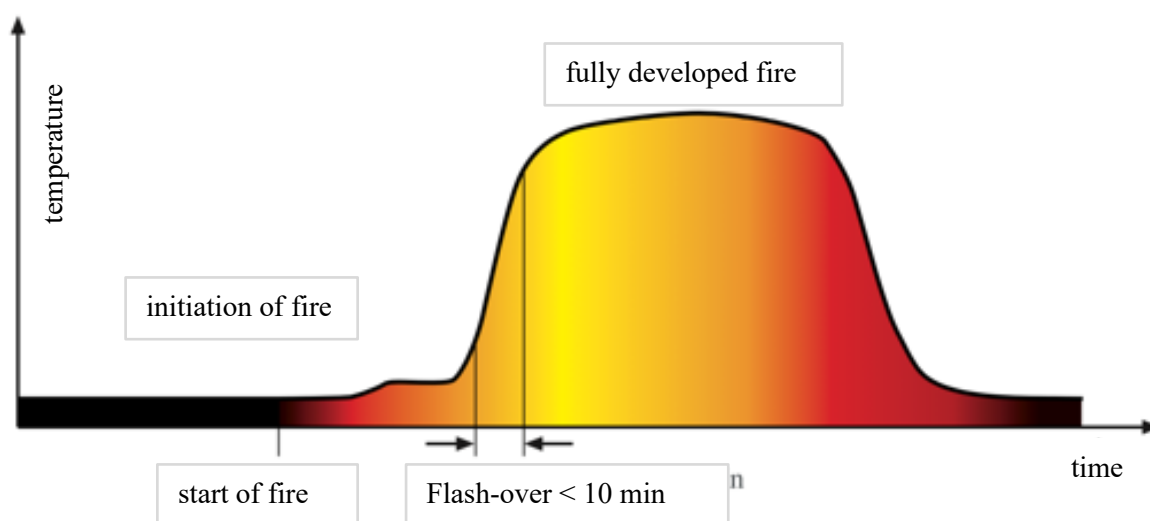


Figure 34 Temperature-time dependency of different stages of a fire [140,141].

**Flame retardants** (FR) can interfere with the degradation and burning cycle.

Typically, FR's can inhibit the degradation mechanism via **solid-phase** reaction or **gas/vapor-phase** reaction. In the solid-phase inhibition, the FR promotes the formation of char at the polymer surface upon heating. The char functions as an insulating barrier between the heat of the flame and the underlying neat polymer material, counteracting the production of new fuel. The degradation rate will decrease [18,30]. Some FR's also release water during their degradation, cooling the surface and merging the energy needed to retain the flame. Secondly, the gas-phase active FR's change the chemistry of the flame. During combustion of the FR's, volatile components are released, which interact in the gas-phase above the burning material and diffuse into the flame. They interrupt the ongoing free radical reactions, which increase the amount of energy needed to sustain the flame (= flame poisoning) [143]. In some cases, FR's act in both the solid- and vapor-phase [18,30]. *Intumescent* FR's contain an acid, a carbon, and a gas source. The solid component degrades under dissipating thermal energy. The visco-elastic material can entrap evolved gases or volatiles, resulting in an intumescence state (foamed). The carbonaceous intumescence coating protects the material underneath [30].

Recently, legislative restrictions banned **brominated FR's** from the use in the E&E market, especially in PCBs. Since the 1960s, polybrominated compounds (i.e., polybrominated biphenyl, PBB) or tetrabromobisphenol A (TBBA), which consists of bromine in the chemical backbone, were used as standard FR's for PCBs. Halogen-containing components (i.e., bromine (Br), chlorine (Cl)) are known to be gas-phase active agents quenching the free radical reaction

and are very efficient in lower concentrations [18]. However, there are concerns with their toxicity.

*Alternatives* to brominated FR's are **halogen-free FR's**, including *phosphorous* (P)-, *nitrogen* (N)- and *inorganic*-based compounds. They are further divided into *reactive* constituents or *inactive* additives. Reactive components are directly bound to the resin's chemical structure / backbone. They usually do not leach over time and are solvent-resistant, resulting in fewer extractable/leachable but may alter the curing kinetics [144,145]. An example of this type of FR is DOPO (epoxidized phosphorous). The primary decomposition reaction yields to char. DOPO is incorporated into the backbone/Epoxy resin network; the P-H bond can link to the Epoxy resin matrix. Since its chemically bound to the Epoxy, it can decrease the  $T_g$  since it is monofunctional [146,147].

Inactive, inorganic FR's are known to be non-toxic, halogen-free, environmentally friendly, are corrosion-safe, and reduce smoke production [144]. Commonly, inorganic additives (antimony oxide) or hydrated fillers, such as aluminum hydroxides (ATH), or magnesium hydroxides (MDH), release water in an endothermic reaction during combustion and can promote char formation. These fillers are inexpensive and non-toxic. However, much higher loadings (50 wt.% of ATH [30]) compared to DOPO are needed, which negatively impacts the overall final properties [144]. Nitrogen-based FR's (melamine) are char promoters usually releasing  $N_2$  gas, which can "foam" the char (= intumescence) [18]. Nitrogen- or phosphorous-containing FR's need to be used in high loadings, and cause a decrease in  $T_g$ , can lead to increased moisture absorption [144,145].

Inorganic FR's include red phosphorous, which is widely used in wires/cables applications. Red phosphorous is a char-promoting FR [144] that enables absorption of heat. During the FR degradation, water molecules are released. These dilute the gas mixture and therefore reduce the fire intensity [144] (Figure 35).

Boehmite, especially, is a good candidate for the new lead-free soldering requirements as decomposition does not start before reaching 340 °C. Boehmite provides reliability in long-term applications such as automotive. Since the overall efficiency of Boehmite is lower than with ATH, it either needs to be used in combination with another FR or to be used with Novolac based Epoxy resin [145]. Using new matrix resin systems can result in a trade-off of the FR-4

performance [144]. Good FR's combinations can be melamine-containing derivatives with Phosphorous [146,147].

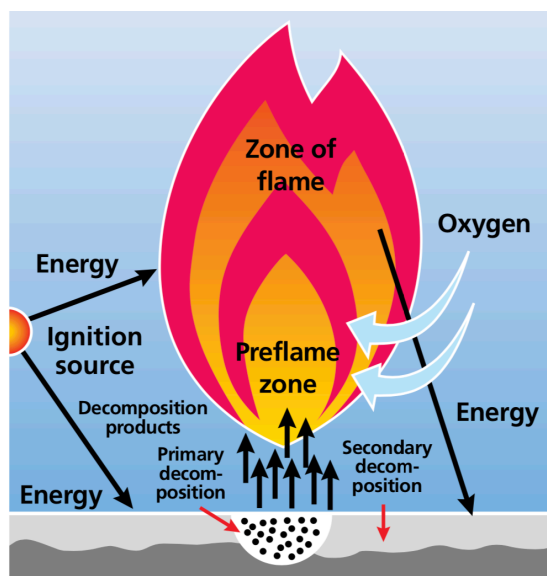


Figure 35 Flame retardancy mode of action for metal hydroxides, such as ATH or Boehmite [145].

### 2.2.2 Characterization of the Fire Behavior

In the E&E industry, flame tests such as the LOI (limited oxygen index) and UL-94 test are well known as standardized methods to classify the material for their flammability. These are small-scale methods whose advantages are low material and time consumption.

The flammability of polymer materials is mainly assessed by their ignitability, heat release (rate), smoke release (rate).

The *Cone Calorimetry Fire Test* is a medium-scale test method developed by the US National Institute of Standards and Technology (NIST). It evaluates the materials's response to a defined, incident heat flux (usually between 35 – 100 kW/m<sup>2</sup>) simulating a forced flammability behavior in a small-scale, real-life scenario according to ISO 5660 and ASTM E1354-92. The test method is based on the principle of oxygen consumption during combustion, indicating a direct relationship between the mass of oxygen consumed and the amount of heat released during polymer combustion [25,148–154]. Since the intensity of the heat radiation can be set utilizing an adjustable radiant heater, it is possible to simulate different fire scenarios: irradiation of an

intensity of  $35 \text{ kW/m}^2$  represents the strength of a wastebasket fire, whereas  $70 \text{ kW/m}^2$  corresponds to a room fire.

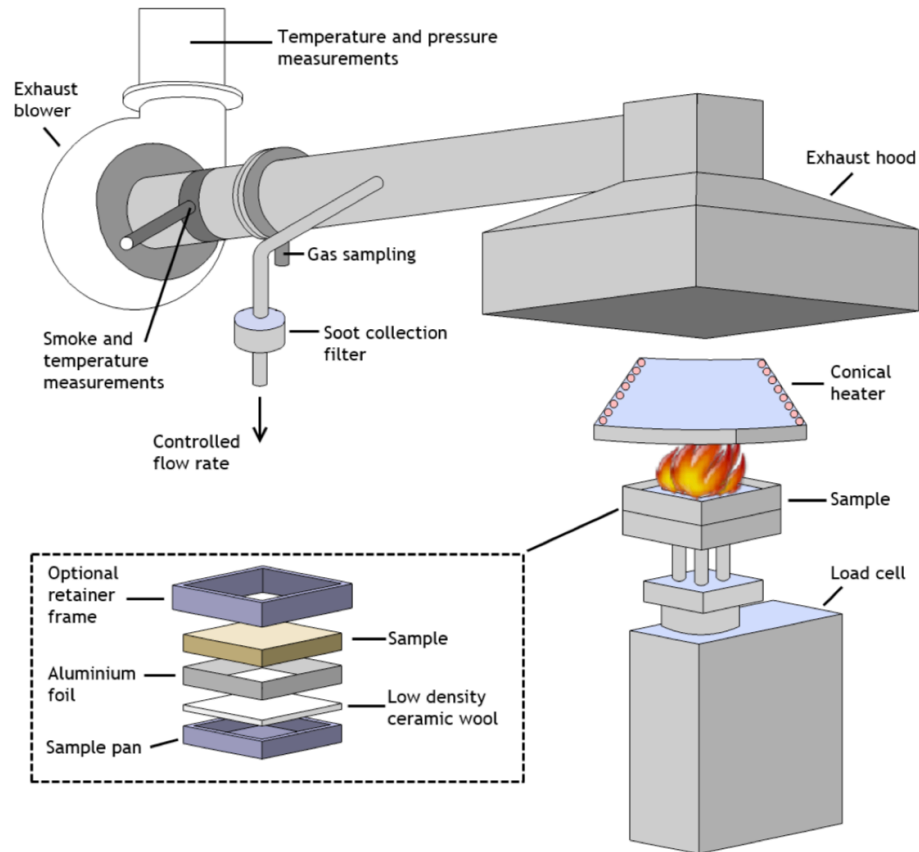


**Figure 36 Schematic set-up of a Cone Calorimeter apparatus [155].**

At the beginning of this fire test, combustion is forced. The heat flux over the surface of the sample leads to the release of volatile. Together with the ambient oxygen, this results in a highly explosive mixture that is ignited by the spark igniter. During the combustion, ambient oxygen is consumed, which is directly correlated to the heat being released by the actual material burned (= heat release rate) and the time to ignition  $t_{ig}$  (from flash-over), which is corresponding to the escape time in real-life *fire scenarios* [148–154] (Figure 37).

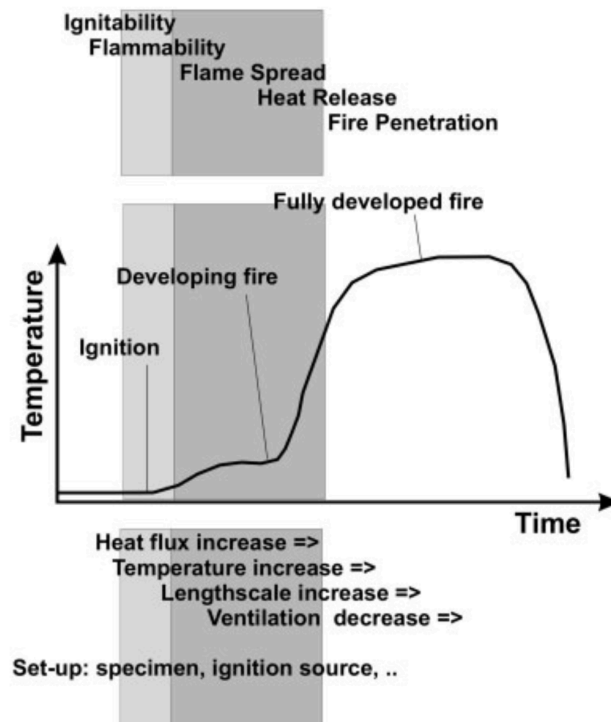


**Figure 37** Parameters accessed by the cone calorimeter and correlation to the fire stages [154].

The **ignition** ( $t_{ig}$ ) time depends on various criteria such as the thermal inertia, critical heat flux, or critical surface temperature for ignition [154]. The **heat release rate** (HRR) is determined by oxygen consumption and can be determined by material-specific properties, i.e., physical, and chemical mechanisms during the combustion. Along with the heat released during combustion, smoke and toxic gases are released. The oxygen concentration in the atmosphere is decreasing. The **total heat released** (THR), the integral of the **heat release rate** (HRR) over time, represents a fire's potential. Both CO and smoke production occur in incomplete combustion processes. That is the case when there is flame-retardant (FR) activity in the gas-phase. In addition, an increase of these values means flame retardants are active in combustion of a cone calorimeter test. The mass of the sample is continuously monitored by a load cell and therefore gives the mass loss rate (MLR) and the mass left as char. Usually, the higher the HRR value, the faster the ignition process starts, and the flame spreads faster along the materials' surface.

The HRR versus time curve shape is affected when char-forming FR are used (Figure 38). The **time until peak heat release rate** (tPHRR) is shortened when a superficial protective layer is formed (e.g., inorganic FR). In contrast, non-charring FR's shift the PHRR to higher times at the end of combustion. This is caused by the thermal feedback when the pyrolysis zone reaches

near the rear surface. While combustion occurs, energy is partially absorbed into the material, which lowers the HRR values; the HRR increases again when the bottom of the sample is reached [148–154]. Other specific parameters are i.e., the *peak HRR (PHRR)*, *total heat released (THR)*, *total heat evolved (THE)*, *mass loss rate (MLR)*, *total smoke produced (TSP)*, *total smoke released (TSR)*, *CO*, and *CO<sub>2</sub> yields* can be determined during one test. The *effective heat of combustion (THE/ML)* and the *effective smoke release (TSR/ML)* can be calculated when dividing the results by the mass loss [148–154]. With FR's being active in the gas-phase, the effective heat of combustion decreases, and the effective smoke release increase simultaneously. In fire scenarios, both the CO and smoke production severely affect the escape time, as most people die from smoke-poisoning rather than the actual flames [153]. Fire resistance is usually indicated with a decreasing trend of the PHRR and total mass loss values and often an increase in  $t_{ig}$ .

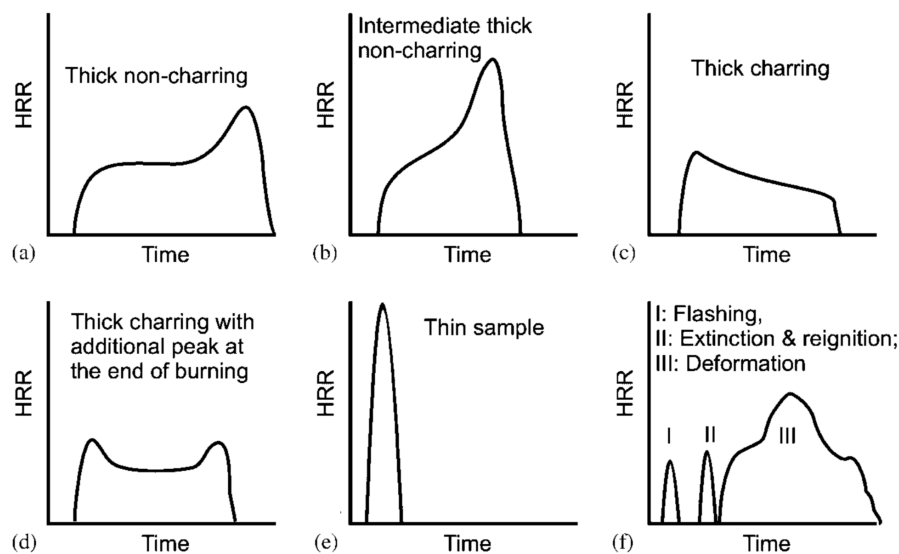


**Figure 38** Typical heat release rate (HRR) curves exhibiting characteristic burning behavior of different materials [154].

To facilitate the interpretation of the results of the Cone Calorimeter, two characteristic values were introduced: the *fire growth rate index (FIGRA)* ( $\text{kW}/\text{m}^2$ ) and the *mean maximum heat release rate (MARHE)*. The fire growth rate FIGRA in  $\text{kW}/\text{m}^2\text{s}$  results from the quotient of PHRR and the time  $t_{PHRR}$ , i.e., the slope of the heat release rate at its maximum. At the same time, MARHE is calculated as the mean value of the maximum heat release rate relative to the

duration of the experiment. In the EU, the MARHE parameter is used for the regulatory assessment of the heat-release potential of combustible materials and components, e.g., in the field of rail vehicles [156]. However, ScharTEL *et al.* state that MARHE should be used with caution because the parameter HRR calculates it and thus disregards factors such as surface flammability and ventilation intensity. Ventilation plays a crucial role in the combustion mechanism as it directly regulates the fraction of fuel in the gas phase. Before ignition, thermal-oxidative decomposition occurs. After ignition, a uniform flame is formed, and pyrolysis is reduced because most of the combustion of the sample takes place in the gaseous phase. The decomposition of the sample mass under the combustion zone takes place under inert conditions. Thermal-oxidative decomposition is only relevant before and during ignition, in the absence of ignition, or minimal flame formation [157].

ScharTEL *et al.* reported that the HRR values measured at heat fluxes  $< 35 \text{ kW/m}^2$  correspond well with UL-94 and LOI measurements. Their studies showed that the UL-94 V0 classification (self-extinguishing) is following HRR values below  $300 \text{ kW/m}^2$  [154,158]. Lyon *et al.* showed a correlation of UL-94 and Cone Calorimetry when the intrinsic heat release is  $125 \text{ kW/m}^2$  [159].

### 2.2.3 State of the Research – *Flame Retardancy*

Epoxy resins' major drawbacks are their high flammability, which can restrict their use in electronics and PCBs unless using FR's [160]. Especially on the PCB substrate level, there is very few studies published regarding flame-retardant mechanisms.

EPA, the US environmental protection agency, published a report on FR's in PCBs [142]. The scientific group studied various FR's in substrate laminates: Phosphorous-FR, Brominated-FR, and a benchmark with no FR. The laminates were tested with and without Cu foil at  $50 \text{ kW/m}^2$  irradiation with Cone Calorimetry. All laminates had a thickness of 3 mm. The results can be found in Figure 39. During measurement, the samples made a cracking sound, which is caused by each layer's delamination. The samples re-ignited when reaching new, undegraded material underneath. The re-ignition can directly be seen in the corresponding HRR results as the curve progresses through multiple peaks. In a second study, the group tested non-halogenated FR's in these laminates. The  $t_{ig}$  was increased from approximately 15 s to over 190 s.

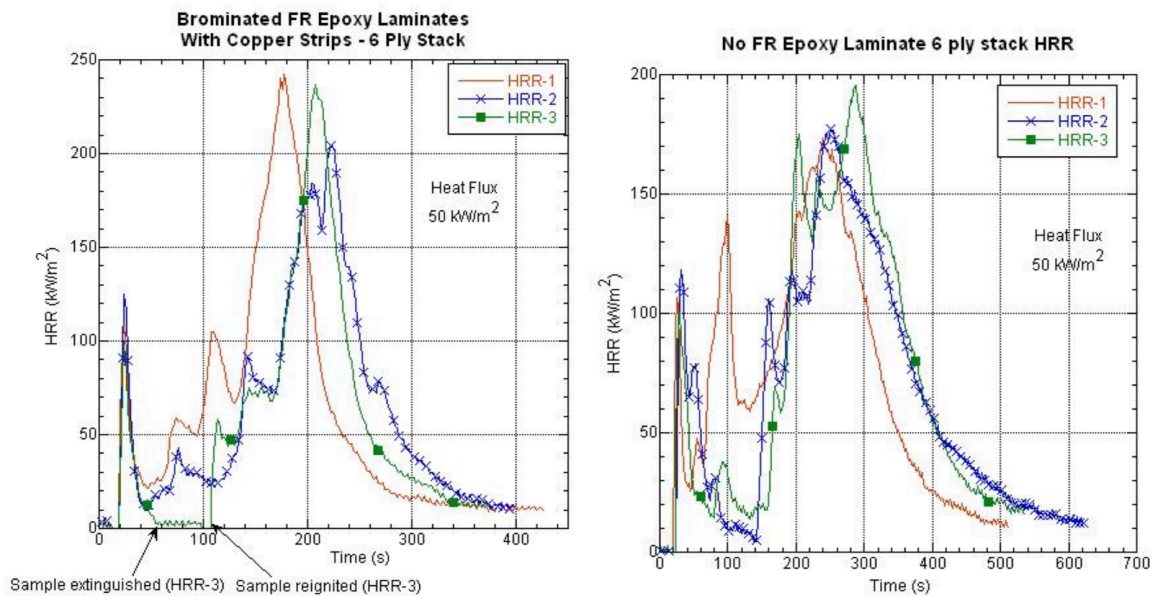


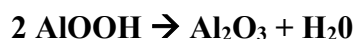
**Figure 39** HRR curve of Epoxy laminates with brominated FR (left) and with no other FR (right) [142].

Tsai *et al.* studied the fire behavior of Epoxy Novolac with UL-94 and with Cone Calorimetry for unfilled and clay-filled GF prepreg substrates [160]. The unfilled laminate failed the UL-94 test, whereas the clay-filled laminate resulted in a V-1 classification. The authors mention a rapid ignition and decomposition during the Cone test. However, the achieved  $t_{ig}$  value was not published.

Compared to the commonly known inorganic aluminum trihydroxide (=ATH), **Boehmite** (=  $AlO(OH)$ ) is a relatively new but very promising candidate. Boehmite as a filler gained more reception in literature due to some of its favorable properties, although it offers less bound water molecules than ATH, thus being a less active FR. However, one advantageous property of Boehmite is its good dispersion behavior in a polymeric matrix [161]. It is thermally stable up to 350 °C during PCB soldering or assembly processes. Furthermore, it offers a low CTE, good copper adhesion, and reduces the overall production costs of PCBs. Boehmite is a halogen-free flame retardant (FR) with an intrinsic thermal conductivity (TC) of 3-10 W/mK. Boehmite is a FR that acts in both the gas- and solid- combustion phase. The combustion process of polymers and the roles of the two steps are well explained in the literature [143]. It decomposes in an endothermic reaction, similar to ATH, to solid  $Al_2O_3$  by releasing water molecules that cool

down the burning system and interact with the ongoing free radical reactions in the gas-phase. In literature, ATH or Boehmite fillers can act as “heat sinks” by inhibiting further pyrolysis due to their endothermic decomposition reaction, which reduced the thermal feedback heat [143]. Additionally, the deposited  $\text{Al}_2\text{O}_3$  acts as a thermal shield against heat and oxygen between the polymer and the flame in the so-called solid-phase [162]. It is known that ATH is more efficient concerning FR compared to Boehmite, however, it can improve charring [163].

Karger-Kocsis listed some favorable properties in his review [161]. Boehmite improves the thermal conductivity, thermal expansion, electrical resistance and breakdown, and mechanical properties (tensile, flexural strength) [161]. However, no mentioning of its flame-retardancy. Sun *et al.* [164] studied Boehmite particles in a DGEBA matrix and evaluated the thermal degradation via TGA,  $T_g$ , and oxygen index (OI). Incorporating 2.3 – 10.2 wt.% of Boehmite, the  $T_g$  increased by approximately 20 °C, the  $T_{d,5\%}$  was 75 °C higher than the neat sample. They claimed that the partial crosslinking ability between AlOOH and the epoxy matrix decreases the decomposition rate and AlOOH acts as a thermal stabilizer. They published a decomposition reaction of neat Boehmite at 480 °C releasing water [164]:



Su *et al.* published a synergistic effect between 10 wt.% Boehmite in combination with 10 wt% of Poly magnesium phosphate in IPDA-cured DGEBA [165]. They studied the FR with Cone Calorimetry and TGA and found a synergy regarding PHRR, THR, and  $t_{ig}$ . A twin-peak appearance in PHRR near flameout was observed. The authors claim with the flame spread, degradation of material underneath the sample holder started.

Neumeyer *et al.* studied Boehmite with a  $D_{50}$  of 1.8  $\mu\text{m}$  in Epoxy Novolac (cured with DICY) combined with DOPO. Self-extinguishment of the samples during the UL-94 testing was observed with the synergistic combination of 1.0 wt.% DOPO with 10 wt.% of Boehmite [166]. However, no testing was conducted using actual prepreg sandwich specimens, and no test methods such as Cone Calorimetry were used to further explain the synergistic fire retardancy mechanisms.

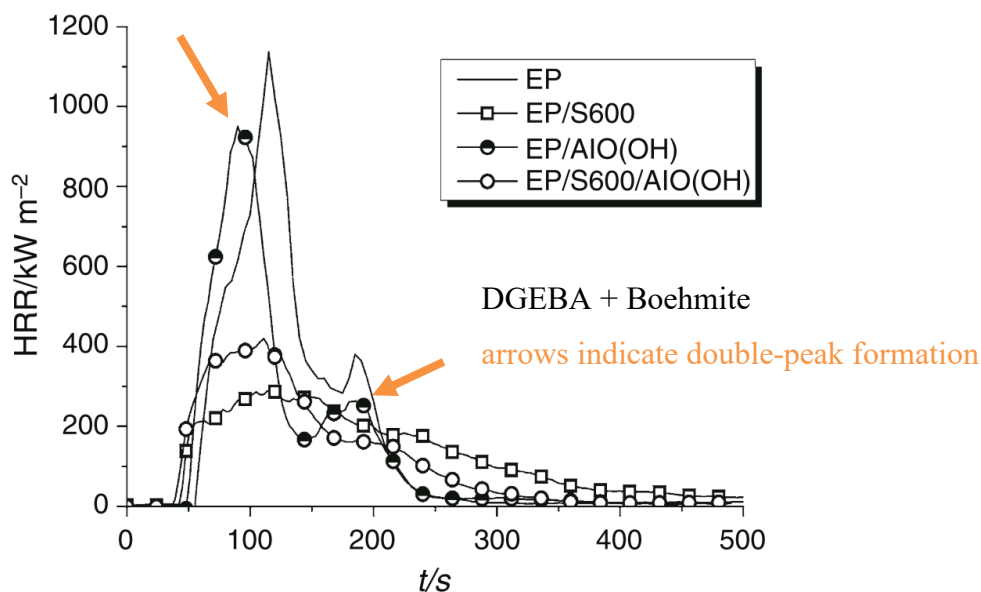


**Figure 40** Heat release rate of DGEBA with 20 wt.% of 2  $\mu\text{m}$  Boehmite (orthorhombic shape) only and in synergistic combination with melamine poly magnesium phosphate (from [165])

Published studies on the flame retardancy behavior of BN in any matrix are limited. Yu *et al.* studied *h*-BN on thermal stability and flame retardancy (TGA and Cone Calorimetry) [167]. They found an increase of the  $T_g$  by 47  $^{\circ}\text{C}$  and a 50 % reduction of PHRR. They claimed that the nano-BN sheets cause a tortuous pathway that delays the release of volatiles and therefore also causes a decrease in heat.

Fischer *et al.* studied *h*-BN in a PA6 matrix [168]. At 20 vol.% *h*-BN, a TC of 1.30 W/mK was reached. However, a better flame-retardancy was achieved by adding 10 vol.% of a flame retardant (Al-diethyl phosphinate). However, a TC value of only 1.14 W/mK was achieved due to the lower intrinsic TC of the phosphinate. Overall, a V-0 rating and a higher LOI value were found.

Summarizing the *State of the Art* for **Boehmite or BN regarding flame retardancy**, there is very little information about these thermally conductive fillers and their performance in FR and especially almost no coherent published work on Cone Calorimetric studies.

In addition, there are still some remaining questions, i.e., what the effect of TC on FR is or what the contribution of thermally conductive fillers on the flame retardant mechanisms is.

There are contradicting assumptions that can be found in the literature of **TC linked to Flame Retardancy**:

- a) *With the increase in TC, rapid heat dissipation of heat from the pyrolysis zone and shielding effects can slow down the ignition or degradation. In addition, the platelet-shaped BN helps to increase the path length of volatile migration to the surface [167].*
  
- b) *With the increase in TC, a faster ignition is assumed to occur, as the ignition temperature might be linked to the degradation and release of volatiles [169].*

Regarding the increased thermal conductivity by using **glass fibers**, both positive and negative effects are discussed. On the one hand, a rapid dissipation of heat from the pyrolysis zone and shielding effects can slow down the ignition or the burning. On the other hand, a faster ignition is enabled, as the ignition temperature is linked to the thermal conductivity.

### 3 Objective and Structure of the Thesis

Recently, the Printed Circuit Board (PCB) industry has faced new challenges impacting the *soldering process*. With the new *RoHS & WEEE directives*, the use of toxic heavy metals such as *lead* (Pb) must be eliminated from this PCB manufacturing step. With lead-free alternatives, the short-term heat distortion temperature that the PCB base substrate must withstand without softening or degradation has increased from 180 °C to 220 °C. Although high-temperature substrates based on bismaleimide triazine, cyanate ester, polyimide, or even PTFE matrices, with a  $T_g > 220$  °C, are already commercially available, their high manufacturing costs due to complex processing steps is a significant downside [22].

Current *State-of-the-Art FR-4 circuit boards*, based on glass-fiber (GF) reinforced Epoxy resins, *are not compatible* with the lead-free **solder assembly at > 220 °C**. Their  $T_g$  is < 200 °C as they are manufactured using a di- or multifunctional-Epoxy resin matrix [22]. To meet the higher  $T_g$  requirement, a new thermoset matrix must be established. Epoxy Novolac resins, cured with a suitable curing agent, can result in glass transition temperatures above 200 °C. In this thesis, Epoxy Novolac cured with the aromatic diethyl toluene diamine (DETDA) is used to achieve the excellent thermo-mechanical properties for the PCB base material. As a first experimental step in this thesis, the curing cycle will need to be optimized, considering the overall  $T_{\text{Processing}}$  of < 230 °C.

In addition, the power density of the electrical circuits has increased tremendously. Significant heat is produced under thermal cycling, leading to hotspots, especially under or close to the embedded chip. The substrate material must be able to dissipate this heat, as this might directly result in *severe degradation* and even a *potential fire hazard*. *State-of-the-Art FR-4 substrate materials* cannot overcome the thermal management sufficiently as their thermal conductivity is known to be below  $\lambda < 0.4$  W/mK. Assembled thermal management parts, such as *heat sinks* or *fan cooling* systems, contrast the current trend of “*miniaturization*” and *lightweight design*. To manage the heat more efficiently, it is known from the literature that the addition of thermally conductive fillers, such as Boron Nitride (BN), can result in thermal conductivities (TC) of  $\lambda > 0.7$  W/mK at filler contents of 15 – 20 vol.% in Epoxy resins [101,113]. Therefore, a novel approach is the *modification of the PCB substrate material itself*. The project partner

of this thesis, Fraunhofer IZM, simulated that a minimum of  $\lambda = 0.7$  W/mK is necessary to distribute heat from the chip throughout the base material efficiently. This thesis aims to introduce BN into Epoxy Novolac formulations of at least 15 vol.% and study the effect on the thermal conductivity in cured resin plates and their GF-reinforced laminates. First, the addition of fillers at these concentrations is expected to increase the viscosity. To ensure its prepreg processability with the *solvent-free direct impregnation* route, ideal processing parameters must be established by optimizing the correlation between filler content and temperature at the coating unit. The known optimal processing window for the solvent-free prepreg processing route is between 200 mPa·s and 50 Pa·s. Secondly, the evaluation of the thermal conductivity with a focus on BN filler content is conducted. Special attention is laid on understanding the interaction of particles and the thermal conductive filler network formation in combination with GF and its increase in fiber volume content (FVC). Experimental results are correlated with scanning electron microscopic images to establish structure-property relationships.

To ensure fire safety in PCBs, FR-4 substrates are manufactured using flame-retardant filler(s) (FR) to meet the **UL-94 V-0** requirement, with no melt dripping and a flame-retardancy of < 10 s after ignition. Especially in automotive applications, *flame retardancy* of the PCB substrate material is essential. In case of over-heating of PCB material during operation, ignition and a possible flame spread must be hindered to surrounding parts in a vehicle. These parts are mostly made of polypropylene which easily ignites and degrades under severe melt-dripping.

Primarily, *tetrabromobisphenol-A* (TBBPA) was used as a reactive FR for PCB substrates which is covalently bound to the (brominated) Epoxy resin matrix [170]. TBBPA is very effective in lower concentrations (ca. 50 wt.% of bromine), however, it is known for its *acute and chronic toxicity* [142,170]. Furthermore, TBBPA is listed on California Proposition 65 as a hazardous substance causing cancer [171]. With the RoHS directive, so-called “green”, *halogen-free* FR were introduced into FR-4 substrates. Most commonly, inorganic *aluminum trihydrate* (ATH), which are low-cost additives, with efficiency at contents of > 25 wt.%. Unfortunately, ATH is not able to withstand the short thermal cycling at 220 °C. At temperatures of 180–200 °C, its thermal degradation is already initiated, and water is released [172]. Boehmite, an *aluminum oxide hydrate* (AlO(OH)), is a relatively unknown flame-retardant filler (FR). However, compared to ATH, Boehmite thermally decomposes at

> 350 °C, however, it has a slightly lower efficiency due to the lower amount of crystal-bound water [164].

Hence, the addition of Boehmite into Epoxy Novolac formulations will result in more thermally stable material. Still, its effectiveness in correlation with concentration will need to be evaluated to meet the UL-94 V-0 requirement. Moreover, the filler combination of Boehmite with BN will need to be assessed in terms of a possible synergistic effect to enhance thermal conductive and flame-retardant properties. Therefore, an optimal filler ratio between Boehmite and BN has to be identified. The thermal degradation is examined with thermo-gravimetric analysis. The flame and fire properties are characterized by Cone Calorimetry with a focus on heat release and time to ignition. Especially, the time to ignition and smoke release is of scientific interest, which Cone Calorimetry can assess. Post-combustion SEM-EDX analysis of the char samples enables establishing modes of actions for BN and Boehmite in both filled resins and their laminates. The role of BN on flame retardancy is not yet well established in the literature. Thus, this thesis focuses especially on the correlation between thermal conductivity and flame retardancy with the final properties to establish structure-property relationships. A particular focus was laid on understanding the relationship between the FVC and flame retardancy. In the end, UL-94 classification, a test method that is more established in the PCB industry, was conducted to help classify the novel base material. Lastly, the optimized laminates undergo additional testing and evaluation for other PCB-relevant properties, such as  $\alpha$ -CTE, water absorption, and dielectric properties.

### **Summary of aims and hypotheses:**

The **overall aim** of this thesis is to develop an innovative, high- $T_g$ , and cost-effective FR-4 substrate with short production cycles that is thermally conductive, flame-retardant, and that complies with regulatory directives.

**Aim 1 – *glass-transition temperature*:** To withstand the temperatures of lead-free soldering processes, the matrix resin system under investigation needs to have a minimum  $T_g$  of 220 °C.

**Hypothesis:** The current FR-4 matrix Epoxy resin needs to be substituted by a novel resin formulation consisting of the phenolic Epoxy Novolac cured with aromatic DETDA towards a  $T_g$  of > 220 °C.

**Aim 2 – thermal conductivity:** To efficiently support the heat management in PCB substrates, a thermal conductivity of at least  $\lambda = 0.7$  W/mK of the resin formulation needs to be achieved.

**Hypothesis:** The incorporation of at least 15 vol.% BN will aid in reaching a thermal conductivity of  $\lambda = 0.7$  W/mK.

**Aim 3 – flame retardancy:** To ensure the overall fire safety of PCB substrates, the classification of UL-94 V-0 must be achieved

**Hypothesis:** The substitution of aluminum trihydrate (ATH) as a standard FR by Boehmite will lead to a more thermally stable and flame-retardant resin system.

The **main technological goal** of this Ph.D. thesis is to fundamentally study and tailor a next-generation *multifunctional*, high- $T_g$  PCB substrate that has higher thermal stability and flame retardancy compared to the current industry’s “*best in class*” marketed **PCL 370HR benchmark** (Figure 41) from Isola [173].

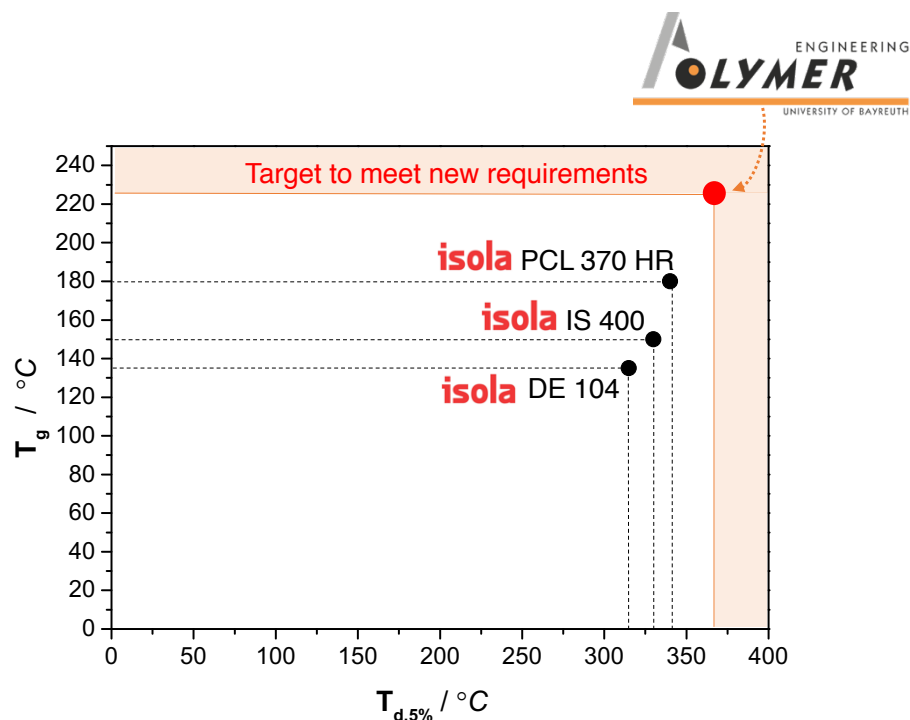


**Figure 41** FR-4 prepregs available at Isola GmbH, including the benchmark of this thesis, the high-performance laminate PCL 370HR.

The **experimental route** of this thesis to achieve the above aims is described in the graphical abstract in Figure 42.

A “*novel*” generation of the FR-4 material should fulfill the technological targets specified in Table 4.

**Table 4 Overview of the technological targets in comparison to the Benchmark PCL 370 HR (Isola).**

System Properties	Benchmark <i>PCL 370HR</i> 	Target 
<b>Prepreg-Processing</b>	Solvent-based dip coating	Solvent-free direct impregnation with a $T_{\text{Processing}} < 230 \text{ }^\circ\text{C}$
<b>z-Thermal Conductivity</b>	0.4 W/mK	<b>&gt; 0.7 W/mK</b>
<b><math>T_g</math></b>	180 °C	<b>&gt; 220 °C</b>
<b>z-CTE</b>	45 ppm/k	<b>&lt; 40 ppm/K</b>
<b><math>T_{d,5\%}</math></b>	340 °C	<b>&gt; 360 °C</b>
<b>Flame-Retardancy (UL-94)</b>	V-0	<b>V-0</b>
<b>Water Absorption (24h)</b>	0.15 %	<b>&lt; 0.5 %</b>
<b>Dielectric Properties (<math>D_k/D_f</math>) at 1 GHz</b>	$D_k < 4.17$ $D_f < 0.0161$	<b><math>D_k &lt; 4.0</math></b> <b><math>D_f &lt; 0.005</math></b>
<b>Mechanics - Flexural Strength</b>	620 MPa (warp) 530 MPa (weft)	<b>420 MPa (warp)</b> <b>350 MPa (weft)</b>
<b>Relative Price Ratio (= based on FR-4 substrate)</b>	1 (= FR-4)	<b>&lt; 4x FR-4</b>

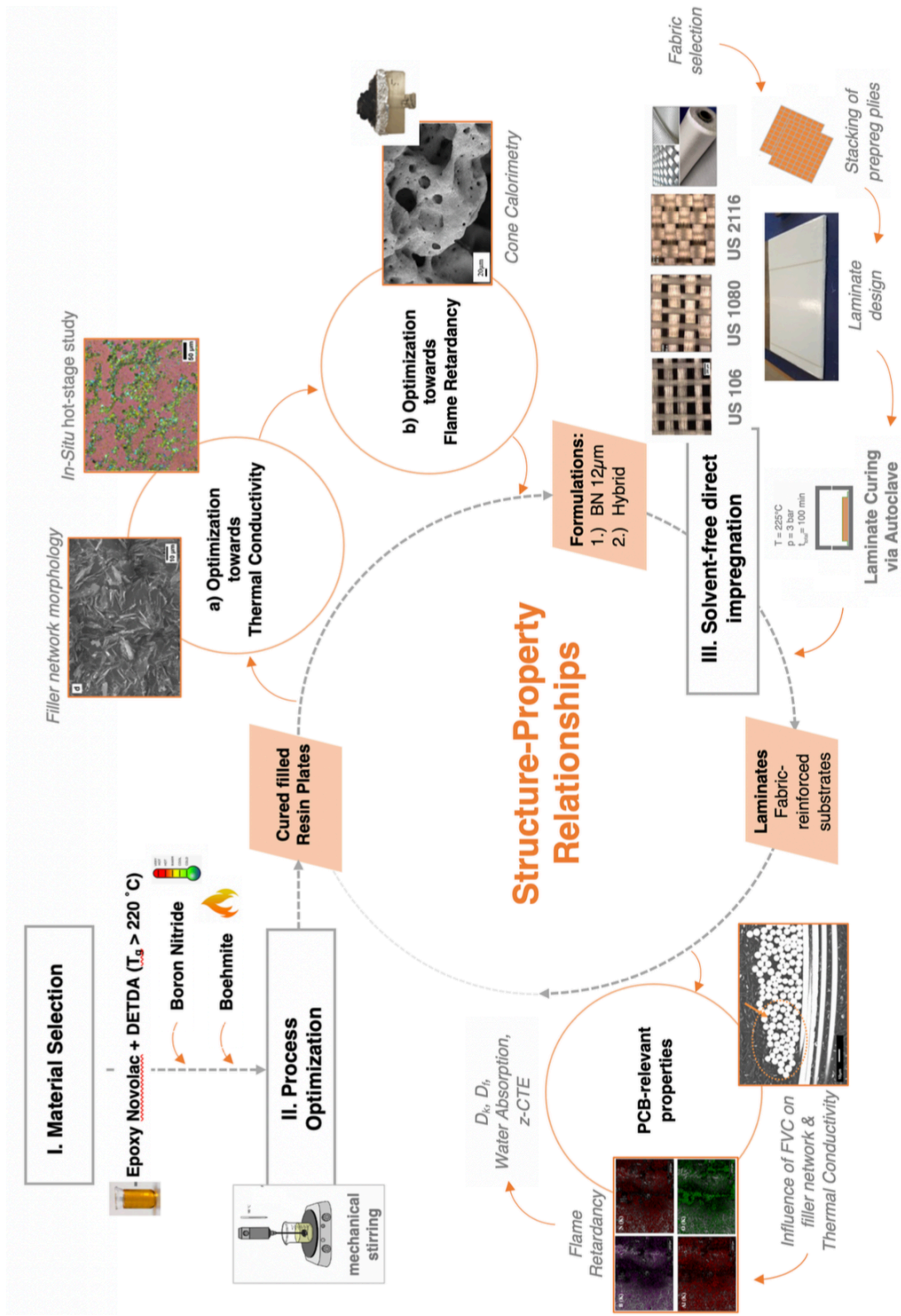


Figure 42 Graphical abstract of the workflow of this Ph.D. thesis.

## 4 Materials & Methods

### 4.1 Materials

All materials under investigation were commercial products and were used as received without any further (surface) modifications.

#### 4.1.1 Resin Matrix

A multifunctional, phenolic Epoxy Novolac (= EN) resin, D.E.N.<sup>TM</sup> 438 from Olin<sup>TM</sup> Epoxy (Stade, Germany) with an Epoxy equivalent of 176 - 181 g/eq was used as a high T<sub>g</sub> reference matrix resin (density of 1.23 g/cm<sup>3</sup>, the price ca. 5 €/kg).

Epoxy Novolac is a standard resin for PCB applications, selected based on the resulting high T<sub>g</sub> values, low water absorption, and chemical resistance compared to other thermosets. Phenolic-based resins offer good long-term thermal and mechanical stability. Due to their aromatic structure, EN resins show excellent fire retardancy with high dimensional stability.

D.E.N. 438 does not contain any solvent, such as MEK (methyl ethyl ketone). Therefore, this resin grade is highly viscous and does not allow high filler degrees at lower temperatures. Its initial viscosity is 31.000 – 40.000 mPa·s @ 25 °C. Consequently, a particular focus was laid evaluating of the processing window as a direct correlation between temperature and filler content.

The Epoxy Novolac D.E.N. 438 was cured with diethymethylbenzenediamine (Araldite XB3473), supplied by Huntsman Advanced Chemicals (Basel, Switzerland) in the stoichiometric ratio of 100:24.1 (price ca. 40 €/kg) [174]. The chemical structures of the matrix EN and the curing agent DETDA can be seen in Figure 43. The curing agent is in a liquid state at room temperature, which helps to improve the processing properties of the Epoxy Novolac resin.

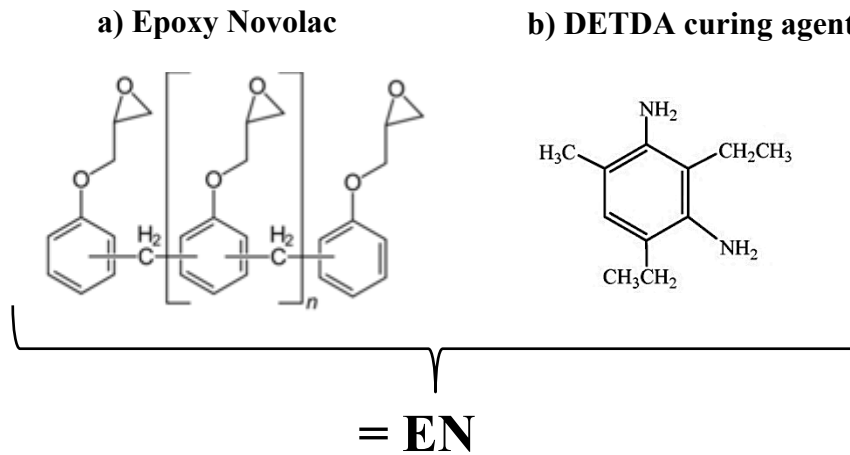


Figure 43 Chemical structures of a) Epoxy Novolac and b) of the DETDA curing agent [174].

#### 4.1.2 Fillers

##### Thermal Conductive Filler - Boron Nitride

As the thermal conductive component, Boron Nitride (BN) was chosen. BN is a non-toxic filler with high electrical resistance, low water absorption, and low thermal expansion [175].

Initially, three *hexagonal* Boron Nitride (= **BN**) types, purchased from Henze BNP (Lauben, Germany) with a  $D_{50}$  of 2.0  $\mu\text{m}$ , 12  $\mu\text{m}$ , and 45  $\mu\text{m}$  were used. All BN types are of (oval) platelet shape and average filler density between 2.27 and 2.35  $\text{g}/\text{cm}^3$ .

After initial investigations, the main BN filler was chosen to be the 12 $\mu\text{m}$ -size (= **BN 12 $\mu\text{m}$** ). This filler has an average particle diameter of 10.5  $\mu\text{m}$  and an aspect ratio of 17.6. The theoretical thermal conductivity is 300  $\text{W}/\text{mK}$  ( $x/y$ ) and 30  $\text{W}/\text{mK}$  ( $z$ ).

The physical properties are summarized in Table 5.

The filler geometry of **BN 12 $\mu\text{m}$**  can be seen in the corresponding SEM micrographs (Figure 44a) and b)). Its evaluated particle size distribution is shown in Figure 44c) indicating a  $D_{50}$  of 10.5  $\mu\text{m}$ . The supplier TDS states a  $D_{50}$  of 12  $\mu\text{m}$ .

**Table 5 Physical properties of the supplier TDS of the thermal conductive Boron Nitride fillers.**

Designation Properties	BN 2 $\mu$ m (=BN2)	BN 12 $\mu$ m (=BN12)	BN 45 $\mu$ m (=BN45)
Commercial Product Name	HeBoFill® 410	HeBoFill® 641	HeBoFill® 501
D <sub>50</sub> Particle Size / $\mu$ m	2	12	45
BET / m <sup>2</sup> /g	20	7	1
Density / g/cm <sup>3</sup>	2.284	2.268	2.290
CTE (x/y)	~ 1 ppm/K	~ 1 ppm/K	~ 1 ppm/K
Aspect ratio	~ 16	~ 18	~ 23
Dk (@ 8.8 GHz)	-	4.0	-
Df (@8.8 GHz)	-	0.0003 – 0.0012	-
Price / €/kg	160	147	150

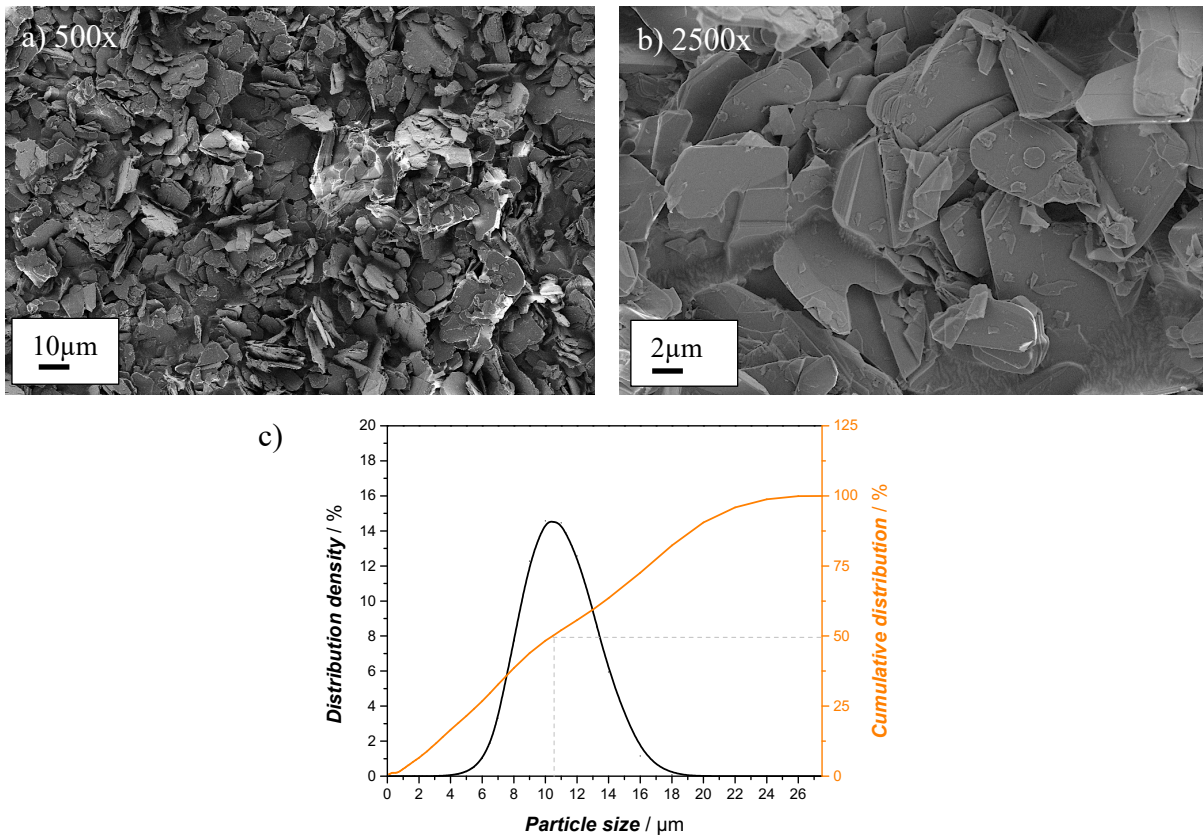


**Figure 44 SEM micrographs of the main thermally conductive component HeBoFill® 641, BN12 (a) 500x and b) 2500x) and c) its particle size distribution indicating an actual D<sub>50</sub> of 10.5  $\mu$ m.**

### Flame Retardant Filler - Boehmite

An (oval) platelet-shaped Boehmite ( $\text{AlO}(\text{OH})$ ) supplied by Nabaltec AG (Schwandorf Germany) with a density of  $3.07 \text{ g/cm}^3$  and a TC of  $10 - 30 \text{ W/mK}$  was used (commercial grade AOH EXS.). Table 6 shows an overview of the physical properties of the BT  $2\mu\text{m}$ . Its corresponding filler geometry and its particle size distribution are shown in Figure 45.

**Table 6 Physical properties according to the supplier TDS of flame-retardant filler.**

Designation	BT 2 $\mu\text{m}$ (=BT2)
Commercial Product Name	AOH EXS
D <sub>50</sub> Particle Size / $\mu\text{m}$	2.0
Specific Surface Area (BET) / $\text{m}^2/\text{g}$	~ 4
Aspect Ratio	10
Cost / $\text{€}/\text{kg}$	~ 3

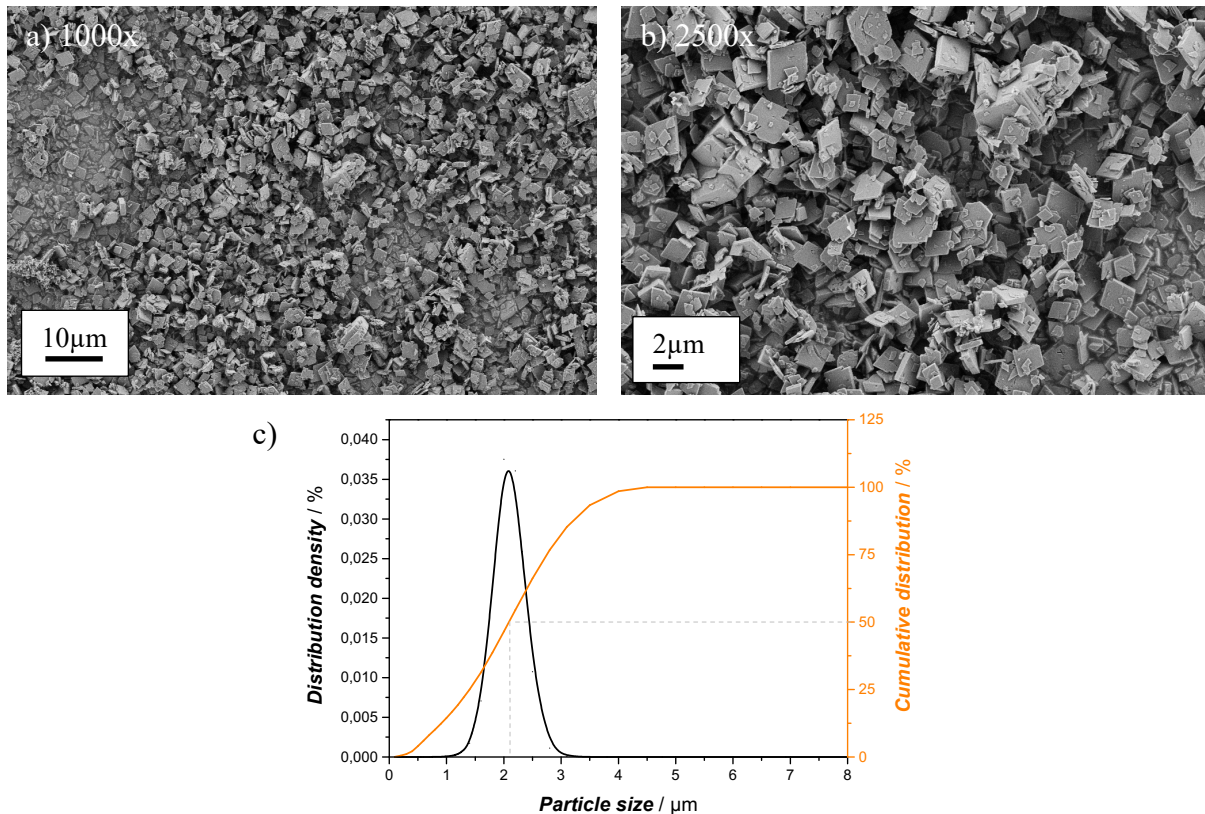


**Figure 45 SEM micrographs of the flame-retardant, Boehmite, AOH EXS<sup>®</sup> (= BT2) at (a) 1000x and b) 2500x) and c) its particle size distribution with an actual D<sub>50</sub> of 2.1  $\mu\text{m}$ .**

### 4.1.3 Glass Fabrics

Three standard E-glass fabrics used in PCB manufacturing with varying areal weights were purchased from PD Interglas Technologies GmbH, Germany (Table 7). The glass fibres have a silane-coating to improve the adhesion to the Epoxy Novolac resin. The fiber bundles (warp/weft) show a plain-weave pattern. Figure 46 shows microscopic images of the US Styles 106, 1080, and 2116 with corresponding areal weights of 25, 49, and 107 g/m<sup>2</sup>.

With increasing fiber areal weights, the thickness of the fiber rovings increases, leading to a smaller mesh size. This is of scientific interest as this might result in barrier effects in highly filled systems.

**Table 7 Overview of the three E-glass fabrics used in this study.**

Designation	GF25	GF49	GF107
Fabric Areal Weight / <i>g/m<sup>2</sup></i>	25	49	107
Commercially known US Fabric Style	US 106	US 1080	US 2116
Finish Type and Content	FE800 (Silane) 0.08 - 0.28 %	FE800 (Silane) 0.08 - 0.28 %	FE800 (Silane) 0.08 - 0.28 %
Yarn Count / <i>threads /</i> <i>inch</i>	56 · 56	60 · 40	60 · 58

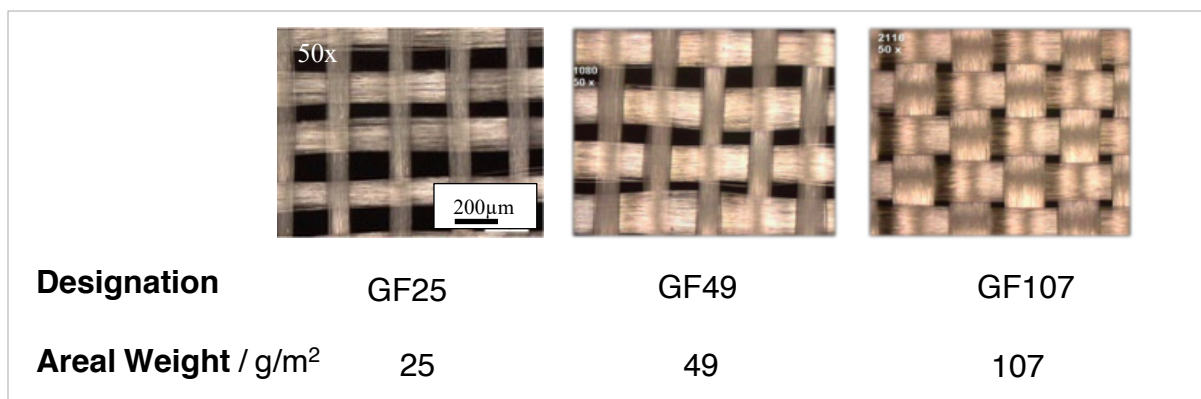


**Figure 46 Overview of the fabric styles GF25, GF49, and GF107, and their corresponding light microscopic images to illustrate the influence of increasing FVC on the mesh size.**

Table 8 shows a summary of all systems used in this thesis with their abbreviations.

**Table 8 Overview of all systems and their abbreviations used in this thesis, including color-coding.**

<b>Systems</b>	Matrix Epoxy Novolac <b>EN</b>	Thermal Conductive Component <b>BN12</b>	Flame- Retardant Component <b>BT2</b>	<b>Hybrid Combination</b>  <i>(ratio 3:1 = BN12 : BT2)</i>
<b>Resin Plates</b>	<b>EN</b>	<b>EN_BN12</b>	<b>EN_BT2</b>	<b>EN_Hybrid</b>
<b>Laminates</b>	<b>EN_GF25</b>	<b>EN_BN12_GF25</b>	<b>EN_BT2_GF25</b>	<b>EN_Hybrid_GF25</b>
	<b>EN_GF49</b>	<b>EN_BN12_GF49</b>	<b>EN_BT2_GF25</b>	<b>EN_Hybrid_GF49</b>
	<b>EN_GF107</b>	<b>EN_BN12_GF107</b>	<b>EN_BT2_GF25</b>	-

#### 4.1.4 Benchmarks

The project partner Isola GmbH provided three FR-4 *State-of-the-Art* materials (= benchmarks). All three benchmarks are produced using Epoxy resin as a base matrix. The fillers used in these benchmarks are considered IP of Isola GmbH and were therefore not disclosed. It is assumed that these are of inorganic nature, i.e., standard FR such as ATH or MDH. Table 9 shows the physical properties of these base materials (provided as cured laminates without Cu lamination!). The overall thickness of these laminates was 1.5 mm.

**Table 9 Physical properties of three commercially available FR-4 substrates that were provided from Isola GmbH. PCL 370 HR is considered the benchmark for this thesis.**

<b>Commercial Product Properties</b>	<b>DE 104</b>	<b>IS 400</b>	<b>PCL 370HR</b>
<b>Functionality of resin</b>	proprietary resin system	proprietary resin system	<b>multifunctional Epoxy resin</b>
<b>Application</b>	FR-4 for automotive / transportation	FR-4 for automotive / transportation	<b>E&amp;E, Automotive, Aerospace</b>
<b>Product Compositions per supplier SDS</b>	35 – 60 % E-glass 40 – 65 % Epoxy Matrix 0 % fillers	35 – 60 % E-glass 35 – 70 % Epoxy Matrix 10 – 25 % Inorganic Filler (SiO <sub>2</sub> )	30 – 70 % E-glass 25 - 60 % Epoxy Matrix 5 – 10 % Inorganic Filler (unknown)
<b>T<sub>g</sub> / °C</b>	135	150	<b>180</b>
<b>T<sub>d,5%</sub> / °C</b>	315	330	<b>340</b>
<b>z-CTE (pre-T<sub>g</sub>) / ppm/K</b>	70	50	<b>45</b>
<b>TC / W/mK (TDS)</b>	0.36	0.36	N/A
<b>TC / W/mK (measured via hotplate)</b>	0.250	0.385	<b>0.380</b>
<b>D<sub>k</sub> at 1GHz</b>	4.37	3.9 (at 500MHz!)	<b>4.17</b>
<b>D<sub>f</sub> at 1 GHz</b>	0.022	0.022 (at 500MHz!)	<b>0.0161</b>
<b>Moisture Absorption / 24h / %</b>	0.30	0.18	<b>0.15</b>
<b>Flammability / UL-94</b>	V-0	V-0	<b>V-0</b>
<b>Flexural Strength / MPa (length/cross-directional)</b>	579 / 448	565 / 455	620 / 530
<b>Young's Modulus / GPa (length/cross-directional)</b>	N/A	25.25/ 22.94	23.97 / 21.91

## 4.2 Processing

### 4.2.1 Processing of filled Resin Plates

The solid resin was heated up to 90 °C in an air circulating oven for 20 min. Both fillers were dried at 120 °C for 15 min to remove adsorbed water before their use. To ensure even wetting and filler dispersion, the resin, and the fillers were mixed at 200 - 250 rpm for 4 min so that the generated shear forces help in thoroughly wetting the fillers. Later, the mixing speed was lowered to 180 rpm for about 15 min. After this homogenization step, the curing agent was added, and the mixing speed was further reduced to 110 rpm to avoid the excess generation of air inclusions. This formulation was then poured into the pre-heated molds (80 °C).

The mixing parameters (*rpm, time, temperature*), *order of addition*, and *filler treatment* (drying steps to remove adsorbed water) were optimized to enhance the filler wetting and resin flow [77].

The maximum filler content for all formulations was determined as 20 vol.%. This is the maximum processable range for solvent-free prepreg production.

The mass fraction of inorganic fillers in volume percent was converted considering the different filler densities for Boehmite 2 $\mu$ m (3.07 g/cm<sup>3</sup>) and the BN 2 $\mu$ m (2.28 g/cm<sup>3</sup>) and BN 12 $\mu$ m (2.26 g/cm<sup>3</sup>). The resin and filler content were also determined via TGA.

The curing cycle of the composites was optimized with an additional post-curing step (*120 °C for 2 hr, 160 °C for 2 hr, 200 °C for 2 hr, 220 °C 2 hr*). The curing rate was evaluated as having a conversion > 99 %.

### 4.2.2 Prepreg Manufacturing

The completely *solvent-free* prepreg production was carried out on a pilot production scale EHA Composites Machinery, Germany. The resin formulations were prepared as in chapter 4.2.1. and then poured into the heated (85 °C) coating unit (Figure 48a)). The uncured resin formulations were then film coated on a siliconized release paper using the direct coating method with a 1.5 m/min production speed. The GF fabric was then introduced onto the resin film, covered with a second siliconized paper. As a release paper, a Mondi G02J1 (88wGLrh) G00J1 of the prepreg's inner and outer side was used. The actual impregnation took place in the

calander unit at 85 °C (Figure 48b)). The prepreg material is heated in the heating zone ( $T = 80\text{ °C}$ ) and then cooled and consolidated by the calander at a pressure of 5.5 bar. Finally, the impregnated fabric is cooled in the cooling zone ( $T = 15\text{ °C}$ ) and rolled up with a tensile force of 70 N. With a circular cutter of an area of  $100\text{ cm}^2$  ( $\text{weight} \times 100 = \text{g/m}^2$ ), quality control checks of the targeted prepreg areal weight were executed. If the desired areal weight was not achieved, the parameters like knife coating distance, calendar roll distance, and temperature were adjusted accordingly. The prepregs with a 200 - 220 mm width was rolled up (Figure 48c), sealed in a vacuum-bag and kept at  $-18\text{ °C}$  until further processing. The production parameters are summarized in Table 10. Table 23 (annex) shows the overall production protocols of all prepregs used in this work.



**Figure 47** Lab-scale prepreg production on an EHA composites Machinery.

The prepreg surface quality, primarily due to the high filler content, was constantly monitored. The production speed and calander roll gap distance were adapted for each system resulting in a constant areal weight of the prepreg.

**Table 10** Overview of the constant prepreg production parameters.

<b>Line Speed / <math>m/min</math></b>	1.5
<b>Tension (Liner Winding) / <math>N</math></b>	40
<b>Tension (Prepreg Winding) / <math>N</math></b>	70
<b>Fabric Tension Pull Station / <math>N</math></b>	5
<b><math>\rho_{\text{Kalander}}</math> / <math>bar</math></b>	5.5
<b><math>\rho_{\text{Pulling Unit}}</math> / <math>bar</math></b>	5.0

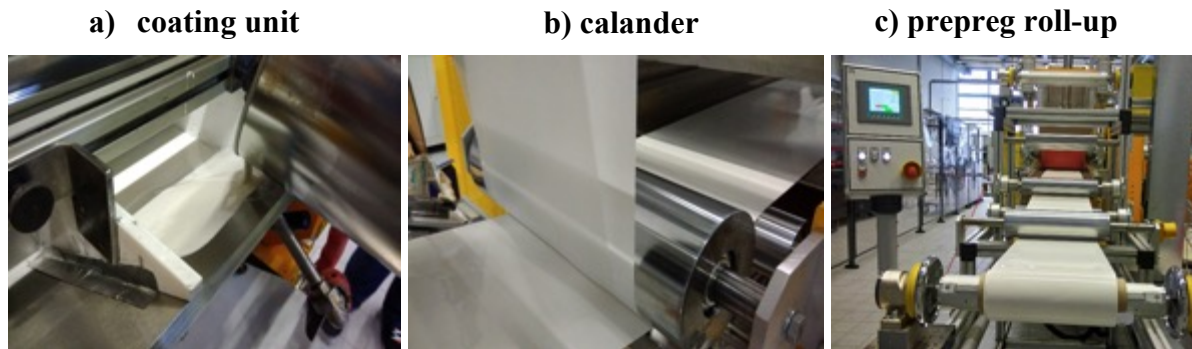


Figure 48 Detailed view of a) the coating unit, b) the calander, where the GF fabrics get impregnated with the resin formulation, and c) the prepreg roll-up for further storage.

#### 4.2.3 Production of the Laminates – *Hand-Lay-Up and Autoclave*

The prepregs were cut into 200 x 200 mm<sup>2</sup> single layers, and roughly up to 35 layers were stacked up by hand-lay-up on a steel plate. The press force used was in between 30 - 45 N.

The average thickness of the unfilled prepreg layers of EN\_GF25, EN\_GF49, and EN\_GF107 were evaluated as 90 µm, 110 µm, and 150 µm (= cured ply thickness, CPT), respectively. The filled prepregs have an average thickness of 110 µm (for the GF25), 120 µm (for the GF49), and 150 µm (for the GF 107). The prepreg lay-up was cured in an autoclave set-up according to the curing cycle under vacuum (< 25 mbar) and 3 bar air pressure (Figure 49). The detailed temperature-pressure profile can be seen in Figure 49. The laminates were cured with the same curing profile as their corresponding filled resin plates. The final laminate thickness for all systems was determined as 3 ± 0.15 mm at the 3 mm section of the laminate.

The following figure shows the autoclave set-up (Figure 50 a)) and an example of a cured sample EP\_BN12\_GF49 (Figure 50 b)) with the optimized laminate design.

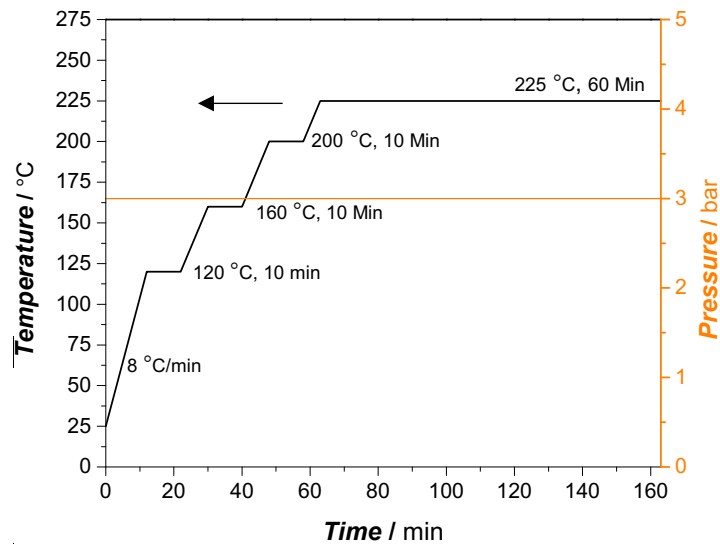


**Figure 49** Temperature-pressure curing profile for the processing of the layered prepregs into laminates.

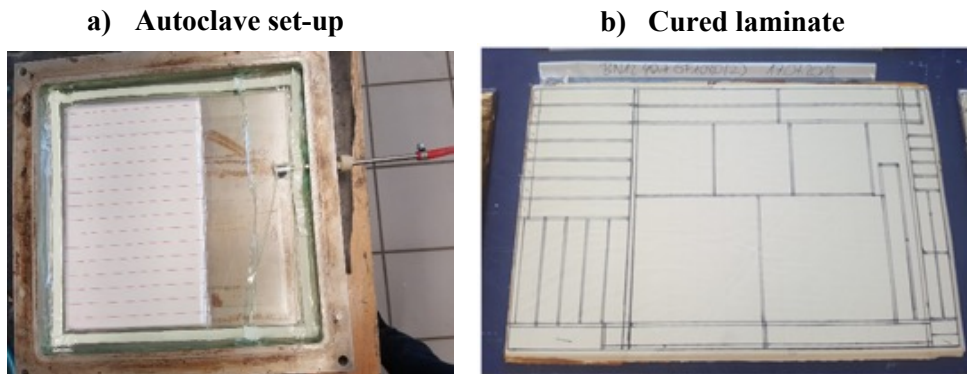


**Figure 50** a) Autoclave set-up of layered prepregs in the vacuum bag and b) the cured laminate with the respective „three-steps“ design layout, exemplarily for the EN\_BN12\_GF49 laminate.

The established completely solvent-free process in this work can be seen in Figure 51.

# Processing - Solvent-free Direct In-line Impregnation

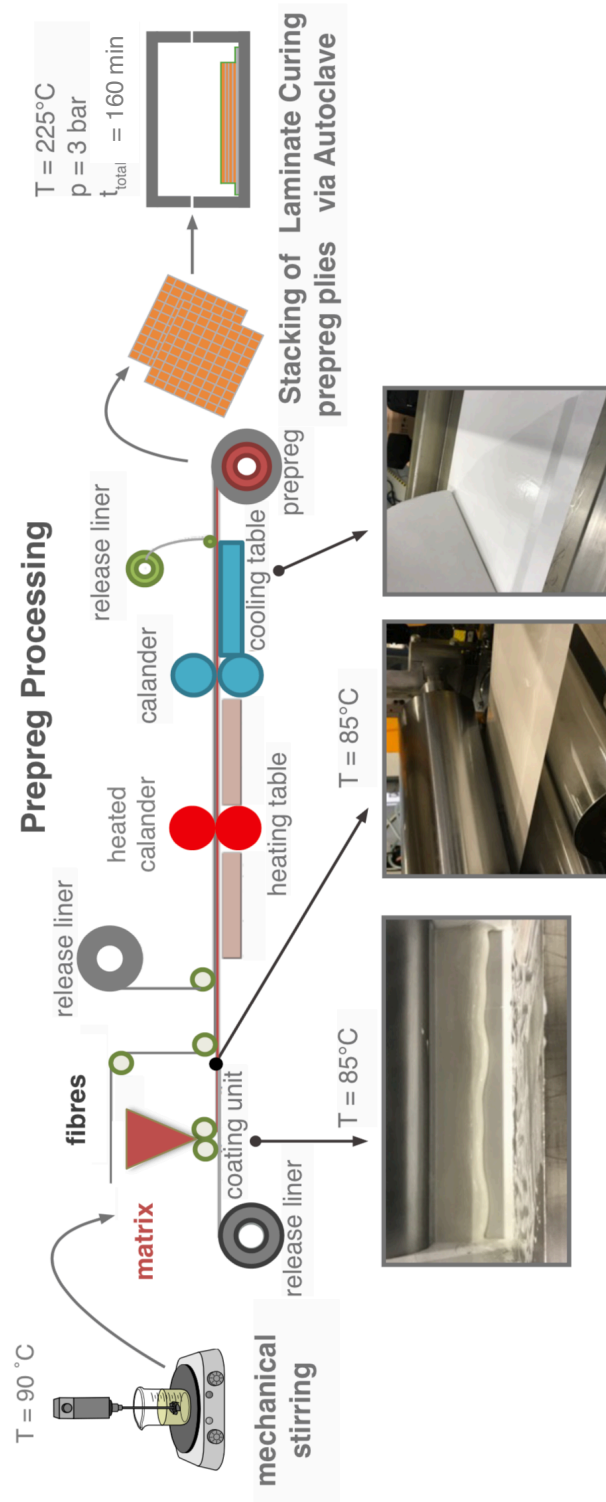


Figure 51 Schematic for the established solvent-free direct *in-line* prepreg production route, from resin formulation – and mixing to prepreg impregnation and the final cured laminate (via *autoclave set-up*).

### 4.3 Characterization Methods

#### 4.3.1 Thermo-Analytical and Physical Methods

##### Heat Conductivity and Temperature Conductivity

###### Heat-Flow Meter

Thermal conductivity measurements were carried out for the *through-plane* direction at room temperature of 23 °C using a heat flow meter Lasercomp FOX50 from TA Instruments (New Castle, United States) according to ASTM C518 and ISO 8301 (and DIN 52612) in specimens with the diameter of 60 mm and a thickness of 3 mm. The samples were polished before measuring using SiC (Silicon Carbide) grinding paper of 500, 1200, 2000 grit sizes and diamond suspensions as low as 1 µm. (Equipment: Struers, Ottensoos, Germany). Each side of the samples was ground on each paper for 4 minutes with 5 kN force and 150 rpm in an anti-clockwise direction and thoroughly cleaned in an ultrasonic bath with distilled water after each grinding step. All measurements were carried out at room temperature 23°C ± 2°C. Each sample was measured three times, and the given values in this thesis are averaged. The accuracy of the Fox50 equipment is ± 3 %, and the reproducibility is ± 2 %.

###### Transient Hot Point Sensor

The *through- and in-plane* measurement were carried out using the transient hot bridge method (THB) THB 100 of Linseis (Selb, Germany). The laminate samples (40 x 40 x 3 mm<sup>3</sup>) were cut in half at the mid-section and were stacked together, once horizontally on top of each other (for z-plane measurement) and once vertically (x/y-plane). A highly temperature-sensitive Kapton-sensor was placed in between using a thermally conductive TiO<sub>2</sub> paste. In addition, a weight of 5 kg (= 50 N) was placed on top of the sensor tip to ensure constant contact pressure on each sample. This method measures the thermal conductivity values in the x/y-plane (*in-plane*) and the z-plane (*through-plane*). The set-up was designed in collaboration with Ph.D. student Johanna Zimmermann from the Chair of Ceramic Materials (University of Bayreuth).

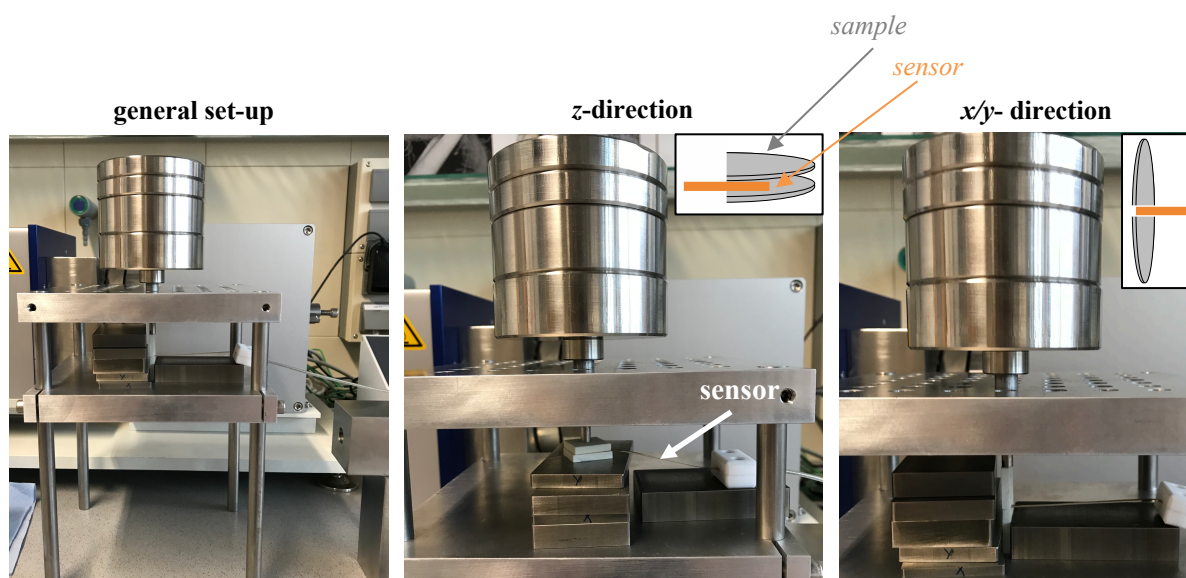


Figure 52 Experimental set-up of the THB (center: z, right: x/y).

### Thermography

Real-time *Thermographic* images and time-temperature profiles were detected with a VarioCam® hr from InfraTec, Germany. The specimens with a diameter of 60 mm and 3 mm thickness were first subjected to an 80 °C pre-heated hot plate and then cooled down to room temperature on a second hot plate set-up. The heating and cooling rates were evaluated using the analysis software *IRBIS*® 3 professional [176]. Snapshots of the movies were taken at 0, 10, 20, 40, and 80 seconds.

### Dynamic-Mechanical Analysis (DMTA)

Dynamic mechanical, thermal analysis (*DMTA*) was performed at a heating rate of 3 K/min ( $N_2$ - purge) from 25 °C- 260 °C in torsional mode at an elastic deformation of 0.1 % and an applied frequency of 1 Hz using the ARES RDA III from Rheometrics Scientific (Germany). The specimens had a rectangular geometry of 50 x 10 x 2 mm<sup>3</sup> (DIN EN ISO 6721-7). The glass temperature was evaluated using the maximum of the  $\tan \delta$  curve. The standard deviation of measured temperatures is  $\pm 0.375$  °C.

### Differential Scanning Calorimetry (DSC)

Differential Scanning Calorimetry was used to evaluate the glass transition temperature and the curing behavior. The measurements were performed under N<sub>2</sub> purge (50 mL/min) with a DSC SDTA 821e from Mettler Toledo. 10 mg of each sample was weighed in 40 $\mu$ L aluminum pans and sealed with a lid. A heating rate of 5 K/min was applied in a temperature range of 25°C to 350°C. For the uncured resin samples, the curing conversion was determined. The T<sub>g</sub> of the cured samples was evaluated with the half-step method. Each sample was measured once.

### Thermo-Mechanical Analysis (TMA)

The dimensional changes in the z-direction (coefficient of thermal expansion, CTE) of each sample were measured with a TMA Q400 EM analyzer from TA Instruments in expansion mode. The specimens of 20 x 10 mm<sup>2</sup> and 3 mm thickness were polished before testing. The measurements were carried out within a temperature range of 25 °C to 300 °C with a heating rate of 3 K/min under an N<sub>2</sub> atmosphere (50 mL/min). A force of 0.05 N was applied during the measurements. The glass transition is determined at the intersection point of two tangent lines. The z-CTE value represents the slope of the curve below and above the T<sub>g</sub>.

### Thermogravimetric Analysis (TGA)

*Thermogravimetric Analysis* (TGA) measurements were conducted using a thermo-gravimetric analyzer (TGA/STDA851e) from Mettler Toledo (Columbus, United States). The samples (15 - 20 mg) were heated from 25 °C to 600 °C under *nitrogen* atmosphere (50 mL/min) and from 600 °C to 900 °C in the *air* (50 mL/min) at a heating rate of 10 K/min to access the fiber and filler residues. To characterize *the char residue and the thermal degradation under inert conditions*, the samples (15 - 20 mg) were heated from 25 °C to 900 °C at a heating rate of 10 K/min under 50 mL/min *nitrogen* purge. The char yield was assessed at 800 °C. The standard deviation of the mass is  $\pm 0.193$ . The degradation temperatures T<sub>d,2%</sub>, and T<sub>d,5%</sub> were evaluated at 2% and 5 % reported weight loss. Each (filled) resin and their GF-reinforced laminates were tested once.

### Rheology

Rheological parameters and the gelation behavior were studied with a deformation controlled MCR 301 rheometer from Anton Paar. The dynamical characterization with a heating rate of 2 °C / min from 25 °C to 200 °C was set under an oscillatory mode at a frequency of 1 rad / s. The measurements were performed with a plate-plate geometry with a diameter of 25 mm. The gap distance between sample and plate was kept at 1 mm.

### Particle Size Distribution

The particle size distribution was determined using a CILAS Ganulometer 850HR from Chrome GmbH, Germany. The results were analyzed with the software “*Quanta*”.

### Density

The density of *cured plates* was determined by displacement method using AG245 balance kit from Mettler Toledo using the Archimedes Principle. By this method, the density of a solid sample can be calculated with the aid of an auxiliary liquid whose density  $\rho_0$  is known (water). All samples were measured in one day at room temperature of  $22 \pm 3$  °C, and the density of water at this temperature is 0.99780 g/cm<sup>3</sup>. The cured plates were weighted in the air (A) and then in water (B). The density  $\rho$  can be calculated with Equation 6.

$$P = \frac{A}{A - B} \times \rho_0 \quad \text{Equation 6}$$

The *density of the fillers* was studied with a *gas displacement pycnometer* system (helium pycnometer), AccuPyc 1330, Micromeritics Instrument Corp., USA. The accuracy for all tested specimens was  $\pm 0.01$  g/cm<sup>3</sup>.

### Water Absorption

To assess the amount of water absorbed by polymer sample when immersed in distilled water (IPC-TM 650-2.6.2.1). The dimensions of specimens used in the test were

50 mm × 50 mm × 3 mm with the edges polished. All samples were dried in the circulating air oven for 1 h at 105 °C, cooled to room temperature, weighed directly after cooling. Afterward, the conditioned specimens were placed in a container of distilled water at room temperature. The water absorption was recorded after 24 h, 72 h, one week, two weeks, three weeks, and four weeks (three samples for each formulation). The specimens were removed from the water and all surface water was removed using a dry cloth. The specimens were weighed immediately. Water content was calculated using the following Equation 7.

$$\text{increase in weight, \%} = \frac{\text{wet weight} - \text{conditioned weight}}{\text{conditioned weight}} \times 100 \quad \text{Equation 7}$$

### Dielectric Properties

The Agilent E4991A RF impedance/material analyzer was used to measure the dielectric constant ( $D_k$ ) and dielectric loss factor ( $D_f$ ) of the cured samples via the capacity method. The dimensions of specimens were 20 mm × 20 mm × 3 mm, and the testing frequency range was from 10 MHz to 1 GHz according to IPC-TM 650-2.5.5.9. To simulate the standard condition for typical applications, the composite samples were dried at 160 °C for 72 h and then kept in the climate chamber for seven days at 25 °C with 50 % relative humidity. The laminate samples were also conditioned at  $23 \pm 2$  °C and  $50 \pm 5$  % *r.h.* for one week. The samples were clamped between two electrodes and measured at the same spring pressure over a frequency range from 1.5 MHz to 1 GHz each time three times at different locations. Three samples each were tested, and the average was used. The standard deviations for the  $D_k$  are in the range of  $\pm 0.3$  and for  $D_f \pm 0.0015$ .

### 4.3.2 Pyrolysis and Fire Behaviour

#### Cone Calorimetry

A *Cone Calorimeter*, iCONE™ Fire Testing Technologies (West Sussex, UK) was used to evaluate the flame retardancy and other essential fire properties. The samples, with a geometry of 100 x 100 x 3mm<sup>3</sup>, were measured in a horizontal set-up with an applied heat flux of 35 kW/m<sup>2</sup> and 23 mm distance between sample and cone heater (Figure 53). The irradiated

surface was 96 x 96 mm<sup>2</sup>. The FIGRA value is calculated by dividing PHRR by the time to PHRR (t PHRR). All samples were conditioned according to ISO 5660-1 at 23 ± 2 °C and 45 % *r.h.* for 24 hours. Two samples of each composition were tested and averaged. The char residues were investigated as received after the cone calorimetric tests with SEM/EDX. All laminate samples were tested with the smooth surface facing the Cone Calorimeter. The cone data reproducibility was tested with three samples of the unfilled, neat EN polymer and with a filled composite sample. The reproducibility was within 1280 ± 168 kW/m<sup>2</sup> (in respect to PHRR).

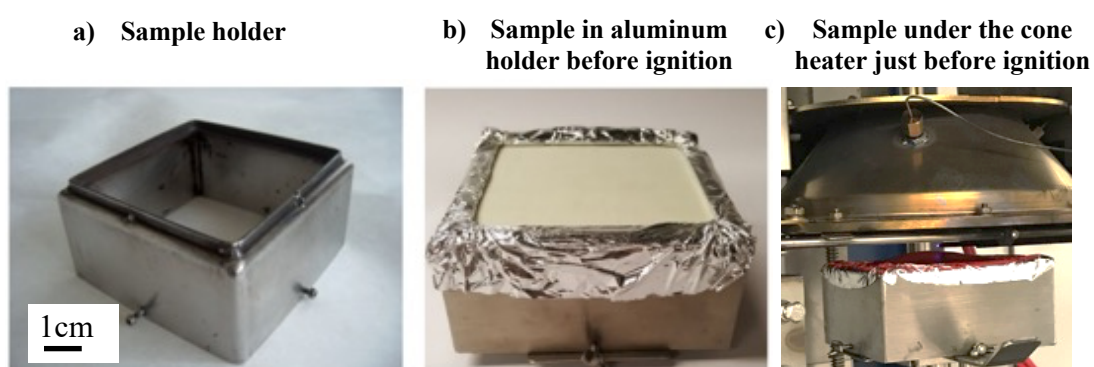


**Figure 53** a) and b) Sample preparation for the Cone measurements exemplarily of the laminate EN\_BN12\_GF49 (adapted from [157]) and c) horizontal set-up of the Cone Calorimeter. A sample before its ignition is shown.

## UL-94

The *Vertical Flame Test* is a test, samples of the geometry of 125 x 13 x 3 mm<sup>3</sup> were vertically fixed to the upper end with a tripod and ignited with a gas burner flame from the bottom. Cotton was placed 300 mm below the sample to indicate any melting drops that may drip off the sample and cause the cotton to ignite upon impact. With a small methane gas burner of about 19 mm height, a small flame was held to the sample twice for 10 seconds, with the time between fire was 10 seconds [157].

### 4.3.3 Mechanical Properties

#### Bending Properties (3-Point Bending)

A *three-point bending* test is carried out to determine the flexural properties of the filled composites (ASTM D-790-03 and DIN EN ISO 178:2003 [177]). The sample size was 80 x 10 x 4 mm<sup>3</sup>. The cut samples were conditioned at 23 ± 2 °C and 50 ± 5 % *r.h.* for 48 hours. Five specimens from each sample were measured and averaged using a Zwick Z2.5 (Zwick Roell, Ulm, Germany). The sample was placed onto two bearings at a defined distance (L = 64 mm), and a force of 2 N was applied on all the specimens with a strain rate of 2 mm/min. The elastic modulus ( $E_f$ ) and the flexural strength ( $\sigma_f$ ) were calculated according to the standard [25,177].

### 4.3.4 Morphological Characterization

#### Optical Microscopy and Hot-Stage

To study *in-situ filler network formation* of uncured resin formulations and their prepregs, a combination of optical microscopy with a hot-stage was used. A droplet of resin formulation or a pre-cut prepreg sample (5 mm x 5 mm) were placed on a microscopic slide with a coverslip on top. The microscopic slide was then affixed inside a Mettler Toledo FP82HT hot stage. The sample was heated from 25 °C to 200 °C with a 10 °C/min heating rate. Microscopic images were captured for different magnifications (2.5x, 5x, 10x, 20x, and 50x) every 5 °C increase using the DM6000 optical microscope by Leica. The images were later visually edited. To assess the morphology of the laminates, optical microscopy was employed at various magnifications. The samples were embedded in Epoxy resin (at RT) and then polished with an automatic grinder. The grinding media used: silicon carbide paper and diamond suspensions with particle sizes of 6 µm, 3 µm, and 1 µm.

#### Scanning Electron Microscopy (SEM)

*Scanning electron microscopic* (SEM) measurements for the laminates were obtained with a Jeol JSM 6510 instrument operating at 15 keV. Samples were embedded, polished (diamond suspension of 6 µm, 3 µm, and 1 µm), and then carbon-sputtered (thickness of coating: 20 nm). All micrographs are in BEC-mode (= backscatter electron composition).

*Energy-dispersive X-ray spectroscopy (EDX)* was used to study the combustion residues of the tested samples from the cone calorimetry test. These measurements were obtained on a Zeiss Leo 1530 instrument operating at 15 keV. Then the pre-conditioned samples were studied by SEM with a field emission cathode for high-resolution micrographs using 15 keV acceleration voltage and 100x magnification. The quantification of the elements was given in wt.%.

### **Ultrasound-Analysis**

*Non-destructive ultrasound* testing was performed by using HFUS 2400 (Air Tech) test machine to assess the quality of the laminates. The tests were done in distilled water at 23 °C at room temperature. A pulse-echo with a velocity of 5900 m/s and an optimized signal processing of 45 dB and adapted high- and low-pass filters were applied. The resulting defect images were created by adjusting the aperture settings for maximum visibility of material defects. C-Scans were then used to study the possible inhomogeneities (pore formation, entrapped air, filler agglomerates) within the laminate.

### **Transmission Electron Microscopy (TEM)**

TEM analysis was performed to investigate the dispersion quality of fillers in the composites. The selected samples were cut to the cube with dimensions of 10 mm × 5 mm × 4 mm, and then thin sections of 50 nm were cut on a Leica Ultracut microtome equipped with a diamond knife. The prepared samples were subjected to a bright-field TEM, LEO922 A EFTEM Carl Zeiss AG, at an acceleration voltage of 200 keV.

## 5 Results and Discussion

### 5.1 Material Selection

#### 5.1.1 Matrix

The selection of suitable polymers for PCB base materials should align with the current higher high-temperature requirements. With lead-free soldering, the short-term heat distortion temperature that the PCB base substrate must withstand without softening or degradation has increased from 180 °C to 220 °C. Although high-temperature substrates based on bismaleimide triazine, cyanate ester, polyimide, or even PTFE matrices, with a  $T_g > 220$  °C are already commercially available, their high manufacturing costs due to complex processing steps is a significant drawback [22]. FR-4 and FR-5 base materials are made of di- and multi-functional Epoxy resins resulting in  $T_g$  of  $< 200$  °C, respectively [22].

To meet this  $T_g$  requirement of  $> 220$  °C, Epoxy Novolac (EN) resin as a new thermoset matrix has been established. Curing with a suitable curing agent can result in glass transition temperatures well above 200 °C. In this thesis, Epoxy Novolac cured with the aromatic DETDA (diethyl toluene diamine) is used as a matrix resin for the PCB base material to achieve excellent thermo-mechanical properties for the PCB base material. Epoxy Novolac, which is already used for PCB applications, was selected based on the resulting  $T_g$  values, low water absorption, and chemical resistance compared to other thermosets. Due to their aromatic structure, their fire and smoke properties are excellent with high dimensional stability. The overall ignitability of Epoxy Novolac is known to be delayed compared to other thermosets [30,32].

The very low viscosity of DETDA as a curing agent aids by mixing with EN in reducing the absolute viscosity of the resin-hardener mixture, which helps in incorporating higher filler loadings. The advantage of aromatic amines is their higher  $T_g$  and better chemical and thermal properties compared to aliphatic amines [25]. The curing of EN with DETDA leads to  $T_g$  usually  $> 177$  °C and even higher with the right curing program, including post-curing steps [178]. The reduced viscosity of the DETDA curing agent compared to phenolic resins is based on the nature of the intermolecular interactions they form. While phenolic resins can form intermolecular hydrogen bonds, the intermolecular binding forces of the DETDA are based on the weaker van der Waals forces.

The temperature-dependent viscosity of EN mixed in a stoichiometric ratio with DETDA is plotted in Figure 54. The viscosity characteristics are typical for Epoxy resins. With increasing temperature, the viscosity decreases until the offset of the crosslinking starts. The curve follows a minimum at 110 °C with a viscosity of 2.5 Pa·s and a maximum of  $4.86 \cdot 10^6$  Pa·s at > 160 °C. The process range for the prepreg pilot line at the University of Bayreuth has a range for viscosities between 50 mPa·s and 200 Pa·s. For this resin system, the cut-off temperature would be at ~ 140 °C.

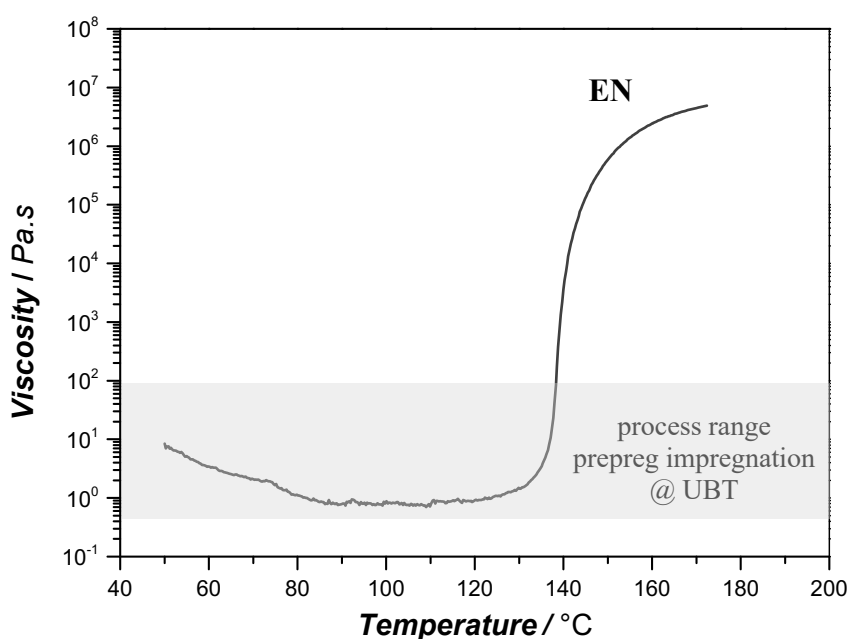


**Figure 54** Viscosity of the unfilled Epoxy Novolac (+ DETDA) in dependency of temperature.

As a first experimental step in this thesis, the curing cycle will need to be optimized for the processing of prepregs, taking into account the overall  $T_{\text{Processing}}$  of < 230 °C. Figure 55 shows DSC measurements of the uncured EN (EN+DETDA) and the curves for the cured samples. A curing profile was suggested by the supplier (curing cycle 1 in Figure 55). A second curing cycle with an additional post-curing step at 220 °C for 2hr (curing cycle 2) resulted in almost a horizontal curve indicating a conversion rate of > 99%. Curing cycle 2 was implemented for all (filled) resin formulations and their laminates. The onset temperature of the curing reaction between DETDA and EN starts at < 100 °C reaching a maximum at 180 °C.

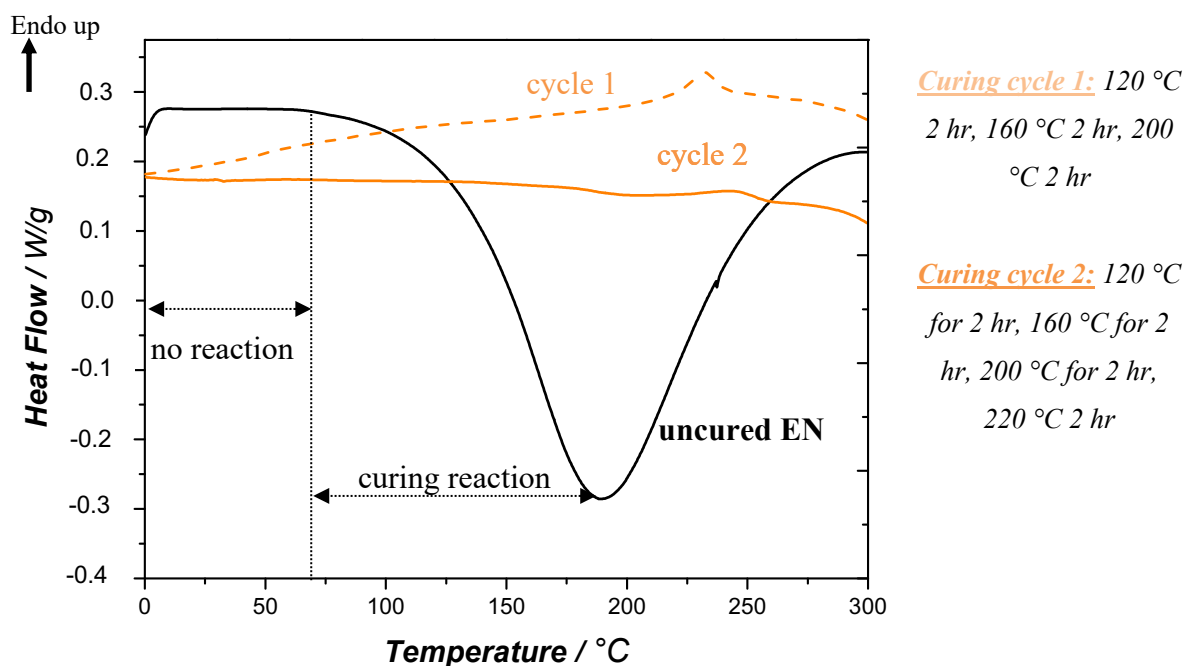


**Figure 55** Differential Scanning calorimeter thermograms of uncured and cured EN for selecting the optimal curing rate.

In conclusion, for the prepreg processing, according to the viscosity plot and DSC results, a temperature window of below 90 °C must be chosen to impregnate the fibers fully with the resin. In the case of filled resins and the prepregs, curing cycle 2 will result in the desired high  $T_g$  range of > 220 °C in the laminates.

Table 11 shows the thermal (-mechanical) properties of Epoxy Novolac (DEN 438) cured with DETDA (= EN). The resin system offers a  $T_{g,DMA}$  of 242 °C, which is well above the desired target of > 220 °C. Measurements with TMA and DSC resulted in  $T_g$  of 233.1 and 233.3 °C, respectively.

The z-CTE (*pre- $T_g$* ) is 71.40 ppm/K. The mechanical properties were also evaluated:  $E_{bending}$ -modulus resulted in 3,050 MPa, the  $K_{IC}$  in 0.63 MPa $\cdot\sqrt{m}$  and a  $G_{IC}$  of 122.05 J/m<sup>2</sup>. The amine-cured, multifunctional EN resin has a brittle nature. Due to the aromatic and the phenolic ring structure, the thermo-mechanical performance is higher but results in low fracture toughness. In addition, the intrinsic thermal conductivity is very low, with a value of 0.199 W/mK, due to its polymeric nature.

**Table 11 Thermo (mechanical) properties of DEN 438 cured with DETDA (=EN).**

Properties	T <sub>g,DMA</sub> / °C	Thermal Conductivity / W/mK (hot-plate)	D <sub>f</sub> @1 GHz	D <sub>k</sub> @1 GHz	Water absorption / 24h
EN	242.7	0.199	0.02303	3.634	0.157

### 5.1.2 Fillers

Based on the motivation of this thesis, the substrate material must be able to dissipate heat. It is known from the literature that the addition of thermally conductive fillers, such as Boron Nitride (BN), is helpful to fulfill the requirements. Boron Nitride (BN) is well-known for its excellent thermal conductivity and its lubricious rheological properties. Three sizes of *h*-BN were chosen: 2 μm, 12 μm, and 45 μm. The detailed investigations and results can be found in chapter 5.2.2.

*Electrically insulating* and non-harmful fillers were selected for this Ph.D. study. Boehmite (BT), a FR filler, is currently “trending” in the PCB market. Boehmite is an intermediate product of the degradation of ATH to Al<sub>2</sub>O<sub>3</sub>. Although ATH has more water bound and has a higher ability to interact with the gas-phase during combustion, its degradation temperature, T<sub>d</sub>, is much lower (ca. 230 °C) than Boehmite (ca. 350 °C). ATH would not be able to withstand the lead-free assembly processing and initiate early material failure.

Initially, three different Boehmite filler sizes were chosen, a nano-size and two 2 μm-sized filler sizes with different geometry (TEM micrographs in Figure 57). The thermal conductivity results and their corresponding microstructure results can be found below (Figure 56). The highest thermal conductivity (*through-plane*) values at 45 wt% filler content (~ 15 vol.%) were achieved with the Boehmite 2 μm *platelet* (0.45 W/mK (125 % increase)) and 0.38 W/mK (90 % increase) for the *nano*-sized as compared to neat Epoxy (0.20 W/mK). Comparing the results of all the fillers, the thermal conductivity of composites filled with **BT 2 μm-platelet (=BT2)** was slightly better than the other Boehmite filler geometries. This can be attributed to the high aspect ratio of the platelet shape of the filler. It provides a higher surface area in contact with the polymer matrix, thus promoting phonon transfer through the composite by reducing interfacial thermal resistance [125]. The corresponding TEM micrographs (Figure 57) show

that a conductive filler network was indeed established. The nano-sized filler is well distributed but does not form any contact point to enable an efficient heat distribution. The evaluation of flame retardancy can be found in chapter 5.2.3.

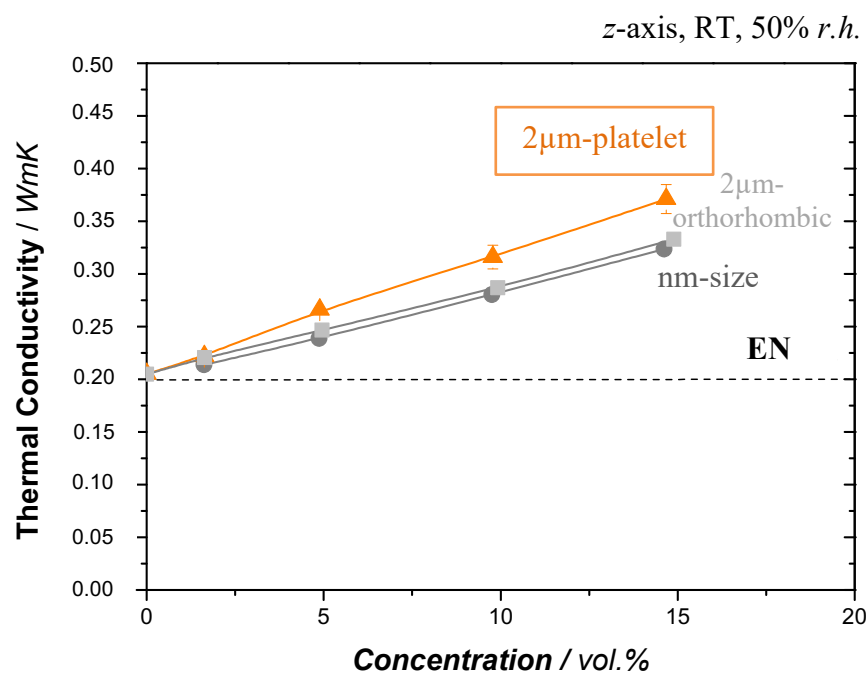


Figure 56 Thermal conductivity of different Boehmite fillers at 15 vol.% (approx 45 wt.%) content in Epoxy Novolac.

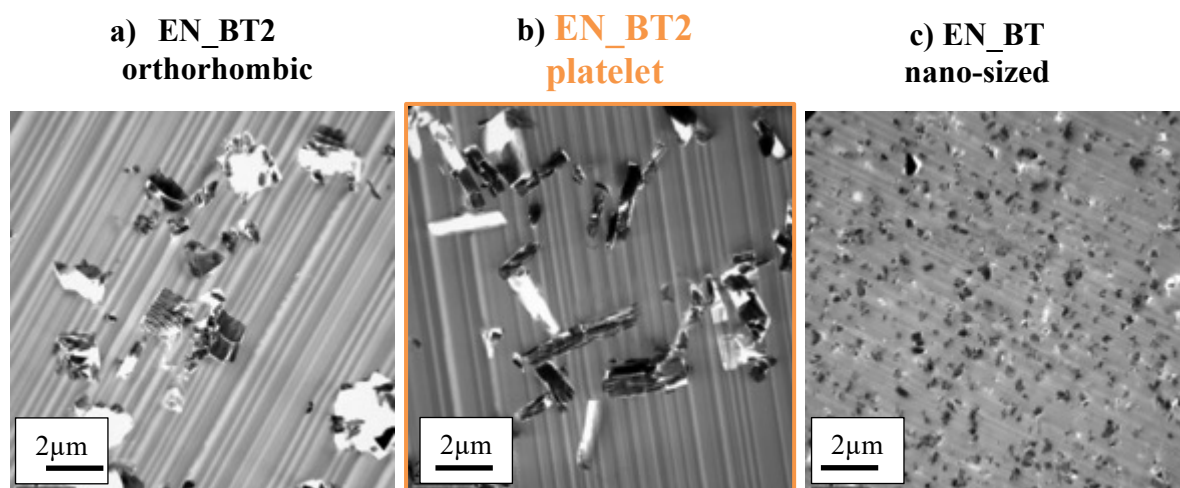


Figure 57 TEM micrographs of various BT-filled ENresins at 45 wt.% content. a) EN\_BT2-orthorhombic ( $\approx 14.6$  vol.%), b) EN\_BT2-platelet ( $\approx 14.7$  vol.%) and c) EN\_BT nano-sized ( $\approx 14.9$  vol.%).

## 5.2 Processing of filled Resin Plates and their Thermal Properties

### 5.2.1 Process Optimization – *filled Resin Formulations*

To process the above-selected materials, the process from mixing to curing needed to be optimized. Overall, the *maximum filler content was set to a maximum of 20 vol.% (~ 45 wt.%)* for the BN fillers to ensure optimal processing and impregnation with the prepreg line. All fillers were dried at 120 °C for 15 min before their use to remove adsorbed water.

The mixing parameters (*rpm, time, temperature*), *order of addition*, and *filler treatment* (drying steps to remove adsorbed water) were optimized to enhance the filler wetting and resin flow.

Firstly, the solid resin was heated up to 90 °C in an air circulating oven for 20 min. To ensure even filler wetting and filler dispersion, the resin and the fillers were mixed at 200 - 250 rpm for 4 min. The generated shear forces reduce in thoroughly wetting of the fillers. After that, the mixing speed was lowered to 180 rpm for about 15 min. After this homogenization step, the curing agent was added, and the mixing speed was further reduced to 110 rpm to avoid the excess generation of air inclusions. This formulation was then poured into the pre-heated molds (80 °C) to support the formulation to flow and distribute within the mold evenly.

### 5.2.2 Optimization towards the desired Thermal Conductivity

#### Influence of Filler Nature

The *z*-thermal conductivity range of the neat (= unfilled) Epoxy Novolac resin (EN) was evaluated to be 0.1995 W/mK in the previous chapter 5.1.1. In addition, it was found that the optimal size resulting in the highest achievable thermal conductivity for the flame retardant is the *2 μm-sized Boehmite with a platelet shape*. According to the *State-of-the-Art*, a platelet geometry presents the most efficient network formation.

The thermal conductivity (TC) of both the platelet-shaped 2 μm Boehmite (BT 2) and the 2 μm Boron Nitride (BN 2) are plotted as a function of their filler content in Figure 58.

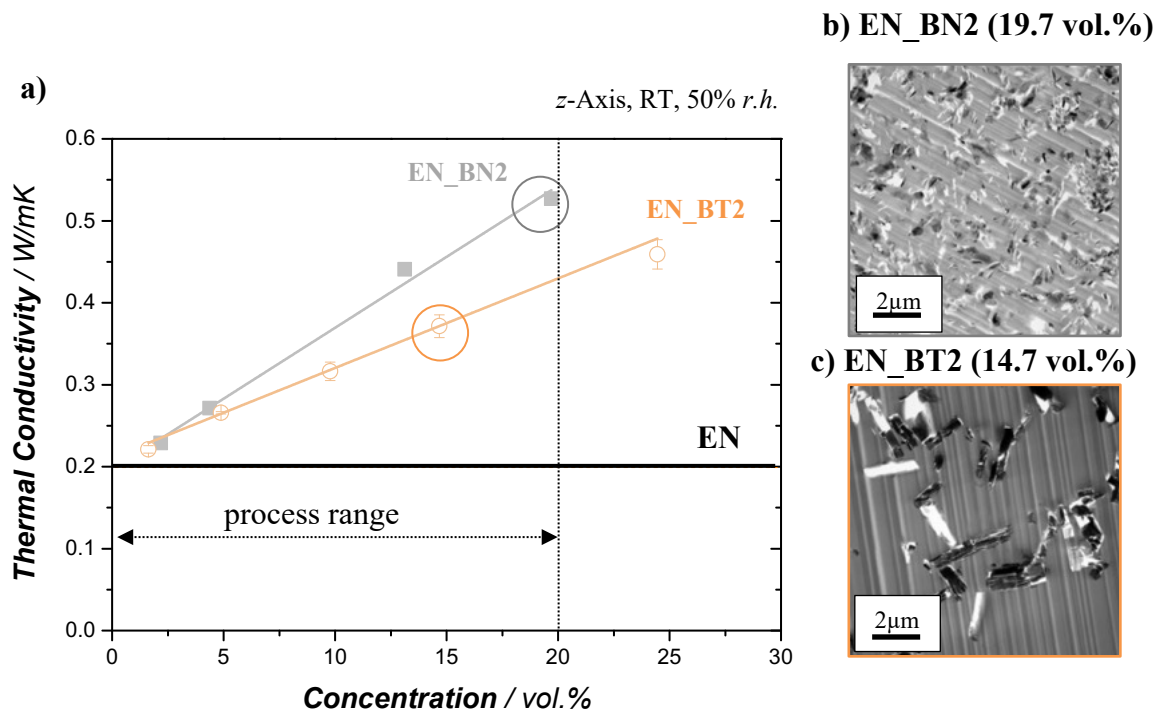
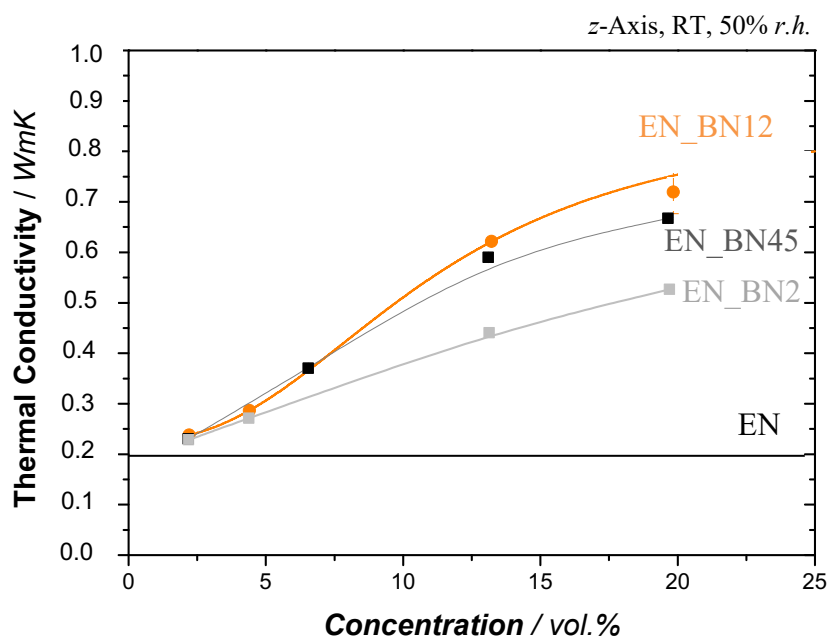


Figure 58 a) Effect of filler nature on the thermal conductivity of filled EN resins depending on filler concentration. b+c) corresponding TEM micrographs of the filler network of b) EN\_BT2 and b) of EN\_BN2 at 45 wt.% (~ 20.vol.%) filler concentration.

The individual addition (= *unimodal distribution*) of Boehmite (BT) and Boron Nitride (BN) to an Epoxy Novolac (0.199 W/mK) shows that the thermal conductivity of the composite was improved with increasing content (Figure 58). The BN2 platelets have a higher impact on the thermal conductivity than the 2 μm BT, resulting in 0.53 W/mK. The TC of BT 2 at 20 vol.% is 0.42 W/mK. The TEM micrographs in Figure 58 show that both fillers are well and dispersed, with a random orientation. The TC value of BN2 is higher than Boehmite, which is mainly governed by its higher intrinsic TC due to its crystal structure. Also, to some extent, BN2 tends to form more agglomerates than BT2, resulting in higher scattering effects of thermal heat. This effect is well-known in literature and is caused by the fillers' difference in *intrinsic thermal conductivity*. The above results are in alignment with findings in literature - from Zhang *et al.* [179], Duwe *et al.* [180], Chiang *et al.* [94], and Yung *et al.* [77].

### Influence of BN Concentration and BN Lateral Size

The effect of increasing *content* and different lateral *BN platelet sizes* and their content in Epoxy Novolac were evaluated in Figure 59 and Table 12. The highest TC results were achieved with BN12 at 19.7 vol.% with a TC of 0.719 W/mK. These results in Figure 59 suggest an *optimum filler size of BN12*.



**Figure 59** Effect of different lateral BN platelet sizes on the *z*-thermal conductivity of EN as a function of filler concentration.

The increase in TC is not only influenced by the filler content but also strongly triggered by the filler aspect ratio (AR) and the BET (*Bauer–Emmett–Teller/theory of gas adsorption on solid surface*) of the BN. The larger the lateral length (diameter) of BN platelets, the higher their AR, resulting in a higher TC. The BET shows a contrary trend, which is decreasing with increasing AR. Moreover, the larger the surface area of the BN fillers, the smaller is their interfacial area shared with the Epoxy Novolac matrix, and the smaller is the TC resistance [135]. Furthermore, the surface appearance affects as well (SEMs in Figure 60).

**Table 12** z-Thermal conductivity of the BN-filled EN resins at 45 wt.% (~ 19.7 vol.%) with varying AR.

Composition	Filler Concentration / vol.%	$\lambda$ / W/mK z-direction	BET / m <sup>2</sup> /g	Aspect Ratio
EN	-	0.19	-	-
EN_BN 2	19.7	0.53	20	16
EN_BN 12	19.8	0.72	7	18
EN_BN 45	19.6	0.66	1	23

Figure 60 shows the microstructure of the EN\_BN2, EN\_BN12 and EN\_BN12 filled resins. The micrographs show a random dispersion and distribution of the BN platelets independent of their aspect ratio at a fixed 19.7 vol.% ( $\pm 0.1$  vol.%) filler concentration in the EN matrix.

At concentrations  $< 5$  vol.%, the barrier effect of the polymer matrix (EN) limits the phonon transport. At a critical filler content of  $> 15$  vol.%, the increase of the thermal conductivity is more prominent. Similar findings were published by Yung *et al.* [77]. They found a critical concentration of various BN filler sizes at ca. 20vol.%. An interfacial bonding between the BN and the matrix seems to be established at the platelet edges, where -OH groups are present. Furthermore, the interparticle distance is much lower, which leads to a misalignment/rotation of the platelets in the direction of flow. A random filler orientation is established (Figure 60), which helps explicitly the heat transport in the z-direction.

BN2 shows a much lower increase in TC as the heat spread is hindered by the scattering effects at each material boundary of the formed agglomerates. Furthermore, it was observed that the viscosity of resins containing BN2 and BN45 was higher, and therefore, filler incorporation and wetting were more difficult. It was observed that the BN45 particles tend to get broken during the processing of the formulation, which was even more evident during the prepreg production and impregnation. **Therefore, these two fillers were not considered moving forward in these studies.** The smoother, more planar surface of **BN 12 is more effective in thermal transport** due to fewer scattering effects.

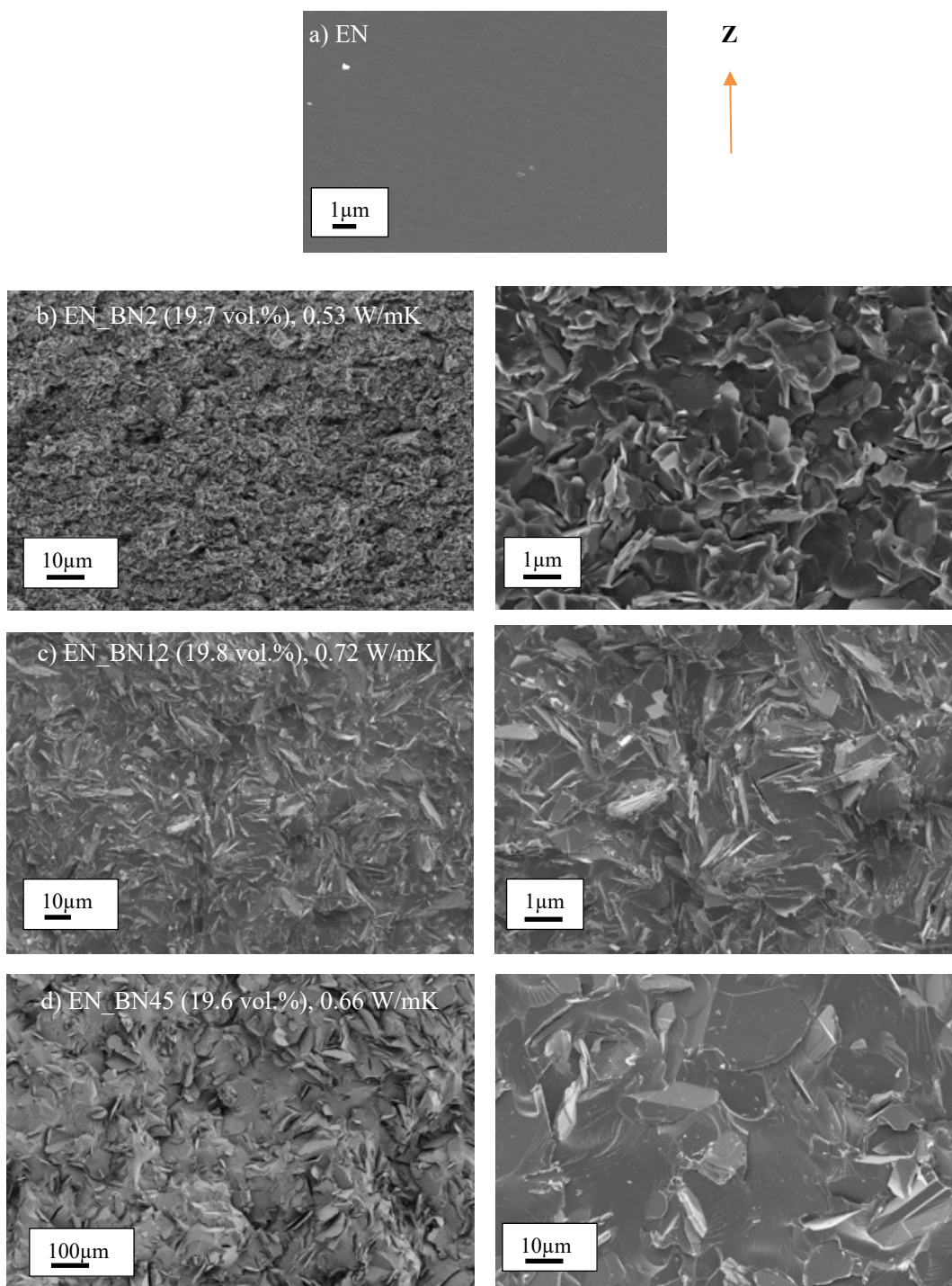


**Figure 60 Influence of the BN platelet aspect ratio on the conductive filler network formation. The SEM micrographs show a) unfilled EN b) EN\_BN2 (19.7 vol.%), c) EN\_BN12 (19.8 vol.%) and d) EN\_BN45 (19.6 vol.%).**

A theoretical model based on *Hatta-Taya* was employed to confirm the above experimental TC results (*z-direction, via heat flow meter*) and the corresponding morphological observations. The Hatta-Taya model includes the actual filler geometry in its equation and is, therefore, more accurate than other theoretical models. This model predicts the “*ideal*” thermal conductivity for platelet-shaped fillers for *in-* and *out-of-plane* orientation, in the *direction of the BN plane* and perpendicular to it (equations 5 and 6). The boundary conditions were defined with 0.1995 W/mK for the TC of the EN matrix, 200 W/mK as TC for the BN, the average platelet length of 15  $\mu\text{m}$ , and thickness of 0.84  $\mu\text{m}$  (evaluated with the help of SEM micrographs of the filler). Figure 61 shows the thermal conductivity results in dependency of the concentration, exemplarily for the EN\_BN12. The linear fits of all three plotted lines, *out-of-plane*, *experimental* and *in-plane*, resulted in an  $R^2$  of  $> 0.98$  for the theoretical values and  $R^2$  of  $> 0.97$  for the experimental, data indicating good approximation. The experimental TC values, especially at higher concentrations, are precisely within the values of the calculated boundaries of 100% *z*-plane versus an orientation 100% *x/y*-plane. This model, therefore, confirms the apparent *random orientation* per the SEM micrographs.

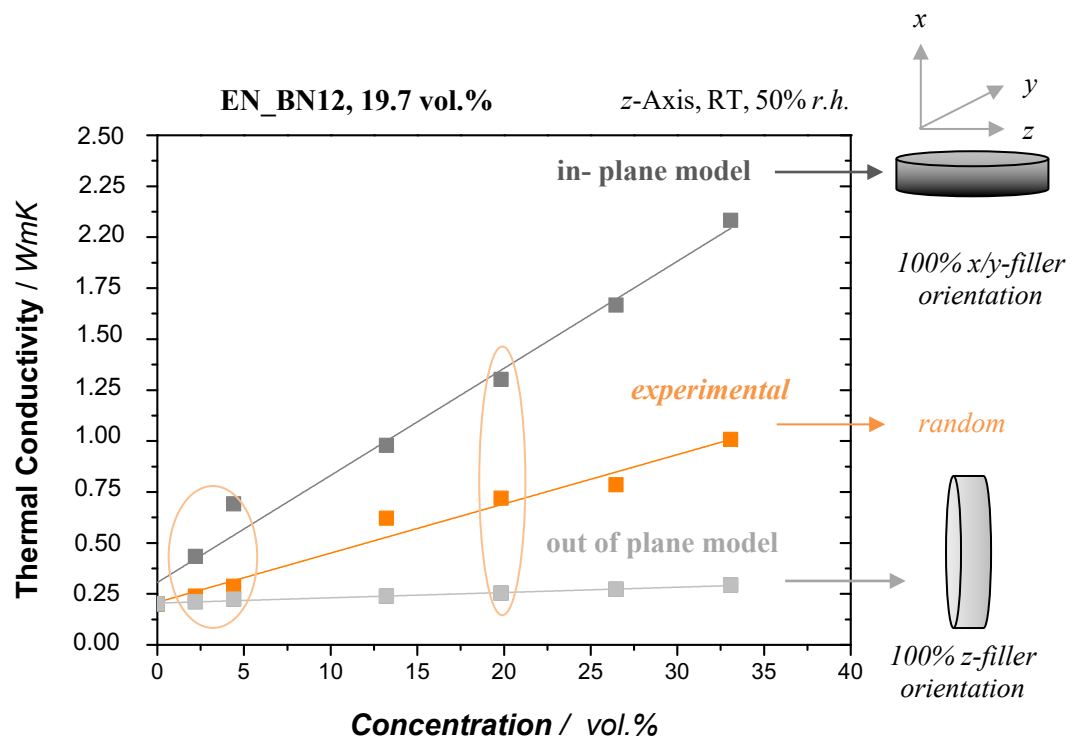


**Figure 61** Thermal conductivity comparison of the experimental and theoretical values based on the *Hatta-Taya* model, exemplarily for the EN\_BN12-filled resin in dependency of concentration.

### Evaluation of Filler Combinations and the Variation of their Ratios

Subsequently, the influence of *filler combinations and their ratios* were studied to improve the overall packing density. In the previous chapter, BT 2 and BN 12 were selected based on their TC results.

By incorporating both 2  $\mu\text{m}$  and 12  $\mu\text{m}$  BN-platelets (= bimodal combination), the packing density of the fillers can be tailored in a smart way, and therefore, the heat transport through the filled resin bulk volume can be optimized. Furthermore, substituting 2  $\mu\text{m}$  BN-platelets with 2  $\mu\text{m}$  Boehmite-platelets (= hybrid combination) shows the *potential to simultaneously establish a low-cost and thermally conductive and flame-retardant-filled resin*. The evaluation of the TC of the bimodal combination of BN (= BN2 and BN12) and the hybrid combination of BN with the flame-retardant Boehmite (= *hybrid*, BT2 and BN12) is shown in Figure 62. The results of the bimodal and hybrid combinations are at a constant filler content of 45 wt.% (= 18.3 / 19.8 vol.%). The corresponding SEM micrographs of the highest TC values are shown below in the graphs.

The thermal conductivity of both formulations, bimodal and hybrid, is higher than their corresponding unimodal formulations (**grey data points**). There is a maximum value for the TC in both cases, which directly correlates with the BN filler size. The thermal conductivity at constant 45 wt% filler content was increased from 0.59 W/mK (unimodal 12  $\mu\text{m}$  BN) to 0.66 W/mK for the bimodal BN combination, BN2 and BN12 (1:1 ratio). Furthermore, the relative composition ratio variation from 1:1 to 1:3 by increasing the BN12 fraction, an even higher TC value was achieved (0.71 W/mK).

The substitution of the BN2 with the Boehmite 2  $\mu\text{m}$  (*hybrid combination*) shows a similar trend. The relative combination of 1:3 Boehmite 2  $\mu\text{m}$  with BN12 in the 45 wt.% formulations (= 18.3 vol.%) leads to an increase from 0.66 to 0.81 W/mK.

The corresponding microstructure shows a homogeneous filler dispersion in the SEM micrographs with random orientation of the BN12 platelets. It can be assumed that the heat path is established mainly with the inter-filler contact of the BN12 platelets at or above the critical filler concentration. These larger BN ellipticals have a slight tendency to be more oriented in z-direction. This leads to a higher heat transfer in the vertical plane of the sample since the intrinsic TC of the BN platelets is strongly dependent on the BN orientation (also see illustration in Figure 61). In both cases, the smaller 2  $\mu\text{m}$  particles fill the gaps between the larger platelets.

With the larger platelet size, the probability for inter-filler contact is higher and, therefore, more likely that form a uniform conductive network is formed. The larger BN12 platelets form the main micro-structure, and the smaller platelets fill the gaps in between, which leads simultaneously to an increase in the packing density but also a higher TC.

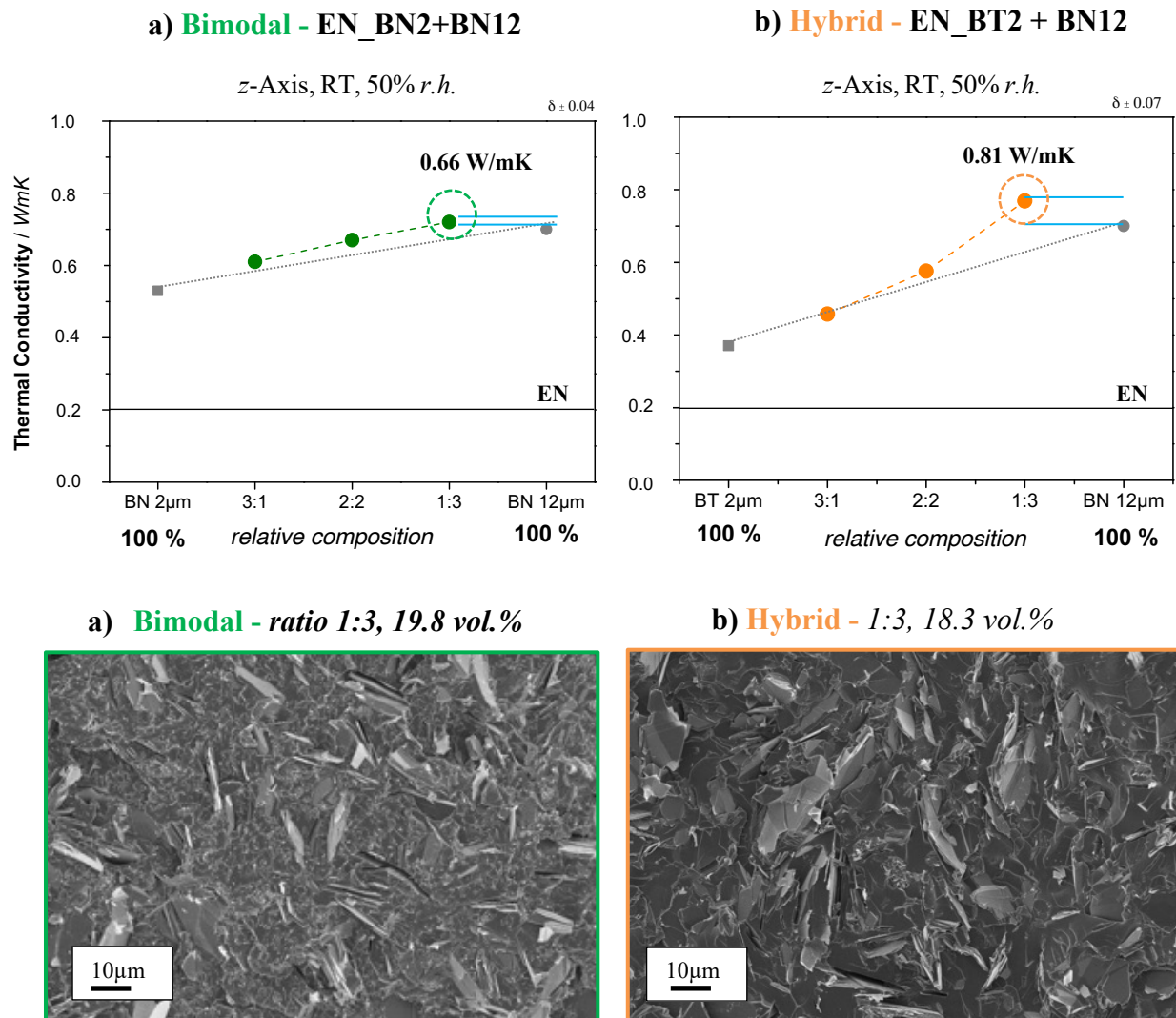
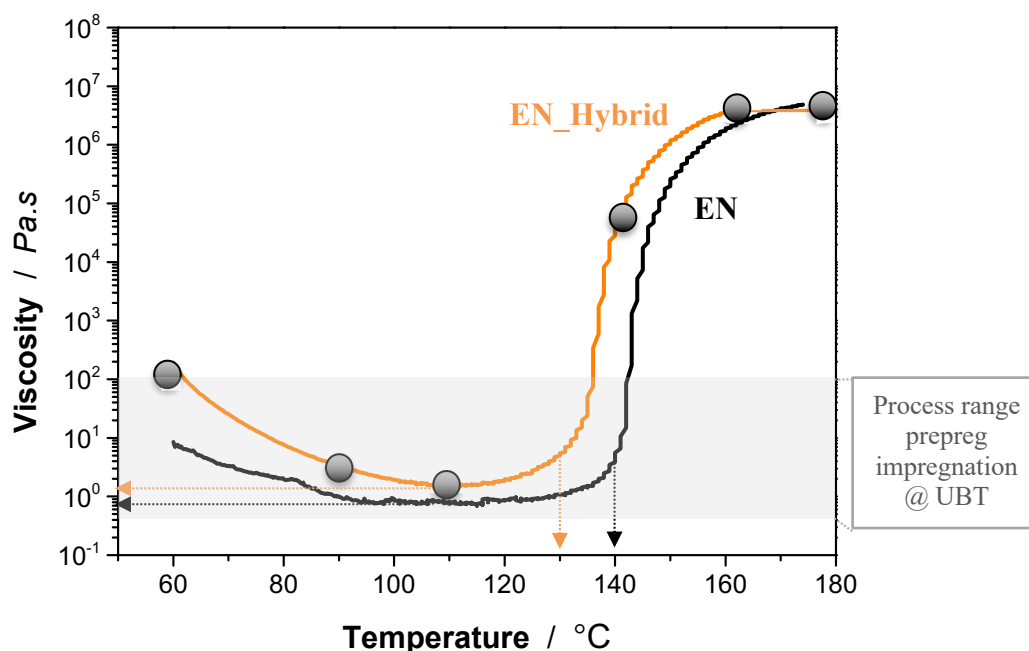


Figure 62 *z*-plane thermal conductivity results and corresponding SEM micrographs of a) EN\_Bimodal and b) EN\_Hybrid. (ratio 1:3 = 2 µm : 12 µm filler size)

### Influence of Fillers on Viscosity and Network Formation - *In-situ Hot Stage Microscopy Study*

To understand the temperature-dependent formation of the filler network, the microstructure of the EN\_Hybrid formulation was studied. With the help of *in-situ* hot-stage optical light microscopy, optical micrographs were taken during the cross-linking reaction. The images were taken at 6 different temperature stages (marked in Figure 63) of this hybrid formulation. The corresponding viscosity plots for the neat EN and the EN\_Hybrid are shown in Figure 63.



**Figure 63** Viscosity plot of the unfilled EN and EN\_hybrid formulation. EN\_Hybrid was studied with *in-situ* hot-stage microscopy, and the highlighted temperatures represent the microscopic images taken.

Firstly, the introduction of both fillers into EN does influence the overall viscosity. The minimum viscosity was evaluated to be at 110 °C. The curve progressions for both unfilled EN and the EN\_Hybrid are similar. However, the onset of the curing reaction is about 10 °C lower for the hybrid formulation (130 °C for hybrid vs. 140 °C for the unfilled EN). With temperatures below < 90 °C at the coating unit, both resin formulations can be processed with the prepreg line as both are within the processable viscosity range of 50 mPas to 200 Pas.

To study the filler network formation during the thermally induced curing reaction, a microscopic image was taken at the lowest temperature at 60 °C (Figure 64). At this stage A, the hybrid formulation shows an excellent *random filler dispersion and distribution*, which was only achieved by the process optimization as explained in chapter 5.2.1. At this temperature, the resin viscosity of the formulation is high, with no resin mobility at all. With the temperature increase to 90 °C, the viscosity slowly starts to decrease. The fillers are still immobile and show an overall random dispersion. At 110 °C, the resin viscosity reaches its minimum. With this onset of resin mobility between 90 °C and 110 °C, the fillers slowly begin to move (Figure 63c)) At this stage, an initial *agglomeration* can be noticed. Reaching 135 °C (stage D), the *gelation* is initiated. The fillers *self-assemble*, and *self-aggregate* are forming a continuous network (indicated by the arrows) as their intrinsic attractive forces are higher than the shielding forces of the matrix. The filler-filler interaction causes a filler rotation and changes to their prior orientation. At stages E and F at temperatures > 160 °C, the viscosity reaches its maximum during the crosslinking reaction. The filler network is “*locked-in*”. The microscopic image in polarized mode (Figure 65) shows that the SEM images in Figure 62b) can be correlated to the findings in the previous chapter: BN12 (green particles) help to establish the main “skeleton” of the network structure, whereas the BT2 fillers assemble into the gaps or adhere to the BN platelets.

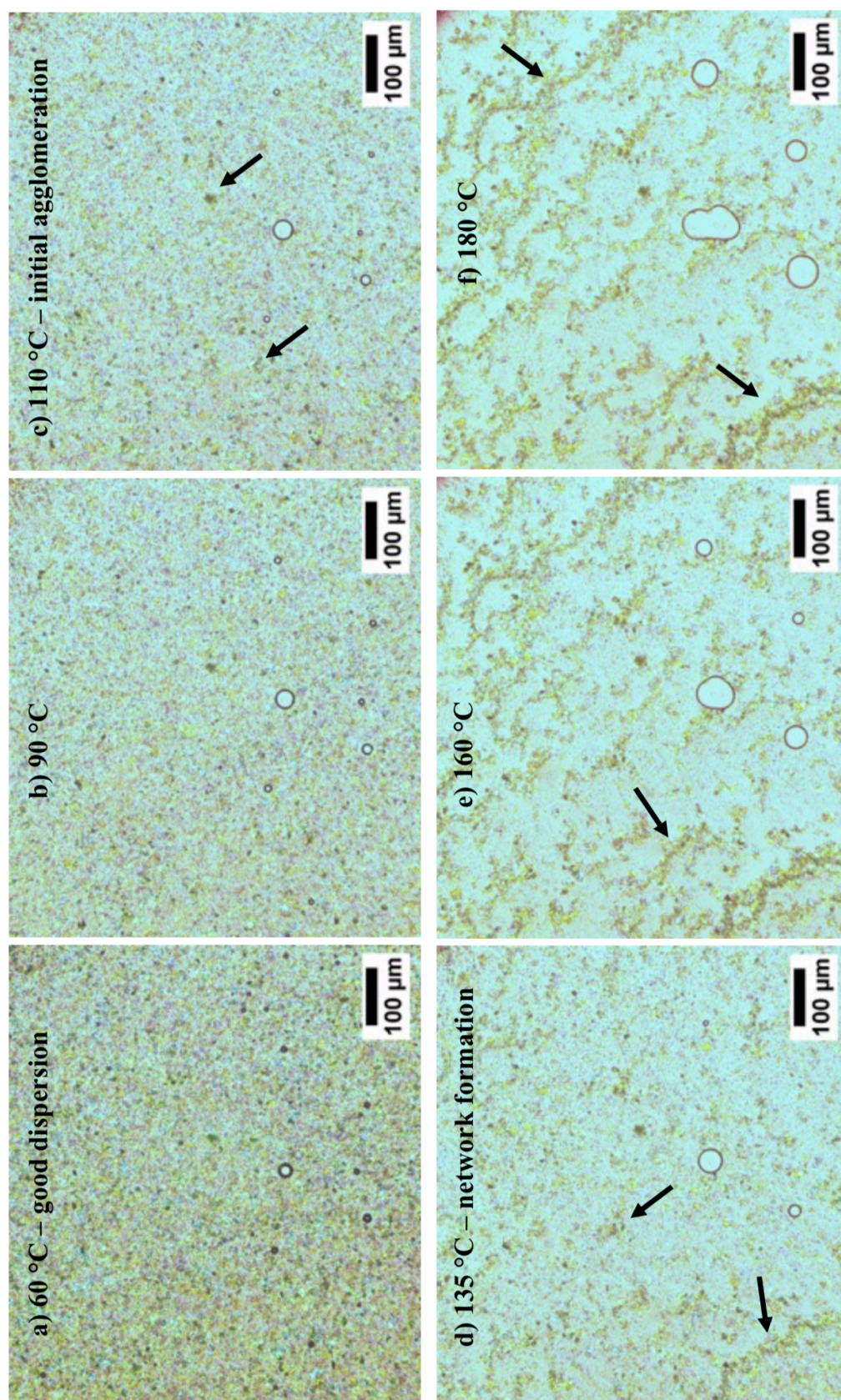
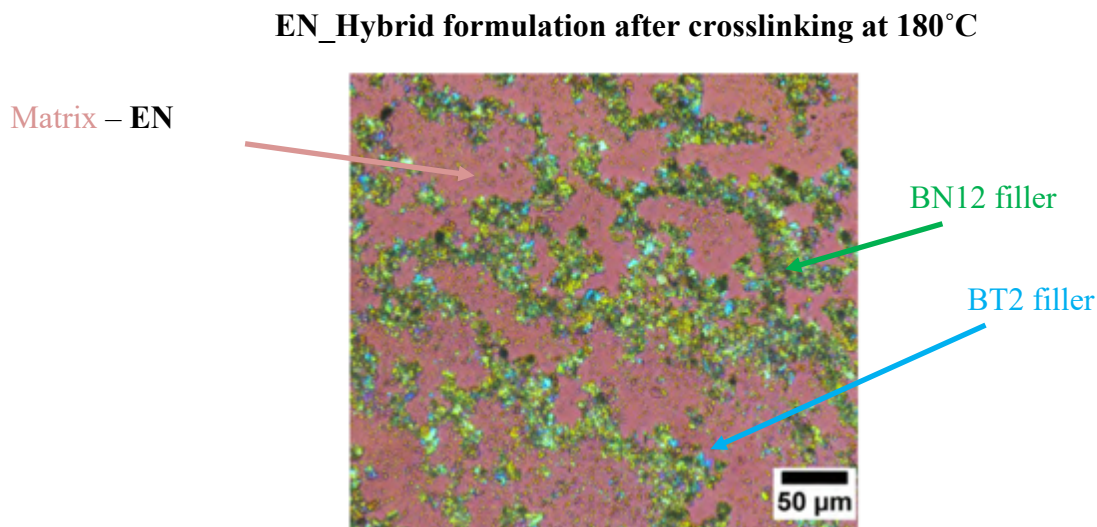


Figure 64 *In-situ* Hot-Stage Microscopy images of the EN\_Hybrid formulation (10x magnification).



**Figure 65** Optical micrograph of the cured state of the EN\_Hybrid formulation in *polarized mode*.

### **Influence of apparent Filler Network Formation on the $z$ - and $x/y$ -Thermal Conductivity**

The TC findings, measured with the heat flow meter in the  $z$ -direction, were further verified with the THB (Figure 66). The advantage of the THB is that the TC can also be measured in the  $x/y$ -axis, whereas with the heat flow meter, the measurements are strictly restricted to the  $z$ -plane only.

The direct comparison of the TC results measured with THB for both  $z$ - and  $x/y$ -directions is shown in Figure 66.

The results indicate that in the  $z$ -direction, the TC is slightly higher than the results perpendicular to it ( $x/y$ -direction). The linear trends for the fillers and their combination can be described as  $y = ax + b$  with a slope ( $= a$ ), intercept  $b$  at 0.2 for the EN matrix. The  $R^2$  for all systems is  $> 0.99$ . The linear fits are in good correlation with the measurements with the heat flow meter in the  $z$ -plane. The THB results for both planes show a similar trend.

In summary, these filled resins show a 3-directional heat spread, aligning with the overall target (chapter 3). Current State-of-the-Art base materials are restricted to 2-directional heat management. FR-4 base materials have a TC of 0.25 - 0.3 W/mK in  $z$ -plane and 0.6 - 0.8 W/mK in  $x/y$ -plane [18].

Literature results also can strongly vary based on the type of gauge and the measurement techniques. Quite often, results are based on simply applying pressure on the samples. Higher pressures can alter the TC result positively.

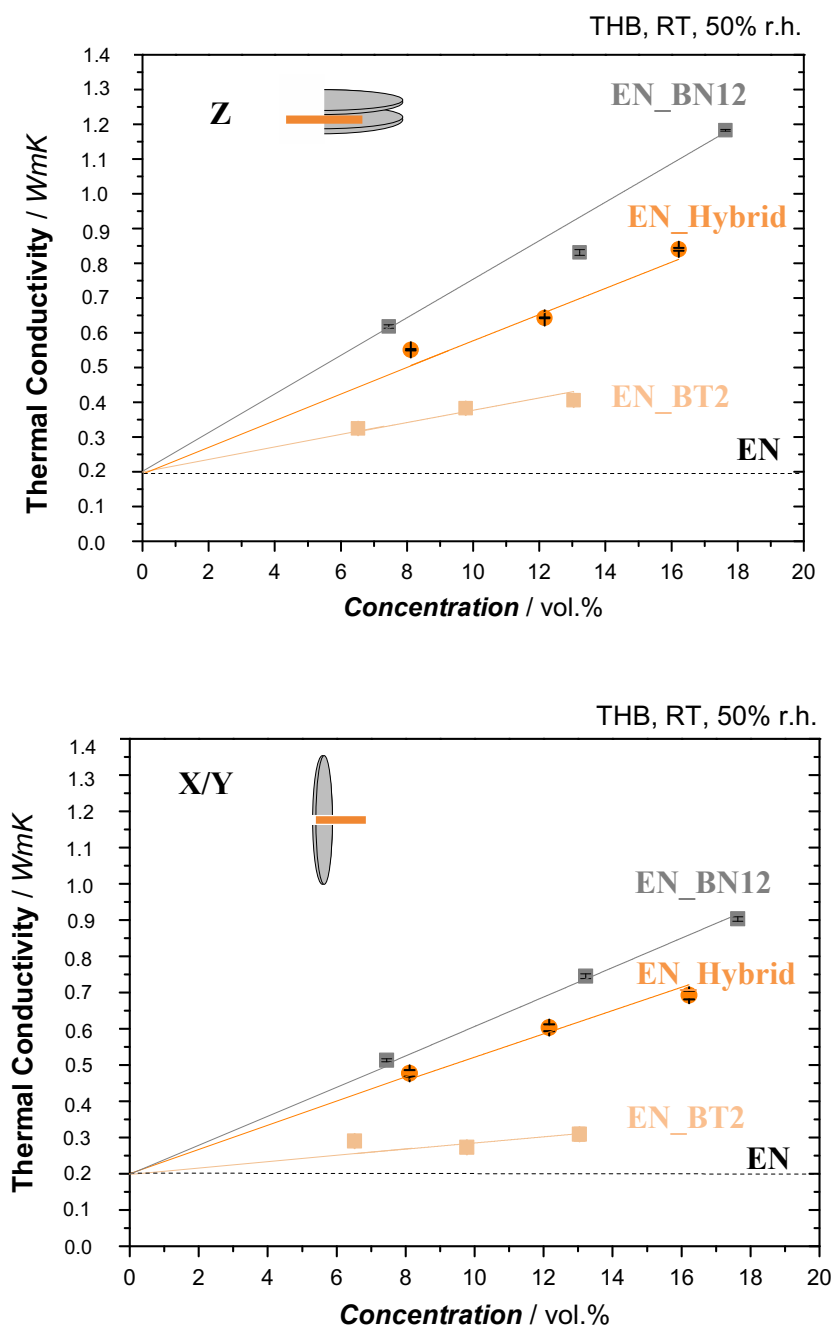


Figure 66 z- and x/y-plane thermal conductivity results for the EN\_BN12 and EN\_BT2 filler and their EN\_Hybrid combination (evaluated with THB).

Xie *et al.* [181] studied the *in-plane* and *out-of-plane* thermal conductivity of *h*-BN polyvinyl alcohol (PVA) composites of a size range between 4  $\mu\text{m}$  and 13  $\mu\text{m}$  and at 19.6 vol.% content. Tape casting forced the alignment of the platelet-shaped fillers. A TC value of 4.41 W/mK (*x/y*-plane) was reported. However, the results perpendicular show a decrease by 50 % due to the 2-directional filler alignment. Similar results were published by Su *et al.* [103] using *h*-BN of 20  $\mu\text{m}$  in a cycloaliphatic Epoxy resin (CER) matrix. At 15 wt.% filler content, *z*-plane values of 0.5 W/mK and 0.8 W/mK in *x/y*-plane were reported. A significant TC increase was found above a filler content of 35 wt.%, with 1.1 W/mK (*z*) and 1.6 W/mK (*x/y*). Their study is based on thin-film resins, and a strong anisotropy of the BN fillers in the *x/y*-plane was claimed to be the main contributor to the high TC values.

### Calculation of the *effective* Thermal Conductivity according to Nielsen

According to Nielsen's *efficiency rule* (Nielsen model), the effective TC is significantly *below its intrinsic thermal conductivity*. Thus, it leads to an increase for the TC in a moderate range. The model by Nielsen was evaluated by using the experimental results for the model calculation. For the intrinsic thermal conductivities of neat EN resin, a theoretical value of 0.20 W/mK and 200 W/mK for EN\_BN12 were used. The calculated ratio  $\lambda_p / \lambda_m$  ( $p$  = particle,  $m$  = matrix) for the formulation investigated in this study is 1000. The mean filler content was determined via TGA of the investigated systems and resulted in 19.7 vol.%.

The *effective TC* of the BN 12 $\mu\text{m}$  filler  $\lambda_{BN,eff}$  was calculated using equation 2. For this, the experimental TC values of BN (= 1.183 W/mK at 19.7 vol.%) and the matrix (= 0.26 W/mK), both measured with THB, were utilized.

The  $\lambda_{BN,eff}$  resulted in 6.05 W/mK for BN 12 $\mu\text{m}$  (literature value: 200-300 W/mK!) and Boehmite a  $\lambda_{BT,eff}$  of 2.19 W/mK (literature value: ca. 30 W/mK!). The value  $\lambda_{\text{hybrid},eff}$  was calculated to be 5.08 W/mK. A similar  $\lambda_{BN,eff}$  was published by Suplicz *et al.* with 8.8 W/mK with *h*-BN of 3-5 $\mu\text{m}$  in size in a PP matrix. His calculations also show that the experimental values are below the anticipated literature values [182].

### **Interim Summary – *Studies on Thermal Conductivity***

Firstly, three Boehmite fillers with various sizes and shapes were studied. It was found that the platelet shape of Boehmite with a  $D_{50}$  of 2  $\mu\text{m}$  (= BT2) resulted in the highest TC.

Secondly, the *influence of the filler nature*, which is well known in the literature, was demonstrated by using BN2 and BT2. BN has a higher intrinsic TC and therefore is more efficiently conducting heat. The BN2 showed higher results but only at *concentrations*  $> 10 \text{ vol.}\%$ . This strongly suggests that interaction between individual filler particles is still required to absorb and transport heat efficiently. Below 10 vol.% filler contents, the TC is *independent of the filler nature*. From the literature, it is known that higher concentrations also lead to higher TC results [66]. The rule of thumb states at least a filler content of 15 - 25 vol.% is necessary to increase the TC by 10 % [66].

The investigation of various BN platelet sizes at  $19.7 \pm 0.1 \text{ vol.}\%$  filler content resulted in selecting the optimal platelet *filler size* of 12  $\mu\text{m}$ . A good filler dispersion was achieved with process optimization. A random filler microstructure was established during curing. This confirms that with increasing lateral size (= increasing aspect ratio), and decreasing BET of the particles, the TC increases. The larger the filler's AR, the sooner a filler-filler interaction was established. BN has a nearly perfect crystal lattice, similar to graphite, which is advantageous for phonon transport with minimal scattering effects [77]. At a critical filler content below  $< 10 \text{ wt.}\%$ , the thermal conductivity is low due to the polymer matrix's thermal barrier effects, limiting the phonon transport. The random microstructure was also confirmed by applying the theoretical *model by Hatta-Taya* that takes the filler geometry, size, and intrinsic TC into account.

Finally, the best thermal conductivity was evaluated as the hybrid filler combination with the combination of BT2 with BN12 in a 1:3 ratio. The fillers were well dispersed in the EN matrix, with a BN12 having a random orientation. It was noticed that a filler network has been established during the curing reaction at the point of the lowest viscosity and hence maximum resin mobility. The well-dispersed fillers self-assemble and -aggregate to a network structure, with BN12 forming the main filler chain and BT2 adhering to the BN or filling into its gaps.

### 5.2.3 Optimization towards the desired Flame Retardancy

Pyrolysis and the flame-retardant behavior are highly important for applying a resin as a matrix for a PCB base material. This thesis evaluated a novel flame-retardant type of Boehmite, which is suitable for the higher soldering processes. In addition, there are not many studies on the role of BN and its thermal conductivity on flame retardancy mechanisms in literature.

The thermal stability and the thermal degradation, especially under air atmosphere, were investigated with thermal gravimetric analysis (TGA). The Cone Calorimeter was used to evaluate time to ignition (tig), the heat release rate (HRR) and its peak value (PHRR), the total heat release rate (THR), the total smoke release rate (TSR), and the residual mass of the laminate samples. Post-combustion morphological investigation of char residues was conducted via SEM-EDX. Based on these morphological studies, the role of each filler type regarding the prevailing flame retardancy mechanism could be identified and used to establish *structure-property relationships*.

#### **Influence of BN and Boehmite Fillers on Thermal Degradation and Pyrolysis Behaviour**

This chapter investigated the influence of the two fillers species on pyrolysis, thermal stability, and flame retardancy in the oxidative and non-oxidative atmosphere.

The concentration of the fillers in the EN matrix was kept constant at 45 wt.% (~19.7 vol.%). The thermo-oxidative degradation of selected filled resin formulations was studied with TGA (Figure 67). The results are summarized in Table 13. The most important characteristic values are the thermal decomposition temperatures at 2 wt.% ( $T_{d,2\%}$ ) and 5 wt.% ( $T_{d,5\%}$ ), indicating the beginning of thermal instability.

The overall glass transition temperature ( $T_g$ ) resulted in a range of  $242 \pm 2$  °C. In general, the thermal stability of the systems has the following order:

$$EN\_BT2 > EN\_Hybrid > EN\_BN12 > EN (= \textit{highest to lowest stability}).$$

The *unfilled, neat* EN has the lowest thermal stability with no char residue left. The thermoset degrades fully under thermo-oxidative (air) conditions. The thermal decomposition is strongly influenced by the monomer, the curing agent, and the crosslinking density [183]. In general, the thermal stabilities of aromatic thermosets are higher than aliphatic [183].

**Table 13 Overview of all filled EN resins' thermal stability and degradation behavior in correlation with their resin- and filler volume contents.**

Composition	$T_{g,DMA}^a /$ °C	$T_{d,2\%}^b /$ °C	$T_{d,5\%}^c /$ °C	Char yield <sup>d</sup> / wt. %	Resin content / vol. %	Filler content / vol. %
EN	242	352	363	0.00	99.7	-
EN_BN12	244	353	368	30.45	86.3	13.7
EN_BT2	242	359	373	29.10	89.6	10.4
EN_Hybrid	242	358	370	29.64	87.8	12.2

<sup>a</sup>  $T_g$  values determined by maximum of  $\tan \delta$ .

<sup>b</sup> Degradation temperature at 2% weight loss under  $N_2$ .

<sup>c</sup> Degradation temperature at 5% weight loss under  $N_2$ .

<sup>d</sup> Residual weight at 800 °C under Air.

In  $N_2$  (*inert*) environment, a C-C bond scission is initiated at elevated temperatures, while under  $O_2$  atmosphere, a radical chain reaction is triggered [184].

The overall  $T_{d,5\%}$  of the matrix EN is 363 °C ( $T_{d,5\%}$ ). The minimum requirement for base materials applicable in PCBs is  $T_{d,5\%} = 350$  °C. This novel resin (EN cured with DETDA) meets *this higher requirement*.

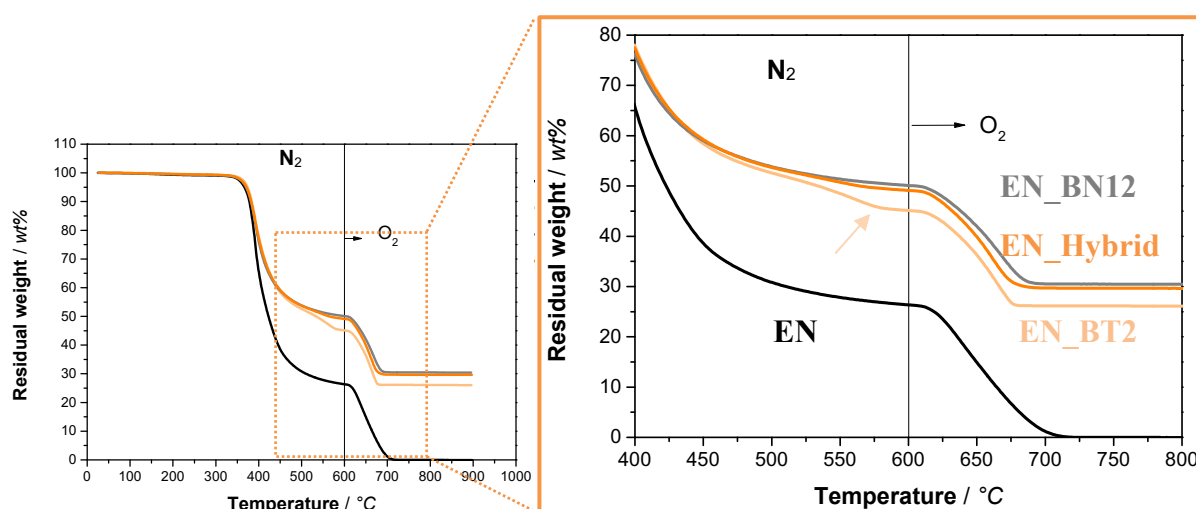


**Figure 67 TGA thermogram of selected EN formulations at constant filler concentration of 45 wt. %.**

The *incorporation of Boehmite and BN fillers* each shifts the onset of the decomposition temperatures,  $T_{d,2\%}$  and  $T_{d,5\%}$ , by up to 10 °C compared to the neat EN resin. This indicates that the incorporation of (low and high) thermally conductive fillers help to spread the surrounding heat and inhibits the diffusion of decomposed volatiles through shielding [125]. A good filler dispersion and interfacial interaction between matrix and filler also lead to higher thermal stability [125], which was achieved in this thesis (compare results in Figure 63a) by process optimization.

Comparing the  $T_{d,2\%}$  and  $T_{d,5\%}$  results, the highest thermal stability shows the EN\_BT2, which is ~ 5-6 °C higher than EN\_BN12. The degradation of the Boehmite-filled resin starts after the initial decomposition of the EN matrix. A closer look at the TGA thermogram shows that the EN\_BT2 has two significant mass loss steps (indicated by an **arrow** in Figure 67). The first step ( $\approx 360$  °C) can be associated with the crystalline lattice change and dehydration of  $\text{AlO}(\text{OH})$ , leading to a phase transition to  $\gamma\text{-Al}_2\text{O}_3$  (intermediate product) [162]. At  $> 500$  °C, Boehmite decomposes entirely by converting to  $\text{Al}_2\text{O}_3$ , which is indicated by an increasing char yield [185,186]. Sun *et al.* studied Boehmite incorporated in DGEBA resin. Their results correlate with the findings above: a higher  $T_{d,5\%}$  BT-filled DGEBA than the unfilled matrix. However, increasing the concentration of BT did not lead to a further shift of  $T_{d,5\%}$  [164]. Boehmite helps absorb heat and supports stabilizing the gas phase above the solid phase by releasing water molecules. Cooling down the gas phase helps to slow down the degradation reaction and therefore shifting the degradation temperature.

The char residues examined with TGA in oxidative conditions show that the incorporation of fillers leads to higher charring effects compared to the neat EN. *This indicates condensed-phase activities for both fillers.* The amount of char formed under oxidative conditions is much higher for the filled resins than the unfilled EN. A high char yield in combination with high initial degradation temperatures describes the effectiveness of flame retardation [187]. BN12 has a slightly higher char yield than BT2, which might be attributed to the initial slightly higher filler volume content and because BN does not decompose in this temperature range.

In general, the matrix decomposes in a first step for the filled resins, as all fillers are more thermally stable. This indicates that there is no interaction between the matrix and the fillers.

### Influence of BN and Boehmite on Flame Retardant Behaviour

The flame retardancy of the filled resins was studied by a Cone Calorimetry. Cone calorimeter tests enable the evaluation of a forced combustion and access to valuable information of the fire-retarding behavior of these materials.

The heat release rate (HRR) in dependency time for the neat EN, EN\_BT2, and EN\_BN12 is plotted in Figure 68. Their filler combinations, bimodal and hybrid, are plotted separately in Figure 69a). The results regarding the total smoke release (TSR) and the heat release (THR) are plotted in Figure 69b and c).

Concerning Figure 68, the exposure to external heat leads to slow degradation of the polymer surface, which causes the release of small fragments/volatiles from the solid- into the gas phase. At a specific critical concentration, these volatiles are ignited by irradiation. The samples start to decompose in air atmosphere under the release of heat and smoke particles into the gas phase [188].

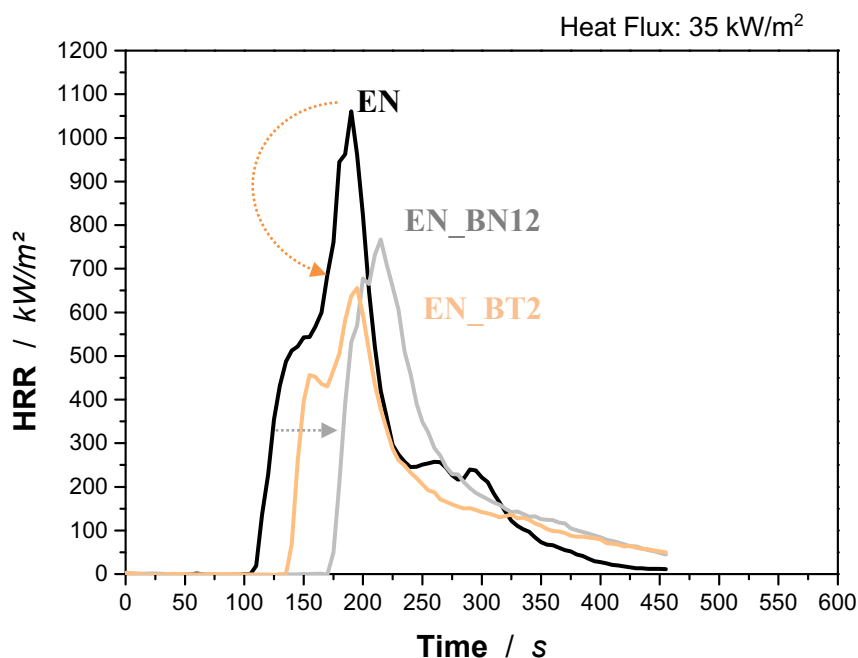


Figure 68 Heat release rate (HRR) of the unfilled EN, the EN\_BT2 - and the EN\_BN12-filled EN resin (applied heat flux 35 kW/m<sup>2</sup>).

The neat EN sample curve progression follows a sharp increase and decreases with the shortest  $t_{ig}$  of all systems. Similar results were published by Unlu *et al.* [189]. This is an indicator for materials with almost no residue formation directly correlated with the TGA results (Table 13) [154]. The neat Epoxy Novolac degrades in the condensed phase (= pyrolysis zone) under random chain-scission into radicals, CO, and CO<sub>2</sub> under a high heat release with a maximum at 1198 kW/m<sup>2</sup>. Especially for amine-cured Epoxies, the first decomposition is undergoing dehydration (or dehydrogenation) of the secondary alcohol, which is formed during those mentioned above radical cross-linking reaction yielding to allylic amines. These radicals cross-link to a more (thermally) stable char [190]. This can be observed in Figure 68 (tiny shoulder) with the reduction of heat release. In a second step, the allylic oxygen bond (C-O) is less stable and can be further scissioned by O<sub>2</sub>. Since the curing agent is amine-based, its weak C-N bond dissociates by forming volatiles [146,189]. These decomposition reactions contribute to the overall charring as amines tend to remain in the solid phase [189,190]. During combustion, it was observed that the EN samples burned uniformly with an intensive flame spreading fully over the total sample surface area. Some char was left, indicating activity mainly in the gas and some extent in the condensed phase, but mainly in gas-phase above solid phase.

A closer look at the HRR curves shows (Figure 68) that the time to ignition ( $t_{ig}$ ), the time to peak heat release rate ( $t_{PHRR}$ ), and the PHRR are strongly influenced by the presence of the inorganic fillers. Compared to EN, the curves for EN\_BT2 and EN\_BN12 show a gradual decrease until flame-out due to char formation.

EN\_BT2 shows a significant decrease of 40 % of the peak heat release rate resulting in 674 kW/m<sup>2</sup>. The  $t_{ig}$  was increased by almost 30 s compared to the unfilled EN. The reduction in PHRR and increase in  $t_{ig}$  were also published by Laachi *et al.* using 20 wt.% Boehmite in a PMMA matrix [191]. The curve of the EN\_BT2 follows a tiny shoulder before reaching its peak maximum. The appearance of this double peak might be correlated to the TGA results, as Boehmite decomposes in two significant steps [164,165]. Wilson *et al.* [192] reported a dehydration reaction of Boehmite at elevated temperatures. At high temperatures (> 340 °C). Boehmite undergoes a dehydration reaction. Water is released, and a thermally stable Al<sub>2</sub>O<sub>3</sub> layer (= ceramic barrier) is formed. The release of water is an *endothermic process*, and it lowers the heat to which the filled resin is exposed, thus lowering its degradation rate. By

releasing water during the degradation reaction, the system is cooled down by reacting with pyrolyzed volatiles in the gas phase and forming an Al<sub>2</sub>O<sub>3</sub>-barrier in the condensed phase.

The PHRR and THE values are affected by gas- and condensed phase flame retardancy mechanisms [193]. While the gas-phase activities suppress the flame, the condensed phase forms active FR residues char, inhibiting the underlying material from decomposing [193]. The much higher char content of the BT- and BN-filled resins indicate higher condensed-phase activity. Compared to the unfilled EN, the total smoke released decreases by 38 % (Figure 69b)). The platelet BT shields the surface by limiting heat transfer and slowing down the degradation reaction [184]. In addition, the decreased smoke release can also be explained in a way that smoke particles (soot) can adsorb to the Al<sub>2</sub>O<sub>3</sub> filler surface [145,194].

For the EN\_BN 12 resin, there is no considerable effect on the PHRR. However, BN causes a significant shift of the  $t_{ig}$  by a total of ~ 60 s. This might imply that:

- a) **the formation of volatiles is either decreased by an efficient barrier effect due to its platelet nature**
- or,
- b) **the time to attain a critical, ignitable volatile concentration in the gas phase above the sample is longer due to its thermal conductive nature.**

The barrier effect given by the platelet shape increases the path length for volatiles to reach the surface [188]. Jin *et al.* investigated *h*-BN (3 μm, 20 wt.%) in a Bismaleimide-matrix [195]. They have published similar observations: *an increase in  $t_{ig}$  and a slight decrease in PHRR*. However, the amount of char residue was negligible. They claimed the poor filler dispersion did not form a heat-protecting layer. Gu *et al.* [169] studied graphite platelets (40 μm) in DGEBA and found a similar phenomenon. They claimed the higher thermal conductivity (1.48 W/mK @ 30 wt.% filler content) for this reduced ignitability. The platelet-shaped BN only reduces the smoke release by 14 % compared to the Boehmite-filled composite. However, the BN shows an influence on the *total release rate* (THR). It can be assumed that the BN sheets migrate to the surface and act as a ceramic barrier inhibiting heat and mass transfer [167]. Also,

the BN supports the heat transfer away from the surface. By spreading the heat, the temperature on the samples' surface changes, and therefore the samples are longer thermally stable.

### **Filler Combinations and their Effect on Flame Retardancy**

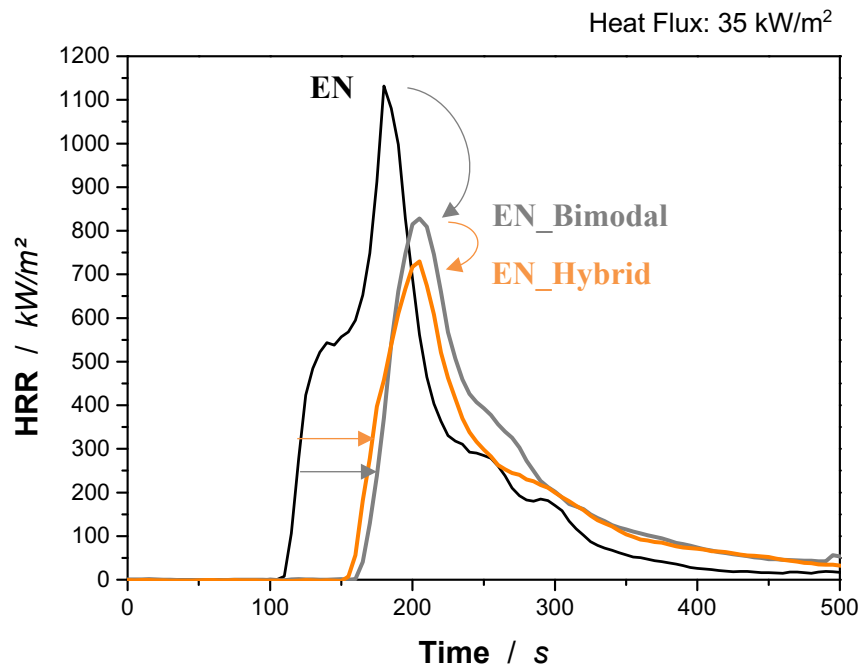
The influence of the filler combination on HRR, TSR, and THR was evaluated in Figure 69. For comparison reasons, the bimodal BN filler combination was also studied.

The *bimodal* combination of BN2 and BN12 leads to the same phenomenon described in the previous sub-chapter for the BN filler: a significant shift of  $t_{ig}$  from 113 s to 164 s, which equals an improvement of 51 s of the  $t_{ig}$ . However, there is no significant effect on the PHRR value (Figure 69a)).

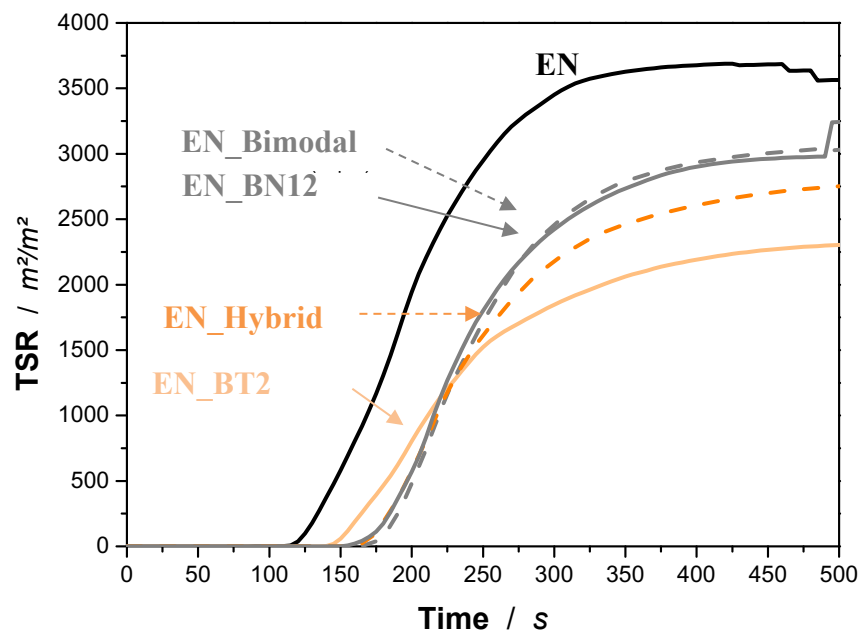
By substituting BN2 with the BT2 (= *hybrid* combination), the PHRR was significantly decreased by 38 %, from 1198 kW/m<sup>2</sup> (neat EN) to 729 kW/m<sup>2</sup>, respectively. In addition, a  $t_{ig}$  shift was observed, which can be attributed to the thermal conductivity of the BN filler (Figure 68). This shows the dual effect of the hybrid formulation compared to the bimodal, which does not contain a FR. This might result from the better dispersion of the BT fillers in the hybrid formulation compared to the BN2 in the bimodal formulation. BN2 tends to agglomerate resulting in a less homogenous distribution. The BT2 particles showed a good dispersion in the EN matrix and higher filler packing density filling the gaps between the BN12 filler. This presumably led to a higher restriction of the migration of volatiles. The pyrolysis gases accumulate underneath the barrier, consisting of Al<sub>2</sub>O<sub>3</sub> and BN, resulting in a significant decrease in TSR (Figure 69b)).

In general, all filled resins showed a higher char residue compared to unfilled EN. Especially, phenol-containing Epoxies, i.e., Epoxy Novolac, are reactive and more inherently fire-retardant and known for their significant heat release and their contribution to charring due to the aromatic component [183]. EN\_BN12 shows a higher TSR but a lower THR compared to the EN\_Bimodal formulation. This can be explained by the more considerable platelet length, which has a higher ability to shield heat.

## a) HRR



## b) TSR



## c) THR

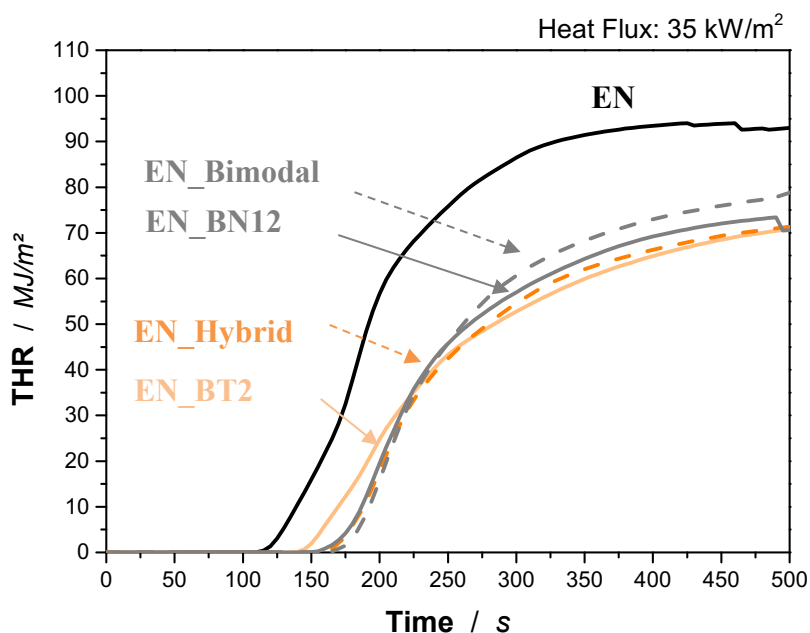


**Figure 69** Evaluation of fire-specific values via Cone Calorimetry for the unfilled and filled EN resins. a) heat release rate (HRR), b) total smoke release rate (TSR) and c) total heat release rate (THR).

In summary, it was found that with only BN (EN\_BN12) alone, the  $t_{ig}$  can be significantly increased, and the TSR decreased. This is due to BN's thermal conductive nature and due to its barrier effect as BN does not decompose. The EN\_Bimodal and EN\_BN12 formulations showed similar overall trends. BN2 was supposed to fill the gaps between the larger BN12 platelets, but no significant effect on the TSR was observed. The EN\_Hybrid and EN\_BT2 both impact FR with the initial endothermic release of water, the smoke release increases slightly, and the formation of the  $Al_2O_3$  (especially for EN\_BT2 in Figure 69b)).

The THR results are very similar for all formulations. The difference between EN\_BN12 and EN\_Bimodal might result from the higher effectiveness of BN12 platelets and their higher intrinsic TC, therefore shielding heat by conducting heat away from the surface.

Furthermore, the *fire growth rate index* (FIGRA), *PHRR*, and *t (PHRR) ratio* were calculated. FIGRA is an index for fire spread and the size of a fire and is used for rating fire-hazardousness [184,195]. The FIGRA value was reduced from 6.6 of the unfilled EN resin to a value of 3.5 for EN\_Hybrid.

### Post-Combustion Analysis of Char Residues with SEM-EDX – *Fire-Retardant Mechanisms*

To establish a *correlation* between the evaluated characteristic Cone Calorimeter parameters and *fire-retardant mechanisms*, the char residues were evaluated with SEM coupled EDX. The EDX quantification was conducted by scanning the surface of the charred samples (Table 14). The SEM micrographs show top- and side perspectives of the char residues (Figure 70 - 72).

Multifunctional Epoxies with an aromatic component offer a high crosslink density and a high pyrolysis resistance, contributing to a stable layer formation [183]. The char formation is generally correlated to the release of “fuel”, which is described as the total heat evolved (THE) parameter [184]. A reduction of heat released is caused by the formation of char or based on a lower polymer content [184]. Levchik *et al.* report in their review that inorganic fillers generally tend to catalyze the degradation of Epoxies [183].

**Table 14 EDX quantification results of the char residues after Cone Calorimeter measurement.**

<b>Composition</b>	<b>B (K) / wt. %</b>	<b>C (K) / wt. %</b>	<b>N (K) / wt. %</b>	<b>O (K) / wt. %</b>	<b>Al (K) / wt. %</b>
EN	-	100	-	-	-
EN_BN12	37	33	9	13	8
EN_BT2	-	68	7	14	11
EN_Bimodal	61	6	30	2	-
EN_Hybrid	39	36	8	10	6

First, for all filled resins, the char resulted in a “foamed” structure after degradation, known as “*intumescence*”. This implies that the top layer must be of dense material, restricting the release of volatiles formed during the degradation of the polymeric matrix into the gas phase [184]. Moreover, a foamed material, in general, has lower thermal conductivity and leads to a temperature gradient from top to bottom of the sample [188].

The *char residue* of the neat Epoxy Novolac sample is very unstable with a very smooth surface (Figure 70a)).

It is majorly composed of carbon, highlighting a complete degradation of the matrix in air atmosphere. Since the char is unstable, the fragmentation of the sample during combustion helped to release the volatiles (oxidized components such as CO, CO<sub>2</sub>) into the gas-phase [188]. The *addition of Boehmite* led to a more rigid char at the surface with a foam-like/porous structure in the core (see side-perspective). The zoomed-in SEM (Figure 70b)) shows a dense, platelet-like surface on the top surface. The elemental composition of this layer consists mainly of carbon, oxygen, and aluminum, indicating the formation of CO, CO<sub>2</sub>, and Al<sub>2</sub>O<sub>3</sub> during the matrix combustion and filler degradation. It is assumed that the volatiles (CO and CO<sub>2</sub>) are trapped under the Al<sub>2</sub>O<sub>3</sub> barrier and contribute to the overall intumescence of this sample [165,191].

The BN-filled char (Figure 70c)) has a compact top, and the main elements detected were boron, carbon, and oxygen. The platelet BN does not decompose at these temperatures, and therefore the filler migrates to the surface, forming a compact layer. This barrier delays the diffusion of pyrolysis gases and the initial ignition. This can be directly correlated with the TSR and THR results from the previous chapter. EN\_BN 12 was higher than EN\_BT 2, as EN\_BN 12 has more microporous channels. BT degrades to Al<sub>2</sub>O<sub>3</sub> and acts as a barrier more efficiently. The elemental quantification indicates a higher probability of matrix degradation into the gas phase. The *bimodal* char morphology is compact at the surface and shows microporous channels in the side perspective (Figure 71). The main elements detected were B and N. The combination of two different platelet sizes of BN, 2 μm and 12 μm (D<sub>50</sub>), forms even more diffusive paths since the smaller platelets can fill the gaps between the larger platelets. The morphology led not only to an increase in thermal conductivity but also to lower TSR and THR. Therefore, the principal mechanism is increasing the diffusive path length and the formation of an insulating barrier restricting heat/oxygen exchange and stabilizing the char [189]. Since the BN platelets migrate to the top surface in an early degradation stage, the volatiles is entrapped, leading to a high level of intumescence.

The *hybrid* char (Figure 72) shows a dense surface but slightly less microporous in the core compared to the EN\_BT 2 sample. The Boehmite decomposes, forming an Al<sub>2</sub>O<sub>3</sub> barrier, the remaining volatiles “foam” the sample leading to a porous structure. The surface scan with EDX identified mainly B, N, and O, but a lower carbon percentage was detected than the bimodal sample.

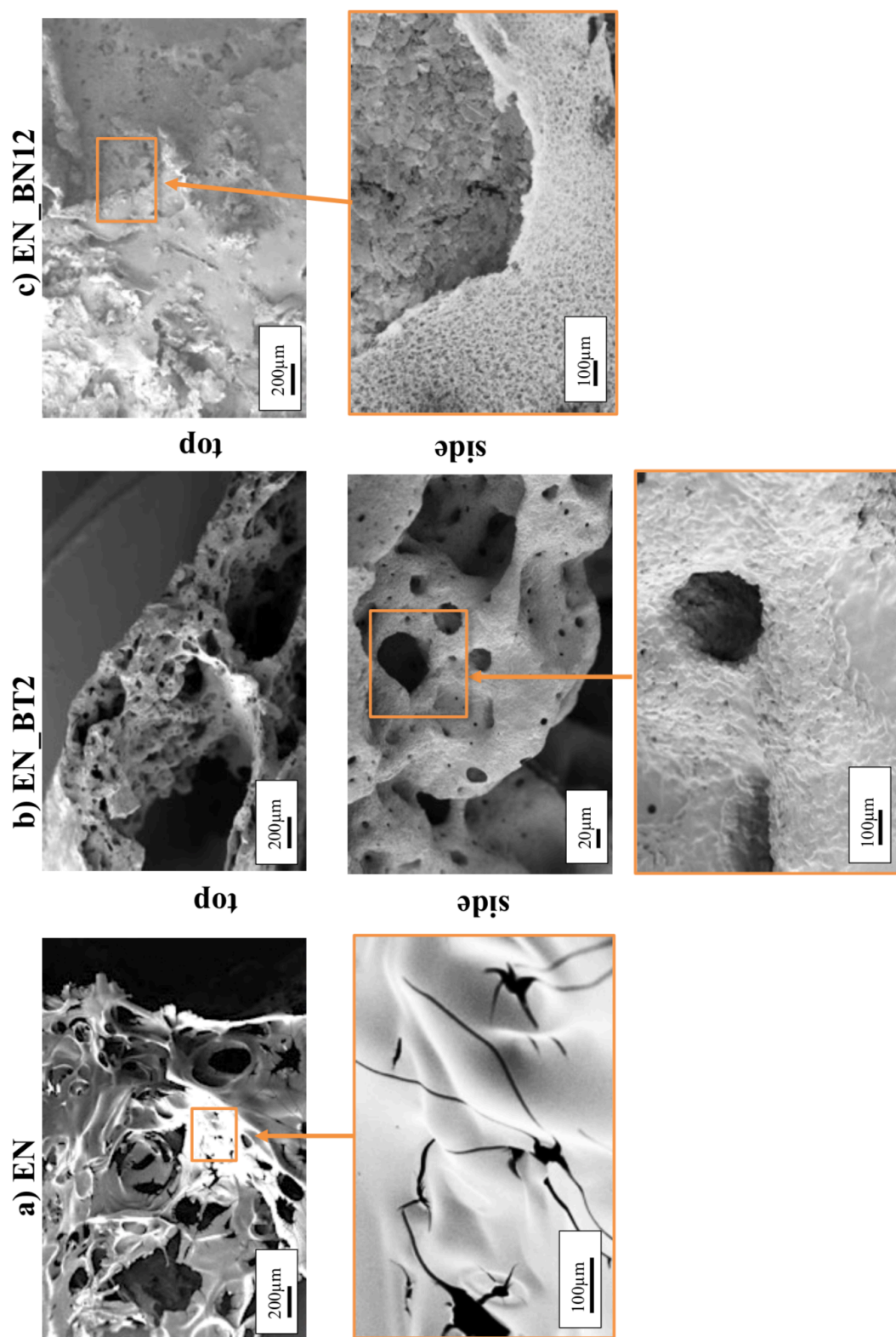


Figure 70 SEM micrographs of the char morphology of the various (filled) resins in top and side view (at different magnifications).

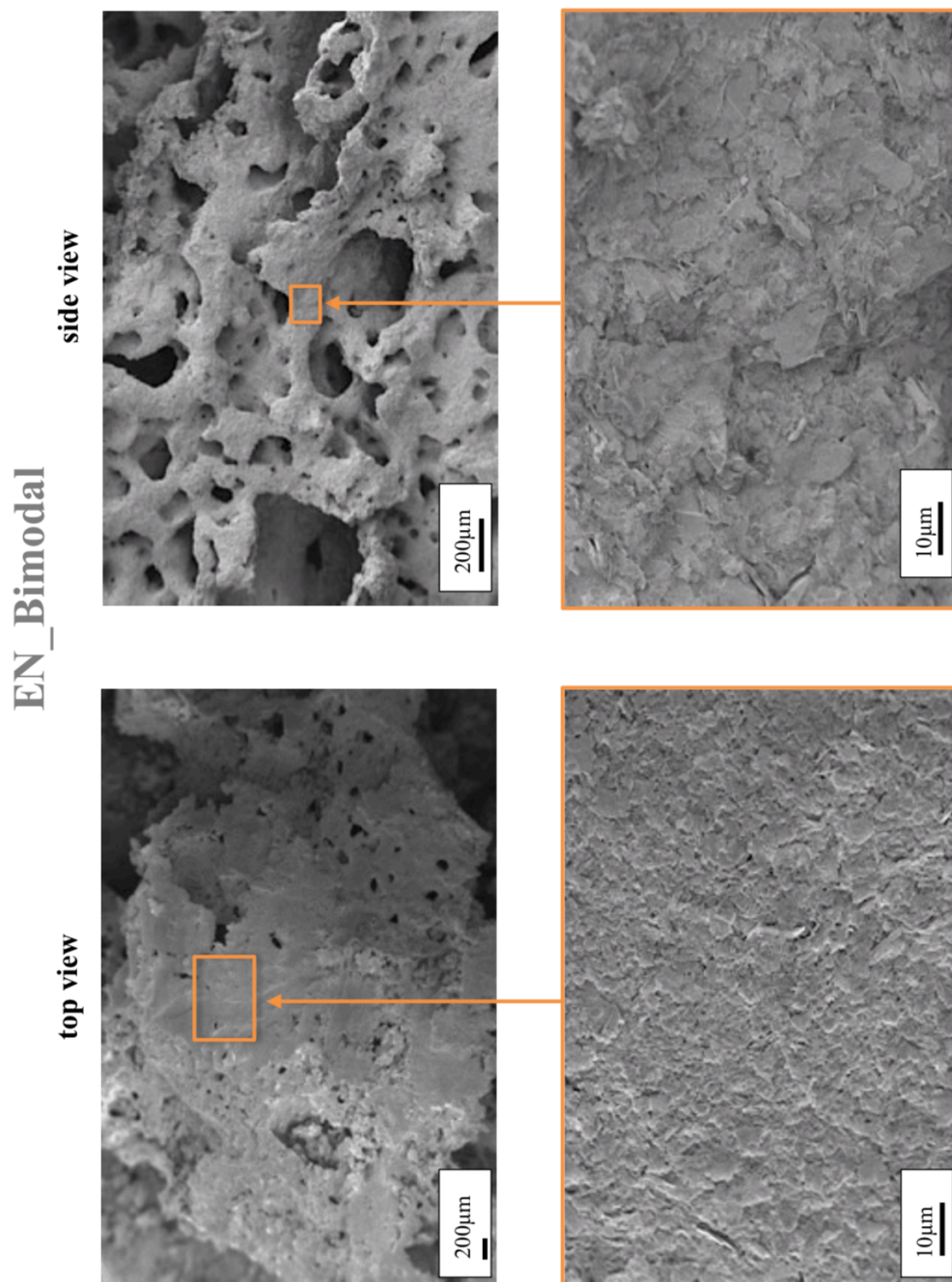


Figure 71 SEM micrographs of the char morphology of the EN\_Bimodal as top and side view (at different magnifications).

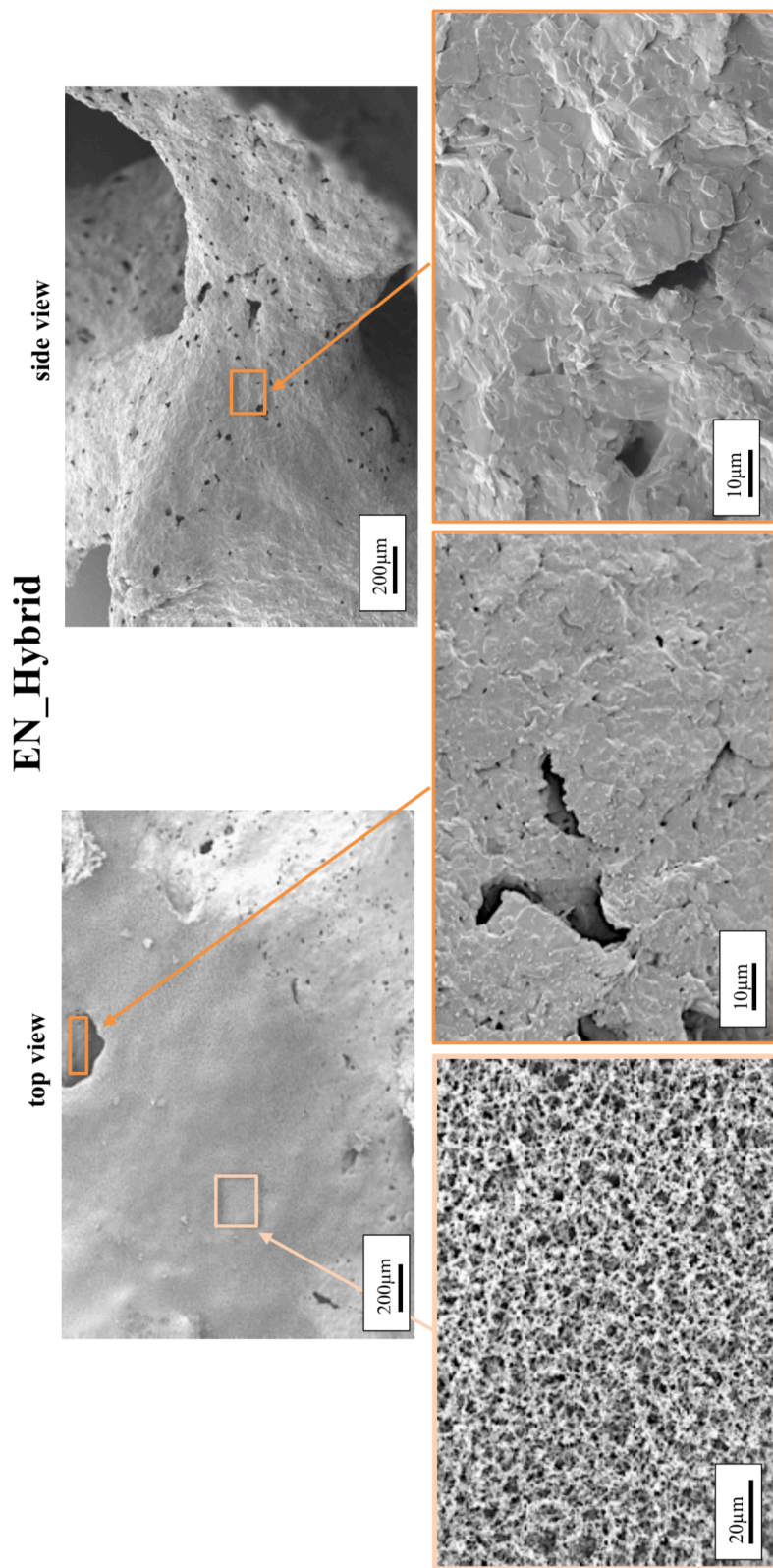


Figure 72 SEM micrographs of the char morphology of the EN\_Hybrid resin in top and side view (at different magnifications).

### Interim Summary – *Studies on Flame Retardancy*

Correlating THR and TSR results with the apparent char morphology indicates that the matrix degradation is higher for the BN-containing formulations EN\_BN 12 and EN\_Bimodal. **BN particles remain in the solid phase as an inactive “FR”** and delay the volatiles' release. In contrast, the Boehmite-containing formulations **EN\_Hybrid and EN\_BT2 restrict the matrix degradation more efficiently by forming the Al<sub>2</sub>O<sub>3</sub> layer. The additional activity in the gas phase** resulted in decreasing both the THR and TSR values.

Lewin and Weil [186] proposed the *synergistic effectiveness* index to identify and verify if a “real” *synergy* between the two fillers exists. Possible synergism is known to show beneficial, improved, or even a superposition of effects using two or more fillers. This synergistic effectiveness is defined as the ratio of flame retardant effectiveness (EFF) between one filler and the EFF of both fillers [186,196]. Yang *et al.* describe synergistic effects if both the condensed- and gas-phase activities lead to improved fire properties [197]. Sut and Scharrel *et al.* introduced the synergy index (SE), which can be calculated based on the PHRR or THE values [165]. If a real synergism exists, then the SE would be > 1. If the ratio ≤ 1, then a combinatoric or even an antagonistic effect is more likely.

The calculated synergy indices indicate combinatoric/antagonistic effects regarding PHRR and THE results. The lowest values regarding PHRR and TSR were accomplished with the unimodal Boehmite, whereas the longest  $t_{ig}$  was attained with unimodal BN. For the hybrid system, the synergy index is slightly higher. However, the SEs indicate a strict combinatoric effect (Table 15).

$$SE = \frac{Y(Epoxy\ Novolac) - Y(combinatoric\ system)}{\frac{X(filler\ 1)}{X(filler\ 1) + X(filler\ 2)} \cdot (Y(Epoxy\ Novolac) - Y(filler\ 1)) + \frac{X(filler\ 2)}{X(filler\ 1) + X(filler\ 2)} \cdot (Y(Epoxy\ Novolac) - Y(filler\ 2))} \quad \text{Equation 8}$$

**Table 15 Comparison of calculated synergy indices for the bimodal and hybrid-filled resins for PHRR and THE indicating combinatoric effects only.**

System	Synergy index (PHRR)	Synergy index (THE)
EN_Bimodal	0.13	0.20
EN_Hybrid	0.22	0.25

### 5.3 Thermal Conductive and Flame-Retardant Properties of Laminates

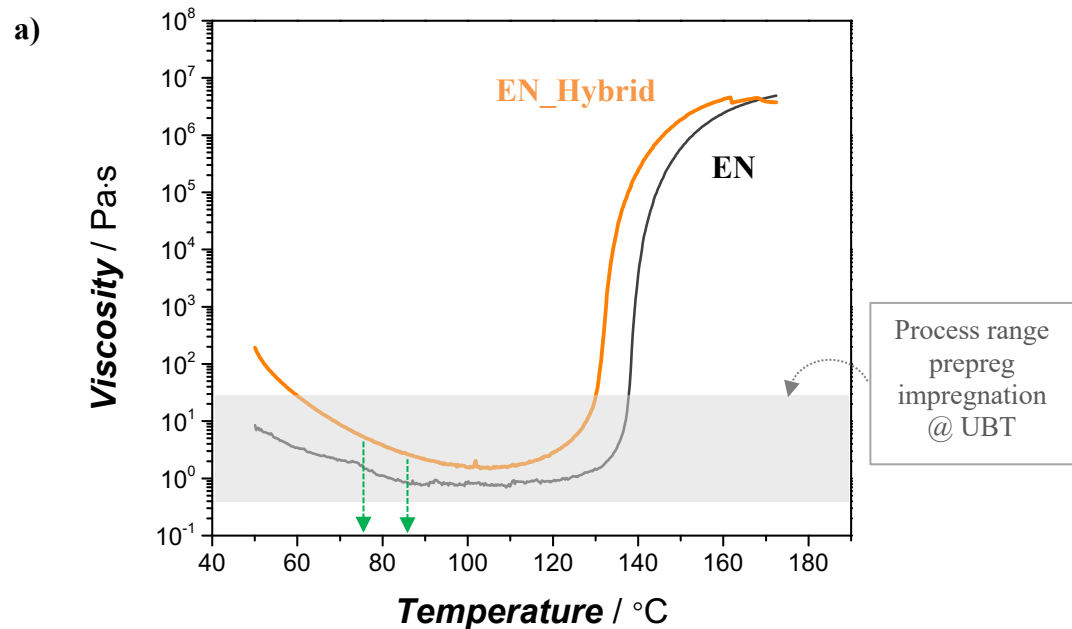
In this chapter, the influence of glass-fibers on the thermal conductivity and the fire behavior of corresponding composites are evaluated. A relation to previous findings of filled resins on filled resins to the behavior of the resin in prepregs will be drawn. For this study, systematically, the FVC was increased under the constraint that the filler content is kept constant! The increase in FVC was achieved using three different standard fabrics with varying areal fiber weights of 25 g/m<sup>2</sup> (= GF25), 49 g/m<sup>2</sup> (= GF49), and 107 g/m<sup>2</sup> (= GF107). As matrix resins the unfilled Epoxy Novolac (EN\_GFXX), the BN 12 μm-filled Epoxy Novolac (EN\_BN12\_GFXX), and the Epoxy Novolac with the hybrid filler combination (EN\_Hybrid\_GFXX) were selected.

#### 5.3.1 Solvent-free direct *in-line* Impregnation – *Prepreg Properties*

##### Prepreg Processing Window

Before prepreg production, it was concluded from rheology experiments that the process temperature needs to be kept at < 90 °C (Figure 54). During prepreg process optimization, a tiny processing window between 75 - 85 °C was determined. A homogenous matrix film was formed within this temperature range on the release paper, whereas higher temperatures led to droplet formation (= porous matrix film) (Figure 73). An inhomogeneous film can directly lead to improper impregnation and the appearance of pores. In general, the overall advantage of the *solvent-free* hot-melt impregnation route is the lower risk of pore formation as there is no

solvent-based volatiles that can be trapped within the prepreg and their corresponding laminates.



b)

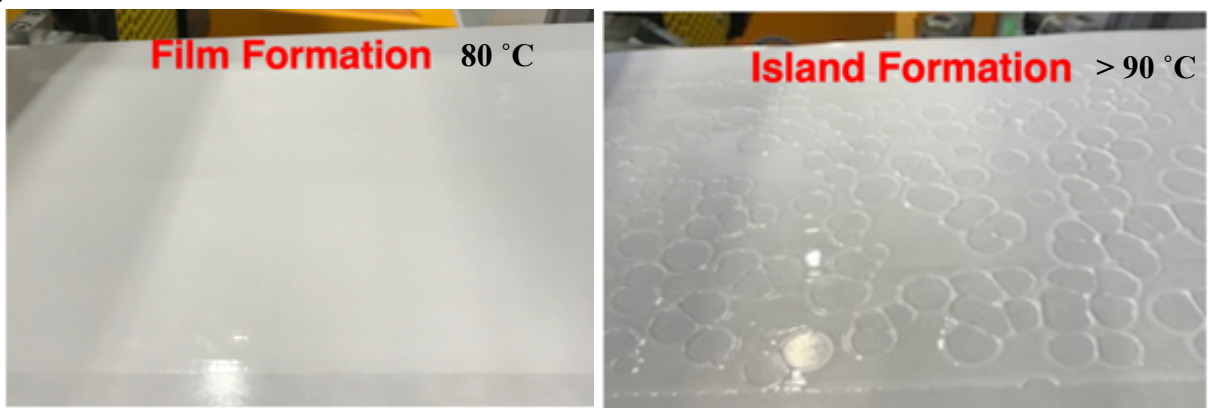


Figure 73a) Viscosities of EN and EN\_Hybrid in dependency of temperature. b) A temperature of 80 °C at the coating head was determined to be optimal to reach a homogeneous film formation. Higher temperatures lead to a droplet „island“ film on the release paper.

### Prepreg Areal Weight

A key parameter for quality inspection is the prepreg areal weight which defines the final cure ply thickness. To compare all laminates, it is crucial to monitor the *prepreg areal fiber weight*. Both the matrix content and the prepreg areal fiber weight can directly be controlled via the film thickness (= gap distance of the coating unit) and the gap in the calander. The prepreg width was kept constant at  $220 \pm 1$  mm. The prepreg areal weights were adjusted as close as possible to the calculated target weights. Table 16 shows, exemplarily for the EN\_GFXX and the EN\_BN 12\_GFXX laminates, the theoretically calculated target prepreg area weight and their actual achieved prepreg area weights. 3 samples were taken from different spots on the prepreg during production. The targeted values were determined based on State-of-the-Art *resin contents*, ca.  $80 \pm 1$  wt.% resin content (= GF25),  $66 \pm 2$  wt.% (= GF49), and  $47 \pm 2$  wt.% resin content for GF107 and prepreg areal weights [18].

The *areal weights* of the produced prepreps (exemplarily for the 25 g/m<sup>2</sup> fabric) were kept constant with a deviation of  $129 \pm 3.1$  g/m<sup>2</sup> (or 2.4 %) (Figure 74). The overall filler content was successfully kept consistent with a tolerance of  $\pm 2.5$  vol.% with the solvent-free route.

**Table 16 Overview of the calculated and practically achieved prepreg areal weights.**

<b>Laminates</b>	<b>Targeted areal weight / g/m<sup>2</sup></b>	<b>Actual areal weights / g/m<sup>2</sup></b>
<b>EN_GF49</b>	3.32	$3.05 \pm 0.15$
<b>EN_GF107</b>	3.90	$3.88 \pm 0.01$
<b>EN_BN12_GF49</b>	3.32	$3.38 \pm 0.01$
<b>EN_BN12_GF107</b>	3.90	$3.94 \pm 0.06$

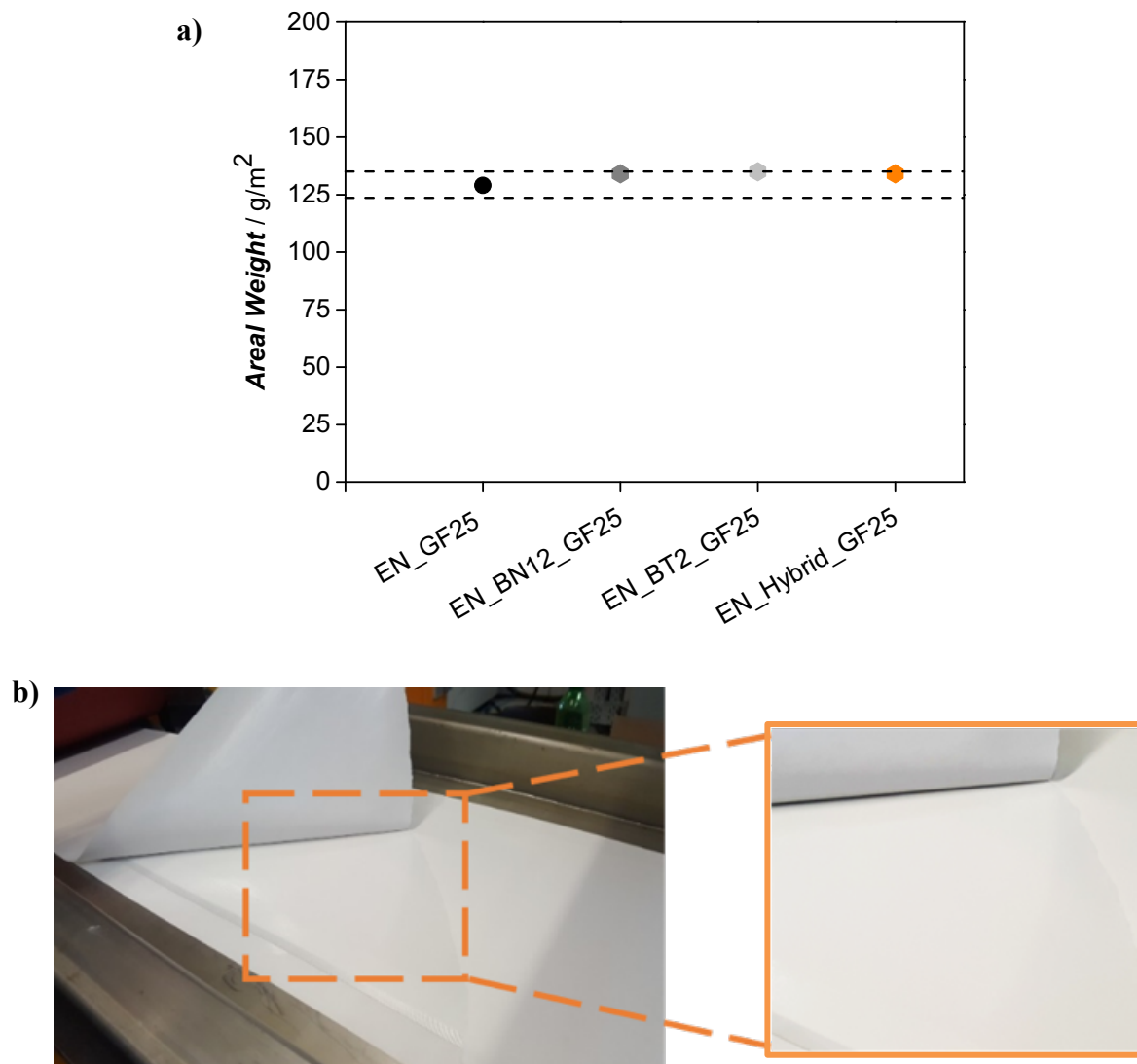


**Figure 74 a) Prepreg areal weights measured during prepreg production exemplarily for the GF 25 prepreps and b) prepreg surface exemplarily for the EN\_Hybrid\_GF49.**

Table 23 (annex) shows an overview of all produced laminates that are discussed in this thesis. Table 24 (annex) lists the resin, filler, and fiber content in both weight and volume percentages and their corresponding *cured ply thickness* (CPT) and laminate densities. All values were averaged, and the standard deviations are given.

The high standard deviation for the *resin contents* is based on the high deviation of the unfilled EN laminates. All filled formulations have a higher intrinsic viscosity than the neat EN and therefore showed less matrix “bleeding” during the curing of the prepreps. The *FVC* is in the range of  $9.5 \pm 1.5$  vol.%; the filler contents have an average of  $14.2 \pm 1.5$  vol.%. The resin

content for the unfilled laminate is the highest with 91 vol.%, whereas the resin content in the filled laminates ranges between  $75 \pm 3$  vol.%.

The average cured ply thickness of the unfilled prepreg layers of EN\_GF25, EN\_GF49 and EN\_GF107 were evaluated as 90  $\mu\text{m}$ , 110  $\mu\text{m}$ , and 150  $\mu\text{m}$ , respectively. The filled prepreps have an average thickness of 110  $\mu\text{m}$  (for the GF25), 120  $\mu\text{m}$  (for the GF49), and 150  $\mu\text{m}$  (for the GF107). The benchmark, PCL 370HR, is offered in CPTs of 51  $\mu\text{m}$ , 64  $\mu\text{m}$ , 102  $\mu\text{m}$  for the GF25, GF49, and GF107. However, it is produced with different fillers at different filler concentrations.

In summary, considering all produced laminates, the increase in FVC was compensated with a decrease in resin content to *keep the overall filler concentration constant* (tolerance of between  $\pm 1.5$  and 2.5 vol.% depending on the formulation). Therefore, both the resin and the fiber content will most influence the final properties, i.e., mainly thermal conductivity and flame retardancy.

### Prepreg Shelf-Life

The *shelf-life* is an important parameter to determine the *storage time and aging behavior* of the prepreps. Exemplarily, the EN\_Hybrid\_GF49 was studied in an *uncured* prepreg state. Prepreg cuts were simultaneously stored at 23 °C *r.h.* and at -18 °C at low *r.h.* for 12 weeks. Figure 75 shows the results for  $T_g$  and the reaction enthalpy that was evaluated via dynamic DSC.

The shelf life of the EN\_Hybrid\_GF49 prepreg conditioned at RT shows only a short period of storage stability of several days. However, whereas kept frozen, this sample is stable for up to 10 weeks before the reaction enthalpy decreases.

The  $T_g$  of the uncured prepreg is an indicator for its tack. The results in Figure 75 indicate a constant  $T_g$  for 12 weeks. Industry-standard for FR-4 prepreps is a stable storage time of 12 weeks below RT and 6 months below 5 °C.

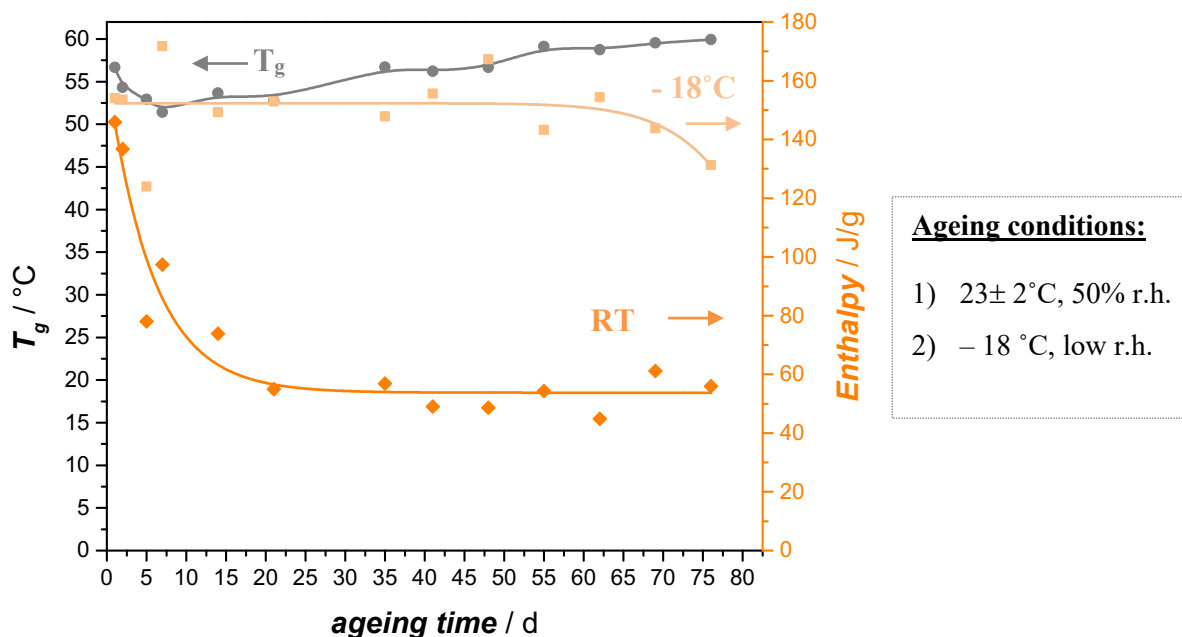
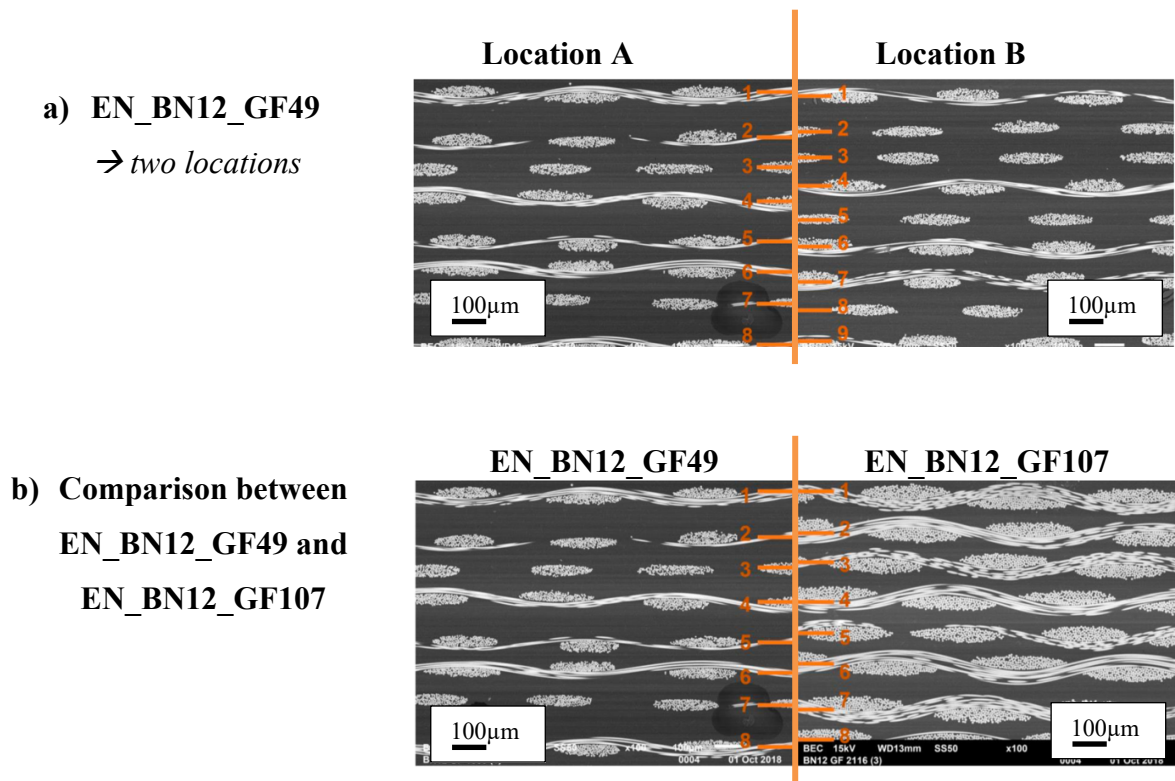


Figure 75 Shelf-life evaluated exemplarily for of the EN\_Hybrid\_GF49 prepreg over a storage time of 12 weeks. The  $T_g$  was evaluated at RT only. The enthalpy was assessed at both RT and  $-18^\circ\text{C}$  conditions.

### Impregnation Quality

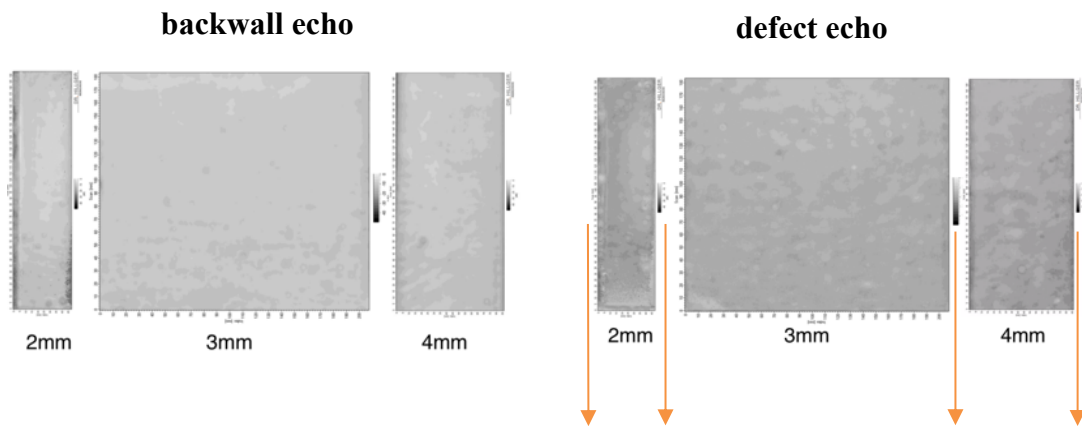
In general, compared to solvent-based impregnation routes, the *degree of impregnation* with this solvent-free method is excellent, despite the absence of solvent (Figure 76). The cavities between the GF strands and the *intra-tow* areas are well impregnated with the matrix. Moreover, the *fiber distance* between two different locations of the EN\_BN12\_GF49 sample was determined on polished sections via SEM (Figure 76). An average tow distance of  $107.5 \pm 14.8 \mu\text{m}$  was selected for the EN\_BN12\_GF49 laminate. Both sample locations show 8 prepreg layers at the same magnification (100x). The SEM micrographs in Figure 76b) show the comparison of fiber tow distance between the EN\_BN12\_GF49 and EN\_BN12\_GF107 specimens. The introduction of the GF107 fabric leads to a lower tow distance, and, the single GF strands increase in width size. Both the inter-and intra-tow areas become smaller and therefore build a much tighter barrier than the GF49 fabric.



**Figure 76** Evaluation of the tow distances in a) same prepreg, i.e., two different locations of the EN\_BN12\_GF49 and b) difference between EN\_BN12\_GF49 and EN\_BN12\_GF107 prepreg (magnification of 100x).

Ultrasonic C-scans were used to detect any *defects*. Figure 77 shows the back wall and the defect echo exemplarily of the EN\_BN12\_GF49 laminate with the three different thickness sections (see laminate design in Figure 77 b). The laminate shows a good uniformity and well-dispersed fillers with only some pores on the lower side of the laminate edges. However, no extensive resin bleeding was observed for all filled systems. One laminate was prepared from one prepreg roll with three different thicknesses, 2 mm, 3 mm, and 4 mm, to accommodate the various testing methods.

### a) Ultrasonic C-Scans



### b) Laminate design



Figure 77 a) Ultrasonic C-scans of the EN\_BN12\_GF49 laminate. b) corresponding prepreg lay-up on the left and the cured laminate to show positions of each sample that were prepared.

### Glass Transition Temperature – *Evaluation of the long-term service temperature*

The *glass transition temperature* ( $T_g$ ) is defined as the temperature at which the glassy state changes into the rubbery or melt state. The material loses its dimensional stability. The temperature at which the long-range translational motion of the polymer chain segments is active [198]. For electronic substrate applications, the glass transition temperature must be above the service temperature of the substrate material, i.e. 200 - 220 °C, especially considering the new lead-free soldering processing at elevated temperatures.

The results of the DMTA measurements are shown in Figure 78 for all systems. The  $T_g$  for all tested laminates is in the range of 230 – 234 °C. The target of  $\geq 220$  °C was thus achieved for all systems. State-of-the-Art FR-4 materials have a  $T_g$  in the range of 140 – 180 °C [14,199].

The results of all three benchmarks, which are currently advertised as “*high-T<sub>g</sub> State-of-the-Art*” materials, only reached values of **150 -180 °C**. The T<sub>g</sub> slightly decreases with increasing fiber volume content by a maximum of – 5 °C. The influence of the fiber volume content on the T<sub>g</sub> is shown in Figure 78. The slope of the fitted curve is negative. A decrease in - 0.300 °C/vol.% °C / per vol.% GF for the hybrid system was calculated, followed by the BN 12 formulation (- 0.222 °C/vol.%), and the EN with a decrease of - 0.061 °C/vol.%.

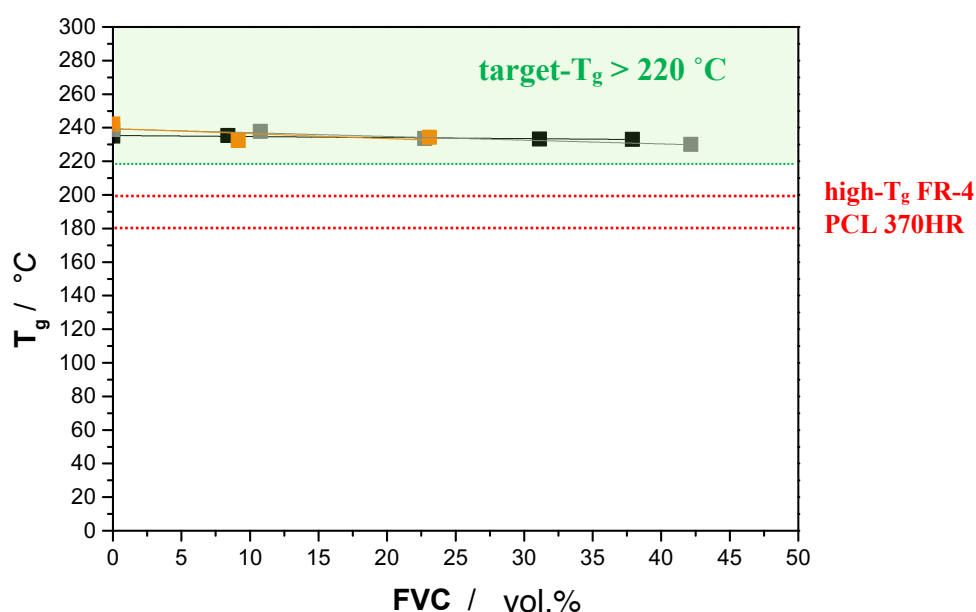


**Figure 78** Glass transition temperatures for the filled resins and their corresponding prepreps (EN, EN\_BN12, and EN\_Hybrid) in dependency of FVC. All systems achieved the target of > 220 °C.

Ratna *et al.* state that the thermoset matrix mainly governs the T<sub>g</sub> since the GF fibers are highly heat resistant [30]. Droste *et al.* pointed out that if the interaction or interfacial adhesion between the fillers and the resin matrix is good, this will inhibit the polymer chains' mobility, resulting in a higher glass transition temperature [200]. Additionally, the incorporation of organosilane-modified GF increases the adhesion between the matrix and the fibers, as the fibers are usually organosilane-modified [30]. Boehmite can establish strong bonds with the EN matrix regarding the fillers due to its -OH functional groups. On the contrary, BN has a smooth surface with almost no functional groups that can initiate any chemical bonding. Only their hydroxyl- and amino-groups at their edges can form linkages with the polymer matrix [82,101,119]. Especially when the BN fillers are well dispersed, the crosslink density increases

and therefore also the  $T_g$ . A better bonding can lead to a stiffer network due to higher filler-matrix interaction, resulting in a higher  $T_g$ . A lower glass transition temperature might indicate a lower crosslink density.

### 5.3.2 Thermal Conductivity of filled GF Prepreg Laminates

#### Influence of Glass-Fibers on the Thermal Conductivity of filled Resin Formulations

The influence of the glass-fibers on the overall morphology (filler dispersion and filler network formation) was studied exemplarily on the GF25 prepreg laminates. TC was evaluated in both  $x/y$ - and  $z$ -direction since the glass fabric has a strong *in-plane* orientation. The effect of an increasing FVC on the TC and the morphology of the laminates was evaluated. The focus was on the following systems: *unfilled EN\_GFXX*, *EN\_BT2\_GFXX*, *EN\_BN12\_GFXX*, and *EN\_Hybrid\_GFXX*.

#### Thermal Conductivity in $z$ -direction of filled GF Prepregs – *Interaction of Fillers and GF*

The thermal conductivity (TC) value was measured in *through-plane* (=  $z$ -plane) of the polished laminate samples with a **heat flow meter**. The TC values of the highly filled GF-laminates and the corresponding filled resin plates are plotted in Figure 79. The filler contents are in the same range for both the filled resins and their corresponding GF25 laminates.

The TC value for EN\_GF25 is 0.181 W/mK, whereas the EN has a value of 0.20 W/mK. The deviation might arise from scattering effects. The thermal conductivity of E-glass is known to be between 0.9 and 1.35 W/mK, depending on the measuring method [123].

Regarding the *influence* of different *filler nature*, the overall trends are analogous to the previous chapter of the (filled) resins. However, the impact of the GF fabric acting as a thermal barrier is apparent (Figure 79).

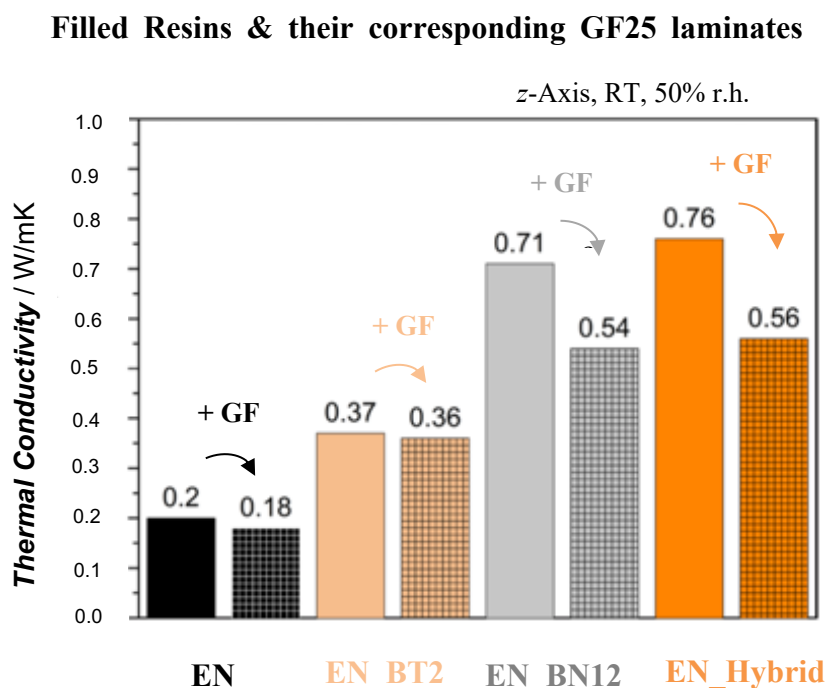


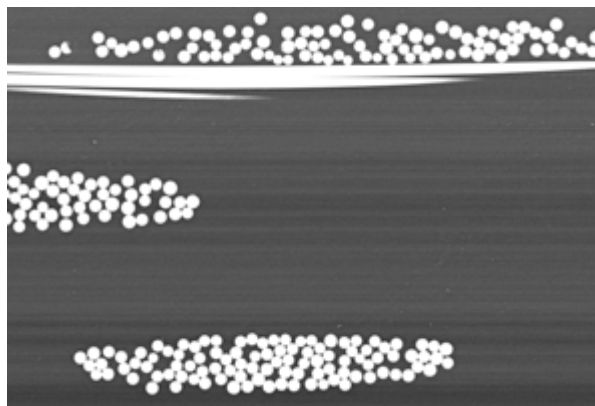
**Figure 79 Thermal conductivity in z-direction of filled EN resins and their GF25 laminates measured via a heat-flow meter.**

The TC of all laminates is slightly lower than the TC of their resin counterparts. Although the GF has a higher TC ( $= 0.9 \text{ W/mK}$ ) than the matrix ( $= 0.2 \text{ W/mK}$ ), the results indicate that the GF acts as a barrier by presumably interfering with the filler microstructure formation. The heat transfer is decreased due to additional scattering effects at the interfaces between *matrix-GF*, *matrix-filler*, *filler-GF*, and *filler-filler*.

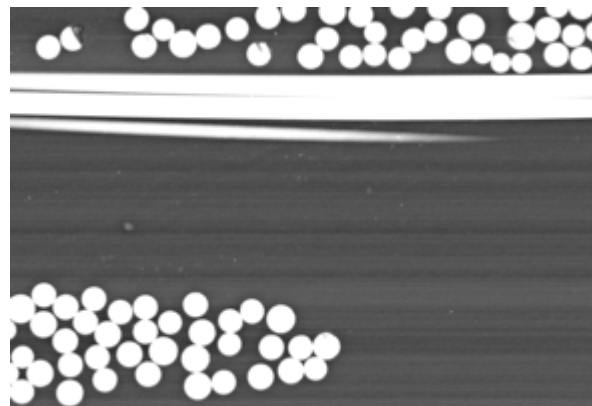
The dispersion quality and the morphology of the fillers in the GF25 laminates were studied with SEM. The laminate cross-sections at a magnification of 500 x and 1000 x can be seen in Figure 80. The first row of the micrographs (Figure 80a) and b) shows the unfilled laminate. The GF tows are well impregnated with the resin matrix. In between the GF tows, one can find the *resin-rich area* (colored in dark grey).

In general, it was observed that the incorporation of various fillers (BT, BN, or hybrid) did not lead to any concentration gradient of the filler particles throughout the laminate. Especially no filtration effects along the *x/y*-axis in between the different prepreg layers are visible due to undergoing resin flow during curing.

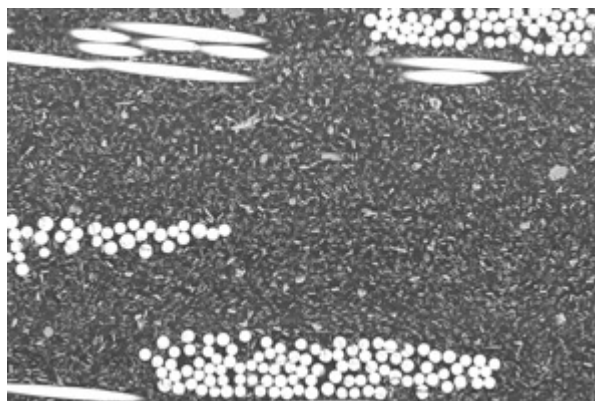
a) EN\_GF25



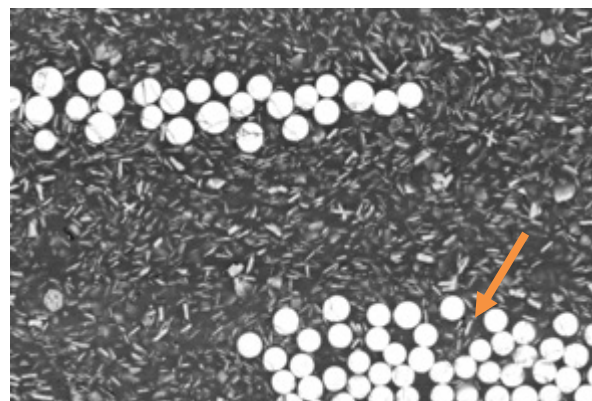
b) EN\_GF25



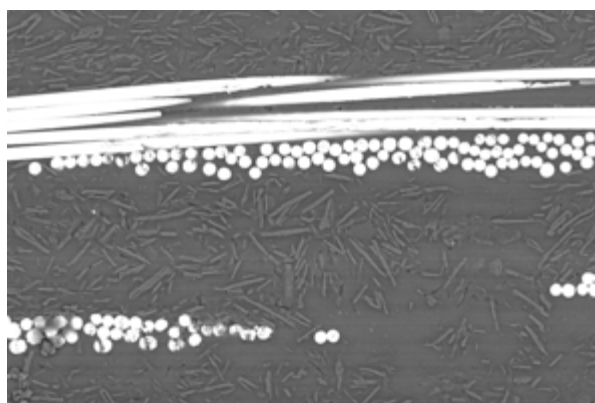
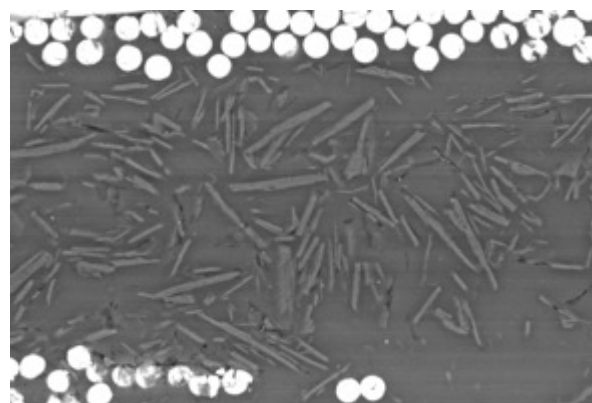
c) EN\_BT2\_GF25



d) EN\_BT2\_GF25



e) EN\_BN12\_GF25

f) EN\_BN12\_GF25 (*inter-tow* region)

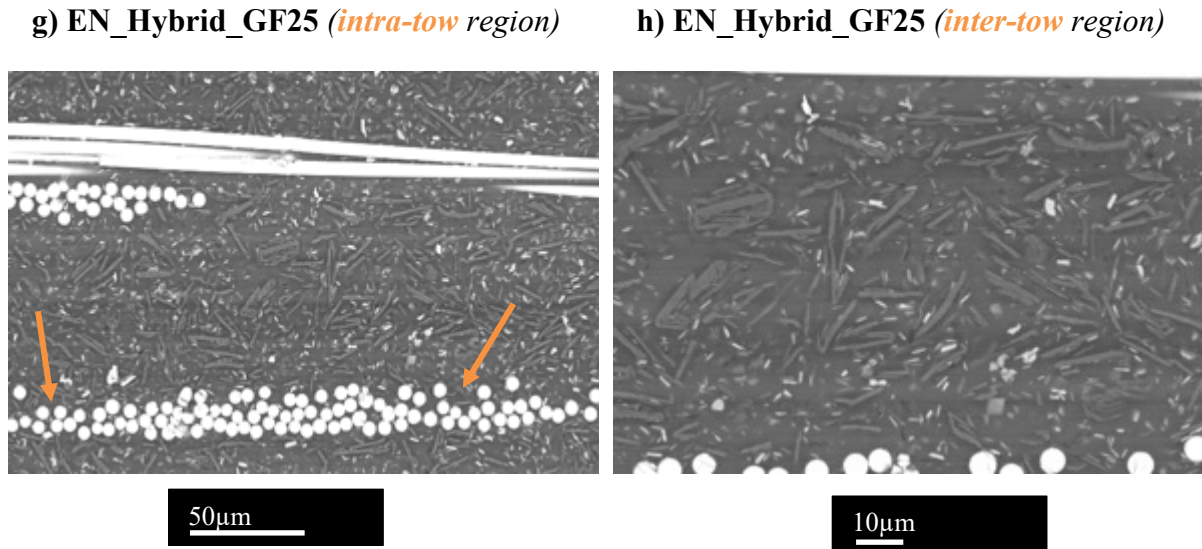


**Figure 80** SEM micrographs of the highly filled prepreg laminates in through-thickness direction indicating the filler dispersion, orientation, and eventual filtration effects for a+b) EN\_GF25, c+d) EN\_BT2\_GF25 e+f) EN\_BN12\_GF25 and g+h) EN\_Hybrid\_GF25.

The addition of 12.7 vol.% of BT2 particles increases the TC of the laminates from 0.181 W/mK to 0.359 W/mK. However, the *z*-plane TC of Boehmite is known to be approximately 30 W/mK in literature. This increase can be attributed to the excellent dispersion and random orientation of the Boehmite particles in the resin matrix, which leads to a dense filler network in the laminate (Figure 80 c) and d)). It can be observed that the BT particles are not only can be detected in the *inter-tow* areas but also infiltrated the *intra-tow* areas.

Moreover, the EN\_BN12\_GF25 exhibits a TC value of 0.545 W/mK at 15.1 vol.% filler content. The fillers particles are uniformly distributed but predominantly within the *inter-tow* areas of the laminate (Figure 80 e) and f). The filler arrangement of the 12 μm BN platelets visible in the SEM micrographs confirms a random orientation with a good-filler-filler interaction similar to the filled resins. Per contra, the *intra-tow* region is not infiltrated by the BN12 filler, as its aspect ratio is too high to infiltrate the tight rovings. The platelets are filtered at the outer corners of these GF rovings and orientate themselves horizontally in *x/y*-direction.

The highest TC value was achieved with the EN\_Hybrid\_GF25 laminate (0.560 W/mK at 14.0 vol.%). Thus, the partial replacement of 12 μm-BN with 2 μm Boehmite results in a TC value comparable to the EN\_BN12 resin formulation. The SEM micrographs (Figure 80g) and h)) show that the larger BN platelets form a filler network in the *inter-tow* region which effectively contributes to the thermal conductivity. The smaller particles attach to the BN

platelets, fill their inter-filler areas, and therefore an optimal packing density can be reached. In addition, the BT fillers can also be detected in the *intra-tow* area suggesting, that their main contribution to the thermal conductivity is to “bridge” the GF barrier. Therefore, the small particles act as “connectors” or “links” between the BN filler network in the *inter-tow* area and the GF barrier.

### ***In-plane- & Through-plane - Thermal Conductivity in GF 25 Prepreg Laminates***

The thermal conductivity of the GF25 laminates in *x/y*- and *z*-direction-dependent was determined by a **transient hot bridge** (THB) sensor (Figure 81). This enables to confirm the findings of the previous chapters concerning the filler network formation and the role of the GF fabric.

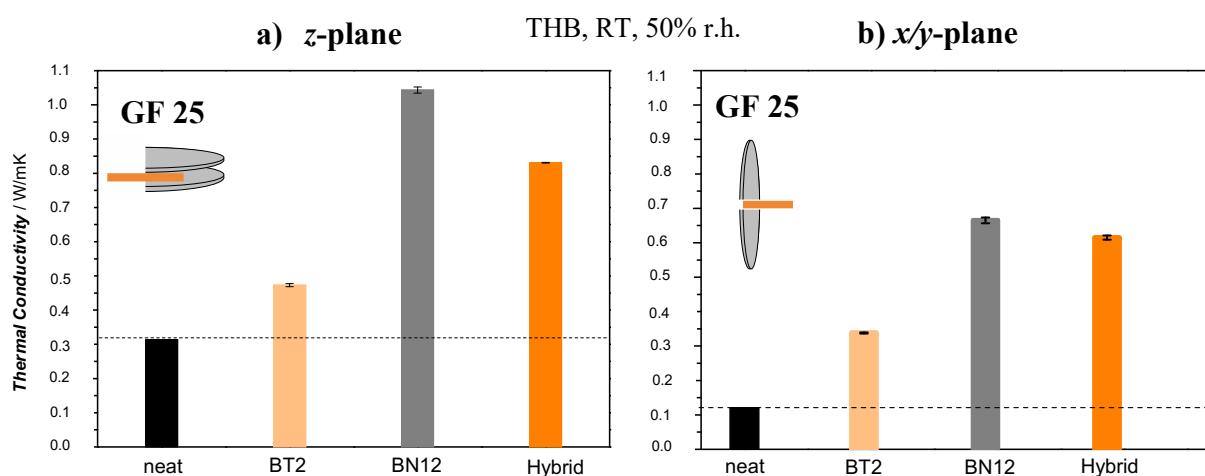


**Figure 81** Thermal conductivity measured with THB a) in through-thickness (*z*-plane) and b) in-plane (*x/y*-plane) direction of the various GF25 laminates.

Values obtained with the THB (Figure 81) are slightly higher than those measured with the heat flow meter (Figure 79). As seen in Figure 81, the *z*-plane TC of the neat Epoxy laminate is 0.314 W/mK, which is considerably higher than the 0.181 W/mK obtained from the hot-plate measurements. This implies that the surface roughness might have a crucial effect. Although the samples for the hot-plate measurement were polished down to 1  $\mu\text{m}$  roughness, the contact area between the measurement plates and the individual sample seems to be lower than the

Kapton sensor. The THB measurement was optimized by embedding the sensor in a thermally conductive paste ( $\text{TiO}_2$ ) to improve the sensor and sample surface interface. In addition, a weight of 5 kN was placed on top of each sample during measurement.

The values in the  $x/y$ -plane are lower than the values measured in the  $z$ -plane. For the BN12  $\mu\text{m}$ , for example, a slight anisotropic effect in  $z$ -plane can be observed. The SEM micrographs show that the BN12 platelets have a random orientation (Figure 80). However, only a few are orientated in the  $x/y$ -direction. The majority is slightly tilted or are oriented in the preferred  $z$ -plane resulting in a higher thermal heat transfer. These values are comparable with the commercially available FR-4 materials with a TC of 0.3 - 0.4 W/mK [201].

**Thermal imaging** cameras are ideal tools to map the heat distribution in electronic components visually. The overall performance load on a circuit board has exceptionally increased due to the miniaturization trend in the electronic industry. The heat generated during use can lead to temperatures as high as 165 °C [123]. The heating rates of different highly filled GF laminates, the EN\_Hybrid\_GF 25 and the EN\_BN12\_GF25 laminate, show the highest and fastest increase in temperature (Figure 82). The EN\_GF25 attains the lowest temperature increase. In general, the non-linear heating/cooling profiles (temperature =  $f(\text{time})$ ) match the trend accordingly with the measured thermal conductivity. The faster a sample heats up, the faster it cools down as well.

The corresponding Infra-Red (IR) images can be seen in Figure 83. Each sample was recorded for a total of 2 minutes. However, the first 30 seconds are most important for heat absorption and heat transfer. The slope of the heating curves lowers after about 40 s approaching a plateau niveau. The EN\_GF25 laminate shows an uneven heat distribution within the sample diameter, indicating that heat absorption, and therefore the thermal conductivity is low. The BN 12 $\mu\text{m}$ -filled laminate has the highest heating rate, closely followed by the EN\_Hybrid\_GF25.

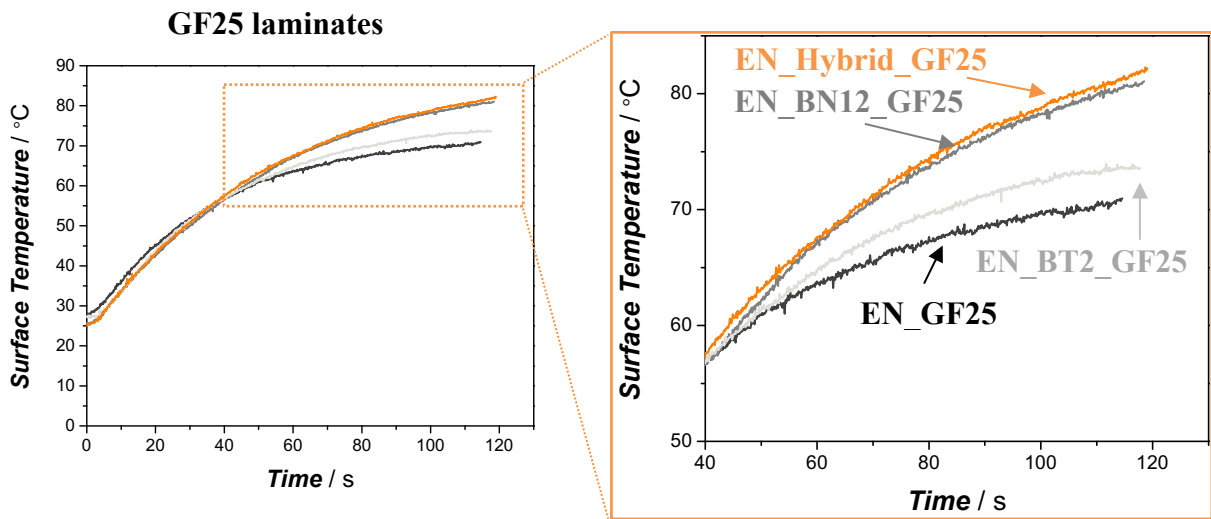


Figure 82 Heating rate profiles of the GF25 laminates recorded with Infra-Red (IR)-thermal imaging.

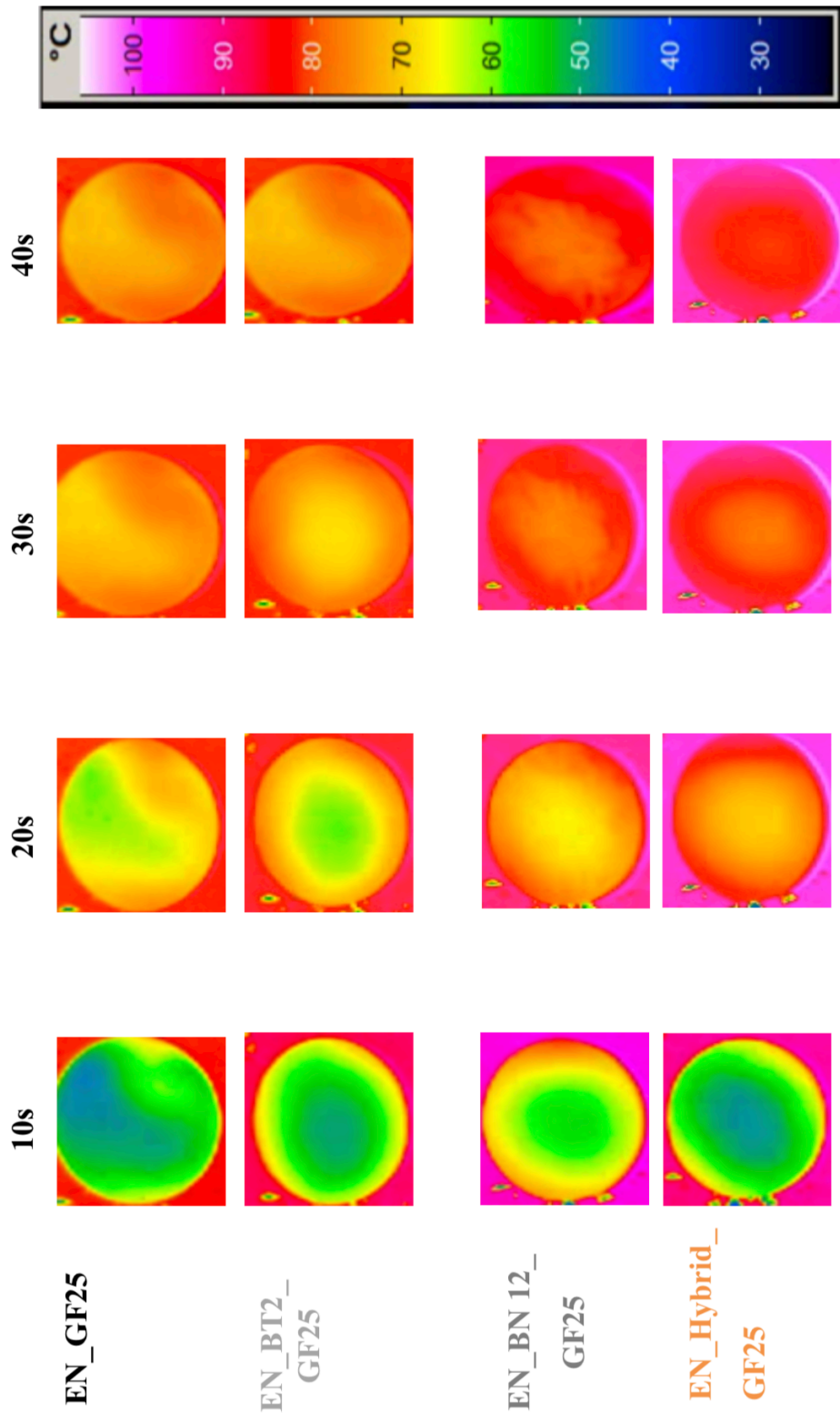
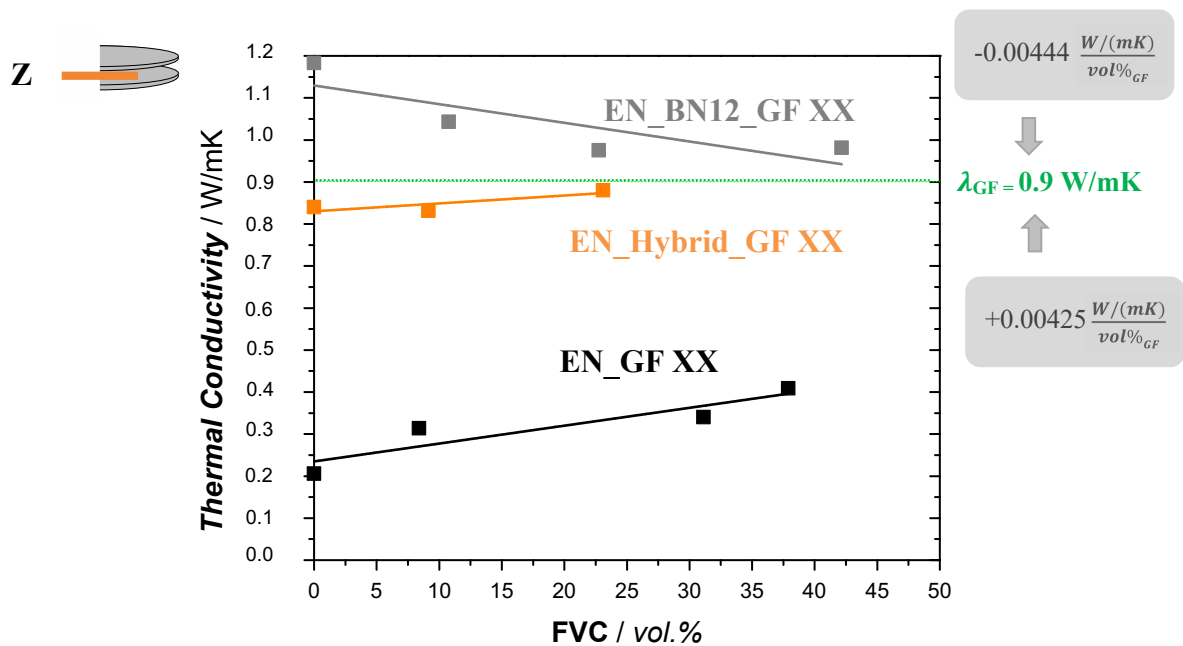


Figure 83 Infra-Red images for the (filled) GF25 laminates indicating different heating rates which are in alignment with their intrinsic thermal conductivity.

### Influence of FVC on the Thermal Conductivity

The influence of an increasing FVC is especially of interest since not only in the PCB- but also in the automotive industry, a wide range of glass fabrics are used to achieve lightweight designs. The chosen fabrics, with areal weights of 25 g/m<sup>2</sup>, 49 g/m<sup>2</sup>, and 107 g/m<sup>2</sup> are commonly used for PCB applications: US Style 106, US Style 1080, and US Style 2117 to adjust different substrate thicknesses in terms of PCB design. Therefore, it is of high interest to analyze the effect of areal weights on the filler microstructure and the resulting thermal conductivity.

The influence of the FVC on the *z*-thermal conductivity measured with THB in for *z*- plane is plotted in Figure 84.



**Figure 84 Influence of FVC on the *z*-thermal conductivity measured with THB.**

The *z*-plane measurements for all systems show that the TC converges to the TC of the glass-fibers, which is 0.9 W/mK. In particular, the EN\_BN12\_GFXX and EN\_Hybrid\_GFXX laminates approach this value with increasing FVC. The BN 12μm filler content is between 15 – 11 vol.% for the GF25, GF49, and GF107, respectively. The TC of the hybrid filled laminates behaves similarly with an increase in FVC. The linear slope of the EN\_GFXX

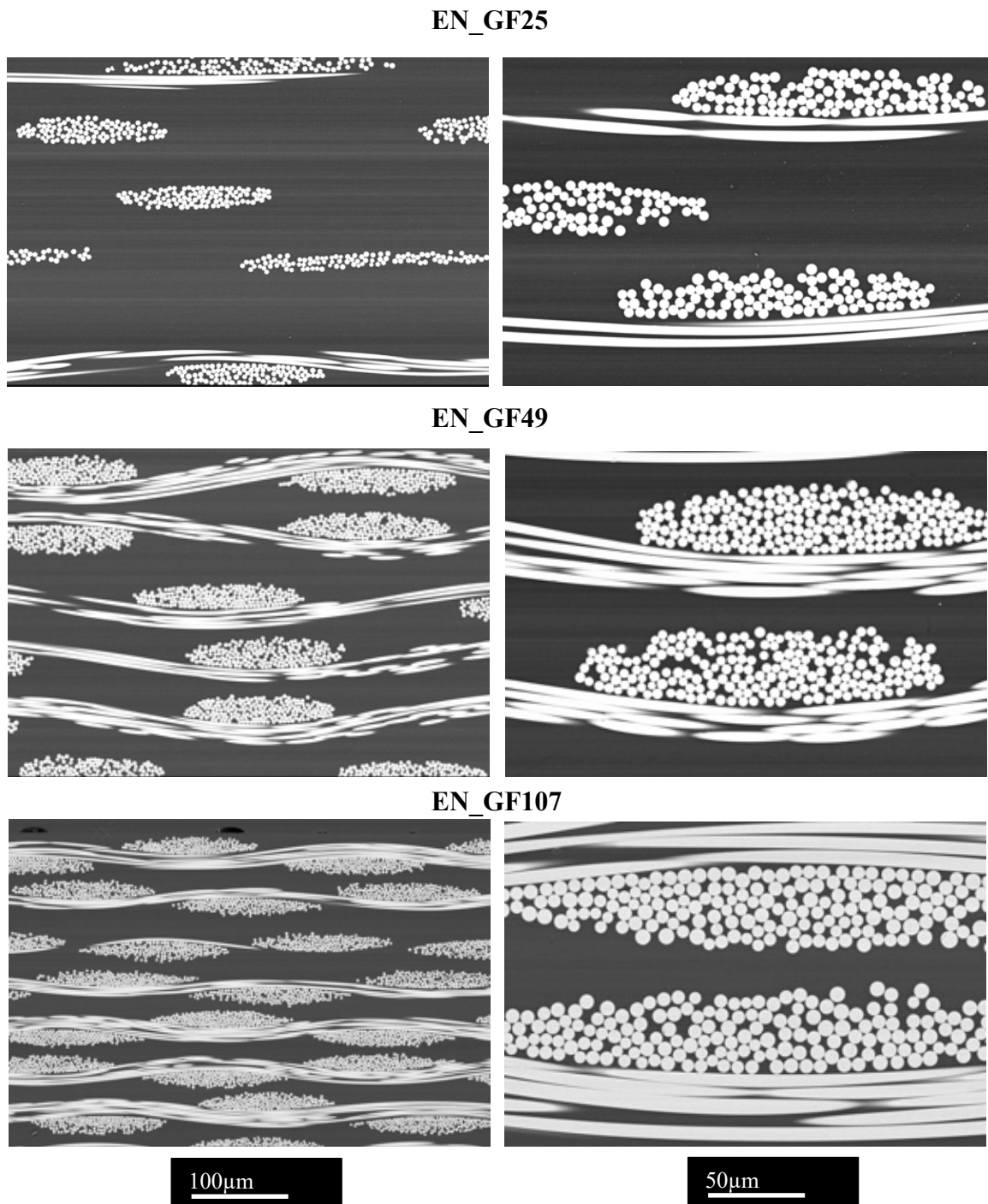
laminates is directly proportional to the increasing FVC and, consequently, the resin volume content reduction. The results demonstrate that the FVC plays a crucial role.

Figure 85 shows the cross-sections of the *neat EN\_GFXX* laminates in increasing order of the FVC: GF25, GF49, and GF107. All three laminates offer good fiber wetting. It can be observed that with increasing FVC, the individual prepreg layer distance decreases. Therefore, the fiber distance is reduced, which leads to a better heat transfer between the prepreg layers. This results in a more efficient heat transfer in both *z*- and *x/y*-plane.

The SEM micrographs of the *EN\_BN12\_GFXX* filled laminates are shown in Figure 86. Similar to the results above on the unfilled laminates, the inter-layer distance of each prepreg layer decreases as the FVC increases. However, in all laminates, the BN platelets can be mainly detected within the *inter-tow* areas in a random orientation and good dispersion. Since the BN is not infiltrating the *intra-tow* area, the GF acts directly as a thermal barrier. This effect is even more pronounced with increasing FVC and caused a lower TC.

A closer look into the resulting microstructure of the *EN\_Hybrid\_GF49* formulation in Figure 87, shows that the filler dispersion is good, associated with a random filler orientation. Furthermore, as already discussed in the previous chapter, the BN 12  $\mu\text{m}$  filler is mainly responsible for forming the *macro filler network*. In contrast, the smaller Boehmite particle fills the BN inter-gaps in the inter-tow area. BN12 particles can also infiltrate the inter-tow GF area forming a *micro filler network* (Figure 87 *intra-tow /inter-tow* area). Boehmite particles are, therefore, able to contribute to the overall TC by overcoming the GF barrier.

Nonetheless, the TC of the hybrid systems is still mainly governed by the high FVC and only little affected by the presence of conductive fillers.



**Figure 85 SEM micrographs of the unfilled, neat laminates in the z-plane direction with increasing FVC for EN\_GF25, EN\_GF49 and EN\_GF107 (200x left, 500x right).**

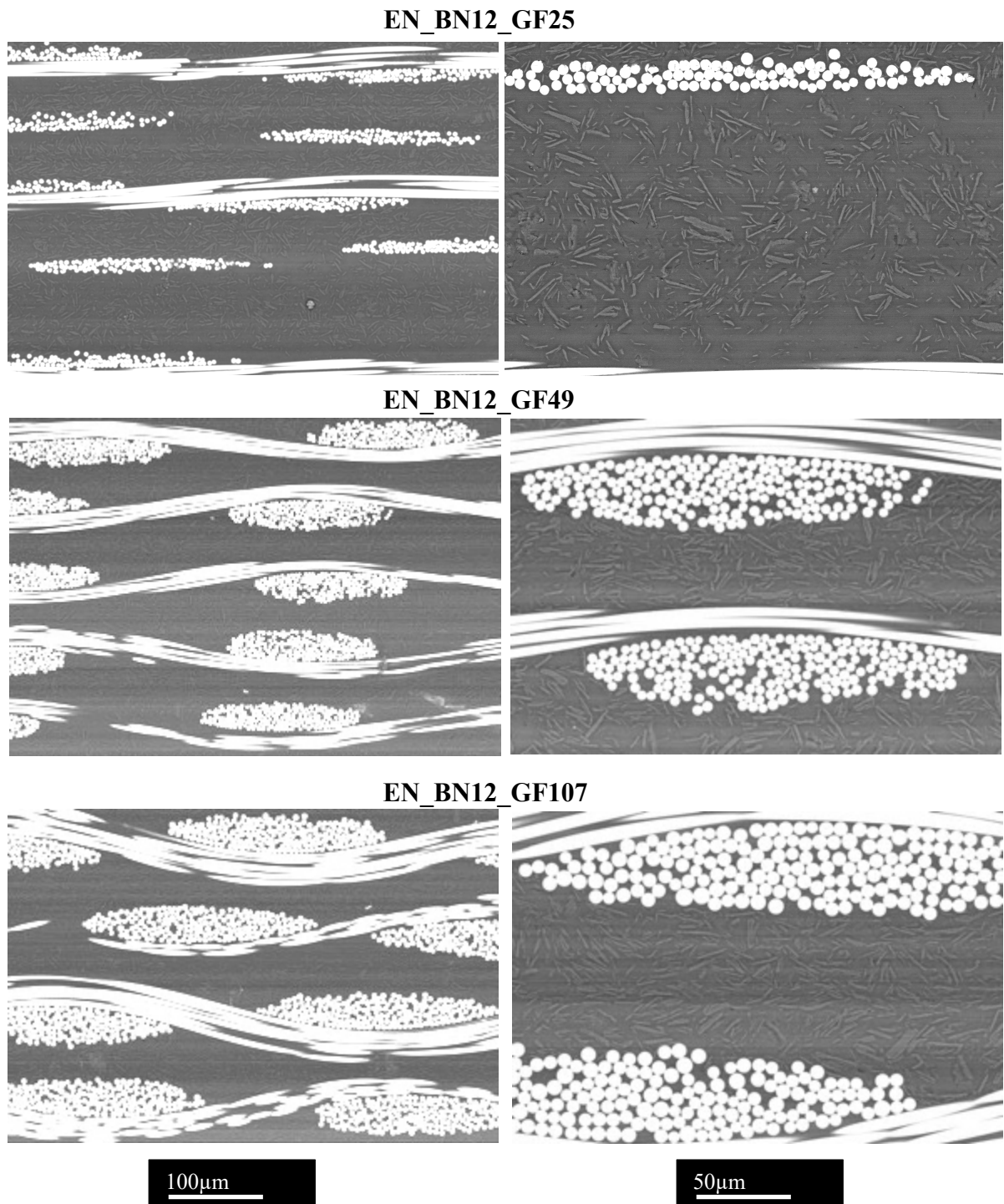


**Figure 86 SEM micrographs of the EN\_BN12\_GFX laminates in z-plane direction in dependency of FVC. The filler dispersion and orientation are visible (200x left, 500x right).**

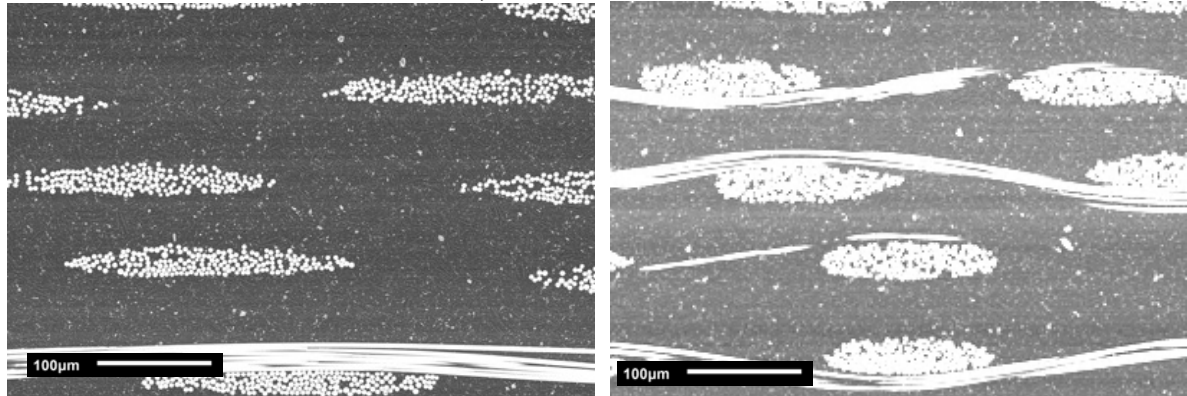
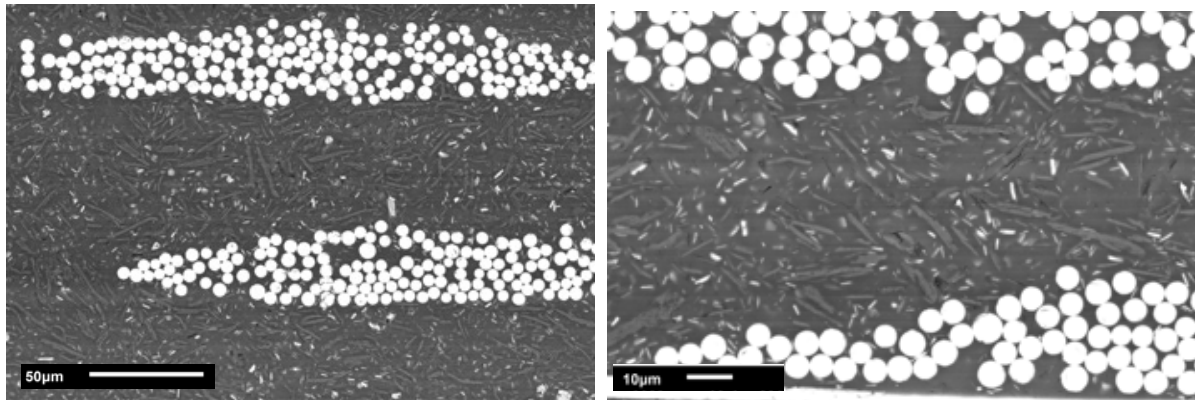
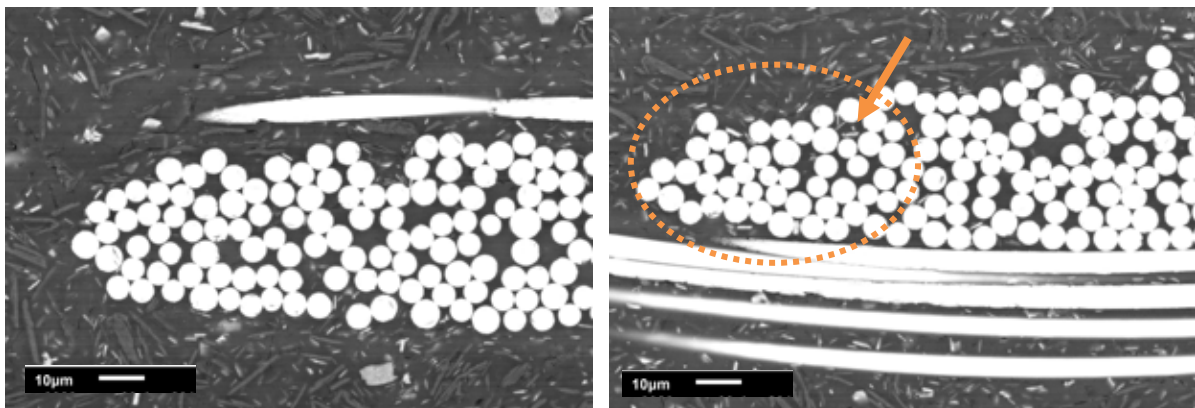
**EN\_Hybrid\_GF49****a) Overview****b) inter-tow area****c) intra-tow area**

Figure 87 SEM micrographs of the EN\_Hybrid\_GF49 laminate in z-plane. Filler dispersion, orientation, and infiltration into the intra-tow area. a) Overview in 200x magnification, b) inter-tow area between two prepreg layers (1000x), and c) intra-tow area of one prepreg layer (500x and 1000x).

Comparing these micrographs with the base material developed in this work above with the microstructure of the benchmark prepregs is very similar although the absence of solvent (Figure 88). The samples studied below are using the GF107 fabric, US Style 2116. The benchmark DE 140 does not contain fillers, whereas IS400 and PCL 370HR contain inorganic fillers. The filler size is assumed to be in the range of  $D_{50} 2 \mu\text{m}$ . Furthermore, it is assumed that either ATH or MDH in a higher concentration were used. Isola did not disclose the filler nature. Considering the production route via solvent-dip, the fillers show a good dispersion with a random orientation. However, it was observed that during this solvent-dip prepreg production, due to the high filler content in the formulation, with time, a gradual filler concentration gradient was formed.

The intra-tow area is infiltrated with the small fillers to some degree. The *thermal conductivity* was studied with hot-plate only, resulting in values of **< 0.38 W/mK in the z-plane**. This supports the assumption that only hydrates, such as ATH and MDH as fillers, were used, which only have an intrinsic TC in the range of the Boehmite. This value is comparable with other commercially available FR-4 (0.3 - 0.4 W/mK) [201].



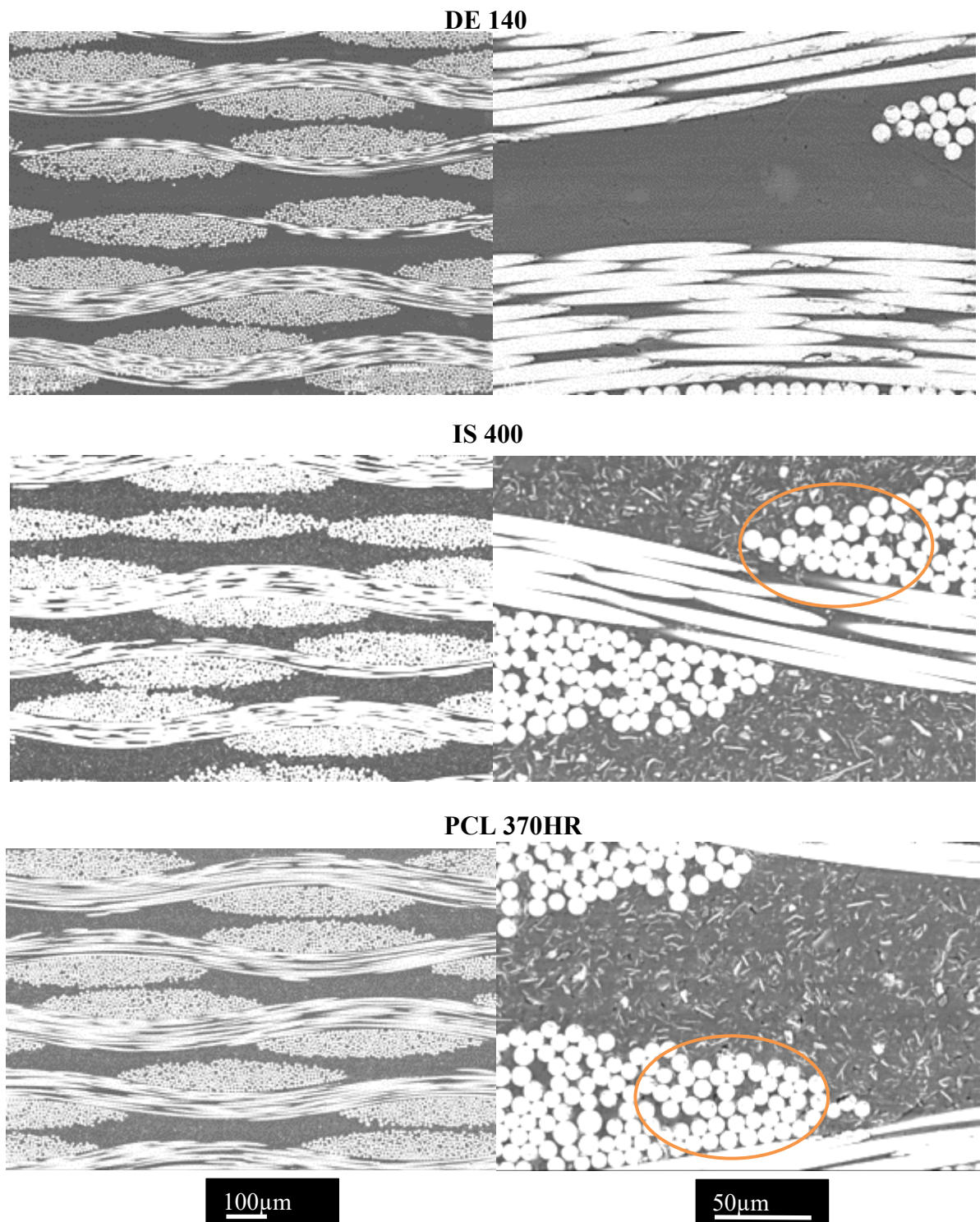


Figure 88 Photograph of the cured laminates and below their corresponding SEM micrographs of the microstructure of *State-of-the-Art* benchmark systems: DE 140, IS 400 and PCL 370 HR (100x left, 500x magnification right).

### Thermal Imaging

Figure 89 shows the results of visual thermographic imaging demonstrating the effect of increasing FVC for the EN\_GFXX and EN\_BN12\_GFXX laminates. Due to the high number of fibers in the GF49 and GF107 laminates, heat absorption occurs very quickly compared to the GF25. Compared to the unfilled laminates, heat absorption in the BN 12  $\mu\text{m}$  filled laminates appears faster.

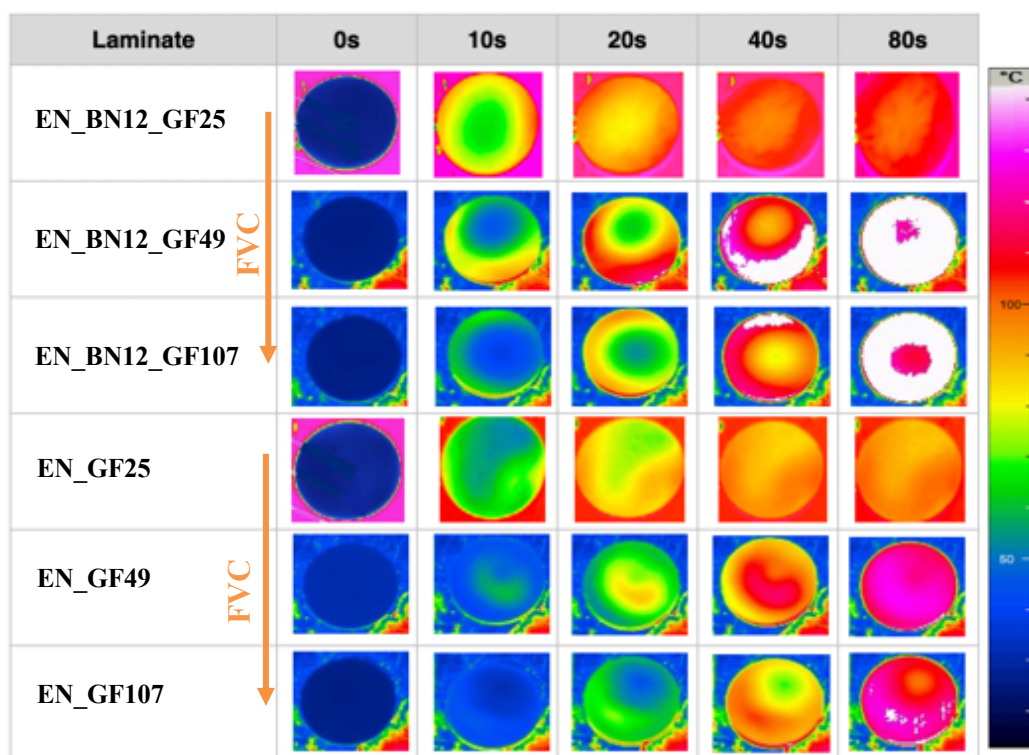


Figure 89 Infra-Red images exemplarily for the unfilled EN\_GFXX and the EN\_BN12\_GFXX laminates in dependency of their FVC.

### Interim Summary – Studies on Thermal Conductivity

In summary, the addition of GF led to TC values that are not exceeding the results of the findings in the filled resins. Furthermore, with the increase in FVC, the TC approached the value of the intrinsic TC of the glass fibers, which is 0.9 W/mK. This was expected since the fibers take up a certain volume content of the resin so that the overall thermal conductivity

increases for the unfilled systems. Furthermore, even the addition of highly thermal conductive BN at the cost of matrix resin (the filler content was kept on the same level with  $\pm 2.5$  vol.%!) could not enhance the TC further.

Although the GF volume content governs the overall thermal conductivity, the filled laminates, EN\_BN12\_GFXX and EN\_Hybrid\_GFXX, presented TC values above the target of 0.7 W/mK. Even though the GF fabric “interferes” with the filler network/microstructure (= *barrier effect*), it contributed to the overall TC of 0.9 W/mK, which helps tremendously in the heat absorption. The *filler network formation mechanisms*, however, are very similar to the findings in the filled resins. The BN forms a macro-sized filler network mainly in the inter-tow areas, whereas the smaller Boehmite filler fits into the small gaps. Furthermore, the BN is also able to infiltrate the GF tows. This micro-structure leads to an improved TC, comparable to EN\_BN12 formulations. This helps lower the GF barrier for the TC and is also cost-effective since the expensive BN is partially substituted with less expensive Boehmite.

In summary, the addition of GF led to TC values that are not exceeding the results of the findings in the filled resins. Furthermore, with increase in FVC, the TC approached the value of the intrinsic TC of the glassfibers which is 0.9 W/mK. This was expected since the fibers take up a great volume of the resin so that the overall thermal conductivity increases for the unfilled systems. Furthermore, even the addition of highly thermal conductive BN at the cost of matrix resin (the filler content was kept on the same level with  $\pm 2.5$  vol.%!), was not able to enhance further the TC.

Although the GF volume content governs the overall thermal conductivity, the filled laminates, EN\_BN12\_GFXX and EN\_Hybrid\_GFXX presented TC values of above the target of 0.7 W/mK. Even though, the GF fabric “interferes” with the filler network / microstructure (= *barrier effect*), it contributed to the overall TC of 0.9 W/mK which helps tremendously in the heat absorption. The *filler network formation mechanisms*, however, are very similar to the findings in the filled resins. The BN forms a macro-sized filler network mainly in the inter-tow areas, whereas the smaller Boehmite filler fits into the small gaps. Furthermore, the BN is also able to infiltrate the GF tows. This micro-structure leads to an improved TC, comparable to EN\_BN12 formulations. This helps not only to lower the GF barrier for the TC but is also cost-effective since the expensive BN is partially substituted with less expensive Boehmite.

### 5.3.3 Pyrolysis- and Fire Behaviour of filled GF Laminates

#### Thermal Degradation and Pyrolysis Behaviour of filled Prepreg Laminates

Table 17 shows the thermal decomposition temperatures at 2 wt.% ( $T_{d,2\%}$ ) and 5 wt.% ( $T_{d,5\%}$ ). The values indicate an initial degradation.

First, it can be observed that with the incorporation of the filler particles into the EN matrix, the decompositions temperatures are shifted by at least + 5 °C. The  $T_{d,2\%}$  and  $T_{d,5\%}$  show a difference of + 10 °C for the EN systems, and + 15 °C for the filled systems, which is in alignment with the findings of the previous chapter (5.2.3).

Secondly, the addition of glass fibers resulted in slightly lower  $T_{d,2\%}$  values, and an increase in  $T_{d,5\%}$  in the GF 25 laminates. However, with increasing in FVC, the thermal stability increases tremendously. The thermal stabilities of conventional FR-4 materials are in the range of  $T_{d,5\%}$  305 -315 °C and are on average 60 °C lower than the novel laminates developed in this thesis. The target value of > 360 °C was achieved for all systems. The highest thermal stabilities were reached with the EN\_BN12\_GF107 and the EN\_BT2\_GF107 specimens exceeding 380 °C.

The char yield of BN-filled laminates is higher compared to the BT-filled systems. In addition, the char yield increases with the increase in FVC. Both effects can be correlated to their high thermal stability, as both BN and the glass fibers do not decompose and remain in the condensed phase.

It has been shown that BT, due to its decomposition step, is active both in the gas and in the condensed phase (see Figure 67), and therefore, the char yield is lower. In addition, the different rheological behavior, especially with the laminates GF49 and GF107, indicates a higher residual strength of the sample, which is vital in the event of fire [202].

**Table 17 Overview of the thermal stability and degradation behaviour of all (filled) Epoxy Novolac resins and their corresponding laminates measured with TGA.**

<b>Composition</b>	$T_{d,2\%}^a /$ °C	$T_{d,5\%}^b /$ °C	<b>Char yield<sup>c</sup> /</b> wt. %
<b>EN</b>	352	363	0.00
<b>EN_GF25</b>	344	370	31.91
<b>EN_GF49</b>	356	373	33.28
<b>EN_GF107</b>	361	378	53.29
<b>EN_BN12</b>	353	368	30.45
<b>EN_BN12_GF25</b>	348	372	39.06
<b>EN_BN12_GF49</b>	356	377	48.59
<b>EN_BN12_GF107</b>	363	380	62.07
<b>EN_BT2</b>	359	373	29.10
<b>EN_BT2_GF25</b>	342	371	36.43
<b>EN_BT2_GF107</b>	367	385	62.23
<b>EN_Hybrid</b>	358	370	29.64
<b>EN_Hybrid_GF25</b>	341	367	39.51
<b>EN_Hybrid_GF49</b>	356	373	49.21

<sup>a</sup> Degradation temperature at 2% weight loss under  $N_2$ .

<sup>b</sup> Degradation temperature at 5% weight loss under  $N_2$ .

<sup>c</sup> Residual weight at 800 °C under Air

### **Influence of Glass-Fibers on the Flame Retardancy of filled Resin Formulations**

The time dependency of the heat release rate (HRR) and the total smoke release rate (TSR) are plotted in Figure 89. To discuss and correlate the results from the cone calorimeter measurements, the fiber, resin, and filler volume contents are given in Table 18.

With the addition of glass-fibers to the (filled) resin formulations, two distinct observations can be made: first, a decrease of the PHRR and, secondly, a shift of the  $t_{ig}$  by - 20 s. Compared to

the results of the filled formulations in Figure 68 and Figure 69, the EN\_GF25 shows the shortest time to ignition ( $t_{ig}$ ) (88 s) and the highest PHRR (686 kW/m<sup>2</sup>). This can be directly correlated to the much higher resin content (approximately 15 vol.%) than the filled laminates.

**Table 18 Overview of the various (filled) prepregs and their corresponding fiber, resin and filler volume contents.**

<b>Composition</b>	<b>FVC / vol. %</b>	<b>Resin content / vol. %</b>	<b>Filler content / vol. %</b>
<b>EN</b>	-	99.7	-
<b>EN_GF25</b>	8.4	91.6	-
<b>EN_BN12</b>	-	86.3	13.7
<b>EN_BN12_GF25</b>	10.7	74.1	15.2
<b>EN_BT2</b>	-	89.6	10.4
<b>EN_BT2_GF25</b>	8.6	78.6	12.7
<b>EN_Hybrid</b>	-	87.8	12.2
<b>EN_Hybrid_GF25</b>	9.2	76.84	14.1

Furthermore, the glass fabric layers tremendously hinder the overall intumescence of the GF 25 laminate samples compared to the resins.

The suppression of the "intumescence" of the sample with 8.4 vol.% fibers (EN\_GF25) leads to higher dimensional stability and a lower loss of rigidity. Intumescence is also an important parameter in a fire scenario since a collapse of the "burning" material can lead to the spread of the fire. Like the unfilled resin, its GF25 laminate shows a double-peak formation during degradation (HRR curve in Figure 90), which is even more pronounced in the laminate.

During the Cone Calorimeter measurements, it was observed that the EN\_GF25 laminate repeatedly ignited. It is assumed that the stacked layers of the individual GF layers shield the underlying matrix from combustion, thus preventing the diffusion of flammable gases to the surface. When the flame reaches the *resin-rich area*, i.e., the *inter-gap* area of overlapping GF strands, the heat release increases due to the discharge of volatiles. The non-combustible fibers remain at the surface. The locally slightly lower resin content (91.61 vol.%) compared to the

surroundings (99.71 vol.%) is an advantage since less “fuel” is locally available for combustion (Table 18). Consequently, the PHRR is reduced by 42.8 %.

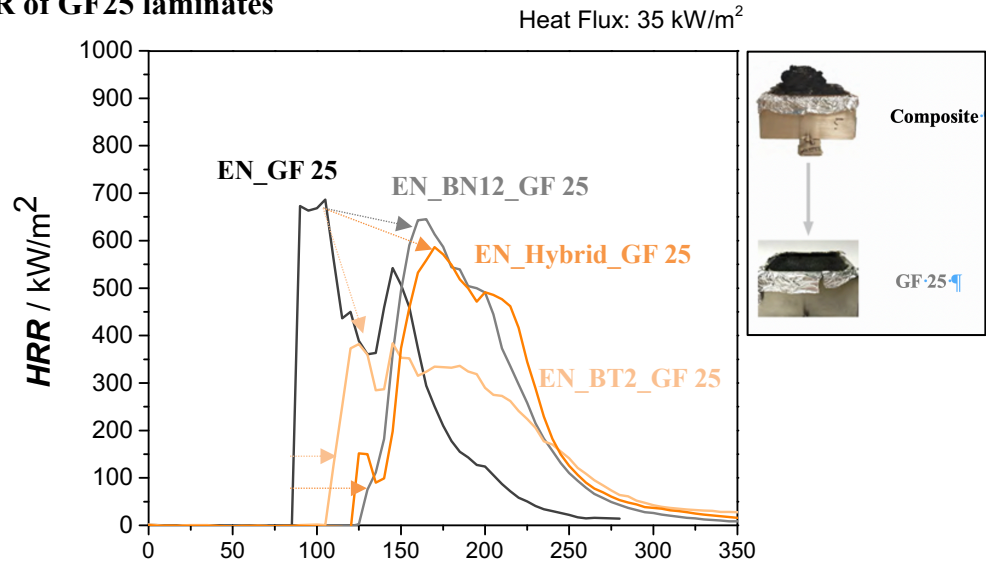
The  $t_{ig}$  is reduced from 113 s to 88 s for the EN systems with the incorporation of fibers. This can be linked to two different mechanisms. The EN\_GF25 laminate (0.314 W/mK, *through-plane*) shows a slightly higher thermal conductivity compared to its neat resin (0.1995 W/mK (*through-plane*)).

Fischer *et al.* conclude in their study that the shorter  $t_{ig}$  is related to the intrinsic thermal conductivity of the GF (approx. 0.9 W/mK) [168]. With an increased thermal conductivity, the heat can be more rapidly transported from the pyrolysis zone (heat dissipation effect) [154,168]. This directly leads to an overall lower burning rate. Also, some studies of GF reinforced polymers claim that the so-called “*Wick*”-effect is responsible for the quicker ignition [168,203].

The Wick effect is a physicochemical anomaly that is strongly dependent on the fiber length and the viscosity parameters and the wettability, spreadability, and flowability of the polymer on the surface of the glass fibers. Due to the surface modification with Si-OH groups, the molten polymer can be easily absorbed, which leads to an increase in the interfacial tension, which improves the flame spread [168,204].

By adding 12.7 vol.% Boehmite (EN\_BT2\_GF25) as a filler, the resin content is reduced to 78.6 vol.%, and the PHRR is reduced from 686 to 383 kW/m<sup>2</sup>. Boehmite is stable up to 350 °C. At temperatures above, it decomposes after the initial degradation of the Epoxy Novolac in a two-step reaction to form an Al<sub>2</sub>O<sub>3</sub> barrier on the surface of the burning sample. This results in a  $t_{ig}$  shift of 23 s and the lowest TSR of all GF 25 laminates. Boehmite, in general, shows a higher effective heat of combustion (THE/ML), indicating a higher activity in the gas phase. The addition of 15.1 vol.% BN (EN\_BN12\_GF25) increases the  $t_{ig}$  even further by up to 130 s. Due to its intrinsic thermal conductive nature and high thermal stability of up to 1200 °C, it is assumed that the external heat flux is dissipated from the surface into the sample, i.e., the surface temperature decreases, and ignition is delayed. However, its PHRR is comparable to the PHRR of EN\_GF25. The hybrid combination of both fillers results in the highest  $t_{ig}$  and  $t(\text{PHRR})$ . The PHRR of 593 kW / m<sup>2</sup> results from a combinatorial interaction between the FR fillers Boehmite and BN.

## a) HRR of GF25 laminates



## b) TSR

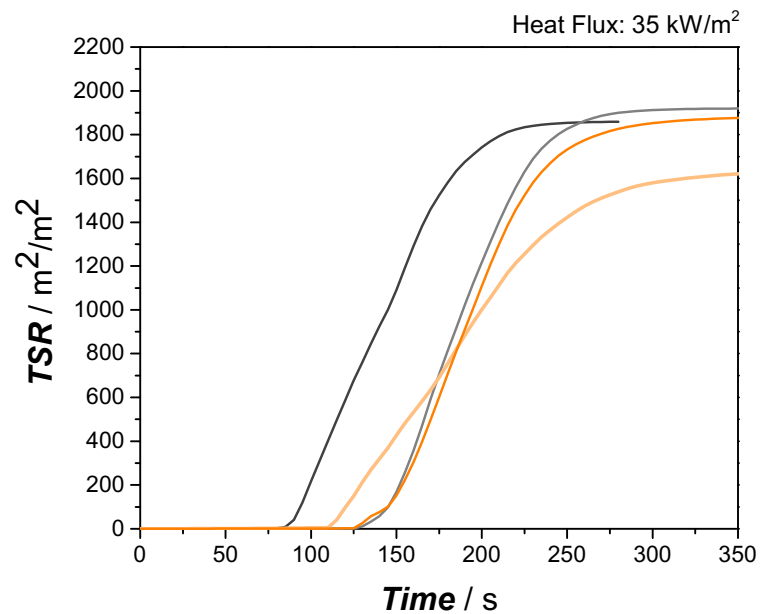


**Figure 90 a) HRR in dependency of time and b) the corresponding total smoke release rate (TSR) in dependency of time for different GF25 laminates measured at an applied 35 kW/m<sup>2</sup> heat flux. The reinforcement with the GF25 fabric led to less intumescence and higher dimensional stability.**

The total smoke release rate (TSR) (Figure 90b) is an important parameter when discussing hazardous fire materials since the release of volatiles (smoke) starts with the ignition of the material. Comparing the TSR results in Figure 69b) for the (filled) formulations with the GF25 laminates can identify the main effect of the glass fabric. The TSR maximums were reduced by almost 50 % for the EN system. The EN\_BT2\_GF25 laminate showed the highest FVC with

10.7 vol.% followed by EN\_BN12\_GF25 and EN\_Hybrid\_GF25 with 8.6 and 9.2 vol.%, respectively. The resin contents were in the range of  $76.5 \pm 2.5$  vol.%. The high efficiency of the FR filler Boehmite is reflected in the lowest TSR, although its filler content of 12.7 by volume is at the lower end compared to the hybrid and BN-filled GF25 laminates. The TSR of the EN\_GF25 and EN\_BN12\_GF25 are at the same level, as their FVC is  $8.5 \pm 0.1$  vol.%. The reduction of the resin content from 91.6 vol.% for the EN\_GF25 to 76.8 vol.% and incorporation of 15.2 vol.% platelets BN12 did not lead to a decrease in the smoke release rate. In summary, similar findings can be observed between the GF25 laminates and their corresponding resin formulations. The HRR and TSR values are the lowest for Boehmite, correlated to its flame-retardant nature and dual activity in the condensed and gas phase. Overall, the addition of glass fibers helps to provide structural stability during combustion. Yet, the GF decreases the  $t_{ig}$  at the same time. This effect is described in the literature as the *Wick-effect*. BN acts primarily heat-stable barrier that counteracts the decreased  $t_{ig}$  due to the presence of the glass fibers. However, BN does not necessarily suppress smoke release.

### **Influence of FVC on Flame Retardancy**

The heat release rate (HRR) and their corresponding TSR are plotted in Figure 91a) and b), focusing on the increase in FVC. The *dotted line in the HRR and TSR plots* corresponds to the resin results; the *increase in FVC* of the laminates is represented by a *color change from light to dark*. Table 19 provides an overview of all evaluated parameters for the main laminate systems. The corresponding fiber, resin, and filler contents are shown in Table 20.

During this Ph.D. experimental work, it was found that the sample thickness and the sample surface roughness have a significant influence on the overall ignition and the fire behavior [154]. All results shown in all figures were measured with the smooth side facing the Cone. The sample thickness of the tested laminates was 3 mm with a tolerance of  $\pm 0.2$  mm, whereas the samples with lower FVC had a thickness at the lower limit of this range, the samples with the highest FVC had a thickness at the upper limit. A smaller sample thickness can result in a lower PHRR, and a faster ramp-down of the HRR as less combustible material is available.

With increasing FVC, for all systems, EN, BN12, and Hybrid, the PHRR decreases (Figure 91a)). The lowest PHRR values were achieved with the GF107 laminates. PHRR values of  $< 400$  kW/m<sup>2</sup> were achieved, an overall reduction of 75 %. In addition, it is noticeable that for

---

all formulations, the  $t_{ig}$  and the  $t(PHRR)$  shift from the highest values for the (filled) resins, with GF25 and GF49 having the shortest values. The values increase again with the GF107, thus not reaching the same level as the resin formulations. The shift of the time to ignition ( $t_{ig}$ ) can directly be correlated to the increase in fiber- and filler content.

**Table 19 Overview of characteristic quantitative results for the combustion behavior of (filled) EN formulations and their GF reinforced laminates measured with the Cone Calorimeter (heat flux of 35 kW/m<sup>2</sup>).**

Composition	$t_{ig} /$ s	t (PHRR) / s	PHRR / kW/m <sup>2</sup>	THE / MJ/m <sup>2</sup>	TSR / m <sup>2</sup> /m <sup>2</sup>	(THE/ML) / MJ/gm <sup>2</sup>	FIGRA / kW/m.s	MARHE / kW/m <sup>2</sup>
EN	113	180	1198	95.3	3774	2.36	6.65	302.3
EN_GF25	88	105	686.3	48.4	1850	2.55	6.53	235.6
EN_GF49	80	100	556.5	50.8	2006	2.60	5.56	233.3
EN_GF107	98	180	315.5	44.9	1711	2.66	1.75	163.8
EN_BN12	175	215	767.0	78.5	3246	2.27	3.56	175.9
EN_BN12_GF25	130	165	655.6	49.4	1919	2.38	3.97	193.3
EN_BN12_GF49	106	125	588.8	40.2	1634	2.19	4.70	179.6
EN_BN12_GF107	135	220	343.9	41.8	1390	2.59	1.56	128.0
EN_Hybrid	163	207	729	72.9	2591	2.46	3.52	169.3
EN_Hybrid_GF25	136	170	593.2	48.0	1870	2.34	3.48	203.7
EN_Hybrid_GF49	109	165	458.3	38.6	1395	2.30	2.77	155.4

FVC  
↓

FVC  
↓

FVC  
↓

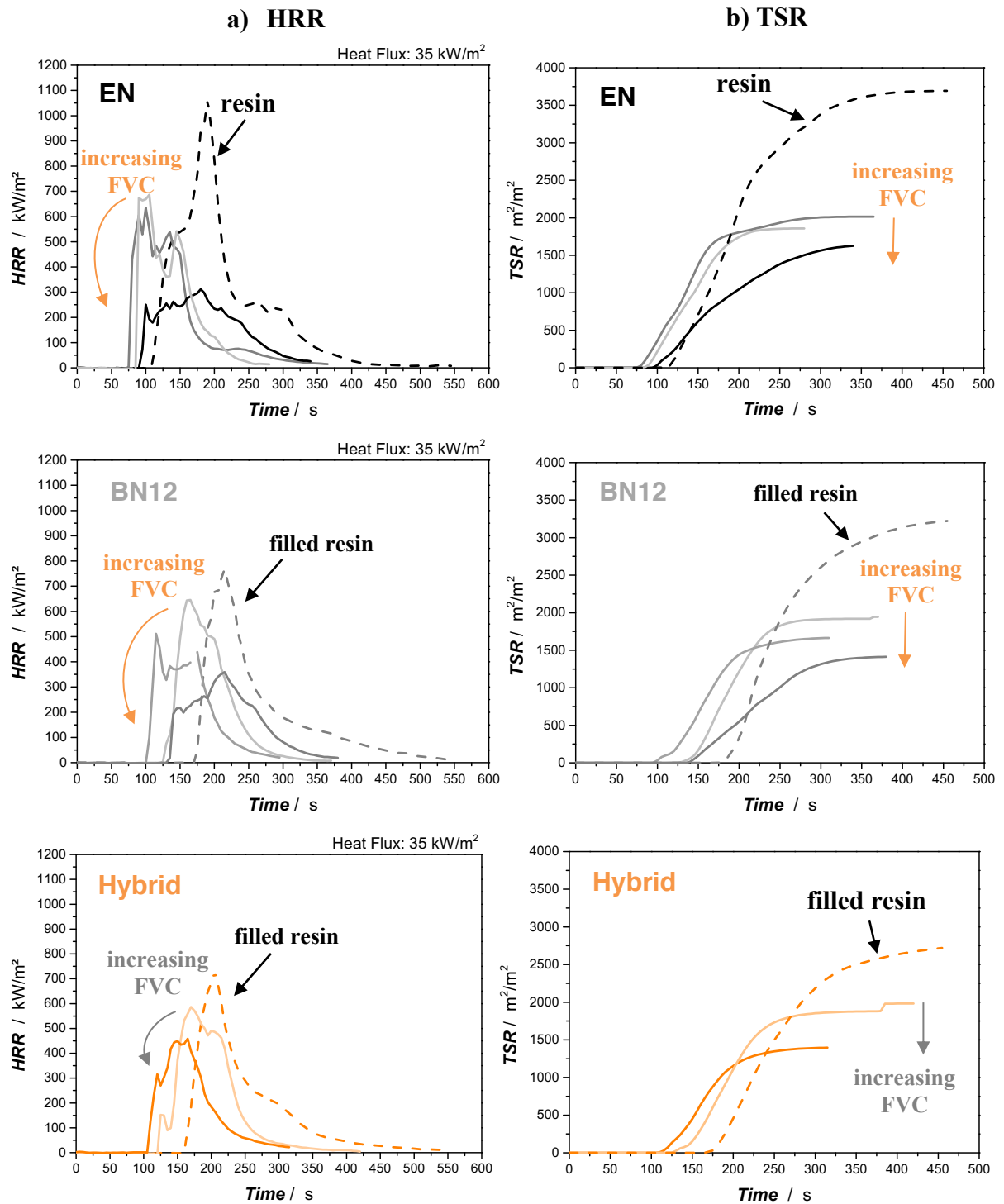


Figure 91 a) HRR versus time curves and b) their corresponding total smoke release rate (TSR) versus time plotted separately for the neat, BN, and hybrid systems in dependency of FVC (applied 35 kW/m<sup>2</sup> heat flux). Dotted lines are the filled resins, gradual color intensity = increasing FVC.

**Table 20 Overview of the various (filled) prepregs and their corresponding respective fiber, resin, and filler volume contents.**

<b>Composition</b>	<b>FVC / vol. %</b>	<b>Resin content / vol. %</b>	<b>Filler content / vol. %</b>
EN	-	99.7	-
EN_GF25	8.4	91.6	-
EN_GF49	31.1	68.9	-
EN_GF107	37.9	62.1	-
EN_BN12	-	86.3	13.7
EN_BN12_GF25	10.7	74.1	15.2
EN_BN12_GF49	22.5	63.2	14.3
EN_BN12_GF107	42.2	46.7	11.1
EN_Hybrid	-	87.8	12.2
EN_Hybrid_GF25	9.2	76.84	14.1
EN_Hybrid_GF49	23.1	65.1	11.8

The shift to shorter ignition time for GF25 and GF49 compared to their resins is due to the so-called “Wick”-effect (see discussion in the previous sub-chapter) and because glass fibers do not decompose. On the other hand, the increase in  $t_{ig}$  for the GF107 laminates results from the reduced resin content and, therefore, lower diffusibility rate of the flammable gases.

The curve progression changes from a sharp (single) peak (resin formulations) to a broader curve with multiple peaks for the laminates with the highest FVC. Shortly before reaching the maximum, a typical sound for cracking was usually heard during the Cone experiment, triggered by the delamination between the GF layer and the matrix due to thermal deformation. Therefore, these alternating fluctuations can be explained by the gradual spread of the flame and the simultaneous breakdown of the individual prepreg layers. When the flame reaches unexposed material, volatiles are immediately released into the gas phase, “re-igniting” the flame. This behavior was accompanied by repeated “*thermal feedback*” to the sides of the samples during measurement (Figure 92). A similar observation was published by Yang *et al.*. They explain the occurrence of multiple peaks for the HRR. The pyrolysis zone reached the

backside of the sample, causing an accelerated degradation with higher activity in the gas phase and even a partial perforation of the barrier layer on the surface [197].

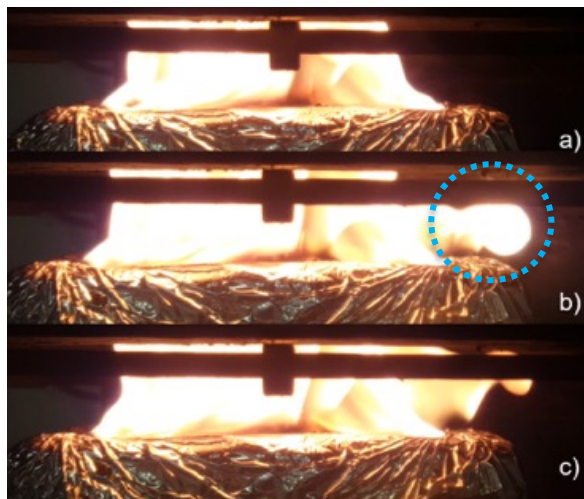


**Figure 92** “*Thermal Feedback*” during combustion of the EN\_BN12\_GF49 laminate: a) before, b) during, and c) immediately after the “cracking” sound occurred.

The TSR (Figure 91b)) is the lowest with the highest FVC. The EN\_GF107 laminate shows a TSR value reduced by 60 % compared to its neat resin; the EN\_Hybrid\_GF49 resulted in 50 % lower smoke production. This is due to the interaction between an increase in FVC, which restricts release when GF remains in the condensed phase, and a decrease in the volume fraction of the EN matrix. In addition, the incorporation of fillers also helps in the suppression of gases. Comparing the GF49 laminates, the lowest value was achieved with the hybrid formulation (Table 19). Primarily the platelet-shaped BN filler helps to restrict the pathway for the volatiles in the condensed phase. The Boehmite filler mainly improves the reduction of the PHHR by its endothermic degradation reaction releasing water, and then the secondary formation of  $\text{Al}_2\text{O}_3$  leads to a decrease in TSR.

The reduction in TSR can be correlated to a decrease in the total heat evolved (THE) which follows a similar trend: EN  $\gg$  BN  $>$  Hybrid in dependency of FVC. The THE/ML gives hints about the apparent flame-retardant mechanisms. The THE/ML increases with FVC for the EN formulations. Although the resin content decreases, the main activity for the unfilled laminates is in the gas phase. In the BN-filled laminates, the THE/ML is almost constant, whereas the Boehmite-filled laminates show a reduction in THE/ML. This supports the assumption that the main FR activity of the Boehmite-filled laminates is in the condensed phase due to the formation of  $\text{Al}_2\text{O}_3$ , which is more effective than BN-filled laminates.

### Correlation between BN and GF and their Effect on Flame Retardancy

The following sub-chapter will focus on the role of the thermally conductive filler BN and its interaction with GF, especially on the influence of the FVC on flame-retardancy, since there are not too many studies on this topic published in the literature.

Figure 93 describes the *correlation between the PHRR and the increase in fiber volume content in the (filled) systems* in the EN\_GFXX and EN\_BN12\_GFXX laminates. The trend lines, which have an exponential decay fit, indicate a direct dependency of heat release rate and the increase of fiber content, and therefore directly correlated to the reduction of resin content. The (filled) resins show the highest PHRR, whereas the PHRR decreases with increasing FVC reaching a minimum with the GF 107. The PHRR is almost on the same level between the unfilled and BN-filled laminates by partially substituting matrix content with the BN filler. Consequently, it can be concluded that the BN filler only has a minor impact on the overall PHRR. **Therefore, the main contributor to the PHRR reduction is strongly dependent on the FVC and independent from the incorporation of the BN.**

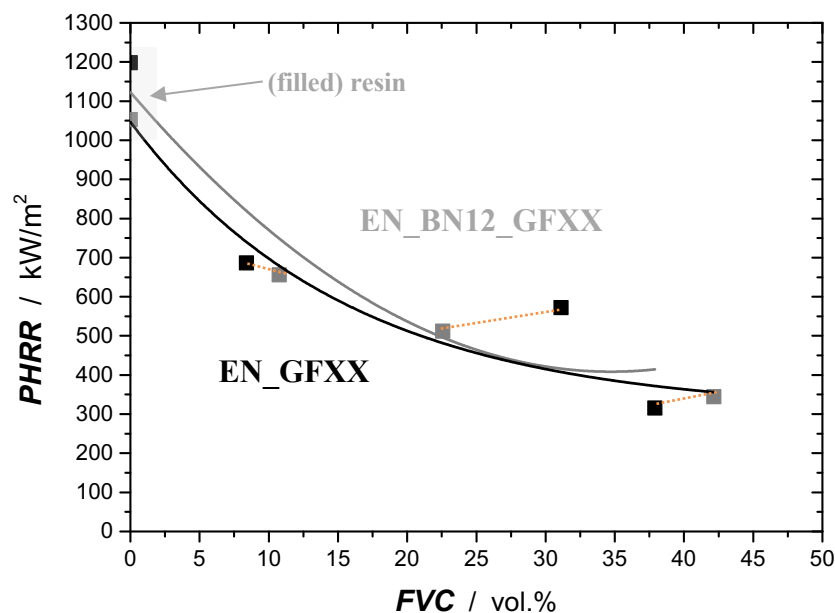
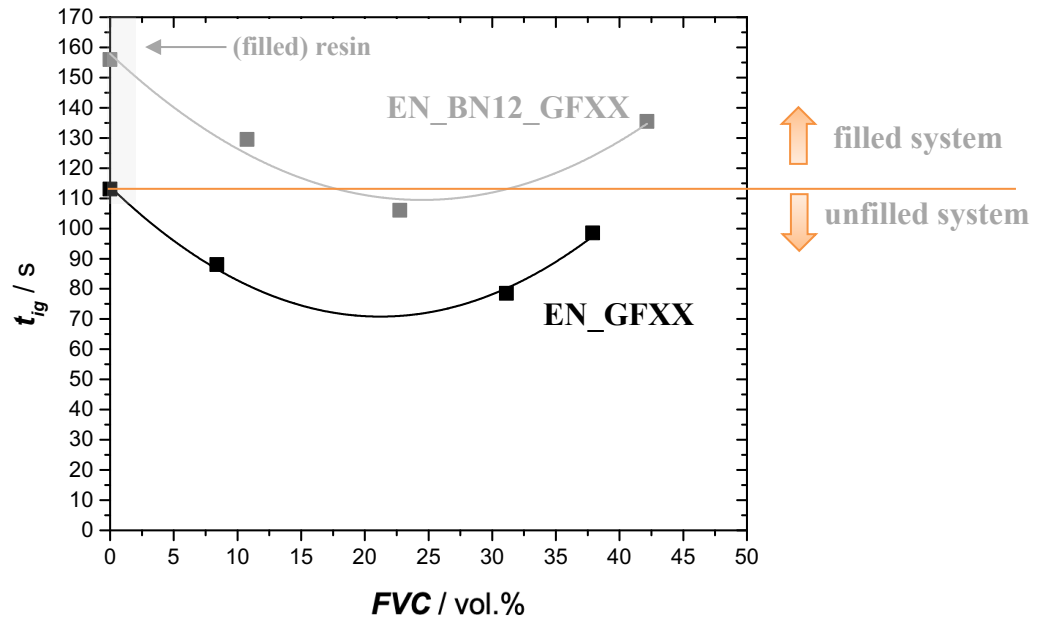


Figure 93 Peak heat release rate (PHRR) as a function of FVC for the (filled) resins and their prepreg laminates of EN (black) and EN\_BN12 (grey).

Figure 94, shows the correlation between  $t_{ig}$  and the increase in FVC. The curves have a parabolic fitting, which approaches a minimum with the GF49 laminates.



**Figure 94** Time to ignition ( $t_{ig}$ ) plotted in dependency of FVC for the EN\_GF and the EN\_BN12\_GF systems.

The addition of filler particles mainly influences the  $t_{ig}$ . This is indicated by a parallel shift of the curves upwards. The addition of *h*-BN thus has a positive effect on the fire behavior (gray curve), which can be attributed to the intrinsic thermal conductivity of the resin and the sample geometry. The thermal conductivity of the BN-filled laminates is higher compared to the unfilled. The BN reduces local heat spots by spreading the external heat into and throughout the sample. Furthermore, the filler platelets hinder the release of flammable gases as their diffusion path increases. The combination of higher thermal conductivity and reduced gas diffusion causes a delay of the ignition time of about 40 - 60 s.

However, the  $t_{ig}$  is the lowest, with the GF49 increasing with the GF107 fabric. One reason for this phenomenon might be the 50 % increase in fiber content between the GF25 and GF49. The filler content is constant, and the described “wick”-the effect is triggered by the glass fibers. In addition, the fabric appearance changes from GF49 to GF107. FVC increases not necessarily the fabric thickness, but the single GF strands broaden, which results in a much tighter mesh. This tighter mesh also hinders gas diffusion and thus impacting the time to ignition.

The decrease in mesh size of the fabric impacts the smoke release (TSR) (Figure 95). With the increase in FVC, the total amount of the smoke released is reduced, and the slope of the smoke release changes, indicating a slowed down or hindered smoke discharge. The FVC is the main contributor to reducing the diffusion of flammable gases from the condensed- to the gas phase. The inhibition is because neither the glass fibers nor the BN actively participates in the combustion reaction in the gas-phase.

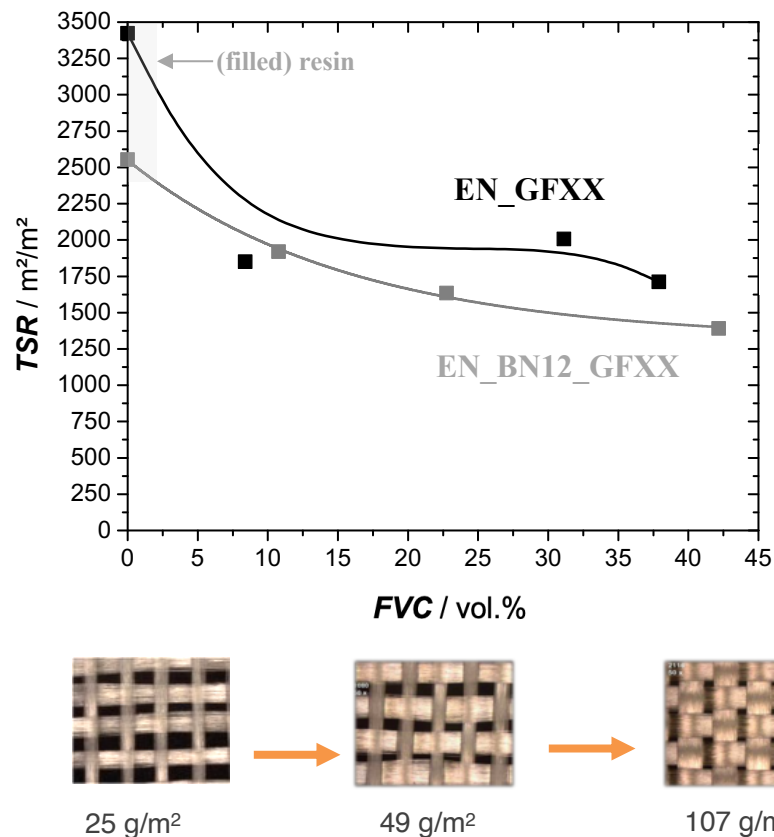


**Figure 95** Total smoke release (TSR) as a function of FVC of the EN\_GF and the EN\_BN12 systems as (filled) resin and their prepreg laminates.

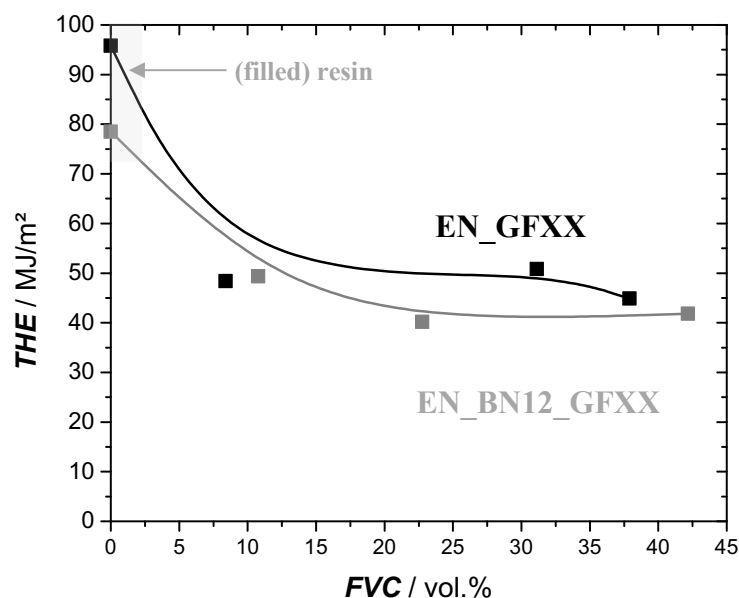


**Figure 96** Total heat evolved (THE, maximum value) as a function of FVC of EN\_GF and the EN\_BN12 systems as (filled) resin and their prepreg laminates.

The total heat evolved (THE) as a function of time is plotted in dependency of FVC in Figure 96. THE is the integral of the HRR concerning total heat output at the end of the test is the THE (total heat evolved) and is, therefore, equal to the fire load on the specimen [154]. The THE strongly depends on the total mass loss (= the difference between the specimen mass and char yield), the effective heat of combustion of the volatiles, and the combustion efficiency in the flame zone. The THE is directly dependent on the FVC content. The THE values decrease rapidly < 10% FVC and then approach a curve plateau at approx. 15 vol.% FVC, very similar to the TSR graph in Figure 95 and the results concerning the PHRR.

Based on these findings above, it can be summarized that the FVC has the main influence on flame-retardancy, and the BN filler has only had a minor influence. A comparison between the unfilled and the BN-filled systems shows that the filler platelets inhibit gas diffusion and shield the released heat. The absorption of external heat from the gas phase leads to a lower THE value.

### Post-Combustion Analysis of Char Residues with SEM/EDX

The charred samples from the cone calorimeter test were further investigated with SEM / EDX. The quantification of the main elements can be found in Table 21.

These results help identify flame-retardant mechanisms and correlate them with the results of the calorimeter made in the previous subsection.

Figure 97 shows the corresponding SEM micrographs for the various GF25 laminates. Both the top surface ( $x/y$ -direction and the side of the char ( $z$ -direction) were scanned.

**Table 21 EDX quantification of the char surface of the GF 25 combusted laminates.**

Composition	B (K) / wt. %	C (K) / wt. %	N (K) / wt. %	O (K) / wt. %	Al (K) / wt. %	Si (K) / wt. %
EN_GF25	6	68	6	9	6	4
EN_BN12_GF25	15	2.3	80	1.7	-	1
EN_BT2_GF25	5	16	3	50	25	2
EN_Hybrid_GF25	10	7	26	33	17	5
EN_Hybrid_GF49 – 100x	7.6	64.5	7.8	16.2	2.2	1.9
EN_Hybrid_GF49 – 500x	7.3	56.9	7.3	20.8	4.3	3.1

Samples with GF reinforcement show higher structural stability on the SEM images in Figure 97 since no pore formation/intumescence or expansion is visible in the  $z$ -axis. The surface morphology of the EN\_GF25 specimens is covered with a very brittle carbonaceous char. Carbon followed by oxygen is the main element of the surface (Table 21). The fibers are covered with a visible glassy or protective layer (side view of the neat sample in Figure 97). It is assumed that the GF strands, impregnated with EN, shield the matrix from decomposition. The main driver for thermal and fire stability is the addition of glass fibers, which do not decompose and therefore provide structural stability.

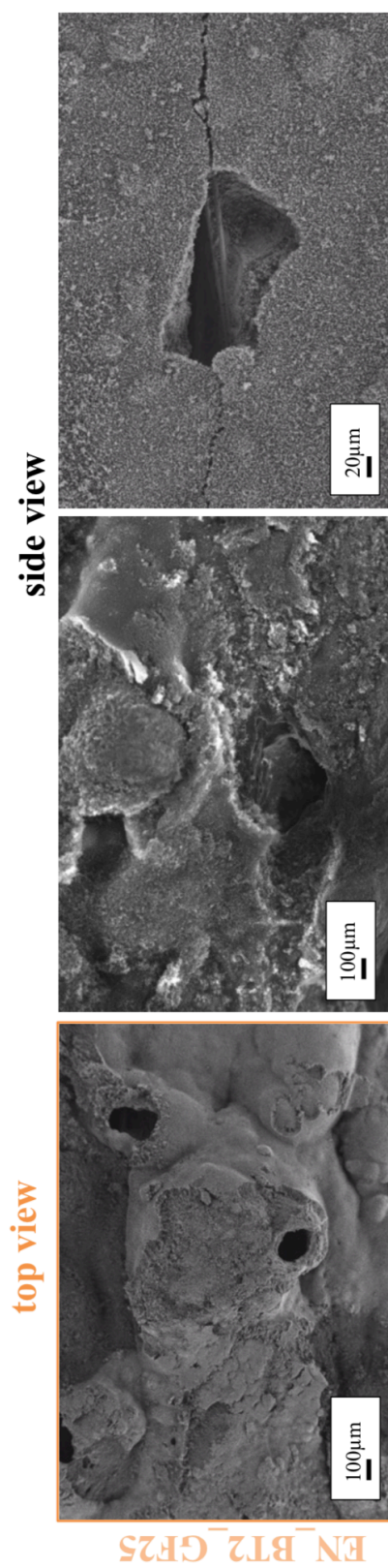
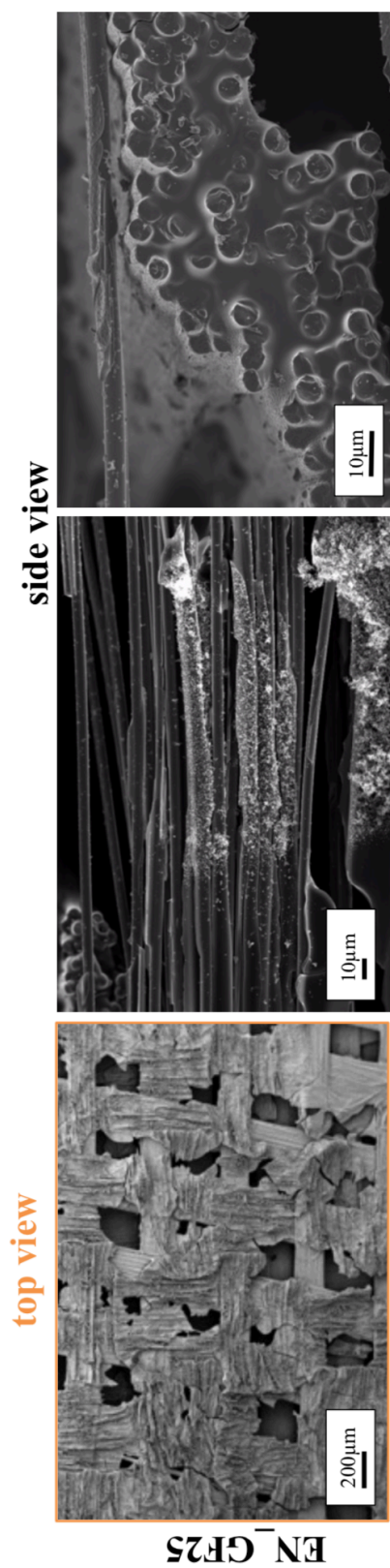
Chow *et al.* studied the char morphology of DGEBA/GF laminates produced via vacuum-assisted resin infusion [205], and found very similar results. The char of the unfilled DGEBA/GF specimens was very brittle, and cracked GF layers are visible. Their EDX study shows oxygen in the layers, which indicates complete matrix degradation [205]. However, no

Cone measurements were conducted. It is known in the literature that the decomposition of Epoxy laminates leads to a release of heat, smoke, soot, and toxic volatiles [146].

The filled GF25 laminates have a surface morphology that is smooth with a noticeable continuous, compact char on top. Also, in the  $z$ -direction, a distinct char covering the GF fabric is notable.

With the FR filler Boehmite (EN\_BT2\_GF25 laminate) addition, a thick char formation on the surface and throughout the sample can be observed (compare Figure 97). The EDX determination shows mainly Al (K) and O (K) as a result, which indicated the formation of an  $Al_2O_3$  ceramic barrier that covers the glass fabric (Figure 98 and Table 21). This compact layer hinders the degraded matrix from reacting with surrounding oxygen to CO and  $CO_2$ . Therefore, the layer is not able to merge into the gas phase Low TSR, THE, and PHRR values, especially for the laminates filled with Boehmite in Figure 90. The gas diffusion is drastically reduced, resulting in a low TSR and THE/ML value, demonstrating the higher effectiveness of Boehmite in the condensed phase. The low PHRR and THE results explain that barrier properties of the surface of the condensed phase not only inhibit the exchange of oxygen and heat but also affect heat dissipation due to their low intrinsic thermal conductivity.

This is in line with the results of Sut *et al.*, which indicate that the main mode of action for Boehmite is an increased formation of intumescent residues, and Boehmite acts as a char stabilizer [165]. The  $Al_2O_3$  layer suppresses the exchange between ambient air and the release of volatiles. The superficial carbon load is very low, illustrating the (degraded) polymer matrix below the ceramic barrier. This layer, therefore, limits the oxidation of carbon to CO and  $CO_2$ , resulting in the lowest PHRR and TSR of all samples. Charring of the surface is associated with lowering these characteristic values [184] and is in strong alignment with the findings in Figure 90 of this thesis. The relatively high carbon amounts detected for this laminate, compared to the EN\_BN12\_GF25 and EN\_Hybrid\_GF25, indicates that smoke particles adsorb onto the filler or char surface [194].



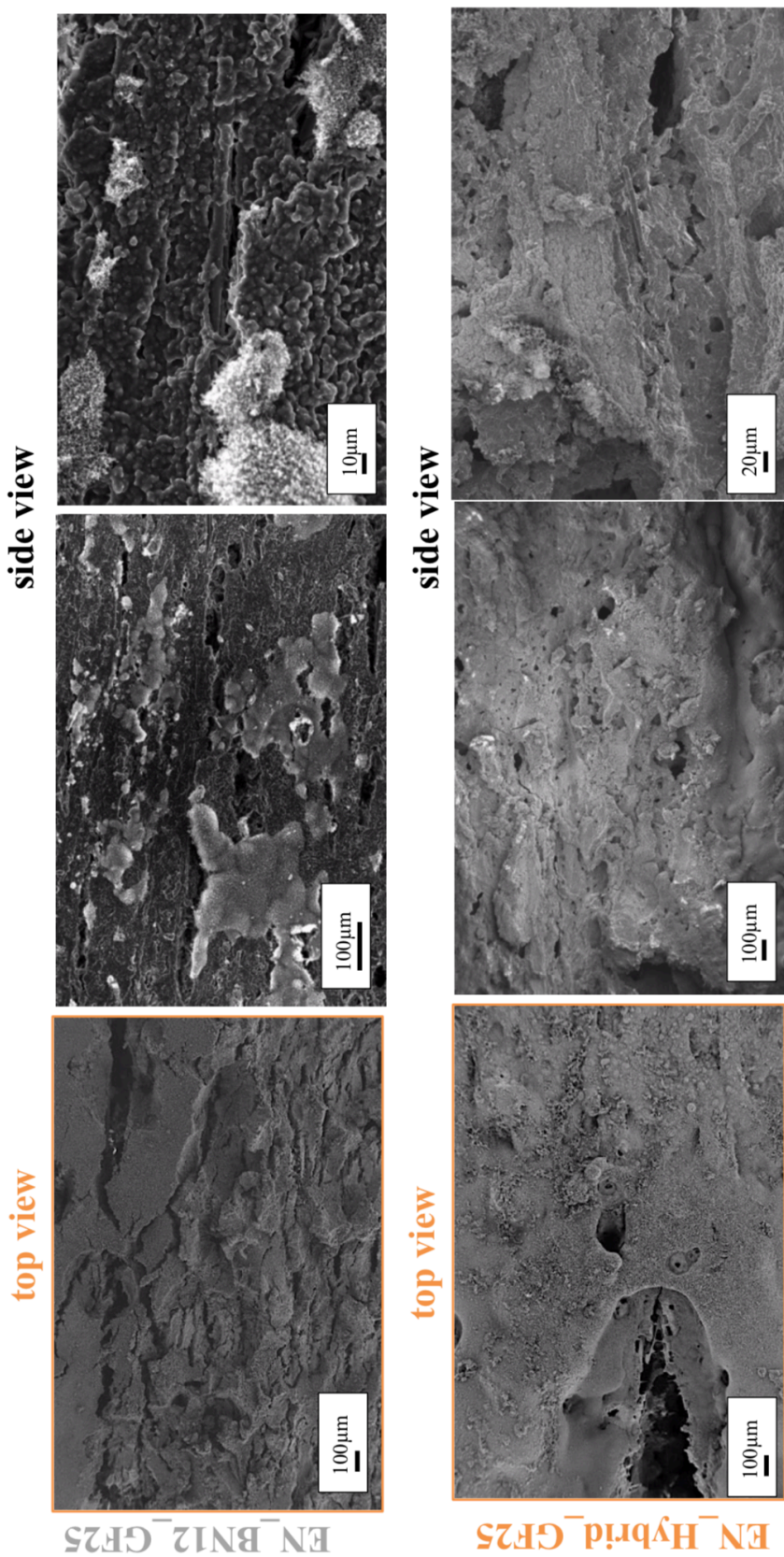


Figure 97 SEM micrographs of the char morphology of the unfilled EN\_GF25, EN\_BT2\_GF25, EN\_BN12\_GF25 and the EN\_Hybrid\_GF25 laminates (top and side views at different magnifications).

The char layer of the EN\_BN12\_GF25 laminate is compact on the surface but cross-sections the char layer is microporous. The char is mainly composed of B (K), N (K), O (K), and C (K) (Table 21). The carbon content compared to the Boehmite sample is lower. This demonstrates that the BN platelets possibly migrate to the surface during combustion (Figure 97, side view). In addition, it is assumed that BN is forming a barrier as the well-dispersed platelets do not decompose. The layer is not as dense as the formed  $\text{Al}_2\text{O}_3$  layer in EN\_BT2\_GF25 (Figure 97) [168]. By releasing CO and  $\text{CO}_2$  during the matrix degradation, the TSR value increases. The TSR value of the BN samples is the highest smoke release of all laminates (compare with Figure 90 and Figure 91). Unlu *et al.* also described in their findings that boron-based compounds' primary mode of action is forming an insulating layer in the condensed phase [189]. The BN laminates, however, showed the highest  $T_g$  and also a slightly higher thermal stability. TGA results in Table 17 and  $T_g$  results in Figure 78 indicate that the BN plays a crucial role in fire resistance. Some studies also showed improvement in thermal stability and flammability for BN fillers [168,206]. The correlation with THE/ML value shows that BN is less effective in the condensed phase than Boehmite. It is too porous in order to properly shield the release of smoke. However, compared to Boehmite the BN-filled laminates had a higher  $t_{ig}$ , where its intrinsic higher thermal conductivity is the main driver. BN therefore is considered as an inactive FR.

The quantification by EDX of the *hybrid*-filled laminate (EN\_Hybrid\_GF25) confirms the occurrence of Al (K) and O (K), which are formed during the degradation of Boehmite.

The C (K) content in Table 21 is very low. (The SEM micrographs in Figure 97 show a dense char in both  $x/y$ - and  $z$ -direction. The formation of  $\text{Al}_2\text{O}_3$  can be detected on the char surface, whereas the BN is seen on top of the GF strands (Figure 98). It is assumed that the migration of the  $\text{Al}_2\text{O}_3$  predominates the migration of the BN platelets.

The comparison of the char residues measured with TGA (Table 17) and the detection with SEM/EDX shows an evident condensed-phase activity of both fillers [193].

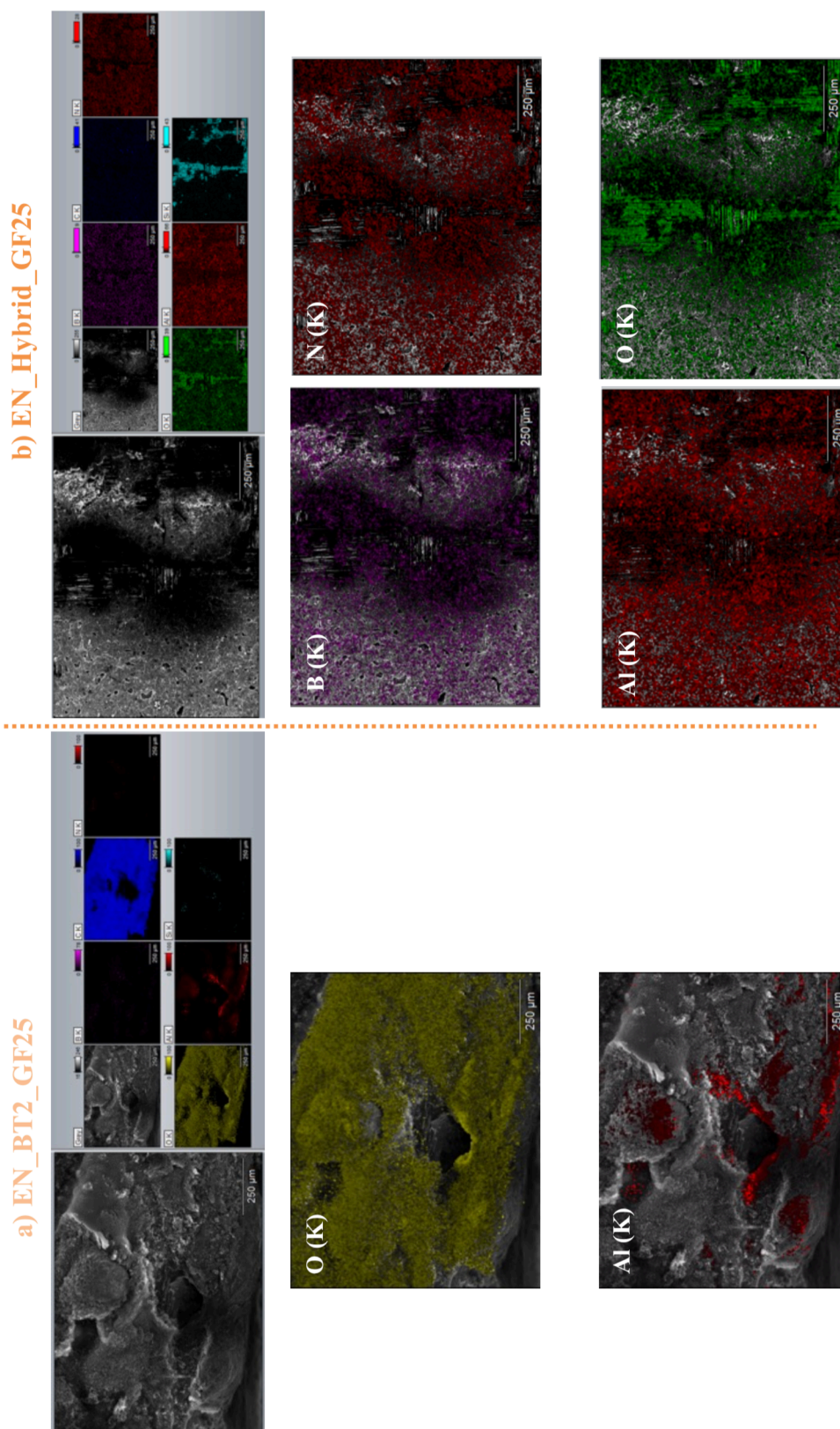
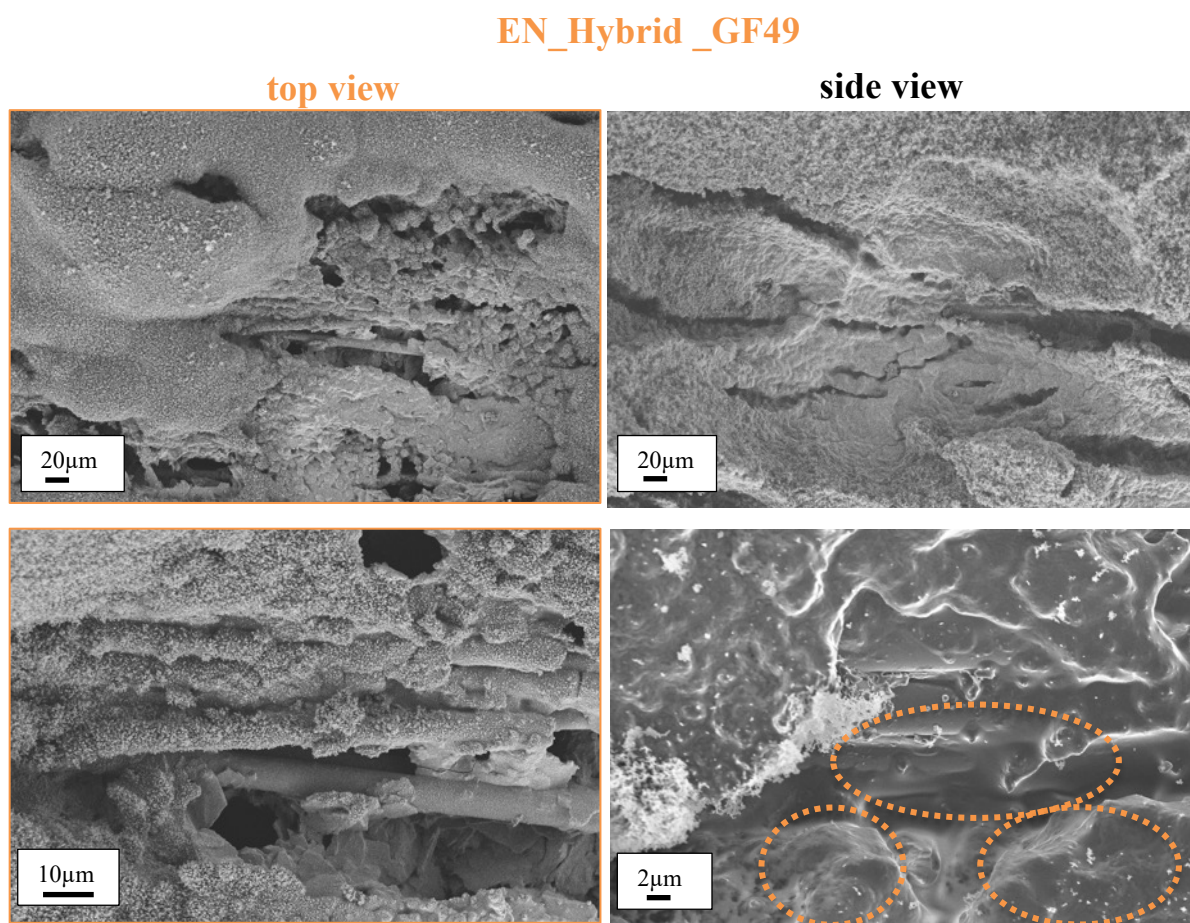


Figure 98 SEM/EDX elemental quantification of the char surfaces of a) EN\_BT2\_GF25 laminate and b) EN\_Hybrid\_GF25 laminate.

---

Moreover, the SEM / EDX analysis of the EN\_Hybrid\_GF49 (Table 21, Figure 98 and Figure 100) also shows Al, O, B and N due to the incorporation of both fillers (Boehmite and Boron Nitride). In the GF49 laminate, the Carbon content is higher (> 56 wt.%) compared to the EN\_Hybrid\_GF25 hybrid laminate. This indicates that an even better insulating layer has been formed, limiting the exchange of volatiles and polymer fragments. The crust layer can be found in both the top and side view of the sample in Figure 99. Additionally, in the condensed-phase, multiple processes can be observed: BN migrates to the surface, helping to shield heat and lower the degradation of Boehmite to  $Al_2O_3$ , which helps as a barrier against the exchange of volatiles and oxygen. This is associated with the lowest quotient of THE / ML and very early self-extinguishing during the combustion in the cone calorimeter. The side-view of the charred samples reveals that the GF has a glassy coating (see orange marking in Figure 99). The EDX analysis also shows that the Al and O elements can be found on the very top surface layer, with Al primarily adsorbing to the GF. It is most likely that the BN will be localized in the inter-tow area of the fabric.



**Figure 99 SEM micrographs of the char morphology of the EN\_Hybrid\_GF49 laminate (top and side views) at different magnifications.**

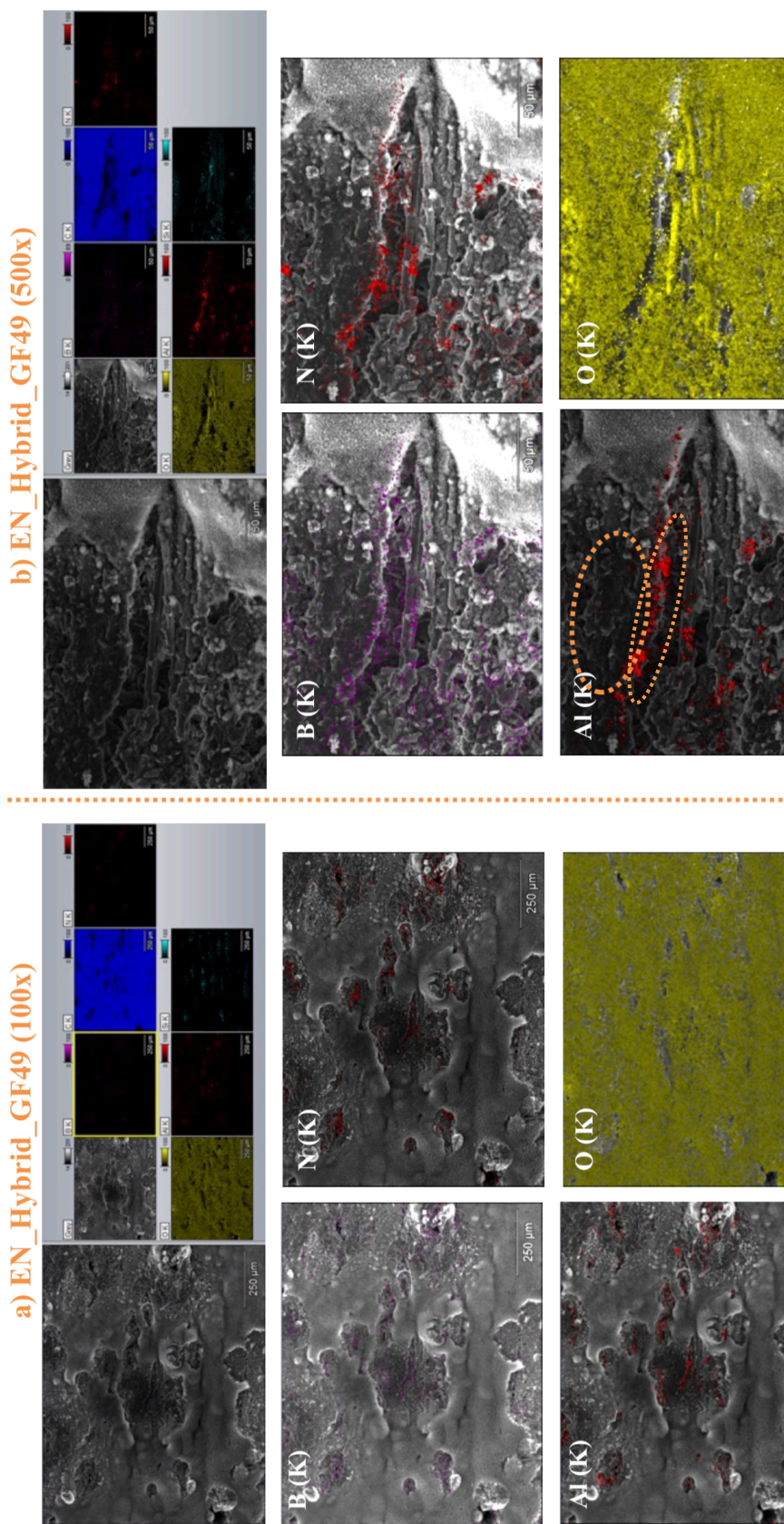


Figure 100 SEM/EDX elemental quantification of the char surfaces of the EN\_Hybrid\_GF49 laminate at 100x and 500x magnification.

### Interim Conclusion - Correlation of Thermal Conductivity with Flame Retardancy

To simplify the Cone Calorimeter data interpretation, FR indices have been introduced to assess the hazard of developing fires. These are the **FIGRA** (fire growth rate = maximum quotient of HRR (t)/t, which equals to PHRR/time to PHRR) and **MARHE** (maximum average rate of heat emission) [154]. The FIGRA and MARHE values of all studied systems can be found in Table 19. The *MARHE index* is a measure of the acceleration of the speed of fire [184]. The lowest FIGRA and MARHE values were achieved with the BT2 directly followed by the hybrid systems. Since the heat emission is drastically reduced with Boehmite, both the MARHE and the FIGRA indices are the lowest for all systems. This is due to the filler's flame-retardant nature and dual activity in the gas- and condensed-phase. The *FIGRA* value is directly influenced by the increase of  $t_{ig}$ , time (PHRR), and the maximum heat release.

For better visibility of the relation between heat release and fire development, Petrella proposed plotting *THE* (as the fire load) against  $PHRR/t_{ig}$  (as the fire growth index) to give a comprehensive assessment of the fire hazard [158,207]. The Petrella plot can be found in Figure 101.

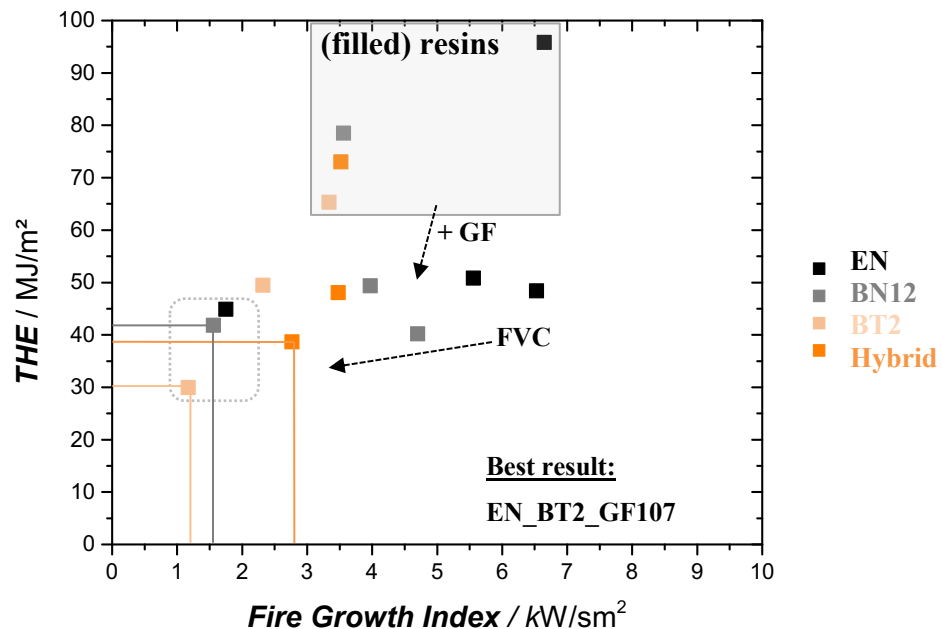


Figure 101 *Petrella plot* – Correlation of THE with FIGRA (fire growth index) summarized for all systems, i.e. (filled) resins and their laminates, in dependency of FVC.

This plot demonstrates clearly that the additions of fillers help to decrease the THE. The THE can be further reduced by adding GF since the fabric reduces mass loss in the condensed phase. The FR boehmite thus influences the flame retardancy and the dominant flame retardant mechanisms. In the filled resins and all laminates, the Boehmite achieved the best results in each FVC category. Due to the missing synergism by using both filler types under investigation. The hybrid system is not able to achieve similar improvements. However, the combinational, hybrid systems still show effective flame-retardancy, followed by BN and the unfilled systems.

One main target of this Ph.D. thesis was to establish a scientific correlation between thermal conductivity (TC) and flame retardancy. A good indicator for flame retardancy is  $t_{ig}$ . The thermal conductivity is plotted against the  $t_{ig}$  for all systems in Figure 102.

The unfilled systems have the lowest  $t_{ig}$  and the lowest TC. With the incorporation of fillers, the  $t_{ig}$  is delayed, but TC values are higher.

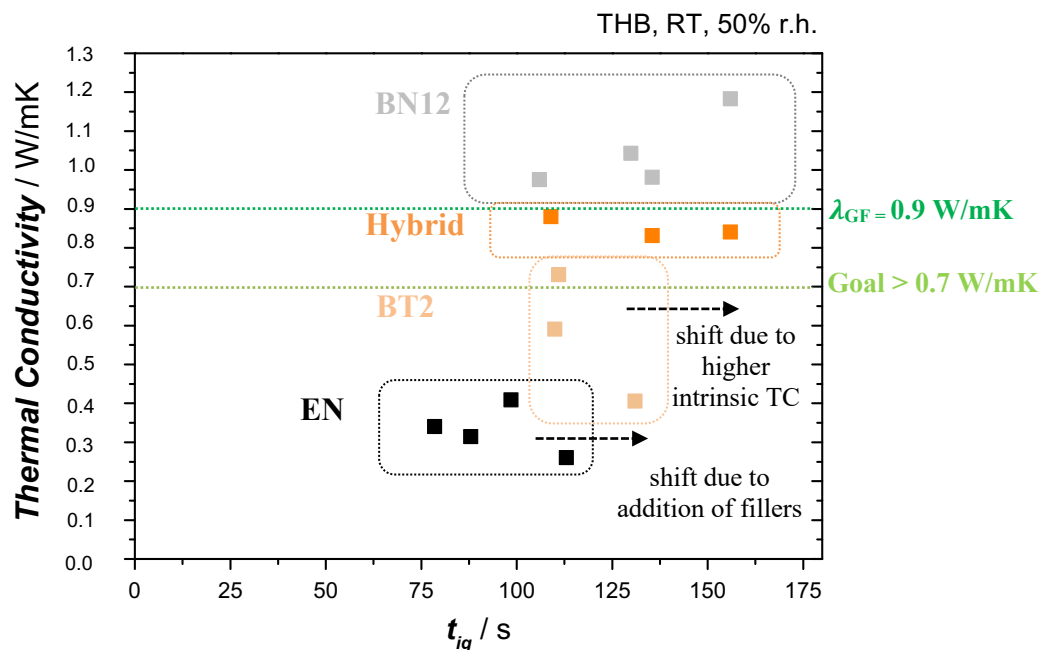


Figure 102 Correlation of the *through*-plane thermal conductivity and the  $t_{ig}$  of the (filled) resins and their corresponding laminates.

The shift in  $t_{ig}$ , therefore, is directly related to the TC. With respect to this correlation, the addition of Boehmite, a filler with a relatively low TC, already helps to shift the  $t_{ig}$ . This effect

is also mainly driven by the higher thermal stability due to the *flame-retardant nature of Boehmite*. The hybrid and BN12-filled systems remain on the same level in terms of  $t_{ig}$ . The increase in TC is achieved with the addition of BN. However, the  $t_{ig}$  is on the same level compared to the hybrid systems. In terms of  $t_{ig}$ , the hybrid filler combinations lead to a synergism; however, it is strictly a combinational effect regarding the TC. Finally, **with increasing FVC, there is no further improvement of the  $t_{ig}$** . The “*Wick*”-effect is assumed to be responsible for an earlier ignition for the GF 25 and GF49 laminates. The  $t_{ig}$  is therefore directly dependent on the TC and the thermal stability of the filled systems. The FVC of GF only affects the TC because the overall TC reaches the intrinsic TC of the GF (0.9 W/mK). GF increases  $t_{ig}$  as they limit the release of volatile substances.

In summary, the fire-specific indices (such as FIGRA, PHRR,  $t_{ig}$ ) show that with the incorporation of fillers, a **combinatoric effect** can be achieved utilizing both fillers’ positive aspects with both fillers. This can also be seen in the significant increase in  $t_{ig}$  when BN is added and in the inhibition of heat transfer due to the shielding effect of the ceramic barrier formed by the decomposition of Boehmite. The char formation of the laminates indicates **condensed-phase actions of the fillers**. Consequently, the combinations between BN and Boehmite suppress the volatile release and increase the materials’ flame-retardant behavior. Moreover, it can be stated that the fire behavior is strongly influenced by the resin content of the laminates and, therefore, also by the increase in FVC. **Neither the BN fillers nor the glass fibers are actively involved in the combustion processes, but they indirectly influence the combustion process due to the reduced resin content**. In addition, the ***h*-BN filler, and the glass fibers, improve the thermal conductivity of the material, which affects the delay of the ignition**. The overall results indicate that the filled resins show the highest fire hazard. They have very high activity in the gas phase due to their high heat release. With their short ignition time and the short time to reach the maximum of the HRR, the FIGRA is also very high. In contrast to this, the fabric laminates mainly have a solid phase activity due to the barrier effect of the fillers and the glass fibers.

In addition, the thermal conductivity of the fillers and GF lead to a heat spread and simultaneous cooling of the fire zone. The laminates have a  $t_{ig}$  that is shifted to lower values, but also the laminates have a much lower PHRR, and finally a lower FIGRA. With increasing FVC, the THE decreases even more due to the even lower matrix content and significant solid-phase

activity of the fillers. The lowest values were reached with the unimodal-filled Boehmite but directly followed by the hybrid system and BN laminate with the highest FVC.

*UL-94* tests are used to classify flame-retardancy in the PCB industry. *UL-94* test was only conducted on some of the laminates. The results are listed below in Table 22. All (filled) resin specimens showed severe dripping due to their high resin content and failed the *UL-94* test. The unfilled EN\_GF25 laminate failed due to its long time until flame extinguishment. The filled GF25 laminates achieved V-1 classification. Overall, V-0 was only achieved with all filled GF107 laminates, i.e., EN\_BN12\_GF107 and EN\_Hybrid\_GF107. With the hybrid filler combination, it was also possible to achieve V-0 (EN\_Hybrid\_GF49 laminate). This demonstrates that BN is not able to provide good FR. The combination with either a high FVC (GF107) or the partial substitution with the FR Boehmite (hybrid) leads to V-0 ratings. It was observed that the EN\_Hybrid\_GF49 also self-extinguished during the Cone Calorimeter tests. These overall results are in good alignment with the Cone Calorimeter measurements. It was shown that excellent fire-retardant properties could be achieved with the filler combination, i.e., high  $t_{ig}$  and low PHRR values. The incorporation of fibers has a significant role in providing the samples' structural stability, which helped prevent melt dripping. An increase in FVC leads to an improvement of the *UL-94* ratings.

Their *UL-94* classification, in general, is **V-0**. The HRR, THR, and TSR results can be seen in Figure 103.

When evaluating the results, it must be considered that the benchmark laminates provided had a total thickness of 1.5 mm. In contrast, the novel base materials examined in this doctoral thesis had a thickness of 3 mm. Therefore, the decrease in thickness by factor 2 has an enormous effect on flame retardancy as the overall amount of fuel is 50 % less in the benchmark. However, comparing the benchmark with the novel substrate, the resin, filler, and FVC are in a similar range (resin content ~ 45 – 46 %, filler volume content 10 – 11 %, and a FVC of 43 – 45 %). With a lower resin content in these benchmark laminates, the heat – and smoke release are strongly reduced.

The HRR curves follow a sharp in- and decrease for the IS400 and the PCL370HR; the DE104 has two main peaks.

Table 22 UL-94 results for the main laminate systems.

Composition	Aftertime /s	ignition of cotton	rating
EN_GF25	132*	no	NR
EN_BN12_GF25	35*	no	V-1
EN_BT2_GF25	> 35*	no	V-1
EN_Hybrid, GF25	28*	no	V-1
EN_BN12_GF49	> 35*	no	V-1
EN_Hybrid_GF49	17.8**	no	V-0
EN_BN12_GF107	10*	no	V-0
EN_BT2_GF107	10*	no	V-0

\* Individual specimen

\*\* set of 5 specimens

The results below correspond well to the GF107 laminates of this thesis. If extrapolating the results, a 3 mm thick sample of the benchmarks would result in a PHRR of 300 - 500 kW/m<sup>2</sup>. The PHRR of all three benchmarks is in the same range as the EN\_Hybrid\_GF107. However, the  $t_{ig}$  is significantly lower compared to the EN\_Hybrid\_GF107. The benchmarks already ignited at ca. 50 s, whereas all systems in this work produced with the GF107 have a  $t_{ig}$  range of 100 -150 s, increasing up to 300 %!

The TSR of the benchmarks is approx. 50 % lower than the systems in this work, and their THR values are approx. 75 % below the values of the hybrid system. The laminate thickness of the benchmarks mainly causes this.

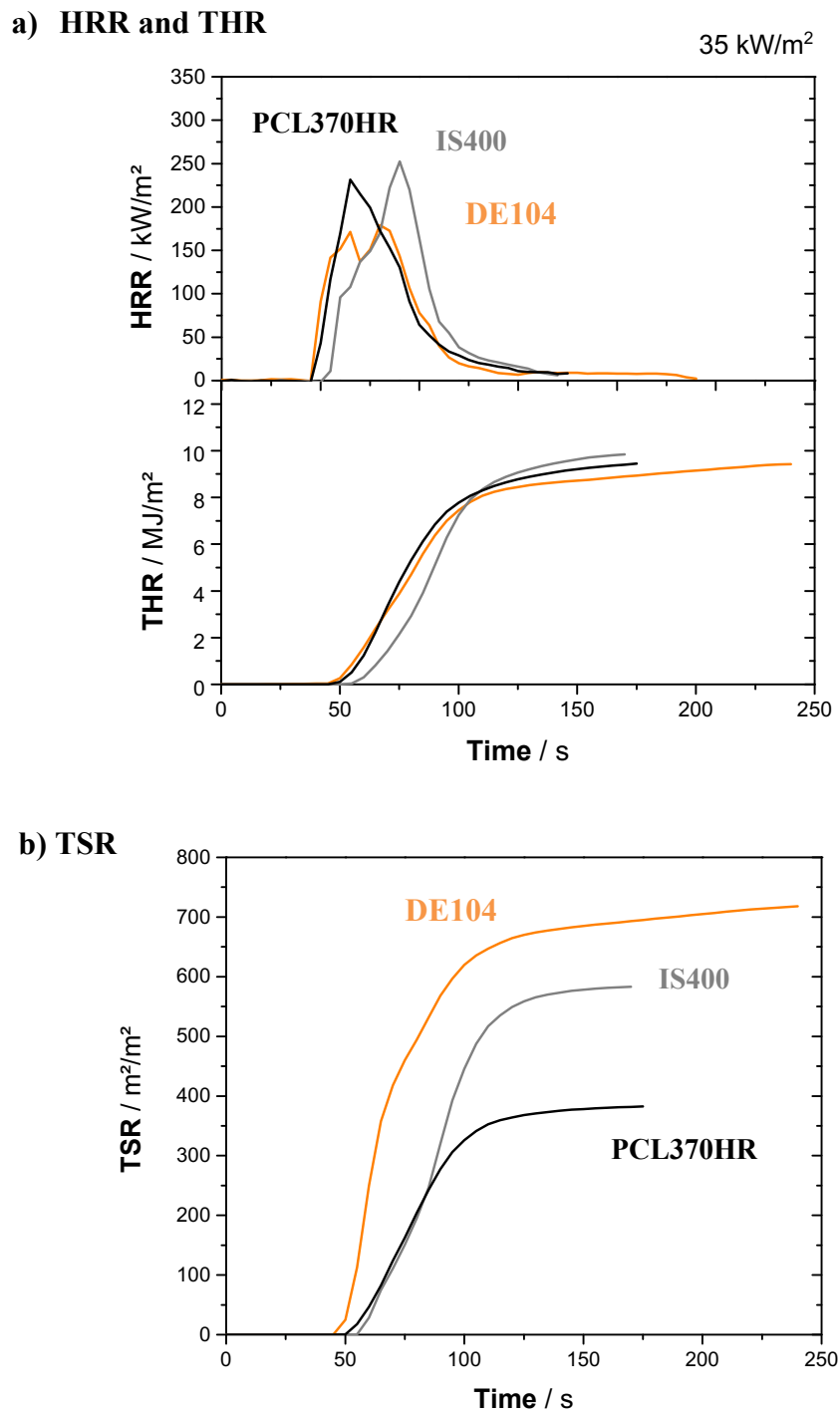


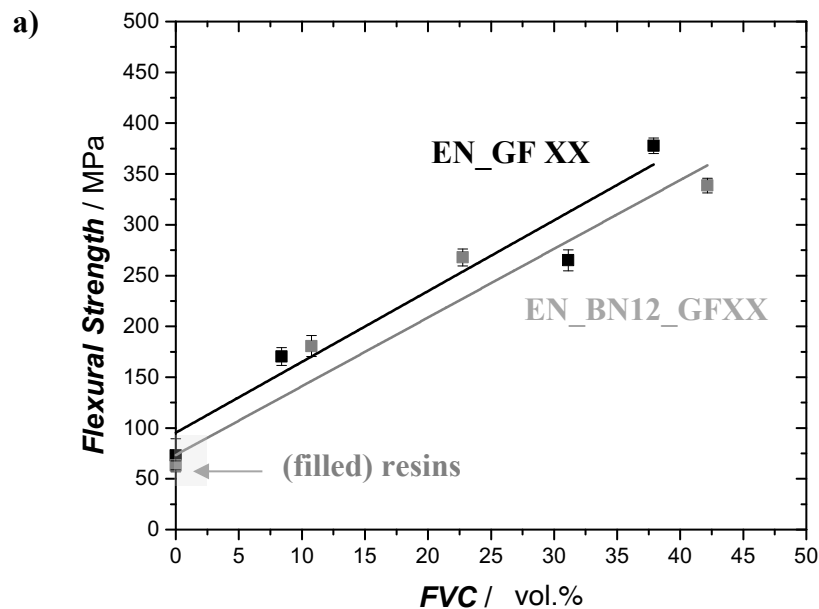
Figure 103 a) HRR in dependency of time curves and their corresponding THR (total heat release rate) versus time and b) the TSR (total smoke production rate) in dependency of time for *State-of-the-Art* benchmark systems measured at 35 kW/m<sup>2</sup> heat flux.

## 5.4 Other PCB-relevant Properties

This chapter evaluates the transfer of these new thermally conductive and flame retardant prepregs towards their application as PCB base material. In the following, the mechanical properties, the coefficient of thermal expansion in the  $z$ -direction ( $z$ -CTE), and the water uptake will be discussed. The focus will be laid on the influence of an increasing FVC.

### 5.4.1 Mechanical Properties – *Flexural Three-Point Bending*

GF-reinforced prepregs, used as base materials in PCBs, are often subjected to cyclic and flexural loads during their application. Compared to metals, GFRP laminates are known to resist flexural loads and fatigue loading because the matrix can redistribute loads to the reinforcing fibers. Moreover, glass fibers/fabric as a reinforcement phase take up more load and act as a “crack arrester”, especially in the transverse direction. To study the effect of different fillers and the increasing FVC, the bending properties were studied. The flexural modulus and flexural strength in dependency of FVC can be seen in Figure 104 for the unfilled EN\_GFXX and the EN\_BN12\_GFXX laminates.



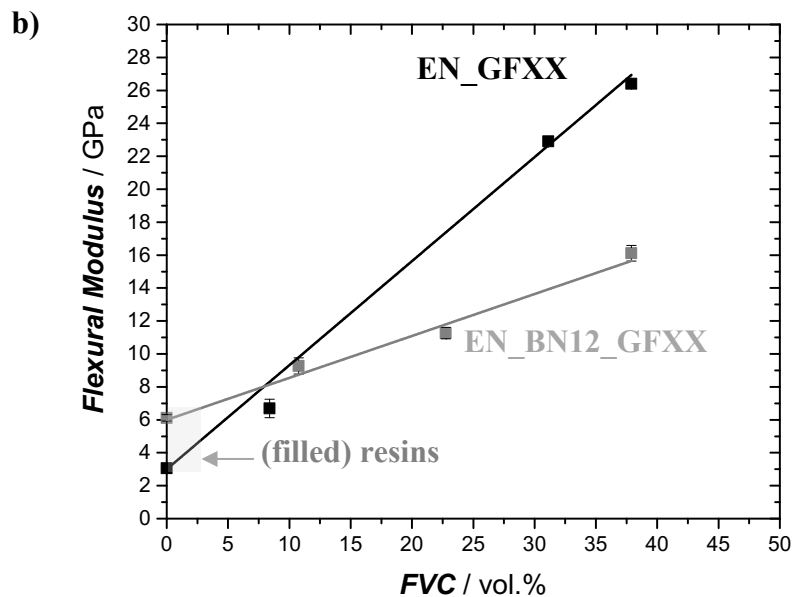


**Figure 104** Three-point bending modulus results in dependency of FVC for the unfilled EN and BN12 filled systems (resins and their laminates): a) flexural strength and b) flexural modulus.

Flexural modulus and strength increase linearly with the fiber volume content. For the unfilled laminates at a higher FVC of > 10 vol.%, the modulus exceeds the modulus of the BN12-filled systems. This is likely due to the ratio between matrix and fiber content. The GF is the major contributor to the modulus increase due to their intrinsic stiffness.

The results of the BN12 laminates suggest that despite a higher interfacial area of these fillers have poor adhesion with the resin matrix. Poor matrix-filler interaction was already proven by the SEM in the previous chapters (5.2.2), as BN only offers functional groups on their edges but not on their smooth, planar surface.

In addition to the increase in flexural modulus, the FVC causes an increase in flexural strength (Figure 104). Sreekala *et al.* reported a similar correlation between fiber content and tensile and flexural properties with GF-reinforced phenol-formaldehyde [208].

The flexural properties of the tested laminates primarily depend on their fiber volume content and the fabric orientation in relation to the applied load direction. Since the GF fabric is under tension during prepreg production, some anisotropy is possible. To study this potential effect, flexural strength was also exemplarily tested in 0° and 90° direction for the unfilled EN\_GF49 laminate (Figure 105). The fabric tension has a negligible impact on the gap size; the main contributor to the overall stiffness are the fibers/rovings in warp-direction (0°-direction). The

results in 90°-direction are lower, as these weft fibers break more efficiently at their interfacial area overlapping the warp fibers. A difference of approx. 100 MPa in strength was observed at the highest FVC.

The benchmark systems have an overall higher flexural strength of > 565 MPa in length (warp)-direction and > 450 MPa in a cross (weft)-direction. This difference may be caused by either a difference in FVC (difference to the novel substrate of 2 vol.%) or filler volume content (contrast to the novel substrate of 1 vol.%), filler geometry, or nature.

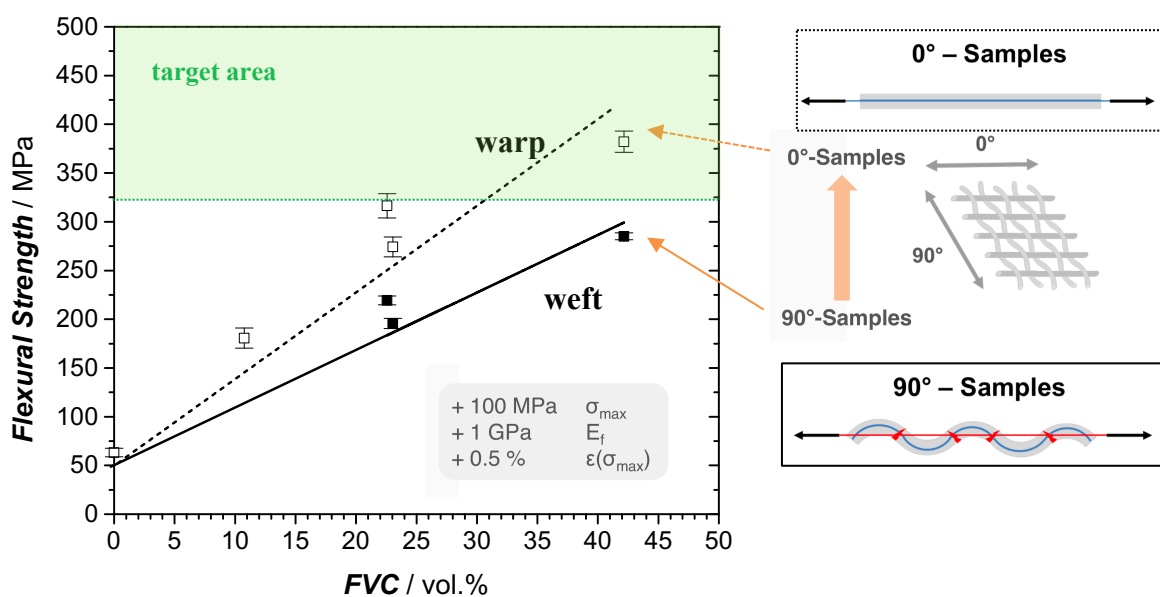


Figure 105 Flexural strength of the EN\_GF laminates in dependency of fabric orientation.

#### 5.4.2 Coefficient of Thermal Expansion (z-CTE)

When laminates are subjected to a temperature change, the mismatch in the *coefficients of thermal expansion* (CTE) of fibers, fillers, and the matrix is causing local stresses, which can take part in local matrix cracking or delaminations [125]. BN has a z-CTE of 1 ppm/K and E-Glass of 4.6 ppm/K [32], and therefore it was expected that fillers or fibers to have a positive impact on the overall z-CTE.

The z-CTE results are plotted in Figure 106 in dependency of their FVC of the laminates. It can be observed that for all systems, the results follow a parabolic fit. The graph also indicates the values of the benchmarks in which FVC is in the same range as the GF107 laminates (ca.

40 vol.%). DE104 has a  $z$ -CTE in the same range as the EN\_Hybrid\_GF49 and the EN\_BN12\_GF107. However, IS400 and PCL370HR have an even lower  $z$ -CTE. This can be attributed to the use of MDH/ATH or SiO<sub>2</sub> fillers.

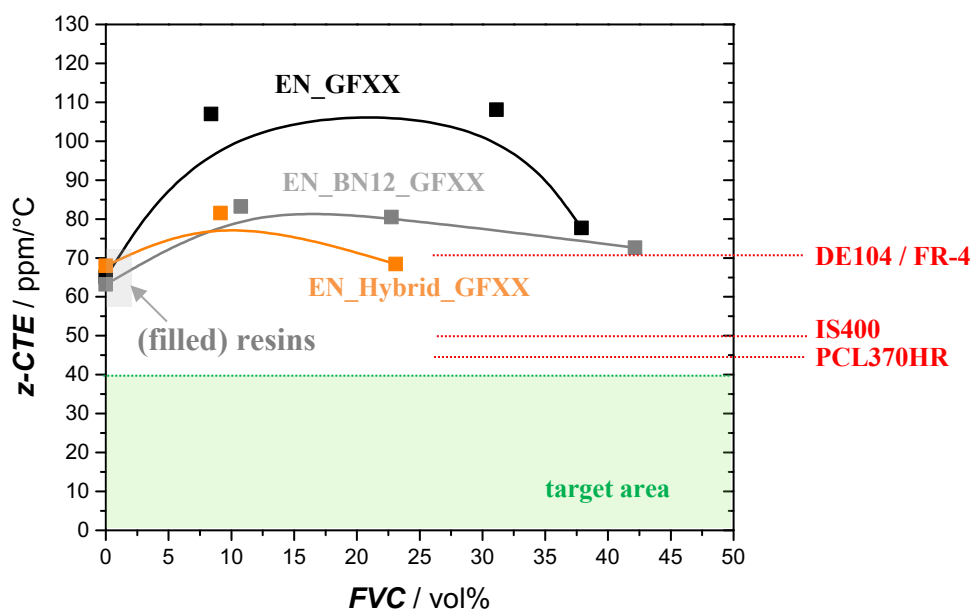


**Figure 106**  $z$ -CTE in dependency of the FVC for all systems.

The target of 40 ppm/K was not achieved for any of the tested laminates. However, the filled systems are much closer to the target than the unfilled, neat composites and their corresponding laminates. FR-4 has a known  $z$ -CTE of 50 ppm/°C below  $T_g$  and 320 ppm/°C above  $T_g$  [22]. Parallel to the surface, in  $x/y$ -direction, the FR-4 substrate has a CTE of 20 ppm/°C, which is close to copper [22].

The CTE of the neat Epoxy Novolac is approximately 65 ppm/K. The addition of BN12 results in  $z$ -CTE of about 65 ppm/K with a fiber content of 0 % by volume. The addition of 15 - 19 vol.% filler and reduces the  $z$ -CTE by -25 % ( $\sim -1.4\%$  /% by volume) in the GF25 laminates. In the filled resins, the filler content is slightly higher than in their corresponding laminates. With increasing temperature, fillers can restrict mobility much more than compared to the GF25 laminates. The covalent bonds between the fillers and the Epoxy matrix might lead to a stronger reduction of the matrix mobility, the latter expressing itself in a more substantial shift of  $T_g$  [125]. Chiang *et al.* reported a mechanical interlock between the organic matrix and the inorganic *h*-BN that restricts the CTE mismatch [94]. Mismatch in CTE can be influenced by

the intrinsic CTE, dispersion, loading, filler size, and shape [89] Apeldorn's research on foamed PEI filled with 25 vol.% of Talkum showed a z-CTE of 64 ppm/K. In the  $x/y$ -plane, the CTE was significantly reduced below 20 ppm/K [24]. The z-CTE, evaluated between 50 and 150 °C, reached values much **closer to copper**. This shows that hydrated fillers help to lower the CTE (see benchmark prepregs), whereas BN seems to increase the CTE although having a very low intrinsic CTE. A study by Tsai *et al.* shows the potential to implement 3 wt.% clay into the EN matrix to reduce the CTE. Their GF laminates showed CTE values between 45 and 56 ppm/K [29]. However, by incorporating clay-based fillers, the water uptake is higher compared to BN. The respective laminates, especially GF25, the microstructure of the fabric consists of overlapping GF strands, forming "pockets", the so-called *inter-tow* areas. Since the fillers are restricted in their mobility by the fabric, the polymer chains can move slightly more. Similar results were reported by Ehrenstein *et al.* Their studies on GF reinforced laminates in dependency of their FVC [32] also revealed a parabolic slope.

### 5.4.3 Dielectric Properties

The dielectric constant ( $D_k$ ) and the dielectric loss factor ( $D_f$ ) of the studied laminates were measured with impedance measurements. The relative permittivity of the dielectric materials was measured, which indicates how easily the material can be polarized in the electric field. The real part of the complex relative permittivity corresponds to the ability of the material to store the energy of an electric field. It is referred to as the dielectric constant  $D_k$ . The dielectric constant of a material should be kept as low as possible to achieve high signal speeds in the application. The imaginary part of the complex relative permittivity ratio to  $D_k$  is given as loss factor  $D_f$ . The lower  $D_f$ , the smaller the signal loss from surrounding electrical signals. A low  $D_k$  value is preferred as high  $D_k$  values increase the signal loss probability.  $D_f$  is a measure of how much an electromagnetic field is absorbed or lost while passing through a dielectric material.

The results for  $D_k$  and  $D_f$  in dependency of FVC are plotted in Figure 107.

*All laminates successfully resulted in a  $D_k$  of  $< 4.0$  (= target).*

The lowest dielectric constant  $D_k$  was measured for EN\_BN12\_GF107, the highest for EN\_GF49. At the same FVC, for both laminates, a parallel curve shift can be observed. Therefore, the ceramic filler particles (the content of 19.7 vol.%) significantly improved the

overall dielectric properties due to their intrinsic electrical insulation and the higher ability for polarization. FR-4 materials (same FVC) have a  $D_k$  of 4.3.

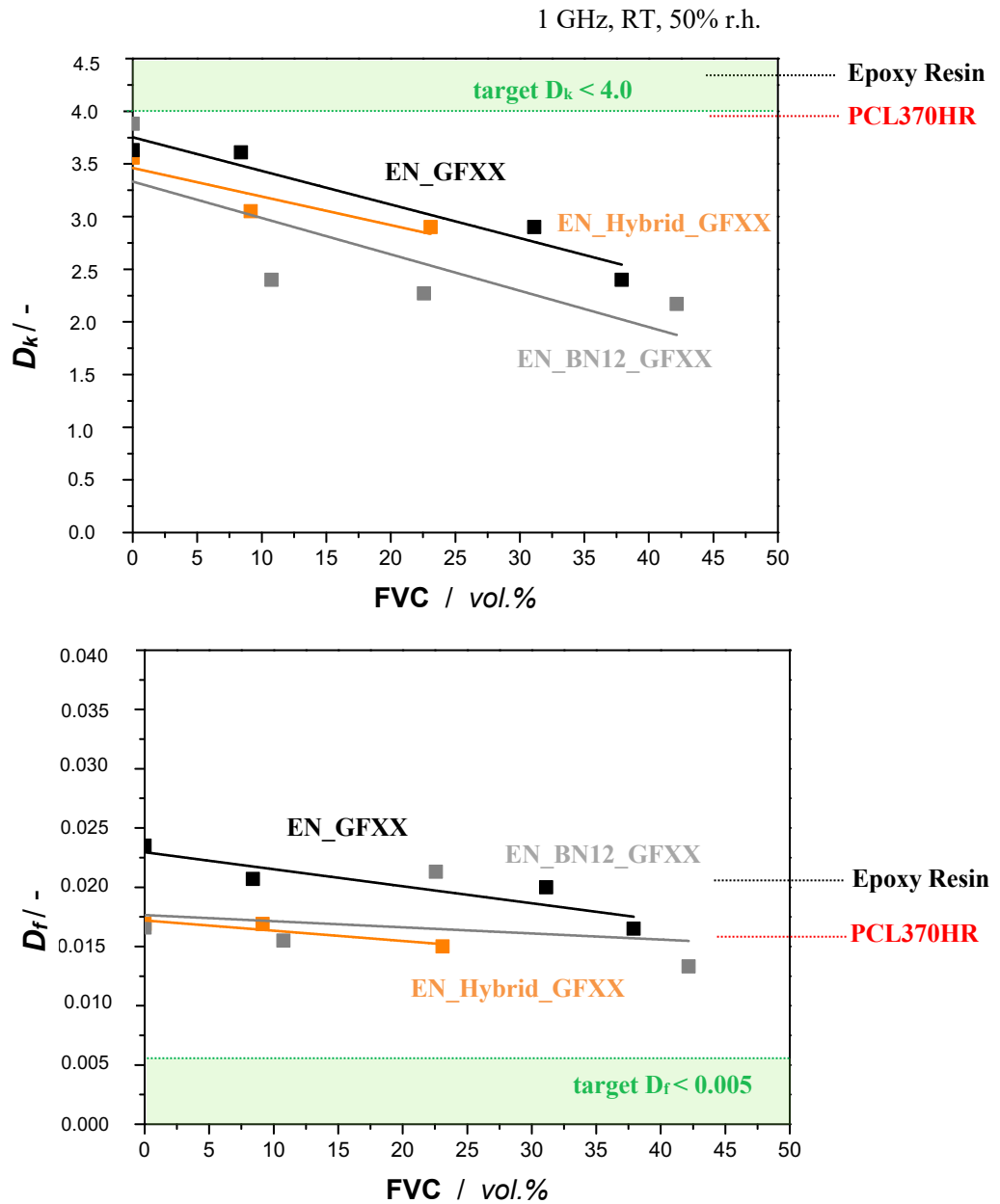


**Figure 107 Dielectric properties in dependency of increasing FVC. a)  $D_k$  and b)  $D_f$ .**

The addition of fillers might lead to a sudden change in polarization of the fillers at higher frequencies [209]. The BN laminates showed the lowest  $D_k$  value compared to the neat Epoxy Novolac and hybrid laminates. The  $D_k$  was reduced by almost a factor of 1. As already seen in

the morphological studies in previous chapters, the good BN filler dispersion contributes to electric current passing. The  $D_k$  values for the conventional FR-4 substrates with a  $T_g$  of 140 °C is at 4.5 at 1 GHz and for the high- $T_g$  substrates with a  $T_g$  of 180 °C at 4.3 at 1 GHz [199]. Both values were reported at 50% resin content. Comparable systems of this Ph.D. study would be GF107 systems that have a resin content between 47 – 62 vol.%.

The  $D_k$  was successfully decreased by a factor of 2. The dissipation factors  $D_f$  of current State-of-the-Art substrates are in the same range as the novel GF107 systems, i.e., 0.016, 0.018 for the FR-4 and the high- $T_g$  FR-4, respectively [199]. FR-4 substrates have a  $D_f$  in the range of 0.018 – 0.022; only cyanate ester-based laminates can reach values of 0.007 [14].

The  $D_f$  values of all systems were slightly above the target of < 0.005. The addition of filler addition resulted in lower  $D_f$  values. The higher surface area of the smaller filler particles probably leads to interfacial losses when the current passes [210]. The EN\_Hybrid\_GF49 laminate exhibits a loss factor of 0.0163, similar to three EN\_BN12\_GFXX laminates.

#### 5.4.4 Water Absorption

The service life of GFRP laminates is generally deteriorating as the moisture uptake increases. Especially, Epoxy resins suffer from high water absorption due to the presence of polar groups (-OH) in their molecular structure [120]. Some Epoxy resins can absorb as much as 20 % water upon saturation, while the current desired value for electronic packaging base materials is < 0.5 % after 24 hours exposure. Water absorption can potentially cause debonding at the fiber/matrix/filler interface through chemical attack and reaction and mechanical-chemical effects such as osmotic pressure [125]. With moisture absorption, the polymer chains are undergoing swelling and lead to delamination. Moreover, moisture absorption in GFRP can change the dielectric properties [211]. According to the literature, the addition of (inorganic) fillers can reduce water absorption, especially with BN [126,212].

In the following, the results of the GF25 laminates are plotted versus the testing time of ca. 30 d (Figure 108a). In addition, the graph below shows the effect of increasing FVC on the water absorption exemplarily for the BN 12 filled laminates (Figure 108b).

The water absorption for the conventional FR-4 substrates ( $T_g$  140 °C) is 0.1 %, and for the high- $T_g$  substrate (180 °C), FR-4 is 0.1 %, which are comparable to the above results [199]. For this project, the target for water uptake was < 0.5 % after 24 hours. The laminates under

investigation fit this criterion and can be used for further applications. The above findings are in alignment with the literature [120,213,214].

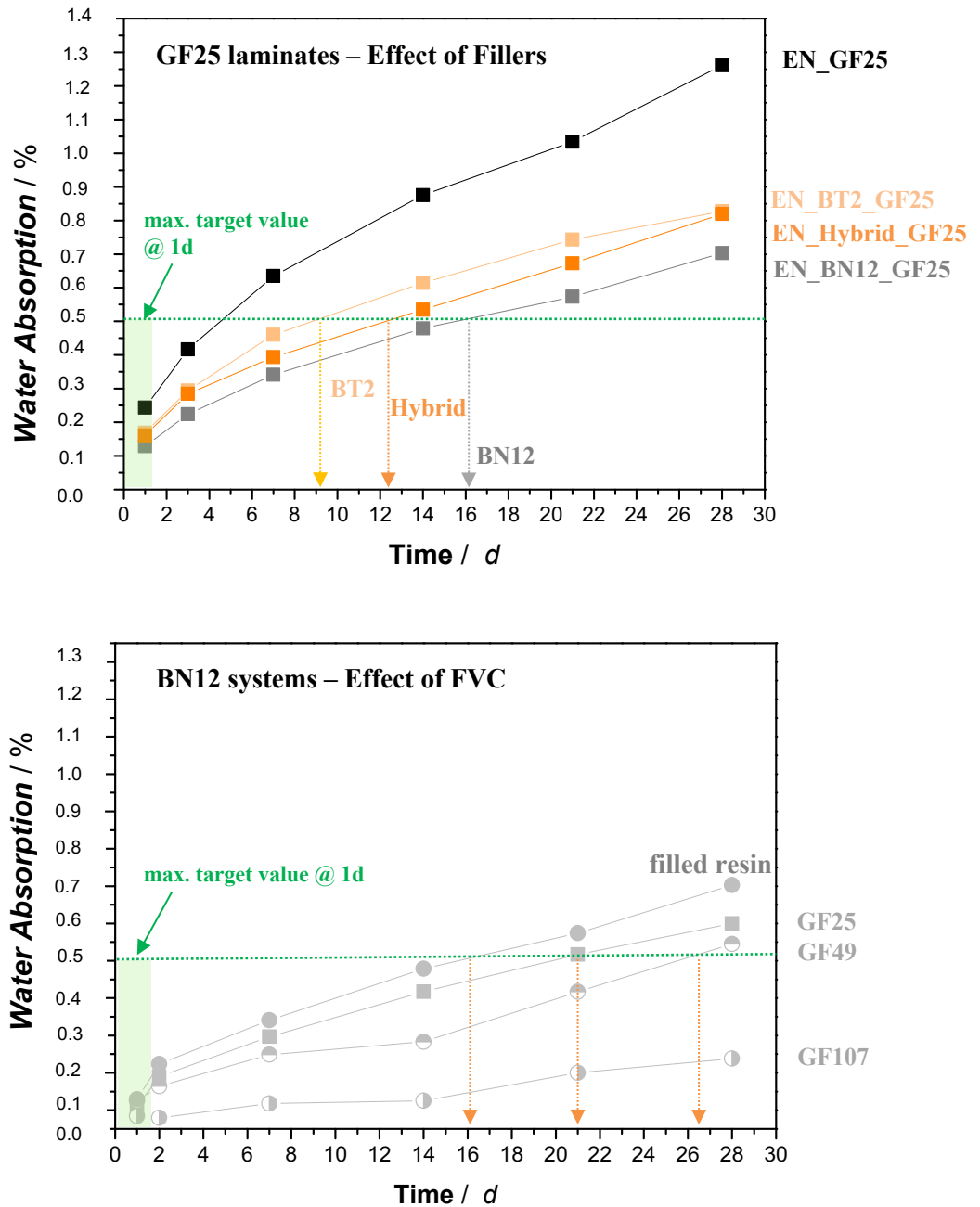


Figure 108 Water absorption results for a) GF25 laminates with fillers of different nature and b) influence of increasing FVC exemplarily for BN12 laminates.

In summary, all laminates absorb water below the target of 0.5 % within 24h. This is per the FR-4 and the benchmark PCL 370 HR, which have a water absorption of approx. 0.2 %.

It is known from the literature that Boehmite, in general, has a higher water absorption than BN. Boehmite has a higher polarity due to its superficial hydroxyl groups, whereas BN has a lower -OH availability. The chemical structure of Boehmite is  $\gamma$ -AlO(OH), which shows that a hydroxyl group is present. However, in literature, it was suggested that the -OH group of Boehmite binds to the multifunctional Epoxy resin during curing [215]. The water absorption of the neat Epoxy GF25 laminate is the highest amongst all and increases from day 1 (0.25 %) to week 4 (1.25 %). As expected, the addition of BN fillers helps in decreasing water absorption. The 12  $\mu$ m BN laminate shows the lowest water uptake. The hybrid laminate offers a water absorption in between the BT and BN laminate, suggesting a combinational effect. With increasing FVC, the water uptake is decreasing (Figure 108b). In general, glass fibers are highly hydrophilic due to the presence of polar groups on their surface, and hence their silanization reduces the hydrophilic nature and therefore increases hydrophobicity. The target value of 0.5 % is surpassed at day 9 for the EN\_BT2\_GF25 laminate, followed by the EN\_Hybrid\_GF25 at day 12 and EN\_BN12\_GF25 at day 16.

## 6 Summary and Outlook

Within the scope of this Ph.D. thesis, the main goal was to develop a novel next-generation multifunctional, high- $T_g$  PCB material with higher thermal stability and flame retardancy compared to the current “best in class” marketed benchmark from Isola, PCL 370HR.

The work focuses on a *solvent-free* prepreg system with a long storage stability whose processing is cost-efficient and has a *short production cycle*.

Overall, a holistic approach along the process chain was considered: *from material selection to processing to the final properties*. To achieve this primary goal, the experimental route started with the material selection taking into consideration overall material costs and ecological aspects, i.e, RoHS directive, that calls for “green” and halogen-free raw materials.

Based on these requirements above, Epoxy Novolac (EN) cured with the aromatic DETDA was selected to achieve excellent thermo-mechanical properties for the PCB base material with  $T_g > 235$  °C.

In addition, *platelet-shaped hexagonal* BN with different *lateral sizes* (e.g., BN2, 12, 45  $\mu\text{m}$ ) ideal candidates to improve the overall thermal conductivity. To provide enhanced flame retardancy and withstand the brief thermal cycling at 220 °C during the lead-free soldering, Boehmite (AlO(OH)) was selected.

The main properties were studied on cured, filled resins. The most promising formulations were then transferred to the filled-prepreg laminates, focusing on increasing fiber volume content (FVC).

As expected, to achieve the target value for the thermal conductivity of  $> 0.7$  W/mK, a minimum of 19.7 vol.% (about 45 wt.%) of platelet *h*-BN 12 $\mu\text{m}$  is needed. This was also the upper limit of filler content regarding processability with the prepreg line due to viscosity limitations. The microstructure revealed a random filler orientation (z-directional) with a high degree of dispersion. A filler-filler interaction established the thermally conductive path. To increase the packing density further and enhance the TC, BN2 was introduced to partially substitute BN12 in a 1:3 ratio. The overall TC value was not higher than the formulation containing only BN12 (0.66 W/mK versus 0.72 W/mK). Because the BN2 has a very irregular shape and filler surface, the scattering effects were too high.

Taking into consideration the overall costs, the *through*-plane (*z*-direction) heat dissipation can be tailored by optimizing the filler size/aspect ratio, and nature which ultimately led to the *hybrid* combination. The partial substitution of BN12 with Boehmite (BT2) decreases not only the overall price of the final laminate (as BN is more expensive by a factor of 50 compared to Boehmite) but also had a *synergistic effect* on the resulting TC of 0.81 W/mK in the filled resin. The microstructure resulted in a main thermal pathway consisting of the larger BN12 platelets with BT2 filling into the inter-gaps. This network formation was studied via *in-situ* hot-stage light microscopy and confirmed the formation during thermally induced curing.

As mentioned above, to achieve a specific threshold value for TC, at least 15 - 20 vol.% of fillers had to be incorporated into the EN matrix. On the prepreg line, the viscosity increase of the resin formulation could easily be controlled by parameters, such as temperatures at the resin holding tank and heating cycles. The solvent-free prepreg processing did not compromise the in the filled resins established random filler orientation. The produced prepregs have a shelf-life of up to 12 weeks stored at -18 °C.

The evaluation of the *effect of the GF content* on the thermal conductivity showed that the GF fabric acts as a (thermal) barrier. Even with an increase of BN12 in the formulation, the thermal conductivity value could not be increased above 1.1 W/mK. This effect was even more significant with increasing FVC, as the TC value approached the intrinsic TC value of the GF 0.9 W/mK. The hybrid filler combination followed the same trend. The microstructure of the hybrid-filled laminate using the fabric with 25 g/m<sup>2</sup> areal weight (EN\_Hybrid\_GF25) showed an efficient increase in packing density which led to a more homogenous *thermal pathway*. Within the *inter-tow* region (*resin-rich* area), most of the random-orientated larger BN12 platelets were detected. The smaller Boehmite platelets filled the gaps between the GF strands (*intra-tow* region). This microstructure helped to bridge the GF barrier leading to a homogenous thermal pathway throughout the laminate.

From a *thermal stability* standpoint, the target of  $T_g \geq 220$  °C and  $T_{d,5\%} > 360$  °C was achieved for all systems and their performance is much better than *State-of-the-Art* benchmarks (see in Figure 109). The achieved values for both  $T_g$  and  $T_{d,5\%}$ , 15 °C higher than the original set targets for this thesis.

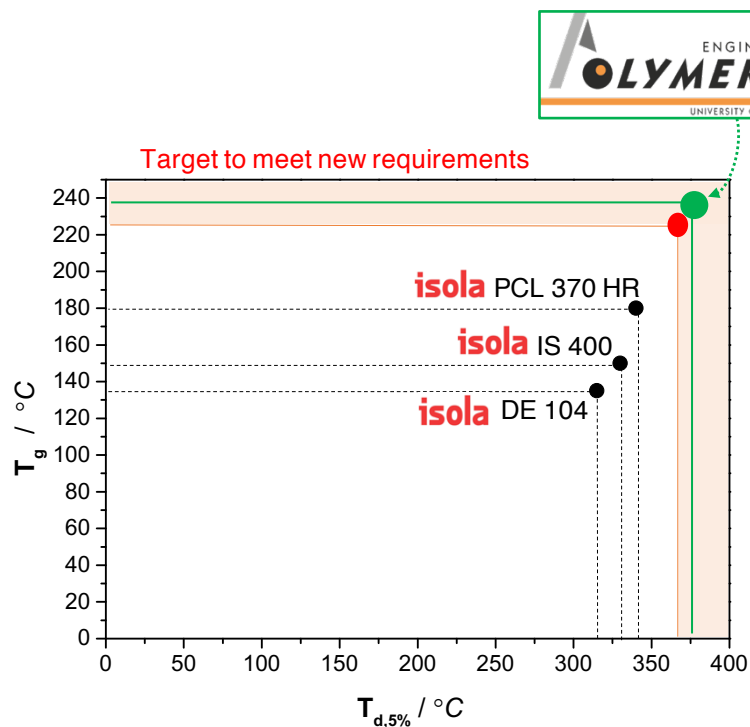


**Figure 109** FR-4 prepregs commercially available (Isola GmbH, this thesis' benchmarks), compared to the high-performance resin formulation developed in this PhD thesis (green data point).

The flame retardancy was studied with Cone Calorimetry, and post-combustion char analysis was evaluated with SEM-EDX. First, the addition of GF led to a more stable, less intumescent char compared to the filled resins. Higher stability is vital in fire scenarios to avoid flame spread. In summary, the primary influence of the filler BN12 was increasing the  $t_{ig}$ . This is attributed to the higher TC, as it delays the diffusion of volatile substances by absorbing thermal energy and supports the temperature distribution throughout the laminate. BN does not decompose and was mainly detected on the char surface, hinting its major contribution as a solid-phase active filler. Boehmite is the major component that has a significant effect on FR. With its reaction to  $\text{Al}_2\text{O}_3$  and therefore its dual-activity in both the gas- and condensed phase, the total smoke release (TSR), the total heat evolved (THE), and finally, the peak heat release rate (PHRR) was significantly reduced; THE and TSR values were decreased by 50 %, the PHRR was decreased by 66 %. The extensive char analysis confirmed the above-described flame-retardancy mechanisms: Boehmite acts as a char stabilizer resulting in a compact char morphology.  $\text{Al}_2\text{O}_3$  was indeed detected on the char surface. The BN-filled char showed that

BN is a rather “inactive” filler migrating to the surface during combustion shielding the release of smoke and protecting the underlying material from heat. The hybrid char revealed a “combinational” effect with the formation of  $\text{Al}_2\text{O}_3$  dominating in the FR mechanism, BN is only migrating to the surface. Comparing the BN12-filled laminates with unfilled laminates at different FVC, it was found that the filler incorporation does not influence the PHRR reduction. With increasing FVC, the heat and smoke release can only be further decreased with the reduction of the combustible matrix. However, the  $t_{ig}$  is influenced by the filler. Both fillers and GF influence the TSR. It was found that especially the closer-meshed woven fabric (GF107) improved the fire properties by inhibiting the diffusion of the flammable gases. Additionally, the incorporation of fillers led to an extension of the diffusion path of volatiles and a much lower PHRR and higher  $t_{ig}$ . In summary, the best FR results (see Petrella plot, THE vs. FIGRA, Figure 101) were achieved with BT only, followed by the hybrid and the BN-filled systems. The correlation between TC and FR showed that with the incorporation of fillers, the  $t_{ig}$  was **increased by up to 25 s**. A **further increase by 25 s** was achieved by using higher intrinsic TC fillers, such as BN. BN, therefore, plays a crucial role by absorbing surrounding heat. Comparing with current benchmarks, this is a **significant increase of up to 100 s**. The delay of ignition is significant since this is considered the time to escape.

UL-94 test passed with the classification of V-1 for the GF25 laminates, V-0 was thus achieved with the hybrid-filled laminate using the  $49 \text{ g/m}^2$  areal weight GF fabric (EN\_Hybrid\_GF49) and all GF107 laminates. All laminates did not show any signs of melt dripping.

A direct comparison between the *standard FR-4* and the benchmark of this thesis *PCL 370 HR* with the *novel hybrid laminate* is shown in Figure 110. **The novel hybrid base material meets almost the entire technical delivery specification, except for the z-CTE**. A potential solution to decrease the CTE can be increasing the overall filler or fiber content in the laminates [50]. The novel prepreg is a very competitive as the water absorption is even lower than for FR-4 and PCL 370 HR. The Df value is in the same range as the benchmark, however, achieved a Dk of  $< 4.0$ , whereas the benchmark and FR-4 are  $> 4.0$  (Figure 110). The prepreps with the highest FVC performed even better in all categories.

A **price increase** was expected in this research project since the BN filler costs about 140 euros/kg. This is very expensive compared to mineral fillers, such as ATH or Boehmite,

with 2 - 3 euros/kg. However, a significant improvement was achieved regarding the thermal properties, i.e.,  $T_g$ ,  $T_d$ , and thermal conductivity with very low water absorption and good dielectric properties.

	FR-4	Benchmark PCL 370HR 	Hybrid Böhmit + BN 	Specifications Smart PVI Box
TC / W/mK	0.35	0.38	<b>0.85</b>	> 0.70
$T_g$ / °C (DMA)	< 180	180	<b>ca. 235</b>	> 220
$T_{d,5\%}$ / °C	315	340	<b>370</b>	> 360
z-CTE < $T_g$ / ppm/K	55	45	<b>55</b>	< 40
H <sub>2</sub> O abs / %	0.20	0.18	<b>0.15</b>	< 0.5
$D_k$ / - @1GHz	4.0	3.9	<b>3.5</b>	< 4.0
$D_f$ / - @1GHz	0.0189	0.022	<b>0.0169</b>	< 0.005
Flame Retard. (UL-94)	V-0	V-0	<b>V-0</b>	V-0
Price ratio	1	N/A	<b>2.68</b>	< 4xFR-4

**Figure 110 Comparison of the technical delivery specification of the *State-of-the-Art* base materials with the novel developed *hybrid* formulation.**

The Printed Circuit Board needs to be designed smartly, as the novel thermally conductive substrate material is higher in price than existing materials. This substrate is a good candidate for its use in areas close to the embedded chip. In surrounding regions, where thermal management is not needed, cheaper substrates can be used. The overall PCB price, thus, is still in a moderate range. This will be ultimately applied in the design process for the upcoming, novel generation of PCBs for wireless charging in E-mobiles, which this thesis is based on (Figure 111) (Smart PVI Box, BMWi 0325916F).

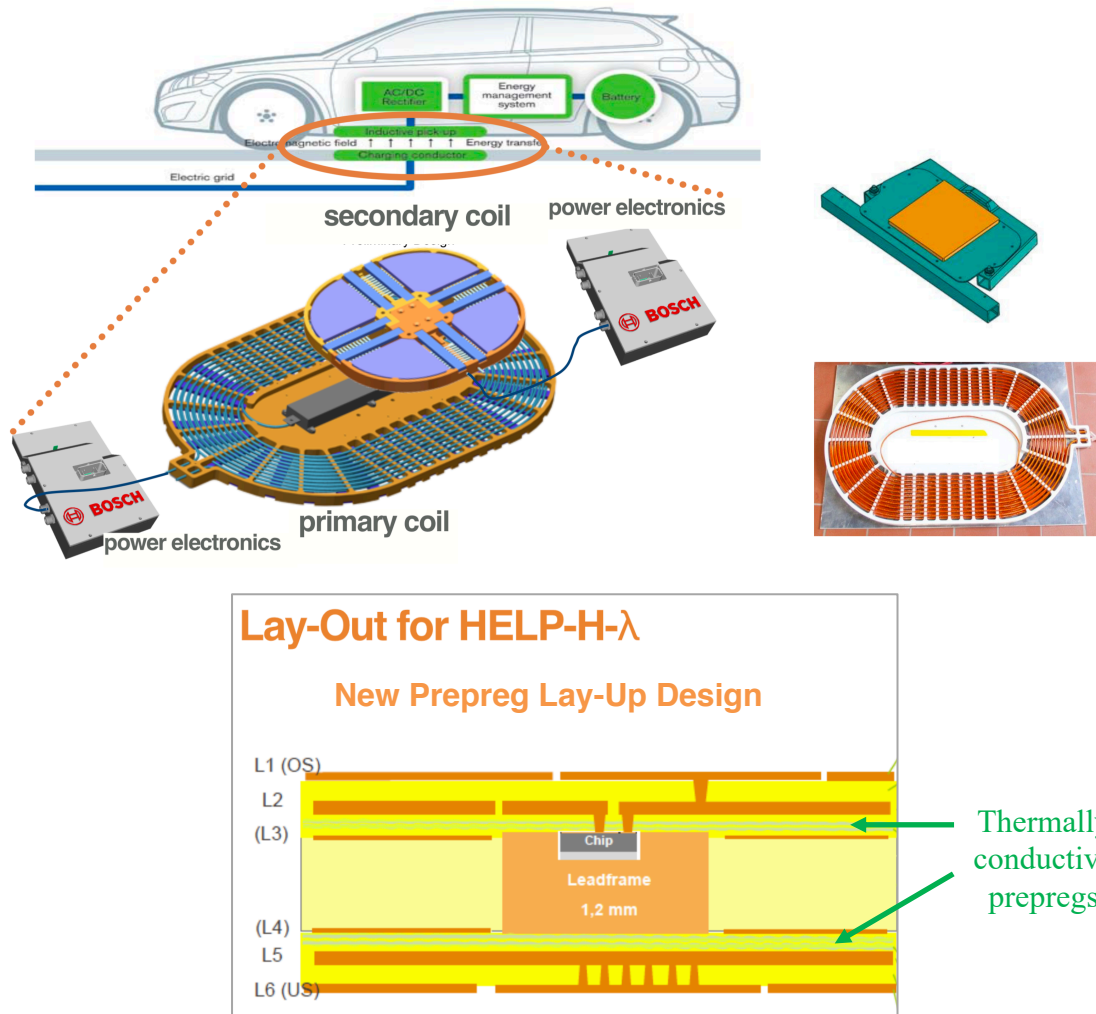


**Figure 111** Incorporation of a thermally conductive prepreg-layer close to the embedded chip (called HELP-H-λ) as part of the project „Smart PVI Box (BMW i 0325916F) (wireless charging for E-mobiles).

Overall, the new substrate made from solvent-free prepregs is very competitive with current prepregs available on the market. Future scientific research might want to investigate achieving the desired  $\alpha$ -CTE and  $D_f$  targets, which are opportunities for further improvement on this novel substrate. This might be achieved by introducing a third filler, such as Talcum. Apeldorn achieved excellent properties in his comprehensive research using Talcum with Quarz and Wollastonite [24,39,65].

As literature showed minor effects on TC, surface functionalization of BN is not economic in terms of processing and cycle times. BN only has a few active functional groups on its surface available for functionalization [134]. Therefore, this will only play a very minor role soon.

The future for thermally conductive polymer composites is emerging: LEDs, E&E (chip packaging), batteries, and solar cells [70].

The emerging battery market, a high-performance thermally conductive system is still lacking. The combination of an organic FR with the inorganic BN fillers would open a niche market. Studies by Lengsfeld [202] and Neumeyer [194] showed that DOPO works great with Epoxy Novolac resin systems. As an outlook for future studies, the FR component Boehmite can potentially be partially substituted with the covalent DOPO modification of the resin backbone, which can even further enhance the FR performance.

## 7 References

- [1] Z. (Die Elektronikindustrie), Deutscher Halbleitermarkt schließt 2018 mit starkem Wachstum ab, *4.12.* (2018).
- [2] BTG Labs, Importance of Adhesion & Composites in Lightweighting Cars, (2019).
- [3] V. Electronics, Automotive PCB Market - What's the future of PCB for Automotive Industry, (n.d.). <https://www.venture-mfg.com/automotive-pcb-capabilities/> (accessed July 3, 2020).
- [4] International Energy Agency, Energy Technology Perspectives 2012, Paris, 2012.
- [5] J. LaDou, Printed circuit board industry, *Int. J. Hyg. Environ.-Health.* 209 (2006) 211–219. doi:10.1016/j.ijheh.2006.02.001.
- [6] PCB-Investigator V11, Simulation mit PCB-Investigator Physics, (n.d.). <https://www.pcb-investigator.com/de/blog/brand-new-physics-simulation> (accessed August 28, 2020).
- [7] PCB Reverse Engineering, PCB -Circuit - Reverse Engineering, (n.d.). <http://www.circuitengineer.com/pcb-circuit-reverse-engineering/pcb-copy-2/> (accessed August 28, 2020).
- [8] Y.X. Fu, Z.X. He, D.C. Mo, et al., Thermal conductivity enhancement with different fillers for epoxy resin adhesives, *Appl. Therm. Eng.* 66 (2014) 493–498. doi:10.1016/j.applthermaleng.2014.02.044.
- [9] K. Kim, M. Kim, J. Kim, Thermal and mechanical properties of epoxy composites with a binary particle filler system consisting of aggregated and whisker type boron nitride particles, *Compos. Sci. Technol.* 103 (2014) 72–77. doi:10.1016/j.compscitech.2014.08.012.
- [10] X.C. Tong, Advanced Materials for Thermal Management of Electronic Packaging, Springer Science & Business Media, 2011, ISBN:9781441977588.
- [11] X.C.. Tong, Advanced Materials for Thermal Management of Electronic Packaging - Thermal Management Fundamental and Design Guides in Electronic Packaging, Springer Science & Business Media, 2011. doi:10.1007/978-1-4419-7759-5\_1.
- [12] D.M. Bigg, Thermally Conductive Polymer Compositions, *Polym. Compos.* 7 (1986) 125–140. doi:10.1002/pc.750070302.

- 
- [13] P. Bujard, Thermal Conductivity of Boron Nitride Filled Epoxy Resin: Temperature Dependence and Influence of Sample Preparation, *Intersoc. Conf. Therm. Phenom. Fabr. Oper. Electron. Components I-THERM '88.* (1988) 41–49. doi:10.1109/ITHERM.1988.28676.
- [14] R. Bissell, J. Conrad, E. Holman, et al., New Low Dielectric Constant, High Tg, Printed Circuitry Substrates, *Isola GmbH.* (2021). <https://www.isola-group.com/resource/new-low-dielectric-constant-high-tg-printed-circuitry-substrates/>.
- [15] K. Devendra, T. Rangaswamy, Thermal Conductivity and Thermal Expansion Coefficient of GFRP Composite Laminates with Fillers, *Conf. Proc. Mech. Confab. 2* (2013) 39–44. doi:2320-2491.
- [16] B. Fan, Y. Liu, D. He, et al., Enhanced thermal conductivity for mesophase pitch-based carbon fiber/modified boron nitride/epoxy composites, *Polym. (United Kingdom)*. 122 (2017) 71–76. doi:10.1016/j.polymer.2017.06.060.
- [17] R.S. Khandpur, Printed Circuit Boards - Design, Fabrication, Assembly and Testing, McGraw-Hill Professional, New York, 2006, ISBN:0071464204. doi:10.1036/0071464204.
- [18] C.F. Coombs Jr, Printed Circuits Handbook, 6th ed., McGraw-Hill, 2008, ISBN:0071510796. doi:10.1036/0071467343.
- [19] M. Goosey, Plastics for Electronics, 2nd ed., 1999, ISBN:978-90-481-4018-3,978-94-017-2700-6.
- [20] R.H. Clark, Handbook of Printed Circuit Manufacturing, 1985, ISBN:0-442-21610-6.
- [21] Luxeon Rebel - Assembly and Handling Information, 2008.
- [22] W.-D. Schmidt, Grundlagen der Leiterplatten-Baugruppen-Entwicklung und Fertigung, 1st ed., Grin Verlag, 2009, ISBN:B00BS70CFM.
- [23] E. Kelley, Re-engineered FR-4 Base Material for Improved Multilayer PCB Performance, in: 2004.
- [24] T. Apeldorn, Untersuchung Leiterplattensubstrat-spezifischer Eigenschaften von ausdehnungsarmen Compounds auf Basis von Thermoplasten, Universität Bayreuth, 2013.
- [25] J.G. Drobny, Polymers for Electricity and Electronics - Materials, Properties and Applications, John Wiley & Sons, Inc., Hoboken, New Jersey, 2012, ISBN:978-0-470-45553-1.

- 
- [26] M. Goosey, *Plastics for Electronics*, Kluwer Academic Publishers, **1999**, ISBN:978-90-481-4018-3. doi:10.1007/978-94-017-2700-6.
- [27] J. Coonrod, Differences Between Thermoplastic And Thermoset Materials, *Rog Blog*. **(2016)**.
- [28] D. Lu, C.P. Wong, *Materials for Advanced Packaging*, Springer Science & Business Media, **2008**, ISBN:0387782184. doi:10.1007/978-0-387-78219-5.
- [29] J.-X. Tsai, Tsung-Yen; Lu, Shau-Tai; Huang, Chin-Jei; Liu, The Structure-Property Relationship of Novolac Cured Epoxy Resin/Clay Nanocomposites, *Polym. Eng. Sci.* **(2008)** 1–9. doi:10.1002/pen.20977.
- [30] D. Ratna, *Handbook of Thermoset Resins*, **2009**, ISBN:1847354106, 1847354114. doi:10.1002/0471743984.vse3011.pub2.
- [31] DOW Chemicals, D.E.N.TM 438 Epoxy Novolac Product Information, (n.d.). [https://www.dow.com/assets/attachments/business/pcm/den/den\\_438/tds/den\\_438.pdf](https://www.dow.com/assets/attachments/business/pcm/den/den_438/tds/den_438.pdf) (accessed January 16, 2019).
- [32] G.W. Ehrenstein, *Faserverbund- Kunststoffe*, 2nd ed., Carl Hanser Verlag München Wien, **2006**, ISBN:9783446227163.
- [33] A. Anastasijevic, Einfluss des Faservolumengehaltes auf das Infiltrationsverhalten sowie die thermischen und mechanischen Eigenschaften von lamianten aus hochgefüllten h-BN Prepregs, University of Bayreuth, **2008**.
- [34] Hexcel, HexPly Prepreg Technology, **(2013)** 35. doi:10.2307/3775933.
- [35] M.W. Jawitz, *Printed circuit board materials handbook*, McGraw Hill Professional, **1997**, ISBN:0-07-032488-3.
- [36] R.A. Normann, *First High-Temperature Electronics Products Survey*, **2005**.
- [37] W. Burr, N. Pearne, F. Stern, Printed circuit board technologies for thermal management, *Circuit World*. 39 **(2013)** 9–12. doi:10.1108/03056121311298909.
- [38] J. Dieterle, *Heat Management in Printed Circuit Boards*, **2010**.
- [39] T. Apeldorn, E. Wolff-Fabris, V. Altstaedt, High-performance substrate based on a highly filled thermoplastic polymer, *Circuit World*. 37 **(2011)** 4–14. doi:10.1108/03056121111101232.
- [40] M. Cygon, High Performance Materials for PCBs, *Circuit World*. 19 **(1992)** 14–18. doi:10.1108/eb046186.
- [41] C. Smith, Gordon, Very ultra thin conductor layers for Printed Wiring Boards, US

- 2004/0185275 A1, **2004**.
- [42] M. Hendricks, Cathy; Kelly, Cathy; Choate, Laminate Composition for Producing reduced curl flat thin core laminate, US 8,263,225 B2, **2012**.
- [43] D.M. Logan, Brook Hedin; Miller, Thermally Conductive Polymer based Printed Circuit Boards, US 2010/0012354 A1, **2010**.
- [44] D.M. Conley, Nicholas Ryan; Logan, Brook Hedin; Miller, Thermally Conductive Printed Circuit Boards, US 2014/0020933 A1, **2014**.
- [45] J.E. Nelson, Robert A.; Dubois, Raymon I.; Collier, Michael A.; Keating, High Temperature Multilayer Flexible Printed Wiring Board, US 2015/0122532 A1, **2015**.
- [46] J. Coonrod, Understanding when to use FR-4 laminates or high frequency laminates, *IPC APEX EXPO Tech. Conf. 2011*. 3 (**2011**) 1991–2016.
- [47] Rogers Corporation, Products - 92ML Materials - Features, (n.d.). <https://rogerscorp.com/advanced-connectivity-solutions/92ml-materials>.
- [48] I. Group, TerraGreen - Halogen-free, very low loss Material - Product Features, (n.d.). <https://www.isola-group.com/pcb-laminates-prepreg/terragreen-laminate-and-prepreg-materials/>.
- [49] I. Group, 370HR - Industry leading, Standard Loss, Thermally Robust Epoxy Laminate and Prepreg - Product Features, (n.d.). <https://www.isola-group.com/pcb-laminates-prepreg/370hr-laminate-prepreg/>.
- [50] C. Zweben, Advances in Composite Materials for Thermal Management in Electronic Packaging, *JOM*. 50 (**1998**) 47–51. doi:<https://doi.org/10.1007/s11837-998-0128-6>.
- [51] M.G. Chemical, High Performance FR-4 for Multi-layered PWB, (n.d.).
- [52] I. Group, I-Tera MT40 - Very Low-Loss Laminate Material, (n.d.). <https://www.isola-group.com/pcb-laminates-prepreg/i-tera-mt40/>.
- [53] I. Group, IS410 - Lead-free Epoxy Laminate and Prepreg, (n.d.). <https://www.isola-group.com/pcb-laminates-prepreg/is410-fr-4-epoxy-laminate-and-prepreg/>.
- [54] I. Group, IS400 - Lead-free, Mid-Tg Epoxy Laminate and Prepreg, (n.d.).
- [55] I. Group, DE104 - Low Tg Laminate and Prepreg, (n.d.). <https://www.isola-group.com/pcb-laminates-prepreg/de104-laminate-and-prepreg/>.
- [56] P. Corporation, Halogen-free Ultra-low transmission loss Multi-layer Circuit board materials | R-5515, (n.d.). <https://industrial.panasonic.com/ww/products/electronic-materials/circuit-board-materials/low-loss/llossr5515>.

- [57] P. Corporation, High thermal conductivity Low transmission loss Halogen-free Multi-layer circuit board materials | R-5575, (n.d.). <https://industrial.panasonic.com/ww/products/electronic-materials/circuit-board-materials/low-loss/llossr5575>.
- [58] H. Chemical, MCL-E-679FG, (n.d.). [www.hitachi-chemical.com](http://www.hitachi-chemical.com).
- [59] C. Raman, A. Murugaiah, B. Xiang, et al., Thermally Conductive but Electrically Insulating Plastics for Thermal Management Applications, *Momentive Perform. Mater. Inc.* (2015) 1–12.
- [60] K. Vasoya, C. Mesa, Optimizing thermal and mechanical performance in PCBs, *Glob. SMT Packag.* (2007) 10–12.
- [61] Würth Elektronik, Basics of Effective Thermal Management, (2011).
- [62] B. Heinz, Heat management of circuit boards, (2011) 1–6.
- [63] S.S. Anandan, V. Ramalingam, Thermal management of electronics: A review of literature, *Therm. Sci.* 12 (2008) 5–25. doi:10.2298/TSCI0802005A.
- [64] Würth Electronics, Basics - Effective Thermal Management, (n.d.). [https://www.wer-online.com/web/en/leiterplatten/produkte\\_/waermemanagement/grundlagen/grundlagen.php](https://www.wer-online.com/web/en/leiterplatten/produkte_/waermemanagement/grundlagen/grundlagen.php) (accessed January 20, 2019).
- [65] T. Apeldorn, C. Keilholz, F. Wolff-Fabris, et al., Dielectric properties of highly filled thermoplastics for printed circuit boards, *J. Appl. Polym. Sci.* 128 (2013) 3758–3770. doi:10.1002/app.38602.
- [66] N. Burger, A. Laachachi, M. Ferriol, et al., Review of thermal conductivity in composites: Mechanisms, parameters and theory, *Prog. Polym. Sci.* 61 (2016) 1–28. doi:10.1016/j.progpolymsci.2016.05.001.
- [67] I. a. Tsekmes, R. Kochetov, P.H.F. Morshuis, et al., Thermal conductivity of polymeric composites: A review, *2013 IEEE Int. Conf. Solid Dielectr.* (2013) 678–681. doi:10.1109/ICSD.2013.6619698.
- [68] C. Heinle, Simulationsgestützte Entwicklung von Bauteilen aus wärmeleitenden Kunststoffen, Universität Erlangen-Nürnberg, 2012.
- [69] Würth Elektronik, Heat management of circuit boards, 2011.
- [70] H. Chen, V. V Ginzburg, J. Yang, et al., Thermal conductivity of polymer-based composites: Fundamentals and applications, *Prog. Polym. Sci.* 59 (2016) 41–85. doi:10.1016/j.progpolymsci.2016.03.001.

- [71] J. Gu, Q. Zhang, J. Dang, et al., Thermal conductivity epoxy resin composites filled with boron nitride, *Polym. Adv. Technol.* 23 (2012) 1025–1028. doi:10.1002/pat.2063.
- [72] M. Donnay, S. Tzavalas, E. Logakis, Boron nitride filled epoxy with improved thermal conductivity and dielectric breakdown strength, *Compos. Sci. Technol.* 110 (2015). doi:10.1016/j.compscitech.2015.02.006.
- [73] L. Huang, P. Zhu, G. Li, et al., Spherical and flake-like BN filled epoxy composites : morphological effect on the thermal conductivity , thermo-mechanical and dielectric properties, *J. Mater. Sci. Mater. Electron.* 26 (2015) 3564–3572. doi:10.1007/s10854-015-2870-1.
- [74] F. Wang, X. Zeng, Y. Yao, et al., Silver Nanoparticle-Deposited Boron Nitride Nanosheets as Fillers for Polymeric Composites with High Thermal Conductivity, *Nat. Publ. Gr.* (2016) 1–9. doi:10.1038/srep19394.
- [75] K. Gaska, A. Rybak, C. Kapusta, et al., A Study of Thermal Conductivity of Boron Nitride Epoxy Matrix Composites, in: 15th Eur. Conf. Compos. Mater., 2012. doi:N/A.
- [76] R. Kochetov, T. Andritsch, P.H.F. Morshuis, et al., Effect of Filler Size on Complex Permittivity and Thermal Conductivity of Epoxy-based Composites Filled with BN Particles, *Annu. Rep. Conf. Electr. Insul. Dielectr. Phenom.* (2010) 3–6. doi:10.1109/CEIDP.2010.5723962.
- [77] K.C. Yung, J. Wang, T.M. Yue, Thermal Management for Boron Nitride Filled Metal Core Printed Circuit Board, *J. Compos. Mater.* 42 (2008) 2615–2627. doi:10.1177/0021998308096326.
- [78] B.L. Zhu, J. Ma, J. Wu, et al., Study on the Properties of the Epoxy-Matrix Composites Filled with Thermally Conductive AlN and BN Ceramic Particles, *J. Appl. Polym. Sci.* (2010). doi:10.1002/app.32673.
- [79] T. Wieme, D. Tang, L. Delva, et al., The relevance of material and processing parameters on the thermal conductivity of thermoplastic composites, *Polym. Eng. Sci.* 58 (2018) 466–474. doi:10.1002/pen.24667.
- [80] J.P. Hong, S.W. Yoon, T. Hwang, et al., High thermal conductivity epoxy composites with bimodal distribution of aluminum nitride and boron nitride fillers, *Thermochim. Acta.* 537 (2012) 70–75. doi:10.1016/j.tca.2012.03.002.
- [81] D.D.L. Chung, *Materials for Electronic Packaging*, Butterworth-Heinemann, 1995, ISBN:0-7506-9314-2.

- [82] I. Isarn, X. Ramis, F. Ferrando, et al., Thermoconductive thermosetting composites based on boron nitride fillers and thiol-epoxy matrices, *Polymers (Basel)*. 10 (2018). doi:10.3390/polym10030277.
- [83] S. Zhou, Wenying, Yu, Demei, Wang, Caifeng, An, Qunlin, Qi, Effect of Filler Size Distribution on the Mechanical and Physical Properties of Alumina-Filled Silicone Rubber, *Polym. Eng. Sci.* (2008) 1380–1389. doi:10.1002/pen.21113.
- [84] G.W. Lee, M. Park, J. Kim, et al., Enhanced thermal conductivity of polymer composites filled with hybrid filler, *Compos. Part A Appl. Sci. Manuf.* 37 (2006) 727–734. doi:10.1016/j.compositesa.2005.07.006.
- [85] M.H.E. Glowania, Untersuchung und Methodenentwicklung zur Steigerung der Wärmeleitfähigkeit von Faserverbundkunststoffen, Hochschule Aalen, 2012.
- [86] Y. Zhao, Z. Zhai, D. Drummer, Thermal conductivity of aluminosilicate- and aluminum oxide-filled thermosets for injection molding: Effect of filler content, filler size and filler geometry, *Polymers (Basel)*. 10 (2018). doi:10.3390/polym10040457.
- [87] X.F. Jiang, Q. Weng, X. Bin Wang, et al., Recent Progress on Fabrications and Applications of Boron Nitride Nanomaterials: A Review, *J. Mater. Sci. Technol.* 31 (2015) 589–598. doi:10.1016/j.jmst.2014.12.008.
- [88] R. Damasch, Bornitrid als multifunktionseller Füllstoff in Polymersystemen, (n.d.). <http://www.keramverband.de/keramik/pdf/07/sem07-13.pdf> (accessed April 19, 2019).
- [89] X. Huang, P. Jiang, T. Tanaka, A review of dielectric polymer composites with high thermal conductivity, *IEEE Electr. Insul. Mag.* 27 (2011) 8–16. doi:10.1109/MEI.2011.5954064.
- [90] A.F. Coonrod, John; Horn, High Frequency Circuit Materials with increased Thermal Conductivity, *High Freq. Electron.* (2010) 40–49. doi:10.1201/9781482277425-61.
- [91] R.F. Hill, P.H. Supancic, Thermal Conductivity of Platelet-Filled Polymer Composites, *J. Am. Ceram. Soc.* 85 (2002) 851–857. doi:10.1111/j.1151-2916.2002.tb00183.x.
- [92] T.L. Li, S.L.C. Hsu, Enhanced thermal conductivity of polyimide films via a hybrid of micro- and nano-sized boron nitride, *J. Phys. Chem. B.* 114 (2010) 6825–6829. doi:10.1021/jp101857w.
- [93] X. Duan, Z. Yang, L. Chen, et al., Review on the properties of hexagonal boron nitride matrix composite ceramics, *J. Eur. Ceram. Soc.* 36 (2016) 3725–3737. doi:10.1016/j.jeurceramsoc.2016.05.007.

- [94] T.H. Chiang, T.-E. Hsieh, A Study of Encapsulation Resin Containing Hexagonal Boron Nitride (hBN) as Inorganic Filler, *J. Inorg. Organomet. Polym. Mater.* 17 (2007) 335–335. doi:10.1007/s10904-007-9105-8.
- [95] H. Ishida, Composition For Forming High thermal Conductivity Polybenzoxazine-based Material and Method, 5,900,477, **1999**.
- [96] H. Ishida, S. Rimdusit, Very high thermal conductivity obtained by boron nitride-filled polybenzoxazine, *Thermochim. Acta.* 320 (1998) 177–186. doi:10.1016/S0040-6031(98)00463-8.
- [97] G.W. Ehrenstein, Polymer-Werkstoffe, 3rd ed., Carl Hanser Verlag München Wien, **2017**, ISBN:9783446422834.
- [98] O. Skrabala, Wärmeleitfähige Kunststoffe: Verarbeitungsinduzierte Eigenschaftsbeeinflussung und deren numerische Vorhersage, Stuttgart, **2016**.
- [99] K. Kim, M. Kim, Y. Hwang, et al., Chemically modified boron nitride-epoxy terminated dimethylsiloxane composite for improving the thermal conductivity, *Ceram. Int.* 40 (2014) 2047–2056. doi:10.1016/j.ceramint.2013.07.117.
- [100] H. Wu, L.T. Drzal, High Thermally Conductive Graphite Nanoplatelet/Polyetherimide Composite by Precoating: Effect of Percolation and Particle Size, *Polym. Compos.* (2013). doi:10.1002/pc.
- [101] K.C. Yung, J. Wang, T.M. Yue, Filled Metal Core Printed Circuit Board, *J. Compos. Mater.* 42 (2008). doi:10.1177/0021998308096326.
- [102] D. Bigg, Conductive Polymeric Compositions, (1977).
- [103] Z. Su, H. Wang, X. Ye, et al., Anisotropic thermally conductive flexible polymer composites filled with hexagonal boron nitride (h-BN) platelets and amine carbon nanotubes (CNT-NH<sub>2</sub>): Effects of the filler distribution and orientation, *Compos. Part A Appl. Sci. Manuf.* 109 (2018) 402–412. doi:10.1016/j.compositesa.2018.03.021.
- [104] R. Kochetov, Thermal and Electrical Properties of Nanocomposites, Including Material Processing, Delft University of Technology, **2012**.
- [105] I. Tsekmes, R. Kochetov, P. Morshuis, et al., Modeling the thermal conductivity of polymeric composites based on experimental observations, *IEEE Trans. Dielectr. Electr. Insul.* 21 (2014) 412–423. doi:10.1109/TDEI.2013.004142.
- [106] P.P. Composites, R.F. Hill, J.L. Strader, Rudimentary Finite Element Thermal Modeling of, *IEEE Trans. Components Packag. Technol.* 30 (2007) 235–241.

- doi:10.1109/TCAPT.2007.898330.
- [107] C. Skrabala, O., Bonten, Orientation behavior of platelet-shaped fillers in plastic suspensions, *J. Plast. Technol.* 12 (2016) 157–183.
- [108] L. Chen, Y. Sun, H. Xu, et al., Analytic Modeling for the Anisotropic Thermal Conductivity of Polymer Composites Containing Aligned Hexagonal Boron Nitride, *Compos. Sci. Technol.* (2015). doi:10.1016/j.compscitech.2015.11.013.
- [109] C. Yu, J. Zhang, Z. Li, et al., Enhanced through-plane thermal conductivity of boron nitride/epoxy composites, *Compos. Part A Appl. Sci. Manuf.* 98 (2017) 25–31. doi:10.1016/j.compositesa.2017.03.012.
- [110] H. Ishida, S. Rimdusit, Very High Thermal Conductivity Obtained by Boron Nitride Filled Polybenzoxazine, *Thermochim. Acta.* (1998). doi:10.1016/S0040-6031(98)00463-8.
- [111] S. Rimdusit, C. Jubsilp, S. Tiptipakorn, High Thermal Conductivity of BN-filled Polybenzoxazines, in: Alloy. Compos. Polybenzoxazines, Engineerin, Springer, Singapore, 2013. doi:10.1007/978-981-4451-76-5.
- [112] Y. Jiang, X. Shi, Y. Feng, et al., Enhanced thermal conductivity and ideal dielectric properties of epoxy composites containing polymer modified hexagonal boron nitride, *Compos. Part A Appl. Sci. Manuf.* 107 (2018) 657–664. doi:10.1016/j.compositesa.2018.02.016.
- [113] S. Chung, J. Lin, Thermal Conductivity of Epoxy Resin Composites Filled with Combustion Synthesized h-BN Particles, *Molecules.* 21 (2016) 1–11. doi:10.3390/molecules21050670.
- [114] M.F. Shafee, M. Jaafar, Effect of Boron Nitride Nano Filler Filled Epoxy Composites for Underfill Application, 9 (2013) 89–98.
- [115] J. Hong, S. Yoon, T. Hwang, et al., High thermal conductivity epoxy composites with bimodal distribution of aluminum nitride and boron nitride fillers, *Thermochim. Acta.* 537 (2012) 70–75. doi:10.1016/j.tca.2012.03.002.
- [116] S. Li, S. Qi, N. Liu, et al., Study on thermal conductive BN / novolac resin composites, *Thermochim. Acta.* 523 (2011) 111–115. doi:10.1016/j.tca.2011.05.010.
- [117] T. Huang, X. Zeng, Y. Yao, et al., Boron nitride / graphene oxide hybrids for epoxy composites with enhanced thermal conductivity, *RSC Adv.* 6 (2016) 35847–35854. doi:10.1039/C5RA27315C.

- [118] C. Teng, C.M. Ma, K. Chiou, et al., Synergetic effect of hybrid boron nitride and multi-walled carbon nanotubes on the thermal conductivity of epoxy composites, *Mater. Chem. Phys.* 126 (2011) 722–728. doi:10.1016/j.matchemphys.2010.12.053.
- [119] S. Choi, J. Kim, Thermal conductivity of epoxy composites with a binary-particle system of aluminum oxide and aluminum nitride fillers, *Compos. Part B Eng.* 51 (2013) 140–147. doi:10.1016/j.compositesb.2013.03.002.
- [120] H. Ishida, D.J. Allen, Mechanical characterization of copolymers based on benzoxazine and epoxy, *Polymer (Guildf)*. 37 (1996) 4487–4495. doi:10.1016/0032-3861(96)00303-5.
- [121] D. Fu, Jifang; Shi, Liyi; Zhang, Effect of Nanoparticles on the Performance of Thermally Conductive Epoxy Adhesives, *Polym. Eng. Sci.* (2010) 1–11. doi:10.1002/pen.21705.
- [122] T. Hong, Jung-Ho, Yoon, Sung-Woon, Hwang, High Performance Heat Sink Composites Incorporating Micron-Sized Inorganic fillers and SN/IN Metal Particles, *Polym. Eng. Sci.* (2012) 1–8. doi:10.1002/pen.23190.
- [123] AZoNetwork UK Ltd, AZO Materials - E Glass Fibre Properties, (2019). <https://www.azom.com/properties.aspx?ArticleID=764> (accessed August 16, 2018).
- [124] M. Chohra, S.G. Advani, A. Gokce, et al., Modeling of filtration through multiple layers of dual scale fibrous porous media, *Polym. Compos.* 27 (2006) 570–581. doi:10.1002/pc.20228.
- [125] M. Suchitra, N.M. Renukappa, The Thermal Properties of Glass Fiber Reinforced Epoxy Composites with and without Fillers, *Macromol. Symp.* 361 (2016) 117–122. doi:10.1002/masy.201400227.
- [126] M. Ge, J. Zhang, C. Zhao, et al., Effect of hexagonal boron nitride on the thermal and dielectric properties of polyphenylene ether resin for high-frequency copper clad laminates, *Mater. Des.* 182 (2019) 108028. doi:10.1016/j.matdes.2019.108028.
- [127] D.M. Bigg, Mechanical, thermal, and electrical properties of metal fiber-filled polymer composites, *Polym. Eng. Sci.* 19 (1979) 1188–1192. doi:10.1002/pen.760191610.
- [128] J.D. Eshelby, The determination of the elastic field of an ellipsoidal inclusion, and related problems, *Proc. R. Soc. London, Ser. A, Math. Phys. Probl.* 241 (1957) 376–396. doi:10.1098/rspa.1957.0133.
- [129] M. Hatta, H., Taya, Equivalent inclusion method for steady-state heat conduction in composites, *Int. J. Eng. Sci.* 24 (1986) 1159–1172. doi:10.1016/0020-7225(86)90011-

- X.
- [130] D. Kumlutas, Thermal Conductivity of Particle Filled Polyethylene Composite Materials, *Compos. Sci. Technol.* 63 (2003) 113–117.
- [131] K. Soga, T. Saito, T. Kawaguchi, et al., Percolation effect on thermal conductivity of filler-dispersed polymer composites, *J. Therm. Sci. Technol.* 12 (2017) 1–8. doi:10.1299/jtst.2017jtst0013.
- [132] N.K. Mahanta, M.R. Loos, I. Manas Zloczower, et al., Graphite–graphene hybrid filler system for high thermal conductivity of epoxy composites, *J. Mater. Res.* 30 (2015) 959–966. doi:10.1557/jmr.2015.68.
- [133] W. Jin, W. Zhang, Y. Gao, et al., Surface functionalization of hexagonal boron nitride and its effect on the structure and performance of composites, *Appl. Surf. Sci.* 270 (2013) 561–571. doi:10.1016/j.apsusc.2013.01.086.
- [134] A. Jin.W., L., Liang, G., & Gu, Jin, W., Yuan, L., Liang, G., & Gu, A. (2014). Multifunctional Cyclotriphosphazene/Hexagonal Boron Nitride Hybrids and Their Flame Retarding Bismaleimide Resins with High Thermal Conductivity and Thermal Stability, *ACS Appl. Mater. Interfaces.* 6 (2014) 14931–14944. doi:10.1021/am502364k.
- [135] S. Chung, J. Lin, Thermal Conductivity of Epoxy Resin Composites Filled with Combustion Synthesized h-BN Particles, *Molecules.* 21 (2016) 1–11. doi:10.3390/molecules21050670.
- [136] L. Wang, W. Wu, D. Drummer, et al., Study on thermal conductive PA6 composites with 3-dimensional structured boron nitride hybrids, *J. Appl. Polym. Sci.* 136 (2019) 1–9. doi:10.1002/app.47630.
- [137] K.A. Wartig, Funktionalisiertes Graphen als Additiv für den Flammenschutz von Polypropylen, Universität Tübingen, 2014.
- [138] P. Kiliaris, Polymer/layered silicate (clay) nanocomposites: An overview of flame retardancy, *Prog. Polym. Sci.* (2010) 902–958.
- [139] F. Wolff-Fabris, Polymeradditive - Flammenschutzmittel - Lecture Notes, n.d.
- [140] E.- European Flame Retardants Association, Flame Retardants - FAQ, n.d.
- [141] K.H. Pawlowski, Wirkungsmechanismen von Bisphenol-A-bis(diphenylphosphat) als Flammenschutzmittel in Polycarbonat/Acrylnitril-Butadien-Styrol-Copolymerisat, Freie Universität Berlin, 2008.
- [142] United States Environmental Protection Agency, Flame Retardants in Printed Circuit

- Boards, **2015**.
- [143] G. Zattini, S. Ballardini, T. Benelli, et al., Safer plasticized polyvinyl chloride synthetic leathers for the automotive industry: Evaluation of alternatives to antimony compounds as flame retardants, *Polym. Eng. Sci.* (**2019**) 1–10. doi:10.1002/pen.25121.
- [144] M. Cygon, M; Hein, M; Choate, Halogen Free Base Materials for PWB Applications, (n.d.). <https://www.isola-group.com/wp-content/uploads/Halogen-Free-Base-Materials-for-PWB-Applications.pdf> (accessed February 4, 2021).
- [145] Pinfa (Cefic), Innovative Flame retardants in E & E Applications. Non-halogenated phosphorus , inorganic and nitrogen flame retardants, *Innovation.* (**2009**) 34.
- [146] M. Rakotomalala, S. Wagner, M. Döring, Recent developments in halogen free flame retardants for epoxy resins for electrical and electronic applications, *Materials (Basel).* 3 (**2010**) 4300–4327. doi:10.3390/ma3084300.
- [147] S. V. Levchik, E.D. Weil, A review of recent progress in phosphorus-based flame retardants, *J. Fire Sci.* 24 (**2006**) 345–364. doi:10.1177/0734904106068426.
- [148] J. Lindholm, A. Brink, M. Hupa, Cone calorimeter – a tool for measuring heat release rate, *Finnish-Swedish Flame Days 2009.* (**2009**). doi:10.1002/fam.
- [149] W.J. Babrauskas, V.; Parker, Ignitability Measurements With the Cone Calorimeter, *Fire Mater.* 11 (**1986**) 31–43.
- [150] J.C. Ronda, M. Galia, V. Ca, Cone calorimetry studies of benzoxazine-epoxy systems flame retarded by chemically bonded phosphorus or silicon, *Polym. Degrad. Stab.* 94 (**2009**) 102–106. doi:10.1016/j.polymdegradstab.2008.10.005.
- [151] G. Beyer, Nanocomposites: A new class of flame retardants for polymers, *Plast. Addit. Compd.* 4 (**2002**) 22–28. doi:10.1016/S1464-391X(02)80151-9.
- [152] S. Pavlidou, C.D. Papaspyrides, A review on polymer-layered silicate nanocomposites, *Prog. Polym. Sci.* 33 (**2008**) 1119–1198. doi:10.1016/j.progpolymsci.2008.07.008.
- [153] L. Wang, X. He, C.A. Wilkie, The utility of nanocomposites in fire retardancy, *Materials (Basel).* 3 (**2010**) 4580–4606. doi:10.3390/ma3094580.
- [154] B. Schartel, T.R. Hull, Development of fire retarded materials: Interpretation of cone calorimeter data, *Fire Mater.* (**2007**) 327–354. doi:10.1002/fam.
- [155] Efectis, Cone Calorimeter - Predicting fire and smoke behaviour accurately and cost-effectively, Bleiswijk, Netherlands, **2019**.
- [156] Railway applications - Fire protection on railway vehicles - Part 2: Requirements for fire

- behaviour of materials and components; German version EN 45545-2:2013+A1:2015, **2016**.
- [157] B. ScharTEL, M. Bartholmai, U. Knoll, Some comments on the use of cone calorimeter data, *Polym. Degrad. Stab.* 88 (2005) 540–547. doi:10.1016/j.polymdegradstab.2004.12.016.
- [158] B. ScharTEL, U. Braun, Comprehensive fire behaviour assessment of polymeric materials based on cone calorimeter investigations, *E-Polymers*. 3 (2003) 1–14. doi:10.1515/epoly.2003.3.1.177.
- [159] R.E. Lyon, Ignition Resistance of Plastics, *Recent Adv. Flame Retard. Polym.* 13 (2002) 14–25.
- [160] T.Y. Tsai, N. Bunekar, C.C. Huang, et al., Novolac cured epoxy resin/fullerene modified clay composites: applied to copper clad laminates, *RSC Adv.* 5 (2015) 95649–95656. doi:10.1039/c5ra18073b.
- [161] L. Karger-Kocsis, J.; Lendvai, Polymer / boehmite nanocomposites : A review, *J. Appl. Polym. Sci.* 45573 (2017). doi:10.1002/app.45573.
- [162] E.S. Ogunniran, R. Sadiku, S.S. Ray, Morphology and Thermal Properties of Compatibilized PA12 / PP Blends with Boehmite Alumina Nanofiller Inclusions, *Macromol. Mater. Eng.* (2012) 627–638. doi:10.1002/mame.201100254.
- [163] G. Camino, A. Maffezzoli, M. Braglia, et al., Effect of hydroxides and hydroxycarbonate structure on fire retardant effectiveness and mechanical properties in ethylene-vinyl acetate copolymer, *Polym. Degrad. Stab.* 74 (2001) 457–464.
- [164] T. Sun, Q. Zhuo, Y. Chen, et al., Synthesis of boehmite and its effect on flame retardancy of epoxy resin, *High Perform. Polym.* 27 (2015) 100–104. doi:10.1177/0954008314540312.
- [165] A. Sut, S. Greiser, C. Jäger, et al., Synergy in flame-retarded epoxy resin, *J. Therm. Anal. Calorim.* 128 (2016) 141–153. doi:10.1007/s10973-016-5934-4.
- [166] T. Neumeyer, G. Bonotto, J. Kraemer, et al., Fire behaviour and mechanical properties of an epoxy hot-melt resin for aircraft interiors, *Compos. Interfaces*. 20 (2013) 443–455. doi:10.1080/15685543.2013.807153.
- [167] B. Yu, W. Xing, W. Guo, et al., Thermal Exfoliation of hexagonal boron nitride for effective enhancements on thermal stability, flame retardancy and smoke suppression of epoxy resin nanocomposites via sol-gel process, *J. Mater. Chem. A Mater. Energy*

- Sustain.* 4 (2016) 7330–7340. doi:10.1039/C6TA01565D.
- [168] A.J. Fischer, Y. Zhong, L. Zhang, et al., Heat propagation in thermally conductive polymers of PA6 and hexagonal boron nitride, *Fire Mater.* (2019) 1–8. doi:10.1002/fam.2753.
- [169] J. Gu, C. Liang, X. Zhao, et al., Highly thermally conductive flame-retardant epoxy nanocomposites with reduced ignitability and excellent electrical conductivities, *Compos. Sci. Technol.* (2017). doi:10.1016/j.compscitech.2016.12.015.
- [170] B.G.L. Prasada Rao S. Kodavanti, Chapter 25 - Polychlorinated biphenyls, polybrominated biphenyls, and brominated flame retardants, in: Ramesh C. Gupta (Ed.), *Biomarkers Toxicol.*, Academic Press, 2014: pp. 433–450. doi:10.1016/B978-0-12-404630-6.00025-7.
- [171] California Environmental Protection Agency, Tetrabromobisphenol A (TBBPA) - California Proposition 65, (2020). <https://www.p65warnings.ca.gov/factsheets/tetrabromobisphenol-tbbpa> (accessed December 28, 2020).
- [172] J. Innes, Ann; Innes, *Handbook of Environmental Degradation of Materials - Chapter 10 Flame Retardants*, (2012) 309–335. doi:10.1016/B978-1-4377-3455-3.00010-9.
- [173] Isola GmbH, 370HR - High-Performance Laminate and Prepreg, (n.d.). <https://www.isola-group.com/pcb-laminates-prepreg/370hr-laminate-prepreg/> (accessed December 6, 2020).
- [174] Huntsman Advanced Materials, Hardener XB3473, (2009) 1.
- [175] Accuratus, Boron Nitride, BN Ceramic Properties, 2020.
- [176] InfraTec GmbH Germany, IRBIS 3 Analysis Software, (2019). <https://www.infratec.eu/thermography/thermographic-software/irbis3/> (accessed May 21, 2019).
- [177] D.D.I. fuer N. E.V., DIN EN ISO 178 Bestimmung der Biegeeigenschaften, 2003.
- [178] Laurenzi S.; Marchetti M., Advanced Composite Materials by Resin Transfer Molding for Aerospace Applications, *Compos. Their Prop.* (2012) 197–226. doi:10.5772/2816.
- [179] S. Zhang, X.Y. Cao, Y.M. Ma, et al., The effects of particle size and content on the thermal conductivity and mechanical properties of Al<sub>2</sub>O<sub>3</sub>/high density polyethylene (HDPE) composites, *Express Polym. Lett.* 5 (2011) 581–590. doi:10.3144/expresspolymlett.2011.57.
- [180] S. Duwe, C. Arlt, S. Aranda, et al., A detailed thermal analysis of nanocomposites filled

- with SiO<sub>2</sub>, AlN or boehmite at varied contents and a review of selected rules of mixture, *Compos. Sci. Technol.* 72 (2012) 1324–1330. doi:10.1016/j.compscitech.2012.04.015.
- [181] B.H. Xie, X. Huang, G.J. Zhang, High thermal conductive polyvinyl alcohol composites with hexagonal boron nitride microplatelets as fillers, *Compos. Sci. Technol.* 85 (2013) 98–103. doi:10.1016/j.compscitech.2013.06.010.
- [182] A. Suplicz, H. Hargitai, J.G. Kovacs, Methodology development for through-plane thermal conductivity prediction of composites, *Int. J. Therm. Sci.* 100 (2016) 54–59. doi:10.1016/j.ijengsci.2012.03.035.
- [183] S. V. Levchik, E.D. Weil, Thermal decomposition, combustion and flame-retardancy of epoxy resins - A review of the recent literature, *Polym. Int.* 53 (2004) 1901–1929. doi:10.1002/pi.1473.
- [184] J. Hausner, B. Fischer, M. Stöter, et al., Increasing time of ignition for PS-clay nanocomposites filled with [Fe(bpy)<sub>3</sub>]<sup>2+</sup>-modified hectorite, *Polym. Degrad. Stab.* 128 (2016) 141–148. doi:10.1016/j.polymdegradstab.2016.03.015.
- [185] E.S. Ogunniran, R. Sadiku, S. Sinha Ray, et al., Morphology and thermal properties of compatibilized PA12/PP blends with boehmite alumina nanofiller inclusions, *Macromol. Mater. Eng.* 297 (2012) 627–638. doi:10.1002/mame.201100254.
- [186] G. Camino, A. Maffezzoli, M. Braglia, et al., Effect of hydroxides and hydroxycarbonate structure on fire retardant effectiveness and mechanical properties in ethylene-vinyl acetate copolymer, *Polym. Degrad. Stab.* 74 (2001) 457–464. doi:10.1016/S0141-3910(01)00167-7.
- [187] Y. Zhang, J.R. Choi, S. Park, Thermal conductivity and thermo-physical properties of nanodiamond-attached exfoliated hexagonal boron nitride/epoxy nanocomposites for microelectronics, *Compos. Part A.* (2017). doi:10.1016/j.compositesa.2017.06.019.
- [188] C. Dong, A. Wirasaputra, Q. Luo, et al., Intrinsic flame-retardant and thermally stable epoxy endowed by a highly efficient, multifunctional curing agent, *Materials (Basel)*. 9 (2016). doi:10.3390/ma9121008.
- [189] S.M. Unlu, S.D. Dogan, M. Dogan, Comparative study of boron compounds and aluminum trihydroxide as flame retardant additives in epoxy resin, *Polym. Adv. Technol.* 25 (2014) 769–776. doi:10.1002/pat.3274.
- [190] M. Rakotomalala, Muriel, Wagner, Sebastian, Döring, Recent developments in Halogen Free Flame Retardants for Epoxy Resins for Electrical and Electronic Applications,

- Materials (Basel)*. 3 (2010) 4300–4327. doi:10.3390/ma.3084300.
- [191] A. Laachachi, M. Ferriol, M. Cochez, et al., A comparison of the role of boehmite (AlOOH) and alumina (Al<sub>2</sub>O<sub>3</sub>) in the thermal stability and flammability of poly(methyl methacrylate), *Polym. Degrad. Stab.* 94 (2009) 1373–1378. doi:10.1016/j.polymdegradstab.2009.05.014.
- [192] S.J. Wilson, The Dehydration of Boehmite, *J. Solid State Chem.* 30 (1979) 247–255. doi:10.1016/0022-4596(79)90106-3.
- [193] B. Schartel, B. Perret, B. Dittrich, et al., Flame Retardancy of Polymers: The Role of Specific Reactions in the Condensed Phase, *Macromol. Mater. Eng.* 301 (2016) 9–35. doi:10.1002/mame.201500250.
- [194] Neumeyer Thomas, Struktur und Eigenschaften neuer, flammgeschützter Prepreg-Matrixsysteme für Anwendungen in der Kabine von Verkehrsflugzeugen, Universität Bayreuth, 2015.
- [195] W. Jin, L. Yuan, G. Liang, et al., Multifunctional cyclotriphosphazene/hexagonal boron nitride hybrids and their flame retarding bismaleimide resins with high thermal conductivity and thermal stability, *ACS Appl. Mater. Interfaces*. 6 (2014) 14931–14944. doi:10.1021/am502364k.
- [196] B. Schartel, C.A. Wilkie, G. Camino, Recommendations on the scientific approach to polymer flame retardancy: Part 2 - Concepts, *J. Fire Sci.* 35 (2017) 3–20. doi:10.1177/0734904116675370.
- [197] W. Yang, Y.R. Zhang, A.C.Y. Yuen, et al., Synthesis of phosphorus-containing silane coupling agent for surface modification of glass fibers: Effective reinforcement and flame retardancy in poly(1,4-butylene terephthalate), *Chem. Eng. J.* 321 (2017) 257–267. doi:10.1016/j.cej.2017.03.123.
- [198] J. Menczel, R. Prime, Thermal analysis of polymers, 2009, ISBN:9780470423837. doi:10.1007/BF01914481.
- [199] C.F.J. Coombs, Printed circuits Handbook, 6th Edition, n.d., ISBN:0071510796.
- [200] A.T. Droste, D.H.; Dibenedetto, The glass transition temperature of filled polymers and its effect on their physical properties, *J. Appl. Polym. Sci.* 13 (1969). doi:10.1002/app.1969.070131011.
- [201] Isola Corporation, Product Data Sheet - FR-406, 2018.
- [202] H. Lengsfeld, Entwicklung flammhemmend ausgerüsteter Epoxidharzsysteme auf Basis

- neuer latenter Kombinationsverbindungen, Universität Bayreuth, **2004**.
- [203] A. Casu, G. Camino, M. De Giorgi, et al., Effect of glass fibres and fire retardant on the combustion behaviour of composites, glass fibres-poly(butylene terephthalate), *Fire Mater.* 22 (1998) 7–14. doi:10.1002/(SICI)1099-1018(199801/02)22:1<7::AID-FAM623>3.0.CO;2-3.
- [204] S. Vaddi, Flammability Evaluation of Glass-Fiber reinforced Polypropylene and Polyethylene with Montmorillonite Nanoclay Additives, University of Alabama, Birmingham, **2008**.
- [205] W.S. Chow, L.N. Chang, M. Jaafar, Flame retardant epoxy hybrid composite laminates prepared by vacuum-assisted resin infusion technique, *J. Compos. Mater.* 49 (2015) 1471–1481. doi:10.1177/0021998314535454.
- [206] S. Madakbaş, E. Çakmakçı, M.V. Kahraman, Preparation and thermal properties of polyacrylonitrile/hexagonal boron nitride composites, *Thermochim. Acta.* 552 (2013) 1–4. doi:10.1016/j.tca.2012.11.011.
- [207] R.V. Petrella, The Assessment of Full-Scale Fire Hazards from Cone Calorimeter Data, *J. Fire Sci.* 12 (1994) 14–43. doi:10.1177/073490419401200102.
- [208] S. Joseph, M.S. Sreekala, Z. Oommen, et al., A comparison of the mechanical properties of phenol formaldehyde composites reinforced with banana fibres and glass fibres, *Compos. Sci. Technol.* 62 (2002) 1857–1868. doi:10.1016/S0266-3538(02)00098-2.
- [209] W.A. Hussain, A.A. Hussein, J.M. Khalaf, et al., Dielectric Properties and a . c . Conductivity of Epoxy / Alumina Silicate NGK Composites, (2015) 282–289.
- [210] C.Y. Zhi, Y. Bando, T. Terao, et al., Dielectric and thermal properties of epoxy / boron nitride nanotube composites, *Pure Appl. Chem.* 82 (2010) 2175–2183. doi:10.1351/PAC-CON-09-11-41.
- [211] P.S. Rao, M.M. Hussain, R. Kishore, Moisture Absorption Evolution of Gfrp Laminates Subjected To Different Environmental Conditions, 2 (2012) 33–38.
- [212] D. Qiang, G. Chen, T. Andritsch, Influence of water absorption on dielectric properties of epoxy SiO<sub>2</sub> and BN nanocomposites, *Annu. Rep. - Conf. Electr. Insul. Dielectr. Phenomena, CEIDP.* 2015-Decem (2015) 439–442. doi:10.1109/CEIDP.2015.7352130.
- [213] P. Marx, A.J. Wanner, Z. Zhang, et al., Effect of interfacial polarization and water absorption on the dielectric properties of epoxy-nanocomposites, *Polymers (Basel).* 9 (2017) 1–16. doi:10.3390/polym9060195.

- 
- [214] C. Zou, J.C. Fothergill, S.W. Rowe, The Effect of Water Absorption on the Dielectric Properties of Epoxy Nanocomposites, *IEEE Trans. Dielectr. ELectrical Insul.* 15 (2008) 106–117. doi:0.1109/T-DEI.2008.4446741.
- [215] M. Jux, B. Finke, T. Mahrholz, et al., Effects of Al(OH)O nanoparticle agglomerate size in epoxy resin on tension, bending, and fracture properties, *J. Nanoparticle Res.* 19 (2017). doi:10.1007/s11051-017-3831-9.

## Curriculum Vitae



<b>Personal Data</b>	Christin Pawelski-Hoell, born 19 <sup>th</sup> July 1987 in Bad Frankenhausen	
<b>Marital Status</b>	married	
<b>Nationality</b>	German	
<b>Education</b>	1994 - 1998	Grundschule Bad Frankenhausen / Bad Rodach
	1998 - 2007	Gymnasium Alexandrinum Coburg Abitur
<b>Apprenticeship</b>	2007 - 2010	Procter & Gamble, Schwalbach/Ts. Degree: Chemical laboratory assistant
<b>Academic Studies</b>	2010 - 2013	University of Applied Science Reutlingen B.Sc. Applied Chemistry
	2013 - 2015	University of Bayreuth M.Sc. Polymer Science
<b>Profession</b>	2015 - 2018	Scientific Employee, Chair of Polymer Engineering University of Bayreuth
	2019 - today	RAUMEDIC, Inc., North Carolina, USA Product Manager Application Technology Extrusion

## **Publications**

### **Begutachtete Publikationen (*Journals*):**

**C. Pawelski, S. Bhagwat, V. Altstädt**

**Thermal, Fire, and Mechanical Properties of Solvent-Free Processed BN/Boehmite-filled Prepregs**

Polymer Engineering and Science, (2019), DOI 10.1002/pen.25184

### **Begutachtete Publikationen (*Conference Proceedings*):**

**C. Pawelski, E. Kang, G. Bakis, V. Altstädt**

**Effect of Filler Type and Particle Size Distribution on Thermal Properties of bimodal and hybrid BN/Boehmite-filled Epoxy Novolac Composites**

AIP Conference Proceedings 2055, 050007 (2019): <http://doi.org/10.1063/1.5084826>

### **Vorträge auf nationalen und internationalen Konferenzen und Tagungen:**

**G. Bakis, C. Pawelski, S. Bard, V. Altstädt**

**Advancements in Thermoset Processing and Material Development**

15<sup>th</sup> Innovations Day, Magic Matrix, Flame Retardancy for Composites and Application, Stade

**C. Pawelski, E. Kang, G. Bakis, L. Honglin, V. Altstädt**

**Effect of Particle Size and relative Composition on Thermal Properties of BN/Boehmite-filled Epoxy Novolac Composites**

Proceedings of the Europe/Africa Conference Dresden 2017 – Polymer Processing Society PPS

**Posterbeiträge auf nationalen und internationalen Konferenzen und Tagungen:**

**C. Pawelski**, S. Bhagwat, V. Altstädt

**Thermally Conductive & Flame Retardant highly-filled Epoxy-Novolac GF-Prepregs for PCBs – Correlation of Morphology & Thermal Properties**

ECCM -18, Athen/Greece, (2017)

**Sonstige Veröffentlichungen**

J. Gensel, L. Klug, G. Niemeyer, T. Neumeyer, **C. Pawelski**, P. Schreier, W. Teubert, U. Wienhold, H. Wörthwein, V. Altstädt

**Novel flame-retardant polymer bead foams**

PPS Dresden 2017 (Poster, 1<sup>st</sup> Poster Prize)

J. Gensel, **C. Pawelski**, V. Altstädt

**Welding Quality in Polymer Bead Foams: An *in-situ* SEM Study**

PPS 32 Lyon (Presentation)

AIP Conference Proceedings **1914**, 060001 (2017); <https://doi.org/10.1063/1.5016721>

J. Gensel, L. Klug, **C. Pawelski**, J. Schwemmer, P. Schreier, T. Neumeyer, V. Altstädt

**Fusion in EPP bead foams: Influence of processing and functional additives**

SPE Foams 2017 (Poster)

**Annex**

**Table 23 Overview of the produced preregs, their detailed production parameters and their corresponding prepeg weights and resin contents.**

Composition	Temperature Auftragswerk /		Temperature Kalandrier /		Temperature Tabela /		Gap Plate / µm	Prepeg		Resin Content / wt. %	Prepeg width / mm	Quantity Produced / m
	°C	°C	°C	°C	areal weight / g/m <sup>2</sup>	(resin+filler) / wt. %						
neat GF 25	70	80	80	70	129	104.00	190	129	104.00	80.62	200	50
neat GF 49	80	80	80	85	131	83.00	180	131	83.00	63.36	200	25
Neat GF 107	80	80	80	85	203	98.00	190	203	98.00	48.28	210	35
BN 2µm, GF 25	855	80	80	85	129	104.00	170	129	104.00	80.62	200	35
BN 12µm, GF 25	85	85	85	80	159	134.00	190	159	134.00	84.28	200	50
BN 12µm, GF 49	80	80	80	85	153	105	190	153	105	68.63	210	35
BN 12µm, GF 107	80	80	80	85	203	98.00	190	203	98.00	48.28	210	35
BN 45µm, GF 25	85	85	85	80	125	100.00	180	125	100.00	80.00	200	33
BN 45µm, GF 107	85	85	85	80	215	110.00	180	215	110.00	88.38	200	35
BT 2µm, GF 25	85	80	80	85	135	110.00	170	135	110.00	81.48	200	47
BT 2µm, GF 107	80	80	80	85	195	90.00	190	195	90.00	46.15	210	35
Hybrid GF 25*	85	85	85	80	134	109.00	210	134	109.00	81.34	200	45
Hybrid GF 49*	80	80	80	85	153	80.00	190	153	80.00	68.63	210	25
Bimodal GF 25**	85	85	85	80	129	104	210	129	104	80.62	200	35

Table 24 Overview of all produced preregs and their corresponding physical parameters and contents.

Composition	Prepreg areal weight / $g/m^2$	Resin Content / wt. %	Fibre Content / wt. %	Filler Content / wt. %	Resin Content / vol. %	FVC / vol. %	Filler Content / vol. %	CPT / mm	Density <sub>lamine</sub> / $g/cm^3$ ***
neat GF 25	129	83.83	16.18	-	91.61	8.39	-	0.090	1.33
neat GF 49	131	51.22	48.73	-	68.90	31.13	-	0.110	1.64
Neat GF 107	203	43.75	56.25	-	62.10	37.90	-	0.150	1.73
BN 2 $\mu$ m, GF 25	129	59.84	18.46	21.70	72.54	11.81	15.56	-	1.52
BN 12 $\mu$ m, GF 25	159	59.02	18.02	22.96	74.05	10.77	15.18	0.110	1.53
BN 12 $\mu$ m, GF 49	153	49.44	31.32	19.24	63.20	22.57	14.27	0.120	1.64
BN 12 $\mu$ m, GF 107	203	35.55	50.62	13.83	46.74	42.16	11.10	0.150	1.83
BN 45 $\mu$ m, GF 25	125	57.44	19.67	22.89	70.69	12.58	16.73	0.115	1.83
BN 45 $\mu$ m, GF 107	215	36.57	48.86	14.52	47.79	40.10	12.10	-	1.80
BT 2 $\mu$ m, GF 25	135	63.80	13.67	22.53	78.61	8.66	12.73	0.105	1.54
BT 2 $\mu$ m, GF 107	195	37.89	48.73	13.38	51.05	40.84	8.47	-	1.84
Hybrid GF 25*	134	63.80	14.68	21.52	76.84	9.15	14.01	0.100	1.50
Hybrid GF 49*	153	50.87	31.97	17.16	65.07	23.09	11.08	0.120	1.64
Bimodal GF 25**	129	58.61	19.00	22.39	71.70	12.31	15.00	-	1.54

\*Hybrid: Boehmite 2 $\mu$ m + BN 12 $\mu$ m, ratio 1:3\*\*bimodal: BN 2 $\mu$ m + BN12 $\mu$ m, ratio 1:3

\*\*\* calculated from TGA results